2020-08-11

Measurement and Simulation of Head Impacts in Mixed Martial Arts

Aidan Meagher
Technological University Dublin

Recommended Citation

Meagher, A. (2020). *Measurement and simulation of head Impacts in mxed martial arts*. Masters dissertation. Technological University Dublin. doi: 10.21427/kr6v-b979

Measurement and Simulation of Head Impacts in Mixed Martial Arts

A Thesis Presented for the Award of Masters by Research by

Aidan Meagher B.Eng. Hons

Technological University Dublin – Tallaght Campus

School of Engineering

Department of Mechanical Engineering

For Research Carried Out Under the Guidance of

Mr. Stephen Tiernan

Submitted to Technological University Dublin

November 2019

Declaration

I certify that this thesis which I now submit for examination for the award of _____, is entirely my own work and has not been taken from the work of others, save and to the extent that such work has been cited and acknowledged within the text of my work.

This thesis was prepared according to the regulations for graduate study by research of the Technological University Dublin (TU Dublin) and has not been submitted in whole or in part for another award in any other third level institution.

The work reported on in this thesis conforms to the principles and requirements of the TU Dublin's guidelines for ethics in research.

(The following sentence may be deleted if access to the thesis is restricted according to Section 4.8 of the TU Dublin Research regulations)

TU Dublin has permission to keep, lend or copy this thesis in whole or in part, on condition that any such use of the material of the thesis be duly acknowledged.

Signature _____ Date _____

Candidate Aidan Meagher

Acknowledgements

Many people have been a part of this journey and I would like to take this opportunity to thank them. Firstly, I would like to thank all the staff at what is now The Technological University Dublin – Tallaght Campus, with special thanks to my supervisor Mr. Stephen Tiernan. Without your support and guidance this would not have been possible.

I would also like to thank Derek Sweeney and the team at CADFEM Ireland. For their support in providing me with a virtual machine for running my simulations free of charge and support for using the model correctly. This study would certainly have not been possible without this generous offer.

Dr. David O Sullivan of Pusan University, South Korea for his willingness to get involved and take time from his busy schedule to take continue this study for the next year.

To my fellow post grads; Adam Kelly, Gary Byrne, Dr. Gemma Newman, Mark Beakey, Niamh Murphy and Tiernan Brennan a huge thanks must go to you all. Thank you for the coffee, laughs, tears and all-round stress relief over the last few years.

Finally, and most importantly, I want thank to my family and friends for putting up with my over-stressed self for the last two years, for providing me with a support structure and generally keeping me on the right track (despite my best efforts). There are no words.

Abstract

This study measures *in vivo* head accelerations in Mixed Martial Arts (MMA) and applies them to a finite element head model to determine the levels of strain within the corpus callosum, thalamus, midbrain and brain stem. Twenty-two elite amateur and professional MMA athletes took part in the study. Ethical approval was granted by the Institute of Technology Tallaght Ethics Committee (REC-STF1-201819).

Participants were fitted with the Stanford University instrumented mouthguard (MiG2.0), a 6 DOF device with a tri-axial accelerometer and gyroscope. The lower threshold for recording data was 10g. All events were video recorded to allow for the confirmation of any impact recorded. The measured head accelerations were applied to a partially validated, 50th percentile male human model managed by the Global Human Body Modelling Consortium (GHBMC).

434 head impacts have been recorded at fourteen out of competition sessions and eight competitive events. No injuries were sustained during the out of competition sessions, while five of the competitive events resulted in an mTBI diagnosis. The mean impact sustained by participants in out of competition sessions was 29.2g and 4917 rads/s^2 while the mean impact in competitive events was 43.5g and 5969 rads/s^2.

The best predictors for strain in the corpus callosum and thalamus were peak linear acceleration in the Y axis and peak rotational velocity combined (R^2 (adj) = 0.48 and 0.493 respectively), in the mid brain and brainstem were peak linear acceleration in the Y axis and peak rotational acceleration about the Z axis combined (R^2 (adj) = 0.741 and 0.805 respectively). The best predictor for a concussive diagnosis was found to be impact duration. Eight of the simulated impacts had durations greater than 15ms for linear acceleration or 25 ms rotational acceleration duration, seven of these sessions resulted in a concussion diagnosis. These results may aid future work in the prediction of mTBI's in sport.

Nomenclature

TBI	Traumatic Brain Injury
mTBI	Mild Traumatic Brain Injury
SRC	Sports Related Concussions
MMA	Mixed Martial Arts
FE	Finite Element
FEA	Finite Element Analysis
CSF	Cerebrospinal Fluid
CNS	Central Nervous System
GHBMC	Global Human Body Model Consortium
SIMon	Simulated Injury Monitor
KTH	Kungliga Tekniska Högskolan
UCD	University College Dublin
UCDBTM	University College Dublin Brain Trauma Model
MPS	Maximum Principal Strain
SCAT	Sport Concussion Assessment Tool
CSDM	Cumulative Strain Damage Measure
CoG	Centre of Gravity
DoF	Degrees of Freedom
WSTC	Wayne State Tolerance Curve
GSI	Gadd Severity Index
HIC	Head Impact Criterion
HIP	Head Impact Power
HITS	Head Impact Telemetry System
CT	Computed Topography
MRT	Magnetic Resonance Topography
IR	Infrared
PCS	Post-Concussion Syndrome
PMHS	Post Mortem Human Subject
PLA	Peak Linear Acceleration
PRA	Peak Rotational Acceleration
NFL	National Football League

PRV	Peak Rotational Velocity
RMS	Root Mean Square
MAS	Mean Adjacent Strain

Table of Contents

Table of Tables

Tables of Equations

Table of Figures

Chapter 1 Introduction

"… People are uneducated about traumatic brain injury. They don't recognize it when it happens to them or their loved ones; they don't know the extent of the public health problem… Without accurate data, how can we begin to address the problem?"

The quote above is from a traumatic brain injury (TBI) survivor, taken at the Congressional Brain Injury Task Force in 2001. Almost twenty years later it still holds true. As of 2018, at least 1.4 million Americans suffer a TBI every year, 235,000 of these require hospitalisation and 50,000 die as result of their injuries [1]. There are many forms of TBI, ranging from severe (skull fracture) to mild (concussion) [2]. The fifth International Conference on Concussion in Sport has defined concussion as a "*complex pathophysiological process affecting the brain, induced by traumatic biomechanical forces*." [3].

Sports and recreation activities are one of the main sources of TBI in the United States of America, with 90% of these injuries being classified as mild traumatic brain injuries (mTBI). In the period 2001-2012, 3.42 million emergency department visits were recorded as a result of a sport related TBI in the US, with the rate at which these injuries occurred increasing throughout the period [4]. MTBI's are particularly difficult to diagnose, as medical imaging techniques show no physical damage to the brain post injury [5]. Several studies have postulated that increased levels of strain in the brain are the cause of mTBI, with several regions being of particular interest [6] [7] [8]. This study investigated that hypothesis by collecting *in vivo* head impact data and applying it to a finite element model to determine the levels of strain in the brain during an impact. In order to do this, several procedures had to be put in place.

- A procedure for collecting the *in vivo* data was be developed, as well as a procedure to analyse this data.
- Once a procedure for collecting data was developed and the data had been analysed, in order to rule out any false positives, data collection could begin.
- A procedure to apply this data to the finite element model and to run the simulated impacts was then developed.
- A method of analysing the simulation data was developed
- Investigate of predictors for strain and concussion from simulation results

An instrumented mouthguard has been viewed as a one of the more accurate options for recording the velocity and acceleration of the head following an impact. This is due to the fact that the coupling of the mouthguard, via the test subjects' dentition, allows for direct recording of the kinematics of the head. As opposed to the recording of data incorporated in an instrumented helmet, for example.

Mixed Martial Arts (MMA) was chosen as the sport to collect data from as it offers a near unique opportunity to collect large numbers of impacts. This is because MMA is a competitive, full-contact sport that involves an amalgamation of elements drawn from boxing, wrestling, karate, taekwondo, jujitsu, Muay Thai, judo, and kickboxing [9]. The fighters wear 110g to 170g gloves and do not wear head protection. A ten-year review of injuries in MMA by Buse et al., in 2006, found that head trauma was the single biggest reason for match stoppages (28.3%) [10]. This is one of few studies to measure *in vivo* head accelerations in an unhelmeted sport [11] [12] [13].

Chapter 2 Literature Review

2.1 Introduction

The following chapter will document the research literature reviewed for this study.

- Anatomy of the human skull, the regions of the brain and their functions.
- Traumatic Brain Injuries (TBI) and the diagnosis of concussion.
- Instrumented devices including helmet mounted systems, devices that are worn on the body and instrumented mouthguards.
- Finite Element (FE) models used in concussion research.
- Brain injury predictors.
- Mixed Martial Arts (MMA), its history, rules and the justification for choosing it for this study.

2.2 Anatomy

In this section the anatomy of the human head and brain will be discussed. This will include the anatomical arrangement, operation and function of the skull, major regions of the brain and some of the areas of the brain that are of particular interest in the study of TBI. Anatomical plane and axes will be defined and their relative directions of motion/rotation will also be discussed.

Particular attention will be paid to the regions that have been highlighted as important in the field of TBI [6] [8] [7]. These include the corpus callosum, mid-brain, brain stem, falx cerebri, cerebellar tentorium and diencephalon.

2.2.1 Skull

The adult human skull consists of 22 bones, 8 forms the cranium and 14 forms the facial structure. The 8 cranial bones create the cranial cavity, which houses the brain. The cranial bones are the occipital, parietal (x2), frontal, temporal (x2), sphenoid and ethmoid, shown in Figure 1. These bones protect the brain from external forces and dictate the overall shape of the brain within.

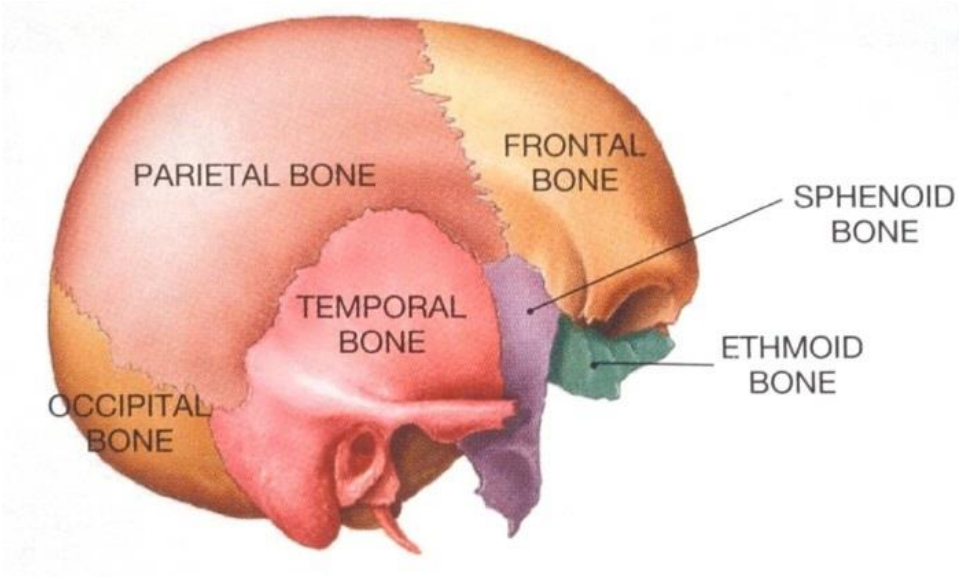

Figure 1: Cranial Bones [14]

Connections between these bones in adults consist of dense fibrous connective tissue called sutures, Figure 2 shows these sutures. There are 4 suture types in the cranial cavity:

1. Lambdoid suture: Connects the occipital and parietal bones in the posterior of the skull. One or more Wormian bones, which are small non-uniformly shaped bones not unlike jigsaw pieces, form part of this suture.
2. Coronal suture: Connects the frontal and parietal bones on the superior of the skull.
3. Sagittal suture: Connects the parietal bones, running from the lambdoid suture to the coronal suture.
4. Squamous suture: Connects the temporal and parietal bones on each side of the skull.

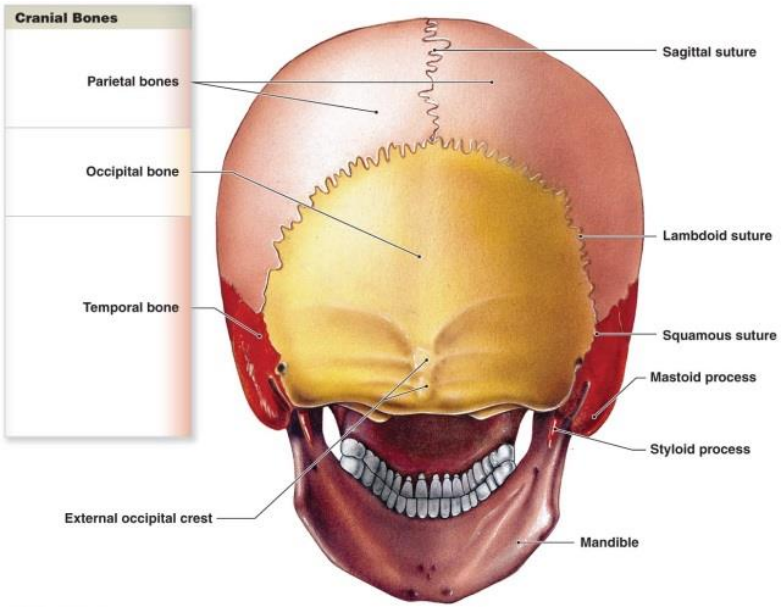

Figure 2: Bones and sutures of the skull in posterior view [14]

2.2.2 Brain

The human brain is mainly comprised of a left and right hemisphere, cerebellum, brain stem and the corpus callosum. It is protected internally by the cranial meninges and cerebrospinal fluid.

The matter of the brain is made up of neurons; these neurons send and receive electrical and chemical signals to and from the brain. The makeup of these neurons can be broken down into “grey” and “white” matter. “Grey” matter consists of the cell bodies of neurons and makes up the cortex of the brain. “White” matter is made up of millions of nerve fibres called dendrites and axons, axons are the medium through which the signal travels and connect the cell body to the dendrite. Dendrites are located at the area at which the signal is to be sent and have a branched structure to allow for the signals to be passed to the area required, shown in Figure 3.

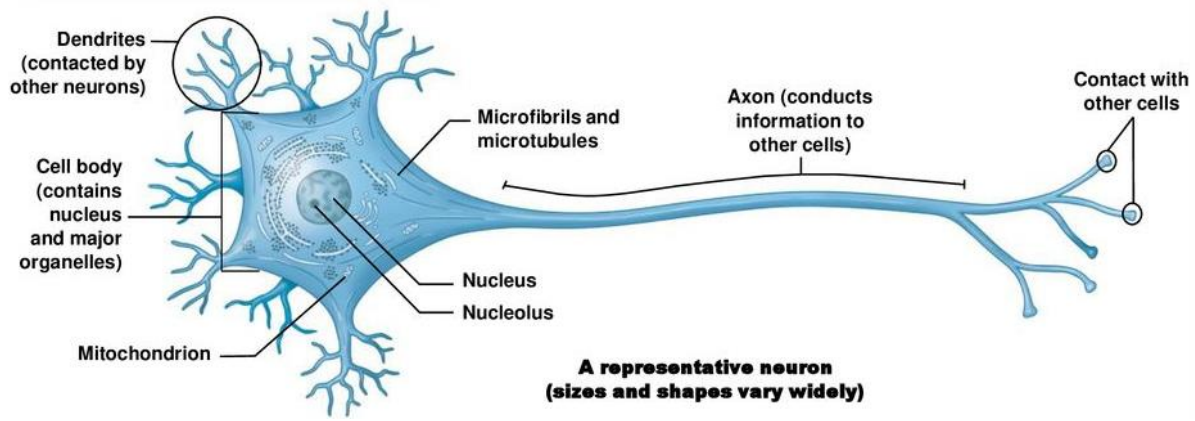

Figure 3: General arrangement of a neuron [14]

2.2.3 Brain Regions

The anatomical structure of the human brain is made up of 6 main regions; the (1) cerebral hemispheres, (2) cerebellum, (3) diencephalon, (4) midbrain, (5) pons and (6) medulla oblongata, with the midbrain, pons and medulla oblongata making up the brain stem, shown in Figure 4. Each region is associated with different functions and has varying cellular structures. Brain size varies by gender, with male brains being approximately 10% larger on average due to the difference in average body size.

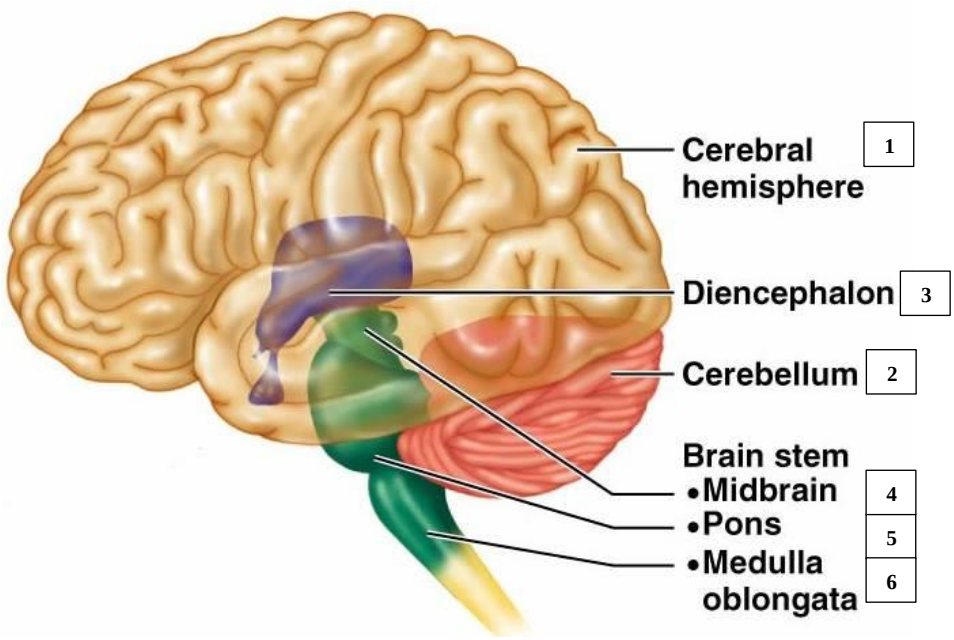

Figure 4: Major regions of the brain [14]

1. Cerebrum: The largest region of the brain consisting of 2 cerebral hemispheres, the left and right hemispheres. The outer surface of the cerebrum is known as the cerebral cortex. The surface of the cerebral cortex is covered in Gyri, raised ridges, and Sulci, shallow depressions, which increase the surface area of the brain. The cerebral hemispheres are made up of 4 lobes; the frontal, parietal, occipital and temporal lobes.

2. Cerebellum: The second largest region of the brain, located posteriorly to the cerebrum. The cerebellum also has 2 hemispheres and is covered by a ridged cerebellar cortex. The function of the cerebellum is to receive signals from the sensory systems of the body and regulate motor function.

3. Diencephalon: Located in the centre of the brain below the cerebral hemispheres, provides the link between the cerebral hemispheres and the brain stem. Consisting of the thalamus and the hypothalamus. The thalamus is the processing centre for sensory signals. As well as being involved in the delivery of sensory and emotional information between the spinal cord and the cranial nerves. And the hypothalamus is the centre for hormone production, emotion control and autonomic functions.

4. Midbrain: Uppermost portion of the brain stem located directly below the diencephalon. It is the processing centre of visual and auditory data, maintains consciousness and generates the reflexive motor responses.

5. Pons: The mid portion of the brain stem, named from the Latin for bridge, the pons is the connection between the cerebellum and the brain stem. It sends sensory data to the cerebellum and thalamus and is the centre for subconscious somatic and visceral motor functions.

6. Medulla Oblongata: The lowest portion of the brain stem, the medulla oblongata connects the brain stem to the spinal cord. It sends sensory data to other portions of the brain stem and is the autonomic centre for regulating the body's visceral functions.

2.2.4 Lobes of the Cerebrum

The cerebrum is physically split into 2 hemispheres; each hemisphere has 4 distinct lobes. These lobes are separated by sulci that are common to all adult human brains. The central sulci separate the frontal and parietal lobes, the horizontal lateral sulci separate the temporal and frontal lobes and the parieto-occipital sulci separate the parietal and occipital lobes. While these sulci are found in all adult human brains, the exact formation of the gyri and sulci of every brain are entirely unique.

1. Frontal Lobe: Located anteriorly, the frontal lobe has many functions including voluntary movement and speech. The pre frontal cortex is a subdivision of the frontal lobe; its functions are in relation to memory, intelligence, temperament and personality.
2. Parietal Lobe: Located posteriorly to the frontal lobe the parietal lobe is the primary sensory cortex. It handles how the brain perceives pain, pressure, heat, taste and vibration.
3. Occipital Lobe: Located at the posterior of the skull the occipital lobe is the visual cortex of the brain. It handles the interpretation of visual stimuli.
4. Temporal Lobe: Located laterally in the cranial cavity the temporal lobe is the auditory and olfactory cortex. It deals with the perception of sounds and smells.

Although these lobes have been listed with certain functions it should be noted that they do not function separately, they have highly complex relationships and function as a whole. Information is passed between lobes and hemispheres, and each lobe could be further divided into specialised areas for each function, shown in Figure 5.

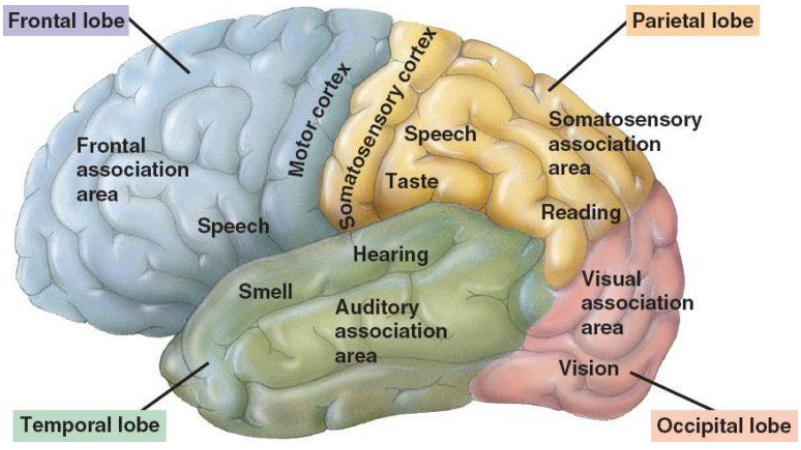

Figure 5: Functions of the Lobes of the Brain [14]

2.2.5 Corpus Callosum

The corpus callosum is a fibrous band of nerves that spans part of the longitudinal fissure of the brain, shown in Figure 6. Located beneath the cerebral cortex it connects the left and right hemispheres and allows each hemisphere to communicate with each other. Comprised of approximately 200 million axons, it is the largest white matter fibre bundle in the brain. Its main functions are:

- Passing of information between left and right hemispheres
- Perception of touch and tactile localisation
- Combining visual data from left and right hemispheres
- Identification of visual data and connecting with language centre

Figure 6: The Corpus Callosum highlighted in red [15]

2.2.6 Cerebrospinal Fluid

Cerebrospinal fluid (CSF) surrounds the entirety of the central nervous system (CNS), with the CNS encapsulating the brain and spinal column. It has a number of functions, including but not limited to the following:

1. Acts as a damper for the delicate surfaces of the CNS
2. Provides support to the brain by surrounding it completely
3. Acts as an exchange medium for nutrients, waste and chemical signals

2.2.7 Cranial Meninges

Within the cranial cavity the brain is protected by the cranial meninges. The cranial meninges are made up of 3 layers; the dura, arachnoid and pia, shown in Figure 7. The main function of the cranial meninges is to provide a protective layer within the cranial cavity.

1. Dura: The outermost layer of the cranial meninges. It is comprised of 2 layers; the outer periosteal and the inner meningeal. The periosteal layer is directly connected to the periosteum of the cranial cavity, meaning there is no space within the cranial cavity superior to the dura matter. Between the 2 layers there is a small gap that contains tissue fluids and allows the veins of the brain to open into the sinuses that direct blood from the brain to the jugular veins in the neck.

2. Arachnoid: An epithelial membrane that covers the brain but does not follow the curvature of the brains surface. It is in direct contact with the inner layer of the dura and has a void, the sub-arachnoid space, between it and the pia layer. The sub-arachnoid space houses Cerebrospinal fluid, which has a damping effect when the cranium is impacted.

3. Pia: The pia is a thin layer that is directly connected to the brains surface, following every fold of the brain and covers cerebral blood vessels where they penetrate the brains surface.

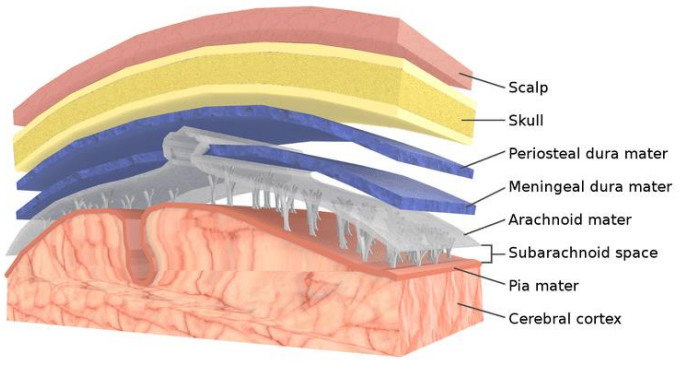

Figure 7: Layers of the Meninges [16]

2.2.8 Falx Cerebri

A meningeal layer of dural matter, the falx cerebri is a sickle shaped layer that separates the cerebral hemispheres vertically in the longitudinal fissure. It is connected anteriorly proximal to the cribform plate and the frontal sinus. In the posterior it connects to the upper surface of the tentorium. Shown in Figure 8.

2.2.9 Cerebellar Tentorium

A further extension of the dural matter, the cerebellar tentorium derives its names form the Latin for "tent of the cerebellum". It separates the cerebellum and the cerebrum in the transverse fissure. It gets its name from its tent like shape, which wraps around the cerebellar hemispheres. Shown in Figure 8.

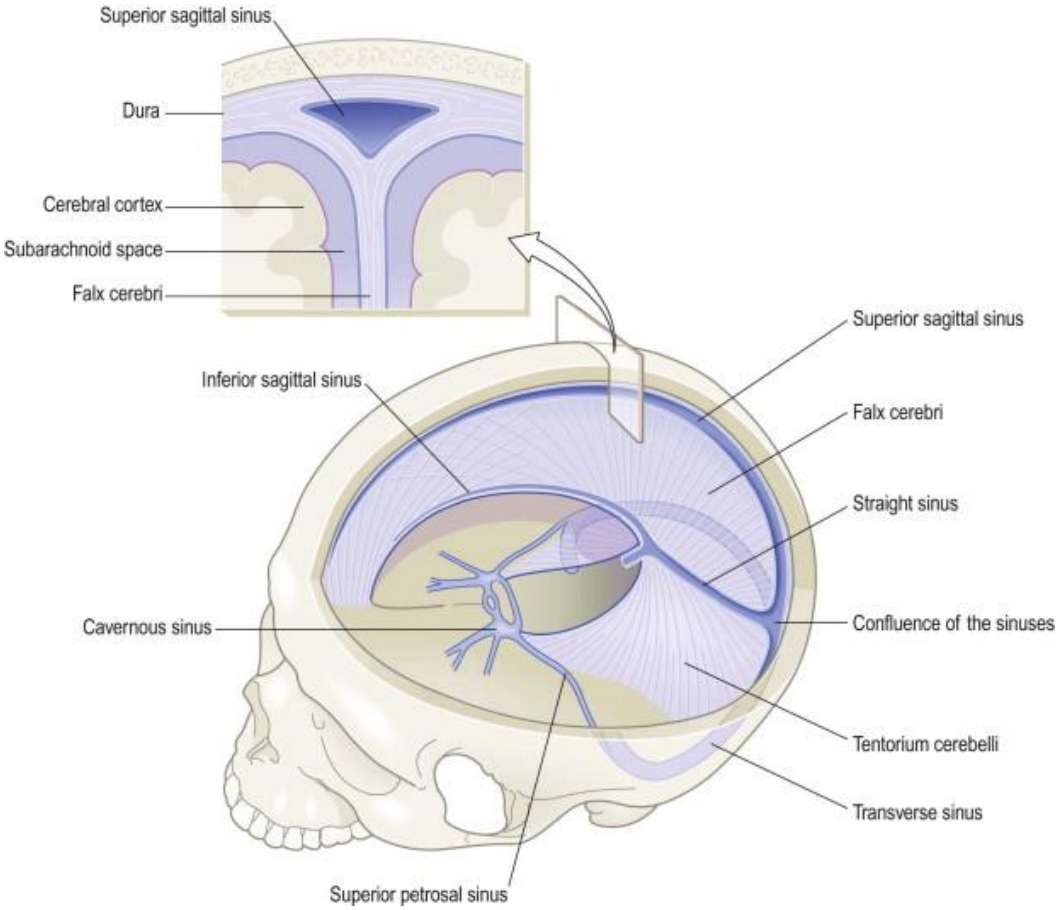

Figure 8: The skull and position of Flax Cerebri and Cerebellar Tentorium [17]

2.2.10 Anatomical Planes and Axes

Shown in Figure 9 are the standard anatomical planes and axes.

Planes:

- The frontal plane divides the body into front and back (dorsal and ventral).
- The sagittal plane divides the body in to left and right (anterior and posterior).
- The transverse plane divides the body in to upper and lower (superior and inferior).

Axes:

- The frontal axis' direction of motion is left to right.
- The sagittal axis' direction of motion is posterior to anterior.
- The transverse axis' direction of motion is inferior to superior.

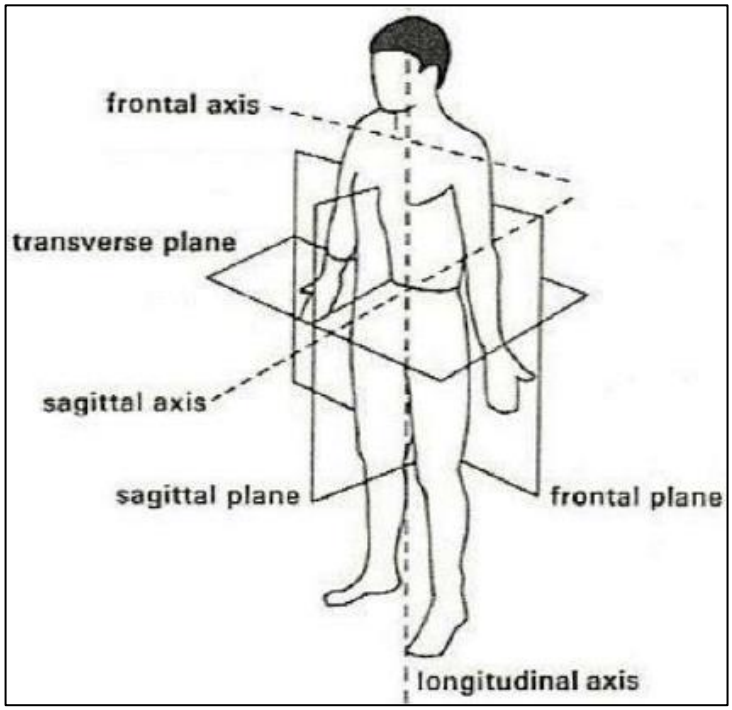

Figure 9: Standard Anatomical Planes and Axes [18]

2.2.11 Anatomy Summary

In this section the regions of the brain that are of interest in TBI have been investigated in terms of their function and operation. Those regions are the corpus callosum, the diencephalon, the midbrain, brainstem, meninges, falx cerebri and the cerebellar tentorium. Some of these regions will be investigated further by performing finite element analysis with *in vivo* impact data.

2.3 Traumatic Brain Injury

In this section TBI will be investigated in terms of its rate of occurrence, severity, symptoms, how it is diagnosed, and long-term effects. Traumatic brain Injury (TBI) is a worldwide health problem, with approximately 2.8 million TBI related visits to hospital in The United States of America in 2013 alone. This includes 2.4 million accident and emergency department visits. Approximately 10% of those resulted in a stay in hospital and there were over 50,000 TBI related deaths. In the period 2001-2010 the rates of TBI related visits to hospital, hospitalisation and deaths have increased by 70%, 11% and 7% respectively. TBI can present in several ways, ranging from the very severe (skull fracture/haemorrhage) to mild (concussion) [2].

2.3.1 Mild Traumatic Brain Injury

Concussion is a mild form of Traumatic Brain Injury (mTBI), the fifth International Conference on Concussion in Sport has defined it as "*a complex pathophysiological process affecting the brain, induced by traumatic biomechanical forces*." [3]. The symptoms of mTBI are wide ranging and can greatly affect the quality of life of the sufferers, with symptoms persisting for weeks or even years in some patients. Sports and recreation activities are one of the main sources of TBI in the United States of America, with 90% of these injuries being classified as mTBI's [4]. Symptoms can be divided broadly into 3 categories; Physical, Emotional and Cognitive.

Table 1: Symptoms of Concussion [2]

Physical	**Emotional**	**Cognitive**
Headache Blurred Vision	Irritability	Cognitive Lethargy
Nausea/Vomiting Dizziness	Depression	Difficulty in recalling new information
Photo and/or Audio-sensitivity	Increased Emotionality	Difficulty in concentrating
Lethargy	Anxiety	
Difficulty maintaining balance	Insomnia	

As can be seen in Table 1, the symptoms of concussion can have wide ranging effects and long terms issues. Some research has shown that as many as 15% of people diagnosed with a concussion may still have symptoms 1 year after injury [19]. MTBI's, such as concussion, are particularly difficult to diagnose as no physical damage to the brain can be observed with conventional imaging methods [5]. Therefore, the diagnosis relies heavily on the self-reporting of symptoms by sufferers. This will be discussed in the next section.

2.3.2 Post-Concussion Syndrome

As well as the symptoms listed above in the Table 1, there are some further diagnoses that can be attributed to an mTBI. The most common of these is Post-Concussion Syndrome (PCS). PCS is defined as the prolonged appearance of the symptoms affecting the sufferer physically, emotionally and/or cognitively. It is thought that PCS effects between 40 and 80% of sufferers of an mTBI, with up to 15% retaining symptoms for up to a year [20] [21].

Although PCS is a relatively common diagnosis, there is to the writer's knowledge no general consensus in the medical world of a clear definition of exactly what PCS is. A study was performed in which physicians who are members of the American College of Sports Medicine (ACSM) were asked to complete a survey related the minimum duration of symptoms and the minimum number of symptoms required to result in a diagnosis of PCS. Respondents had a wide variance in both these questions, with 26% opting for a duration of 2 weeks, 20.4% for between 2 weeks and 1 month, 33% requiring 1 to 3 months and 11% over 3 months. When responding in relation to the number of symptoms required, the variation was wide. 55.9% requiring just 1 symptom, 17.6% requiring 2 symptoms, 14.6% and 3.2% requiring 3 and 4 symptoms respectively [22]. Clearly a general consensus would greatly benefit both those working in the field of diagnosis and those in the concussion research field.

2.3.3 Methods of Concussion Diagnosis

Due to the fact that no physiological changes are visible with conventional imaging techniques, the clinical diagnosis of concussion is entirely based on symptom reporting, cognitive function and neurological screening. The most common test is the Sport Concussion Assessment Tool (SCAT), a standardised concussion evaluation tool, developed in 2004 by the Concussion In Sport Group (CISG). The assessment combines a graded symptom checklist, cognitive tests (five-word recall, delayed recall and Maddocks' questions) and neurological function tests (speech, eye motion/pupil reaction, gait assessment and pronator drift) [23]. It is recommended that a base-line SCAT assessment should be taken for comparison to an assessment taken post impact. The latest version of the SCAT test is the SCAT5, revised at the 5th International Consensus Conference on Concussion in Berlin 2016, can be found in Appendix 1.

Concerns have been raised in the sporting community about this method of diagnosis, as participants could quite easily intentionally perform poorly on their base-line assessment. This means that the difference between base-line results and the results in the post injury assessment are less pronounced and as such could potentially mask injuries. Furthermore, the under-reporting of symptoms is a serious concern, with as many as 45% of athletes not reporting concussions [24]. The reasons given by the athletes for not reporting symptoms was that they did not consider it a serious injury and that they did not want to leave the game. Under-reporting or not reporting symptoms is a serious problem in the world of sport and drives the need for a rigorous method of diagnosing concussion.

2.3.4 Traumatic Brain Injury Summary

In this section sports and recreation have been highlighted as one of the main causes of TBI, with the vast majority of these being mTBI's. The method of diagnosis, symptoms, and potential long-term effects have been examined and as such highlights the need for research in the field. This study aims to investigate mTBI's as a result of sports and recreational activities.

2.4 Instrumented Devices

Various devices for recording head impact data in sports have been used over the last 60 years following the Committee on the Medical Aspects of Sports of the American Medical Association's recommendation in 1961. They varied in design from instrumented head bands, skin patches, helmet mounted systems, and instrumented mouthguards. The most popular of these different instrumented devices will be discussed in this section.

Some of the earliest devices were developed in the early 1970's, with Moon *et al.* (1971) developing a headband that was worn under a helmet in American Football [25]. Several iterations of this design were developed over the next 10 years, all having serious issues with accurately measuring kinematics. These issues including recording many 400g+ impacts recorded that did not result in an injury for the wearer, highlighting the difficulty in accurately measuring *in vivo* impact data [25]. Similarly, in 1983 Morrison, investigated head impacts in American Football with an instrumented helmet. As with the previous studies impacts, extremely large linear accelerations (500g+) were recorded [26]. It wasn't until 2000 that instrumented helmets were utilised in a study again, when Naunheim *et al.*, compared data from high school ice hockey, American football and soccer. Naunheim found that peak accelerations from heading a soccer ball were far greater than those recorded from non-injurious ice hockey and American football impacts [27].

As well as helmet mounted devices, wearable devices have also been tested over the years. Some of these designs include instrumented headbands and skin patches. Reebok developed an instrumented head band, the Checklight [28]. It utilises a traffic light system for reporting the severity of impacts, indicating that the impacts were either "Mild/Intermediate/Severe". Although the manufacturers did not disclose how these impacts were classified. Similar to the Checklight device, Triax Technologies developed an instrumented head band. In validation studies performed by the manufacturers they found good agreement with reference devices. Although further studies discovered that the accuracy diminishes as the impacts become more severe and that root mean square (RMS) errors range from 18 – 85% depending on the impact location [28].

The X-Patch is a skin patch system developed by X2 Biosystems, Seattle WA. It is designed to be attached behind the ear, directly on the mastoid bone of the wearer. Data is gathered with 3 gyroscopes and 3 single axis accelerometers. Linear acceleration data is transformed to the head CoG by way of rigid body transformations, while rotational acceleration is calculated by five finger differentiation of rotational velocity data [29].

Several studies have called the accuracy of this device into question. In 2015, Siegmund *et al.* performed a cadaveric validation study using the X-Patch. Three helmeted cadavers were fitted with an X-Patch and dropped onto three different impact locations (forehead, side and rear boss) and from a range of heights (3 to 142cm). They found that the X-Patch overestimated PLA by 64+/-41% and PAA by 370+/-456% across all tests [30]. Also, in 2015 Nevins *et al.* performed further validation work with the X-Patch. An unhelmeted Hybrid III head and neck was fitted with an X-Patch and mounted on a sled. It was impacted with different sports balls (softball, lacrosse ball and soccer ball) that were fired at the dummy with a pneumatic cannon at a range of velocities (10 – 31m/s). They found linear acceleration results were promising for the softball and soccer ball experiments, while the lacrosse ball and rotational acceleration results were poor. The authors stated that this was likely due to the low sampling rate of the X-Patch [31]. To the best of this authors knowledge, this system is no longer in production and the company that produced it has ceased to exist.

Give this area of research was started in the United States of America, the vast majority of the published work in the area is from the US. There is a lack of data in Europe, with some work being done in Australia and New Zealand [32] [33]. This work will be discussed in this section and section 2.7.5, Head Accelerations Recorded in Sports.

2.4.1 Head Impact Telemetry System

In 2003 Greenwald *et al.* developed a helmet mounted system, the Head Impact Telemetry System (HITS), the first commercially available system of its kind [34]. Developed by Simbex; Lebanon, New Hampshire, it records *in vivo* impact data by means of a nine-accelerometer array that is mounted in an American football helmet. The system includes hardware for the acquisition of the data and for radio frequency (RF) telemetry. These are mounted within commercially available American football helmets, thus removing the need for customised apparatus. Figure 10 shows the cost difference between HITS and a customised approach. As the accelerometer array is mounted in the helmet, an algorithm is used to transform the linear and rotational impact data to the head CoG, this data is transmitted wirelessly to the acquisition system in real time [34].

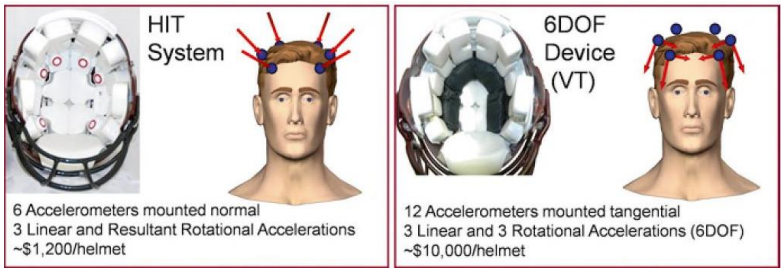

Figure 10: HITS vs. Custom 6DOF helmet arrangement [35]

The HITS has been validated in many studies, in both laboratory and real world conditions [36] [37] [38] [39] [40] [41] [42] [43] [44]. Many of these laboratory-based validation studies were conducted using a Hybrid HIII anthropomorphic test device (ATD). With Rowson *et al.* (2001) finding just a 4% difference in linear acceleration between HITS and measured values from a nine-accelerometer array placed at the CoG, this study also found there to be a 17% difference in angular accelerations. This resulted in the development of a new algorithm and the implementation of a 12 accelerometer array [41]. Furthermore, Jadischke in 2013 conducted a study investigating the role the size of the helmet may play in the transference of impacts [44]. This study, unlike the previously mentioned ones, examined various helmet sizes on a Hybrid Head III. Linear impactor tests were conducted using a medium and large helmet equipped with 3-2-2-2 array of accelerometers. It found the RMS error for linear accelerations was 59.1%, and the absolute error was greater than 15%.

Although this system's accuracy has been called into questions in several studies such as these discussed above, it is still the most commonly used system. It has been used in studies of American Football [36] [45] [46] and boxing [47]. Having been in use since 2003, this system has recorded a huge database of impacts [48] and will continue to be used until a more accurate system is developed for helmeted sports.

2.4.2 Instrumented Mouthguards

Many different arrangements for instrumented mouthguards have been tested over the last 50 years, with much of the early work being conducted by Hertz and Ewing in relation to car crash kinematics. In more recent years work has been carried out to investigate head impacts in sport and the skull/brain kinematics involved.

An instrumented mouthguard has been viewed as a potentially more accurate option for the recording velocity and acceleration of the head during an impact as the coupling of the mouthguard, via the test subjects' dentition, allows for direct recording of the kinematics of the head, rather than the recording of sensors incorporated in an instrumented helmet, for example.

2.4.2.1 Custom Mouthguards

In 2007 Higgins *et al.* conducted a study to determine whether attaching an accelerometer to a custom-built instrumented mouthguard, fitted to a Modified National Operating Committee on Standards for Athletic Equipment (NOCSAE) headform, would provide a more accurate representation of the linear acceleration experienced than an instrumented helmet [49]. No significant differences in acceleration or severity were shown between the headform and mouthguard. Helmet mounted sensors were shown to greatly overestimate acceleration and severity of impacts. It should be noted that only linear acceleration was recorded in this study, although the authors noted that rotational acceleration has been previously reported as a potential cause of Traumatic Brain Injury (TBI).

Paris et al (2010) conducted a study to investigate the accelerations of the head during the heading of a soccer ball by means of a custom-made mouthguard containing an AD ADXL250 Dual Axis Accelerometer Chip with the X-axis oriented anteriorly and the Y-axis superiorly. Four launch speeds and distances were tested and compared to a soccer ball being dropped onto a sphere, made of resin, fixed to a force plate. The results of this found a good correlation with experimental results for impact force, duration and velocity [50].

A similar study was conducted by Kara *et al.* (2012) using a custom-made mouthguard, fitted with a tri-axial accelerometer, to measure linear and angular acceleration of the head during the heading of a soccer ball [51]. The subject was tasked with heading the soccer ball launched at a range of velocities, up to 12m/s; this was recorded using a high frame rate camera. From this visual data ball velocity pre and post impact was calculated, which allowed for the calculation of the impulse force.

2.4.2.2 X2 Impact Mouthguard

Created by X2 Biosystems, this mouthguard has been used in a study to investigate head impact accelerations in amateur rugby union players across a season, King *et al.* 2015 [11]. It can compute peak linear acceleration (PLA), peak angular acceleration (PAA), Head Injury Criterion (HIC), the azimuth and elevation of the PLA. For this study the players were fitted with a mouthguard instrumented with a low power, high-g tri-axial accelerometer (H3LIS331DL) and a tri-axial gyroscope (L3G4200D; ST Microelectronics). Impacts were defined as having a linear acceleration greater than 10g, 100 milliseconds of data were recorded, 25 pre impact and 75 post impact. The measures of impact severity were defined by impact duration, linear acceleration and angular acceleration. Linear acceleration was sampled at 1 kHz and angular velocity at 800Hz. Angular velocity was then interpolated to 1 kHz and filtered. Linear acceleration values were transformed to the centre of gravity of the head, while angular acceleration was calculated using the 5-point stencil method from recorded angular velocity values.

Thirty-eight players, mean age 22 years +/- 4 years, in 19 matches over the 2013 season experienced a total of 20687 impacts, ranging from 10 to 165g with no concussions recorded. Players were subjected to a mean of 77 impacts per game or 1379 impacts per players per season, mean linear acceleration was 22g, mean angular acceleration 3990 rads/s^2 and the mean impact duration was 12 milliseconds. Mean linear and angular acceleration was found to be similar to that of High school American football and some collegiate American football, though lower than female youth soccer players. The majority of impacts recorded in this study were categorised as mild severity impacts and no concussions were recorded.

2.4.2.3 Cleveland Mouthguard (IMG)

The Cleveland Clinic began work in 2008 on an Intelligent Mouthguard (IMG) in order to provide the medical field with a way of accurately gathering head impact data for sport and military applications. The IMG measures 3 degrees of freedom (DOF) linear acceleration, 3 DOF angular velocity, impact duration and direction. Capture time is 125ms and samples at a rate of 4kHz with a bandwidth of 22kHz. IMG linear acceleration is filtered with a low-pass 4-pole Butterworth filter at 250Hz, post filtering the angular velocity was differentiated with a finite difference algorithm in MATLAB to compute angular acceleration.

Bartsch *et al.* 2013 conducted a study to determine the accuracy of the IMG printed circuit board (PCB) in benchtop validation tests. 2 single DOF drop tests were conducted, linear and angular acceleration, tested at impacts ranging from 10g to 175g and 850rad/s^2 to 10,000rad/s^2 respectively [52]. Linear drop tests were conducted on a custom-built aluminium drop tower. The IMG PCB was mounted on a rail and dropped on to 12 foam pads of differing stiffness. Angular acceleration tests were conducted by mounting the PCB on a stationary rotating block, which was then struck with a pad. The padding, striking and struck weight and inertia were held constant to generate a range of impact durations. Reference measurements for linear acceleration were collected by a single axis 500g linear accelerometer, sampled at a rate of 10kHz and filtered with a four-pole low-pass Butterworth filter at a bandwidth of 250Hz. Angular acceleration reference measurements used a pair of 500g linear accelerometers and two 210rads/s angular rate sensors, filtered similarly with a bandwidth of 160Hz.

These tests showed that the IMG PCB had a high level of correlation to the reference measurements, with $R^2 > 0.99$ for linear acceleration and $R^2 = 0.98$ for angular acceleration. Despite this high level of correlation angular acceleration measurements showed high levels of inaccuracy, 17%, when averaged over the ranges of impacts. Further validation testing of the IMG gyroscopes and accelerometers was conducted, again by Bartsch (2014). 3 experiments were conducted; a benchtop level drop test incorporating linear and angular tests, *in vitro* linear impacts and *in vivo* tests in boxing and American football [53]. The benchtop tests were conducted in a manner similar to that of the previous work detailed above, utilising reference measurements for comparison. Multiple impacts were conducted at different impact heights for linear and angular tests. On this occasion the authors created a gyroscopic correction factor to deal with insufficient gyroscope bandwidth, increasing it from 110Hz to 370Hz. Following this correction both linear and angular tests fit the linear regression models well, $R^2 = 0.99$ for linear and $R^2 = 0.99$ for angular following the application of the gyroscopic correction factor.

In vitro linear impacts were compared to a "gold standard" reference 3-2-2-2 accelerometer package in a modified Hybrid III headform. The modified headform was fitted with a custom moulded IMG and an American football or boxing headgear. A linear impactor powered by compressed air was propelled at the headform at velocities up to 8.5 m/s and impacted the headform at varying angles, in increments of 22.5° around the z axis. *In vivo* tests on American football players and boxers was also conducted, with the football players taking part in three 15 to 30-minute practice sessions and the boxers taking part in five 3-minute sparring sessions while wearing the custom moulded IMG. The lower threshold for triggering data recording was set at 15g and the participants were recorded throughout the sessions. The authors of this paper determined that the IMG can be used as a single event head impact dosimeter when certain conditions are met; the mouthguard – skull coupling is maintained; the skull is treated as a rigid body and the harmonics fall within the ranges used in the study. It should be noted that the writer of these validation studies is an employee of the Cleveland Clinic.

2.4.2.4 Stanford Mouthguard

Developed in Stanford, this mouthguard is a 6 DOF device designed for *in vivo* data collection. The mouthguard is moulded to the wearer's upper dentition by way of a custom dental mould. The most recent version, with published results, incorporates a tri-axial gyroscope (ITG3500A) to detect angular rotation and a tri-axial accelerometer (H3LIS331DL) to measure linear acceleration, sample rate of 800-900Hz for linear acceleration is and 900-1000Hz for rotational acceleration respectively and a bandwidth of 184Hz and 500Hz respectively.

In order to ensure that only data from true impact events is collected, this device utilises a proximity sensor (AMS TMD2771) with an infrared receiver-emitter pair to confirm the guard is coupled with the test subject's upper dentition. A support vector machine (SVM) method, trained using frequency domain features, is also used to differentiate impact and non-impact events. A lower threshold of 10g has been set to trigger recording data along with a time period of 50ms pre impact and 150ms post impact. Rotational acceleration is calculated by differentiating the rotational velocity data using the five-point stencil method. Also contained in the device is a microprocessor (ST STM32L151) and a memory chip (STM25P16) to allow for wireless processing and storage of the data. Only when all conditions are met will the device record data, the data is transformed linear acceleration data is transformed to the centre of gravity (CG) of the 50^{th} percentile male human head. This is achieved in post processing.

Validation testing of an earlier iteration of this device was conducted by Camarillo *et al* 2013. The tests were carried out using an Anthropomorphic Test Device (ATD) which was fitted with a Riddell Revolution Speed Classic helmet. The ATD was impacted with a horizontal linear impactor across five impact sites (2 facemask and 3 helmet locations) and varying impact velocities were tested (2.1 to 8.5m/s). The ATD was fitted with a tri-axial accelerometer at the CoG, with 3 single axis accelerometers offset perpendicularly from the CoG and 3 single axis angular rate gyroscopes aligned with the axes of the tri-axial accelerometer for all impact tests [54].

Peak linear and angular acceleration and peak angular velocity from all impact tests for the ATD and mouthguard were compared by means of linear regression analysis. Peak linear acceleration measurements were close with r^2=0.96 and m=1.01. Peak angular acceleration measurements were under predicted by the mouthguard with r^2=0.89 and m=0.90, while individual impact sites had r^2=0.71 to 0.98. Peak angular velocity had a close correlation across all impact sites with r^2=0.98 and m=1.00. Results for linear and angular acceleration had a greater variation across impact sites.

A further study was conducted by Kuo, Calvin et al 2016, into the effect that the mandible has on results. They conducted drop tests on a helmeted ATD and PMHS, from varying heights and impacting various sites. They introduced 3 mandible states; no mandible, unconstrained mandible and clenched mandible [55].

When testing the ATD all 3 mandible conditions were used; no mandible had the mandible removed entirely, unconstrained had the mandible articulating freely and clenched had the mandible had a preload force of 300N applied. When testing the PMHS only the unstrained state was tested so as to test the worst-case scenario. All tests were conducted with both ATD and PMHS wearing a Riddell Steed Helmet. 6 locations and 3 heights were tested, with accelerations ranging from 15g to 150g.

These tests determined that the no mandible and unclenched states performed the best, with m ranging from 0.79 – 0.997 and r^2 from 0.87 – 0.994, Table 2 details these results in full. The results from the unclenched mandible series of tests showed poor results, with m ranging from 1.15 – 1.72 and r^2 from 0.16 – 0.82.

Table 2: Effect of the mandible on bench-top tests [55]

	No Mandible	**Unclenched Mandible**	**Clenched Mandible**
Peak magnitude angular velocity	m=0.997 r^2=0.994	m=1.15 r^2=0.72	m=0.99 r^2=0.99
Peak Linear acceleration	m=1.04 r^2=0.96	m=1.45 r^2=0.82	m=1.1 r^2=0.96
Peak Angular acceleration	m=0.76 r^2=0.91	m=1.72 r^2=0.16	m=0.79 r^2=0.87

Location specific results determined that impact site location can have a large bearing on mouthguard accuracy, with vertex, frontal and frontal oblique impacts in the unconstrained mandible state resulting in the highest overestimation. This may be due to the direction of the acceleration vector being aligned with the pre-dominate mandible direction of movement. This direction of movement potentially increases the movement of the mandible and, in turn, increases the loading of the mouthguard. The results of these 2 studies have shown that mandible state and impact location play a large role in the accuracy of mouthguard results, with helmeted/unhelmeted also having an impact. Although mandible state is problematic to determine *in vivo*, it is important to be aware of and will be discussed in later sections of this study.

Further validation of the mouthguard sensors was conducted by Wu et al 2016 [56]. 3 model systems were tested, helmeted cadaver head drop (no neck), unhelmeted cadaver head drop (no neck) and dummy head linear impact (with neck), at medium to high linear acceleration levels at common impact locations. For each impact high bandwidth accelerometer and gyroscope measurements were recorded and they were defined as ground truth skull kinematics.

Having first determined injury criteria and bandwidth requirements for both skull kinematics and brain deformation, bandwidth requirements for accelerometer and gyroscope were then determined. Analysis of the accelerometer found that a bandwidth of greater than 500Hz is required for most kinematics-based injury criteria, unhelmeted > 500Hz and helmeted 200-400Hz. For deformation-based criteria a bandwidth of < 200Hz for helmeted and 400Hz for unhelmeted is required. In short, unhelmeted systems require a bandwidth of greater than 500Hz which may also be sufficient for helmeted systems. Analysis of the gyroscopic data found that a bandwidth of greater than 1000Hz is required for several of the tested kinematics-based injury criteria, with the helmeted dummy model demonstrating that a bandwidth of 500Hz is required for angular velocity and 740Hz is required for angular acceleration.

2.4.3 Instrumented Devices Summary

In this section several different types of instrumented devices have been investigated. The most used of these is the HITS, which is a helmet mounted system. This is unsuitable for this study as MMA participants do not wear helmets, the same applies to any of the headband type systems. The X-Patch was a skin mounted patch and as it is no longer in production it is also unsuitable for this study.

Instrumented mouthguards prove to be an excellent option in MMA, as all participants must wear a mouthguard while competing/training. The Stanford mouthguard is solely a research tool, is one of the most recently developed systems and has several validation studies published with good levels of accuracy and performance. Although it is not without its disadvantages, validation studies have shown mandible states play an important role as well as the bandwidth required for accelerometers and gyroscopes. The Stanford mouthguard was chosen for this study based on this.

2.5 Brain Models

Due to the ethical issues with performing *in vivo* head impact tests in human subjects, finite element analysis (FEA) provides an excellent alternative. Much of the early work, automotive and military fields, used very simplified models. FEA allows for the creation of detailed models of the human head/body and this will continue to improve as computational power increases.

Many models have been created over the last 50 years, with one of the first being created by Hardy and Marcal in 1971 [57]. They created a 2-dimensional human skull model for use in the automotive industry, in order to predict the deformation of the skull in a car crash. As the adoption of PC's has increased, in the time since the Hardy and Marcal model, the complexity of models has grown. This is even more so in recent years as the use of virtual machines with many CPU's allowing for more complex models.

This section will cover some of the most popular models in use today. As will become apparent in the following chapter, the models are all validated from the same historical cadaver tests. Nahum and Trosseille are used intracranial pressure validation for comparison, while Hardy is used for displacement validation [58] [57] [59].

2.5.1 Global Human Body Modelling Consortium Model

A full body model which was developed by The Global Human Body Modelling Consortium (GHBMC). It was designed for use in the automotive industry. The consortium is made up of 7 automotive manufacturers; Fiat Chrysler Automotive LLC, General Motors Co., Honda R&D Co., Hyundai Motor Co., Nissan Motor Co., Groupe PSA, Renault S.A., and Takata Corp. The GHBMC M50 Detailed Occupant, version 4.5 released on September 1st 2016 is the model used for this study and is shown below in Figure 11.

The geometry for the model is based on computed tomography (CT) and magnetic resonance imaging (MRI) scans of an adult male who met the criteria for height and weight of the 50th percentile adult male of the United States of America, criteria shown in Table 3 [60]. A total of 72 scans were completed of the individual, containing a total of 15,622 images. Averages of the morphology of an average male was found from literature and compared to the individual. The model itself is sagittally symmetric and is made up of 418 individual parts, including but not limited to: bones, muscles, ligaments, organs, tendons, blood vessels and skin. The total volume and area of the subsequent model was compared to the literature and was found to closely agree [61].

Figure 11: M50 – Detailed Occupant Model and M50 – Head/Neck isolated Model

Age (years)	**Weight (kg)**	**Height (cm)**	**BMI (kg/m^2)**
26	78	174.9	25.7

Table 3: GHBMC Subject Data

The M50 GHBMC model is made up of 2.19 million elements, 1.26 million nodes and 1036 individual parts. The head model, which is of particular interest to this study, is partially validated by way of 35 sets of experimental data. Table 4 details these validation cases [60]. Due to the fact that the whole body has been shown to have little effect on short duration impacts, an isolated head and neck model is being utilised for this study [62]. This greatly reduces the computational time for simulations. As this study utilises an isolated head and neck model, the focus will be on the validation, contact definitions and material properties of the head and neck. The isolated head and neck model is shown in Figure 11. It is made up of 488,453 elements, 510,501 nodes and 436 individual parts. The material properties for the entire model are too numerous to list in their entirety, material properties for all the brain parts are listed in Appendix 2.

Mao *et al.* 2013 simulated a total of 35 cases in order to validate the head and neck model for brain pressure, brain motion, skull response and facial response. [60]. Brain pressure validation was conducted by simulating 6 cases from Nahum (1977), the study re-pressurised the head of a post mortem human subject (PMHS) and impacted it with a rigid impactor, which was covered in a variety of different materials, and at a variety of velocities [58] [60]. Case 37 from Nahum's study was chosen as the baseline case to compare with, as it had reported the details of contact force and head accelerations. The acceleration profile from case 37 was morphed in order to generate acceleration profiles for the 5 remaining cases. The results of these simulations are shown in Table 4.

Table 4: Brain Pressure comparison of Nahum (1977) to experimental data [58]

Case Number	**Peak Acceleration (km/s^s)**	**Front (kPa)**		**Parietal (kPa)**		**Posterior Fossae (kPa)**	
		Exp.	Model	Exp.	Model	Exp.	Model
36	2.3	136	169	79	97	-64	-77
37	2	141	143	74	75	-60	-69
38	2.42	139	179	66	103	-65	-79
43	2.23	271	164	222	94	-18	-75
44	1.52	102	103	20	51	-3	-52
54	2.34	275	173	180	100	-64	-78

As can be seen above, the simulated results from the 6 Nahum cases matched the experimental data quite well, Table 4. Further validation of brain pressure was conducted by recreated one case from Trosseille (1992), MS-428-2, [59] in which a PMHS was suspended in a sitting position and impacted at a velocity of 7m/s with an impactor of 23.4kg [59]. Pressure transducers were placed in the sub-arachnoid space and the ventricular system in order to measure pressure in these regions [60].

The results of these tests are shown in Figure 12. Pressure in the frontal, lateral ventricle and 3rd ventricle regions matched well but not in the occipital region [60].

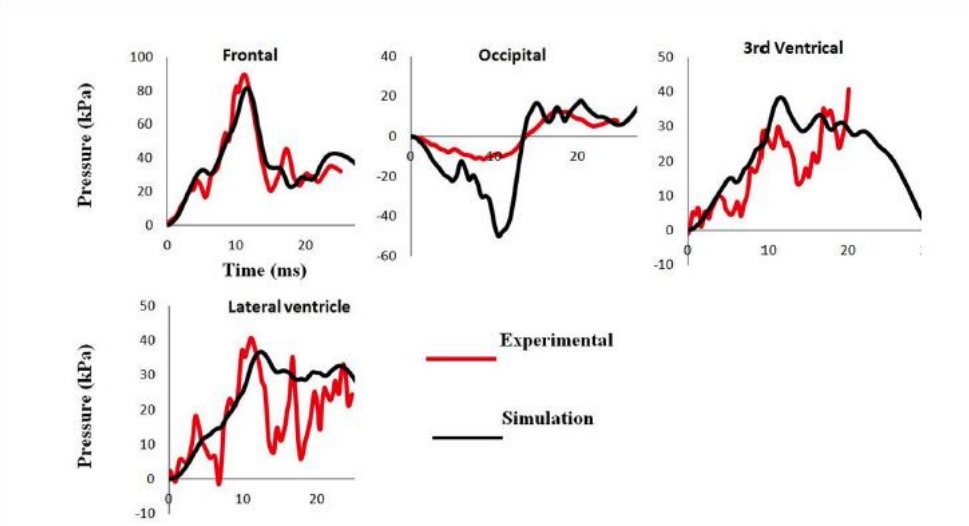

Figure 12: Comparison of experimental and simulated results for Trosseille MS482-2 [60]

Mao *et al.* 2013 also validated brain motion by recreating 8 impacts that were performed by Hardy *et al.* (2001, 2017), these impacts utilised an X-ray system in order to track the movement of neutral density targets (NDT's) that had been placed in the brain of a PMHS [63] [64]. The results from these simulations demonstrated that the motion of the brain matched that of the Hardy experiments, with magnitudes differing by a maximum of 2.6mm between simulations and experimental data [60]. As this study is concerned with mTBI's the validation studies for skull response and facial response will be omitted, as they deal with fractures of the skull and facial bones. The details of these validations are in Table 5. MTBI's are in the mild range of head impacts, injuries which do not normally result in bone fractures.

2.5.1.1 GHBMC Material Properties

Since the advent of FE models many studies have attempted to measure the material properties of human and animal brain tissue, both *in vivo* and *in vitro*, in order to improve the response of models. Beginning in the 1960's with Dodgson 1962 who conducted *in vitro* creep tests on samples of mouse brains [65]. Testing of human brain tissue began in the 1970's with Galford and McElhaney 1970 who examined both monkey and human brain *in vitro,* also with creep tests. They found that the brain tissue could be considered as a viscoelastic material for strains in the region of 30% +/- 10% [66]. Several studies agree with this finding and based on these many modern FE models utilise a linear viscoelastic material model for brain tissue [67] [68] [69]. In the development of the GHBMC, a viscoelastic material model in combination with a large deformation theory was chosen for brain tissue. This material model can be considered elastic in compression and viscoelastic in shear. Equation 1 shows the expression for the shear modulus of a viscoelastic brain material [70].

$$G(t) = G_\infty + (G_O - G_\infty)e^{-\beta t}$$

Equation 1: Shear Modulus of a Viscoelastic Material [70]

Where: G_O is the short-term shear modulus
G_∞ is the long-term shear modulus
β is the decay constant
t is the duration

The values for the material properties of the GHBMC were defined by reviewing a historical data set of mechanical tests on human and animal brain tissue [60]. This data set contained a wide variety of testing methods including tension/compression, shear and indentation [71] [72]. As well as this data set, the writers Mao *et al.* 2013 had access to an in-house set of data, which is unpublished to the best of this writer's knowledge. From this they defined the short-term shear modulus of grey matter to be 6KPa and the long-term modulus to be 1.2KPa. The white matter was defined as being 25% stiffer than the grey matter.

The CSF, a fluid that occupies the subarachnoid space has been modelled as layer of brick elements using a viscoelastic material model despite the fact that it is a fluid. In reality, its density and viscosity are similar to water. In order to best replicate the behaviour, a bulk modulus of 2.19GPa was chosen. As well as a short-term shear modulus of 500Pa and long-term shear modulus of 700Pa. Table 6 details the material properties for all of the viscoelastic parts in the GHBMC head model [60].

The skull bones were modelled as piecewise material model. A study by Wood *et al.* 1971 found that there were no changes in the elastic modulus, breaking strain and breaking stress for any of the bones of the skull due to age, layer or type of bone [73]. Due to these findings, no regional differences are present on the material properties for any of the bones of the skull in the GHBMC. The bones of the skull, both inner and outer, we defined as having an elastic modulus of 10GPa based on early work by McElhaney *et al.* 1970 [74]. The elastic modulus for the diploe layers of the skull were based on the work of Melvin *et al.* 1970 and was defined as 0.6GPa [75]. The data for the bridging veins was determined based on the work of Delye *et al.* 2006, who conducted tensile tests of the bridging veins taken from cadavers. The elastic modulus for the bridging veins was defined as 0.03GPa [76]. Table 8 details the material properties for all piecewise parts in the GHBMC head model.

The remaining parts of the brain were defined using an elastic material model, this includes the skin, falx, tentorium and meningeal layers. Table 7 details the materials properties for the elastic parts of the GHBMC brain.

Table 5: Experimental Data for Head Model Development

Model Development Target	Literature first author, year	Description	Number of experiments used for model development	Loading case numbers (i.e. – Simulation setting numbers)
Brain Pressure	Nahum, 1977 [58]	Frontal impact on forehead Test ID: 36, 37, 38, 43, 44, 54	6	6
	Trosseille, 1992 [59]	Frontal impact Test id: MS 428_2	1	1
Brain Motion or pressure if motion not reported	Hardy, 2001 [64]	Sagittal plane, offset to CG Test id: C383-T3, C755-T2	2	2
	Hardy, 2007 [63]	Sagittal plane, aligned to CG Test id: C241-T1, C241-T6	2	2
		Sagittal plane, aligned to CG Test id: C241-T1, C241-T6	2	2
		Coronal plane, offset to CG Test id: C380-T4, C393-T4	1	1
		Coronal plane, aligned to CG Test id: C380-T3	1	1
		Horizontal plane, offset to CG Test id: C380-T5	1	1
Skull response	Yoganandan, 1995 [77]	Frontal 45-degree impact, head constrained Test id: 8	1	1
		Vertical impact, head constrained Test id: 7, 9, 11, 12	4	4
		Occipital 35-degree impact, head constrained Test id: 10	1	1
	Hodgson, 1970 [78]	Frontal horizontal impact Cadaver number: 1504, 1536, 1581, 1582, 1589, 1615	5	3
Facial response	Nyquist, 1986 [79]	Nasal impact Test id: 20, 29, 34	3	3
	Allsop, 1988 [80]	Zygoma impact, head constrained	8	1
	Allsop, 1988 [80]	Maxilla impact, head constrained	6	1
Brain contusion	Nahum, 1976 [81]	Frontal impact Test ID: 17, 18, 19, 26, 27, 31	6	6

Table 6: GHBMC Viscoelastic Brain Parts Material Properties

Part	Material Type	Material Model	Density (kg/m^3)	Bulk Modulus (GPa)	Short Time Shear Modulus (GPa)	Long Time Shear Modulus (GPa)	Decay Constant
Cerebellum	Viscoelastic	Kelvin Maxwell	1060	2.19	6.00e-6	1.20e-6	0.0125
Cerebrum Gray Lower	Viscoelastic	Kelvin Maxwell	1060	2.19	6.00e-6	1.20e-6	0.0125
Cerebrum Gray Upper	Viscoelastic	Kelvin Maxwell	1060	2.19	6.00e-6	1.20e-6	0.0125
Corpus Callosum	Viscoelastic	Kelvin Maxwell	1060	2.19	7.50e-6	1.50e-6	0.0125
Thalamus	Viscoelastic	Kelvin Maxwell	1060	2.19	6.00e-6	1.20e-6	0.0125
Lateral Ventricle	Viscoelastic	Kelvin Maxwell	1040	2.19	5.00e-7	1.00e-7	0.0125
Mid Brain	Viscoelastic	Kelvin Maxwell	1060	2.19	1.20e-5	2.40e-6	0.0125
Brain Stem	Viscoelastic	Kelvin Maxwell	1060	2.19	1.20e-5	2.40e-6	0.0125
Cerebrospinal Fluid - Cerebrum	Viscoelastic	Kelvin Maxwell	1040	2.19	5.00e-7	1.00e-7	0.0125
Basal Ganglia	Viscoelastic	Kelvin Maxwell	1060	2.19	6.00e-6	1.20e-6	0.0125
Cerebrospinal Fluid - Cerebellum	Viscoelastic	Kelvin Maxwell	1040	2.19	3.00e-6	6.00e-7	0.0125
Third Ventricle	Viscoelastic	Kelvin Maxwell	1040	2.19	5.00e-7	1.00e-7	0.0125
Sagittal Sinus	Viscoelastic	Kelvin Maxwell	1040	2.19	5.00e-7	1.00e-7	0.0125
Sagittal Sinus Anterior	Viscoelastic	Kelvin Maxwell	1060	2.19	5.00e-7	1.00e-7	0.0125
Cerebellum White	Viscoelastic	Kelvin Maxwell	1060	2.19	7.50e-6	1.50e-6	0.0125

Table 7: GHBMC Elastic Brain Parts Material Properties

Part	Material type	Material Model	Density (kg/m^3)	Young's Modulus (GPa)	Poisson's Ratio
Pia	Elastic	Elastic	1100	0.0125	0.35
Tentorium	Elastic	Elastic	1100	0.0315	0.3
Arachnoid – Cerebrum	Elastic	Elastic	1100	0.012	0.35
Arachnoid – Cerebellum	Elastic	Elastic	1100	0.012	0.35
Falx	Elastic	Elastic	1100	0.0125	0.35
Dura	Elastic	Elastic	1100	0.0315	0.35
Dural Sinus	Elastic	Elastic	1100	0.0315	0.35

Table 8: GHBMC Piecewise Brain Parts Material Properties

Part	Material Type	Material Model	Density (kg/m^3)	Young's Modulus (GPa)	Poisson's Ratio	Yield Stress (GPa)	Tangent Modulus
Bridging Veins	Bi-Linear	Piecewise	1130	0.03	0.48	0.00413	0.0122
Dipole	Bi-Linear	Piecewise	1000	0.6	0.3	0.004	0.02
Skull Outer	Bi-Linear	Piecewise	2100	10	0.25	0.09	0.5
Skull Inner	Bi-Linear	Piecewise	2100	10	0.25	0.09	0.5

2.5.2 Simulated Injury Monitor Model

The Simulated Injury Monitor Model (SIMon) was developed in 2003 as a tool for assessing the potential for TBI's in car crashes [68]. SIMon was designed with the target of simulating an impact of less than 150ms, on a high-end PC in less than 2 hours, in order to reduce computational cost. To achieve this model has been reduced to contain as few different parts as possible, thus reducing the number of calculations being run per simulation. A head only model, consisting of the following parts:

- Rigid Skull (Hexagonal Elements)
- Dura-CSF layer (Hexagonal Elements)
- Brain (Hexagonal Elements)
- Falx Cerebri (Hexagonal Elements)
- Bridging Veins (Beam Elements)

When compared to the GHBMC, the SIMon model has far fewer parts. The 50^{th} percentile model SIMon has a total mass of 4.7Kg, with the brain comprising 1.5Kg of this. It is made up of 10475 nodes and 7852 elements (7776 hexagonal solid and 76 beam elements). A soft tie-break contact type was chosen for the skull to dura-CSF and from the dura-CSF to the brain.

Model validation was again carried out by comparing with Hardy's brain displacement experiments. Some refinement of the brain properties was made in order to better fit the Hardy results, with the following properties being those that correlated best with Hardy's.

$$G_o = 2.4\text{kPa}, G_\infty = 1.2\text{kPa and } \tau = 0.01 \text{ sec}$$

The development of this model has shown that a simplified model can be utilised in the study of TBIs. The study also found that impacts received laterally result in more brain damage and may experience greater accelerations (both linear and rotational). Several improvements have been made including, using a quasi-linear constitutive model for the brain tissue and modelling the falx cerebri with shell elements.

2.5.3 Kungliga Tekniska Högskolan Model

The Kungliga Tekniska Högskolan model (KTH) was developed in the Kungliga Tekniska Högskolan (Royal Institute of Technology), Sweden in conjunction with Wayne State University, USA, in 2002 [82]. The aim was to create a scalable FE model of the human head and to validate it against 3 sets of data from cadaveric experiments for 3 impact directions; lateral, frontal and occipital. The model is broadly made up of the following parts and tissue properties:

Table 9: Tissue properties for KTH development [82]

Tissue	Young's Modulus (MPa)	Density (kd/dm^3)	Poisson's ratio
Outer table/face	15000	2.00	0.22
Inner table	15000	2.00	0.22
Diploe	1000	1.30	0.24
Neck Bone	1000	1.30	0.24
Neck Muscles	0.1	1.13	0.45
Brain	Hyperelastic/Viscoelastic	1.04	0.4999994 - 0.4999997
Cerebrospinal Fluid	K=2.1 GPa	1.00	0.5
Sinuses	K=2.1 GPa	1.00	0.5
Dura Matter	31.5	1.13	0.45
Falx/tentorium	31.5	1.13	0.45
Scalp	16.7	1.13	0.42
Bridging Veins	EA=1.9N		

Where: K=Bulk Modulus and EA=load/unit strain

The model is comprised of 19350 nodes, 11454 brick elements, 6940 shell and membrane elements and 22 truss elements. As this is a scalable model, the size of the head and neck can be scaled to better suit the subject being studied. The other models discussed in this section have been 50th percentile approximations, whereas the the KTH model allows for the study of the 50th percentile and any subset of the population and even subject specific cases.

The dura and skull are modelled with a tied-node contact definition. The CSF is modelled with a sliding contact that allows no separation. This was achieved by modelling a further pia matter layer, tied to the dura matter. Doing so allowed for sliding in the tangential direction and transferring loads radially.

This model was again validated by comparing with Hardy's and Nahum's experiments. The results of some of these experiments are shown below in Figures 13 and 14 [82].

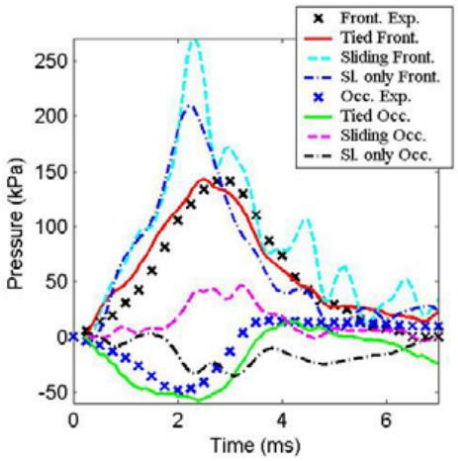

Figure 13: Comparison of Nahum exp. 37 and KTH contact definition experiments [82]

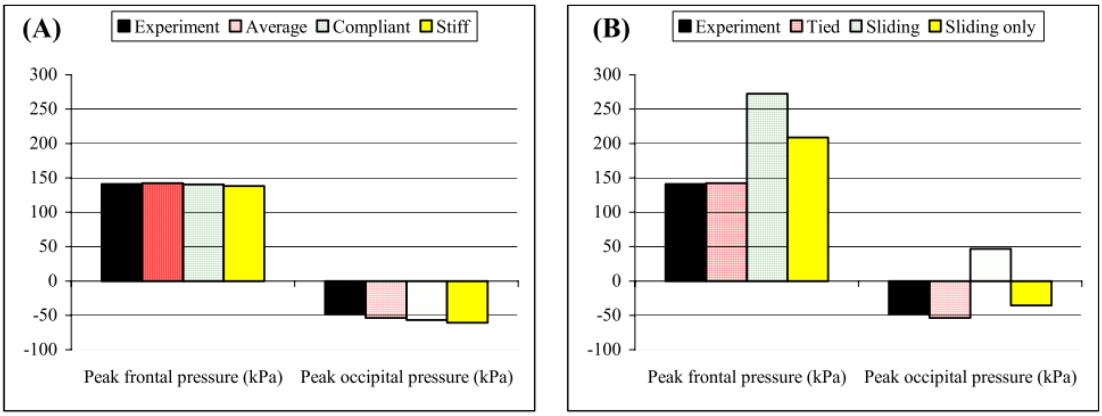

Figure 14: Summary of Nahum pressure experiments vs KTH simulations [82]

2.5.4 University College Dublin Brain Trauma Model

Developed by Horgan and Gilchrist in University College Dublin (UCD) in 2003, the UCD Brain Trauma Model (UCDBTM) is used to simulate pedestrian accidents. The model was generated from Computed Topography (CT), Magnetic Resonance Topography (MRT) and colour images [83].

The model is comprised of several parts; scalp, skull, dura, pia, CSF, falx, tentorium, right and left hemispheres, cerebellum and brain stem. The material properties of the parts are shown in Table 10. While the physical properties of the model are reported as skull weight of 4.017kg, as per experiment 37 from Nahum, with the brain being 1.422kg [58].

Table 10: UCDBTM material properties [83]

Material	**Young's Modulus (MPa)**	**Poisson's Ratio**	**Density (kg/m^3)**
Scalp	16.7	0.42	1000
Cortical Bone	15000	0.22	2000
Trabecular Bone	1000	0.24	1300
Dura	31.5	0.45	1130
Pia	11.5	0.45	1130
Falx and Tentorium	31.5	0.45	1130
Brain	Hyperelastic	0.499981	1040
Facial Bone	5000	0.23	2100

The model is again validated by comparing with Nahum's experiments. It should be mentioned that there were several iterations of this model generated in order to investigate varying contact definitions and material properties. The model described above is known as the "Baseline" model, 5 further versions were created. They are: sliding boundary, grey-white ventricular matter, 3 element CSF, and projection mesh and morphed. The "Baseline" model is comprised of 10192 hexahedral elements, with 7318 making up the brain matter and 2874 making up the CSF.

Further versions of the skull were generated with varying element densities, ranging from 9000 to 50000 elements. These versions have varying mesh densities, element types and CSF thicknesses. They are as follows:

1. Fine mesh – brick element with CSF thickness of 1.3mm
2. Medium mesh - brick element with CSF thickness of 1.3mm
3. Thick mesh - brick element with CSF thickness of 1.3mm
4. Fine mesh - brick element with CSF thickness of 3mm
5. Fine mesh – shell element with CSF thickness of 1.3mm
6. Fine mesh – shell element with CSF thickness of 1.3mm
7. Shell element with CSF thickness of 3mm

Versions 5 and 6 have varying mass which is unreported and the mesh quality of version 7 is also unreported. Validation was carried out on version 2, Medium mesh – brick element with CSF layer of 1.3mm.

2.5.6 Brain Model Summary

All of the models investigated in this section were developed in the same time period and have some similarities; in that all attempt to approximate the 50th percentile male and are validated using the same Hardy, Nahum and Trosseille datasets for intracranial pressure and displacement. The differences are clear when the complexity of the models is examined.

The SIMon model was created with one of the main objectives being that a simulation could be run on a high-end pc in under 2 hours. In order to achieve this, the model has as few parts as possible. Reducing the computational times and costs. The KTH model was developed to be a scalable representation of the human head and as such the complexity is reduced to allow for this. While the UCDBTM has several versions, with different setups in terms of mesh densities and CSF thicknesses. These SIMon, KTH and UCDBTM models have tens of thousands of nodes and 7852, 18416 and 9000-50000 (depending on the version of UCDBTM) elements each respectively.

Whereas the GHBMC head and neck model has 488,453 elements, 510,501 nodes and 436 individual parts. Making it the most detailed of the models in use today. Given it is also a head and neck only model, the computational time required is comparable to that of the SIMon model. This level of detail as well as the option of obtaining a head and neck only model was the reasoning behind choosing the GHBMC model for this study.

2.6 Brain Injury Predictors

Various methods of predicting brain injury have been proposed over the last 50 years, some based on kinematics and some based on FE measures of regions in the brain. Kinematic measures can be 3 degree of freedom (DoF), based on linear translation only or rotational only. They can also be 6 DoF based, including both linear and rotational. FE measures attempt to make a prediction based on the mechanical behaviour of the brain in a FE model and may include but are not limited to; strain, strain rate and intra-cranial pressure. Both FE and kinematics-based measures will be discussed in the next section.

2.6.1 Wayne State Tolerance Curve

Some of the earliest work in this area was conducted at Wayne State University, and investigated the effects of concussive impacts on anesthetised animals. The animals were subjected to accelerations for a given period of time. This resulted in what is now known as the Wayne State Tolerance Curve (WSTC), shown below. This curve found that the human head can withstand high accelerations for a short duration and lower accelerations for a longer duration.

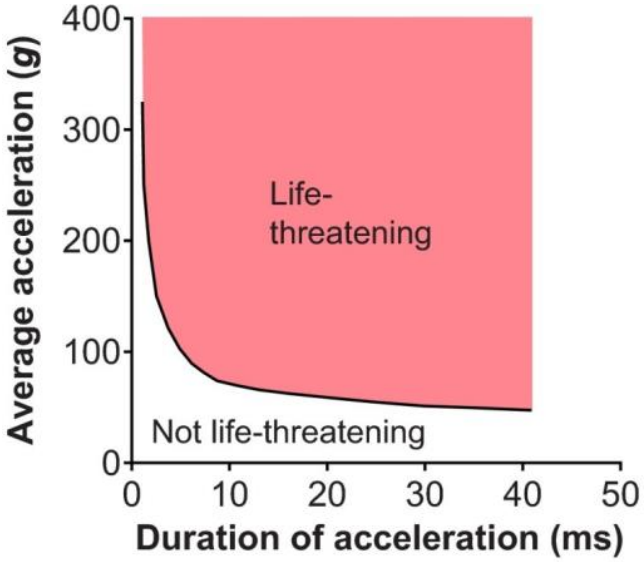

Figure 15: Wayne State Tolerance Curve [84]

Figure 15 above shows the Wayne State Tolerance Curve, with any point above the line, within the Life-Threatening area of the graph, being potentially injurious [84].

2.6.2 Gadd Severity Index

Building on the work of the Wayne State, Gadd developed a mathematical equation in order to determine the severity of an impact. The equation is shown below.

$$SI = \int a^{2.5}\, dt$$

Equation 2: Gadd Severity Index equation [85]

In this equation SI is the Severity Index, α is the weighted acceleration to the power of 2.5 and t is the time duration of the acceleration. A score of >1000 for SI would mean the subjects life is at risk. This index received some criticism due to the fact that low accelerations over a long period of time were not accounted for. It was expanded upon by Versace from the Ford Motor company in conjunction with the National Highway Traffic Safety Administration; this became known as Head Injury Criterion (HIC).

2.6.3 Head Injury Criterion

A continuation of the previous work by Gadd, the Head Injury Criterion (HIC) is based on the WSTC and the Gadd Severity Index. The equation is shown below. It treats the head as single mass structure.

$$HIC = \max_{(t_1,t_2)} \left\{ (t_2 - t_1) \left[\frac{1}{t_2 - t_1} \int_{t_1}^{t_2} a(t)dt \right]^{2.5} \right\}$$

Equation 3: Head Injury Criterion Equation [86]

Where a is the resultant linear acceleration at the head CoG. The main difference between this and the Gadd Severity Index equation is that the impact duration is calculated in the term: $(t_2 - t_1)$, although it is not without its own issues. Namely, a study by Hodgson et al. (1972) showed that this equation is only applicable to short durations [86]. Both HIC and Gadd's equation only take linear acceleration into account, despite the fact that it has been shown that rotational acceleration plays an important role in TBI's [87].

2.6.4 Head Impact Power

Developed by Newman et al (2000), Head Impact Power (HIP) treats the head as a single mass structure, much like HIC [88]. It is calculated using linear and rotational accelerations that are measured at the head CoG of a Hybrid III anthropomorphic test device (ATD). The equation is shown below.

$$HIP = \underbrace{C_1 a_x \int a_x dt + C_2 a_y \int a_y dt + C_3 a_z \int a_z dt}_{\text{Linear Contribution}} + \underbrace{C_4 a_x \int a_x dt + C_5 a_y \int a_y dt + C_6 a_z \int a_z dt}_{\text{Rotational Contribution}}$$

Equation 4: Head Impact Power Equation [88]

The C_n coefficients represent approximations of the mass and the moment of inertia for a 50th percentile human head [89]. a_x,a_y, a_z are the linear and rotational components.

Where: $C_1, C_2, C_3 = 4.5kg$

$C_4 = 0.016Nms^{-2}$

$C_5 = 0.024Nms^{-2}$

$C_6 = 0.022Nms^{-2}$

The calculation is time dependent and the HIP score will be based on a 50th percentile human head, which makes it a of particular interest for this study as both the FE model and instrumented mouthguards being used assume a 50th percentile human head. Equation 4 outputs a maximum value for HIP during the entire impact and the units are in kilowatts (kW).

2.6.5 Head Accelerations Recorded in Sports

Many studies have recorded the magnitude of linear and rotational accelerations induced in participants of sports. Mean values for peak linear acceleration (PLA) and peak rotational acceleration (PRA) from the studies that include concussion data will be reported, although the number of these studies is limited. Many studies report PLA and PRA but do not report concussion data.

In one of the largest data sets of its kind, Duhaime et al. 2012 recorded 486,594 impacts from 3 collegiate football teams and 4 ice hockey teams using the HITS. Forty-eight concussions were reported, 31 of which could be linked to an individual impact. Of those that were linked to an individual impact the PLA and PRA was found to be 86.1g (+/- 42.6g) and 3620 rads/s^2 (+/-2166 rads/s^2).

Beckwith *et al.* 2014 conducted a study using the HITS system where 1,208 high school and collegiate football players were tracked [45]. 105 injury cases were reported in this study, impacts received directly prior to a concussion diagnosis were found to have a PLA of 112.2g (+/- 35.4g) and PRA of 4253 rads/s^2 (+/- 2287 rads/s^2). Similarly, Broglio *et al.* 2010 conducted a study using the HITS system and recorded 54,247 impacts from high school football players, 13 concussions were recorded [90]. From these impacts they determined that a PLA of > 96.1g and PRA of > 5582.3 rads/s^2 increased the probability of a concussion in a high school athlete. Eckner *et al.* 2011 [91] conducted a similar study, where 95 high school football players wore the HITS system for 4 years [91]. Over 100,000 impacts were recorded and 19 concussions were reported. Unfortunately, they did not report the PLA or PRA for the impacts recorded or for the impacts that resulted in a concussive diagnosis.

Several studies utilised the HITS system to record impacts in American football, Beckwith *et al.* 2011 instrumented the helmets of 314 collegiate football players and recorded 286,636 impacts [92]. They reported a 50^{th} percentile PLA and PRA of 20.5g and 1400 rads/s^2 respectively, and the 95^{th} percentile PLA and PRA of 62.7g and 4378 rads/s^2. In a further study using the same data set Rowson *et al.* 2012 examined 57 concussive impacts and determined that the non-concussive impacts had a mean PRA of

1230 rads/s^2 and mean peak rotational velocity (PRV) of 5.5 rads/s [48]. Concussive impacts had a mean PRA and PRV of 5022 rads/s^2 and 22.3 rads/s respectively.

Zhang *et al.* 2004 conducted a study where 24 helmet to helmet collisions from professional American football were reconstructed using the WSUBIM, they reported tentative linear acceleration thresholds of 66g, 82g and 106g for a 25%, 50% and 80% probability of a concussion respectively [93]. They also reported rotational based thresholds of 4600 rads/s^2, 5900 rads/s^2 and 7900 rads/s^2 for a 25%, 50% and 80% probability of a concussion.

2.6.6 Strain

Long postulated as a potential predictor for TBI, strain in the tissue of the brain is particularly difficult to measure *in vivo* and as such has been the focus of many decades of research. Shear strain was first proposed as a cause of TBI by Holbourn *et al.* in 1943. They conducted a study where a physical model of a human skull was created, with the brain tissue being modelled as a gel. This model was subjected to large angular accelerations and a shearing deformation of the gel was observed [94]. The first to attempt to observe the motion of brain tissue directly were Pudenz and Shelden in 1946. They removed the upper skull bone of a Macaque monkey and replaced it with a transparent window and recorded the motion using high speed footage. From these experiments they postulated that rotation of the brain was the most important factor in a brain injury [95].

Following these early studies, much research was conducted utilising X-ray technology to attempt to directly measure the relative motion of the brain tissue and skull. In 1966 Hodgson *et al.* used flash X-Ray technology, in conjunction with an intravascular contrast and lead targets implanted in the brain, to observe the motion in anesthetised canines. The patterns of motion they observed indicated that the response of the brain was mainly driven by shear forces. They also observed that the targets all returned to their original positions, indicating that the deformation was elastic in nature [96]. In 1974 Shatsky *et al.* utilised X-ray technology to investigate brain motion in primates. They observed motions in the region of 2-3mm and estimated strain of 8.6% for a temporoparietal impact [97].

More recently, in 1992 Trosseille *et al.* conducted a cadaveric study where they implanted accelerometers into the brains of five cadavers. The cadavers were placed in a sitting position and were impacted, high speed video footage was taken. Head accelerations, cerebral tissue accelerations and CSF pressures were recorded. This study provides the data for many of the most popular FE models in use today, including the model used for this study [98]. Following this, in 2001 Hardy *et al.* attempted to directly measure the motion of the brain tissue in re-pressurised cadavers, by implanting neutral density targets (NDAs) into the brain. They then used x-ray technology to track the NDAs during an impact. They determined that peak displacements were in the order of 5mm and that motions were either a loop or figure of eight patterns. This study is also used for FE model validation [64].

In 2000, Meaney *et al.* conducted a study where they investigated the mechanism behind axonal injuries, by straining the optical nerve of a male guinea pig. Based on these tests and statistical analysis, they determined that Lagrangian maximum principal strain (MPS) was the best predictor of axonal injury and were one the firsts to propose MPS based injury thresholds [99]. Since then, MPS has been widely used in many studies that investigate TBI and several other injury thresholds has been proposed. These will be discussed in the upcoming sections.

2.6.6.1 Maximum Principal Strain

The first of the FE based brain injury predictors; Maximum Principle Strain (MPS) is the maximum first principle Green-Lagrange strain in an element within a region or part of the brain model. It is widely used as the main metric for finite element based brain injury predictors; it is the maximum tensile strain in the longitudinal direction [6] [87] [100] [101] [8] .

2.6.7 Cumulative Strain Damage Measure

The second of the FE based brain injury predictors, Cumulative Strain Damage Measure (CDSM) is a predictor based on the volume fraction of a region of brain tissue that exceeds a certain value for MPS. The most commonly used versions of this predictor are $CSDM_{15}$ and $CSDM_{25}$, which calculate the volume fraction of the region that have MPS values over 15 and 25% respectively.

2.6.8 Published Injury Thresholds

In 1998 McIntosh *et al.* conducted a study to investigate the dynamics involved in mTBI's in Australian Rules Football, Rugby Union and Rugby League. 100 medically diagnosed concussion cases were studied, 97 of which involved direct impacts to the head. None of the sports in their study require protective head gear. The dynamics of the impacts were determined by analysing video footage, from which the impact location, type of impact and velocities of bodies before and after the impact were calculated. Using these values, they then determined the initial and final momentum, the change in velocity and head impact energy. They determined the mean change in velocity and head impact energy for the 97 head impact cases were 4m/s and 56J [102].

In 2009 Frediche *et al.* reconstructed 27 of the impacts from the previous study in MADYMO in order to further improve the understanding of the dynamics involved in sports related TBI. Full human body models were used to reconstruct the impacts in MADYMO, allowing the full dynamics to be captured including; initial velocities of the subjects, morphometric analyses, and estimates of masses of the bodies involved. The outputs to be investigated from these simulations were HIP, HIC_{15}, PLA, PRA, change in peak linear and rotational velocity. Based on the results of the 97 simulations they found mean values of 13,715W, 103g, and 8020 rads/s^2 for HIP, PLA. and PRA respectively [103].

Using the same 27 concussive cases from the previous study and 13 non-concussive cases Patton et al. used the accelerations determined by Frediche *et al.* and applied them to the

head CoG of the KTH brain model. The level of maximum principle strain in the grey and white matter, brain stem, thalamus, midbrain, corpus callosum, and cerebellum were recorded. Univariate logistical regression was performed on the simulation results and tentative thresholds for a 50% probability of a concussion occurring were found to be; 15%, 15% and 27% in the thalamus, corpus callosum and grey matter respectively. The study also determined mean levels of strain for the cases where a concussion had occurred of; 25%, 26%, 31% and 47% in the midbrain, thalamus, corpus callosum and grey matter respectively, Table 11 [6].

Viano *et al.* (2005) conducted a study where 28 National Football League (NFL) impacts were recreated and simulated using the Wayne State Head injury Model (WSUHIM), with 22 concussions [8]. Impacts were recreated using a Hybrid HIII ATD and the resulting accelerations were applied to the WSUHIM. This study found that strain in the thalamus and midbrain were the best predictors for symptoms such as memory loss and general cognitive problems. Tentative thresholds for mean strains to cause a concussive injury in these regions were determined to be; strains of 38% and 34% in the thalamus and midbrain respectively. And the mean strain for non-injury in the thalamus and midbrain were determined to be 23% and 21% respectively [8].

Kleiven *et al.* (2007) conducted a study where 58 impacts from the NFL were reconstructed and simulated using the KTH model [7]. Several regions of the brain were investigated; brainstem, midbrain, corpus callosum, thalamus, white matter and grey matter. The strain in each of these regions was reported and further tentative thresholds for mean strain in the corpus callosum and the grey matter for a 50% probability of a concussion occurring were 21% and 26% respectively [7].

Further work conducted by Hernandez *et al.* into many different FE and kinematic based brain injury predictors found that maximum principle strain in the corpus callosum had the lowest deviance across all the predictors analysed. In this study they also found that of the 6 DoF kinematic based predictors, HIP performed the best and had the 3rd lowest deviance of predictors examined [101]. Post *et al.* examined the relationship between impact duration and strain in the corpus callosum and discovered that as the duration of an impact increases, the magnitude of rotational acceleration required to cause injury decreases [87].

In the development of HIP, Newman *et al.* reconstructed 12 helmet to helmet impacts from American Football. Impacts were reconstructed in a laboratory setting, using Hybrid III ATDs instrumented with nine accelerometers allowing for the calculation of both linear and rotational accelerations. One of the ATDs was mounted on a carriage and dropped vertically into another. From these reconstructions they produced a MTBI-HIP risk curve. From this curve they calculated a HIP of 12.8kW correlated with a 50% probability of a concussion [89].

Based on the combined work of McIntosh, Frediche and Patton in determining the thresholds, as well as the analysis by Hernandez, the maximum principle strain in the corpus callosum has been selected as the main FE based TBI predictor for this study. The strain in the midbrain, brain stem and thalamus will also be compared with the published thresholds. Table 11 summarises these thresholds. Furthermore, as highlighted by Post, the impact duration will also be analysed. Based on the work by Newman, Hernandez and Frediche, HIP will be investigated as the main kinematic based TBI predictor.

Table 11: Summary of Published Strain Based Injury thresholds

Study	Model	Region	% Strain	Comment
Patton [6]	**KTH**	Midbrain	25%	Mean for Concussive injury
		Corpus callosum	31%	
		Thalamus	26%	
		Grey matter	47%	
		Midbrain	13%	Mean for non-concussive injury
		Corpus callosum	12%	
		Thalamus	10%	
		Midbrain	15%	50% probability of concussion
		Corpus callosum	15%	
		Grey Matter	27%	
Viano [8]	**WSM**	Midbrain	34%	Mean for Concussive injury
		Thalamus	38%	
		Midbrain	23%	Mean for non-concussive injury
		Thalamus	21%	
Kleiven [7]	**KTH**	Corpus callosum	21%	50% probability of concussion
		Grey matter	26%	

2.6.9 Brain Injury Predictors Summary

In this section several different metrics from brain injury predictors have been examined, some being based on kinematics. With GSI and HIC using linear acceleration only and not taking impact duration into account. And HIP, taking linear and rotational acceleration into account but only being applicable to the 50^{th} percentile human head.

MPS is a metric based on FE model outputs and is independent of kinematic based metrics. It is the most widely used metric of its kind, with many studies utilising it across many sports and in accident recreation [6] [7] [8] [87] [100] [101] [104]. CSDM is a further FE model output-based metric derived from the levels of MPS exceeded in regions of the brain during a simulated impact. As MPS is the fundamental metric and that much of the work in concussion has been utilising it, with several thresholds for concussion published in terms of MPS, it was chosen as the main FE based predictor to be investigated for this study.

HIP is a time dependent formula, which takes both linear and rotational acceleration into account. The equation also uses anthropometric data for a 50^{th} percentile human head, aligning with the FE model and instrumented mouthguards used in this study. For these reasons it has been chosen as the main kinematic based TBI predictor.

2.7 Mixed Martial Arts

Mixed Martial Arts (MMA) is a combat sport that incorporates several different disciplines including but not limited to; striking, grappling, Brazilian Jiu Jitsu, wrestling, boxing and Muay Thai. MMA style competitions have been recorded as far back 648BC [105], while MMA in its current form started in the United States of America in 1993 with Ultimate Fighting Championship (UFC) 1. It wasn't until 2001 when the UFC was acquired by a new owner (Zuffa LLC) that the health of the participants was addressed more fully and a set of unified rules and weight classes were implemented. Since 2001 MMA has seen a massive increase in the number of participants and fans, with it now being one of the fastest growing sports in the United States. News reports suggest some 5.5 million teenagers and 3.2 million children under 13 are actively participating in the sport in the United States alone [106].

Amateur MMA is governed by the World Mixed Martial Arts Association (WMMAA) and the International Mixed Martial Arts Federation (IMMAF). These federations were founded independently, with the WMMAA being founded in 2012 by Vadim Finkelchtein and the IMMAF by August Wallen. In 2018 in an effort to push for Olympic recognition the federations merged to form the IMMAF – WMMAA [107].

In 2014 the IMMAF produced the first set of unified rules for amateur MMA, latest revision March 2017, which lays out how fights would be judged; a system of warnings, definitions of fouls and forbidden techniques, weight divisions, medical requirements for participants, the personal protective equipment to be used, the dimensions of the cage, scoring techniques and how the winner of a fight would be decided. This document is available in full in Appendix 2.

Also created was a set of unified rules for youth participants, latest revision February 2019 rev B, it is similar to the previously mentioned rules but also defining the age ranges in which youth participants would compete.

Further medical requirements have been implemented in Ireland for participants of MMA, with the formation of Safe MMA in 2012. Safe MMA regulates the medical standards for MMA in the UK and Ireland, working closely with the Irish Amateur MMA Association, the Ulster Amateur MMA Association, the United Kingdom Mixed Martial Arts Federation and the International Mixed Martial Arts Federation. To participate in an event organised by any of these federations or associations medical clearance must be provided by Safe MMA, known as a "passport". There are several different types of "passports" provided by Safe MMA (Table 12). As well as the requirements listed in Table 8 blood tests are also required, with confirmation of the participant being clear of the following blood borne diseases: HIV, Hepatitis B and Hepatitis C [108]. Safe MMA addresses the issue of competitor safety practically and in the simplest way possible, with its system of standardised and voluntary, fighter medical clearance. A Safe MMA passport includes:

- Confidential database for competitors' well-being and current medical status
- Member promotions only using athletes found within the registered database
- Listed promotions upholding medically advised suspensions
- Affordable cost: Not-for-Profit medically led project with specially negotiated blood test rates.
- Access to sports based medical advice that fighters can trust

As part of the Safe MMA regulations, "at event" medical examinations are required for all participants. In Ireland these are conducted by Code Blue, a team of medical professionals that provide medical support. Code Blue is made up of professionals in emergency medicine and the ambulances services. They provide an on-site medical centre, where all participants will be examined pre- and post-fight, medical support ring side and transfers to hospital as required. They are fully accredited by the Irish Medical Council, An Bord Altranais and The Pre-Hospital Emergency Care Council (PHECC) [109].

Table 12: Safe MMA fighter medical requirements

Professional		Amateur	
Type	**Requirements**	**Type**	**Requirements**
M1	• Yearly medical examination • Six-monthly blood tests • Pre and post-fight medical examinations (at event)	M1	• Yearly medical examination • Yearly blood tests • Pre and post-fight medical examinations (at event)
M3	• Yearly medical examination • Six-monthly blood tests • Pre and post-fight medical examinations (at event) • Dilated pupil eye tests • One-off MRI of the brain • MRI of the brain every 3 years		
M5	• Yearly medical examination • Six-monthly blood tests • Pre and post-fight medical examinations (at event) • Dilated pupil eye-tests • One-off MRA of the brain and neck • Yearly MRI of the brain	M5	• Yearly medical examination • Yearly blood tests • Pre and post-fight medical examinations (at event) • One-off MRI of the brain

2.7.1 MMA Summary

As MMA involves a more diverse physical interaction among athletes than boxing, it may result in higher injury rates yet with less significant head trauma [110] [111]. Boxers are limited to hitting their opponent in the head and body whereas MMA fighters can use a multitude of fighting techniques with the inclusion of wrestling and Brazilian jiu-jitsu. In a 10-year review of professional MMA matches, head trauma was found to be the single most common reason for match stoppage at 28.3% [10]. 15% of the 115 MMA athletes surveyed, by Heath and Callaghan in 2013, reported a history of at least 1 knockout [112]. Ngai and colleagues found during a 5-year period, regulated MMA event injuries were similar to other combat sports, with only 3% of matches ending in concussion [113].

As MMA participants are required to wear a mouthguard at all times during practice or competition, it was seen as an excellent opportunity to collect *in vivo* impact data by way of an instrumented mouthguard. A further consideration was that MMA is an individual's sport and as such makes recording of video footage considerably easier than that of an American Football team, for example. Focusing the camera on a single participant allows for confirmation of impacts to be considerably simpler, as just a single camera is likely to capture most impacts. It was with this in mind that MMA was chosen as the sport to conduct this study, as MMA provides a unique opportunity to gather *in vivo* head impact data.

2.8 Literature Review Summary

In this chapter several important topics for investigation have been defined, as well as some of the methods to be used. This includes the brain regions of interest, the definition, symptoms, effects and diagnosis of mTBI, the device being utilised for collecting *in vivo* impact data, the model being utilised for simulating data the predictors for predicting an mTBI and the sport in which data was collected.

The regions of interest have been chosen based on their function and previous studies, which have highlighted their role in mTBI study. They are the corpus callosum, brain stem, midbrain and thalamus.

The Stanford mouthguard was chosen due to the fact that it provided a unique opportunity to collect *in vivo* data in an unhelmeted sport and because it is one of the best performers of all instrumented devices available.

The GHBMC model was chosen as it is one of the most detailed models available, with good validation studies in the literature and was possible to utilise an isolated head and neck model which reduces the computational power and cost.

MMA was chosen as it provides an excellent opportunity to gather *in vivo* head impact data. Competitors are required to wear a mouthguard during all bouts and training sessions, meaning there was little change required in the participants behaviour. MMA also provides an excellent arena to gather head impact data due to the fact that up to 25% of all MMA bouts end as a result of head trauma. Also due to the fact that the sport itself is 1-on-1, this make recording of video footage considerably easier than other sports commonly studied in mTBI studies.

These combinations of factors are the driving force behind the design and decisions made for this study.

Chapter 3 Study Design

3.1 Introduction

The aim of this study is to measure and simulate head impacts in MMA. The measurement of these impacts is achieved by way of an instrumented mouthguard. The section below, 3.2 Mouthguards, will describe in detail the process. The head accelerations recorded by the mouthguards will be applied to a head simulated model. This process will be described in the next chapter, Chapter 4.

The study had 22 participants, all of whom gave their written consent to take part; ethical approval was granted by the Institute of Technology Tallaght Ethics Committee (REC-STF1-201819). The consent form is available in full in Appendix 3.

While the purpose of this particular study is to measure and simulate head impacts, this study is part of a much larger project. The author of this thesis is part of the Concussion Research Interest Group (CRIG). CRIG is a multi-discipline, multi-institute group of science, engineering and medical researchers working in the field of concussion research. Along with the measurement and simulation of impacts there are other aspects of the project. Our partners in the Smurfit Institute of Genetics, Trinity College Dublin, postulate that damage to the blood brain barrier (BBB) is a contributing factor in the mechanism behind concussion. In order to investigate this, participants are asked to make themselves available to have a gadolinium contrast injection MRI, to capture a baseline of their "uninjured" brain. It is important that this baseline scan is as clean as possible, in that it should take place as long as possible after any previous head impact. Then when the participant has taken part in a competitive event, they will have a further MRI, in order to compare to the baseline scan. These scans are provided by St. James Hospital, Dublin radiology department and are supervised by an emergency medical professional. The research in this area is on-going.

Further testing is carried out on the participants in the form of cognitive testing, undertaken by neurologists from Beaumont Hospital, Dublin. They are investigating the potential link between eye tremors and the diagnoses of concussion. Research in this area is also on-going.

Also, as part of the project, there is a physiotherapist who is conducting SCAT 5 tests on the participants after each event. This has just recently begun and the data from this is limited.

The final aspect of the project is to investigate the existence of a blood bio marker that indicates whether a concussive injury has occurred. The discovery of a bio marker would be the “holy grail” in this field. As it would be the least intrusive and most cost-effective method of diagnoses. This research is conducted in Trinity College, Dublin and is also ongoing.

In this chapter the processes developed to take manufacture and configure the mouthguards, field data collection and review video footage of events will be detailed. In the final section the statistical techniques being used in this study will be explained.

3.2 Mouthguards

All participants in this study have been provided with 2 mouthguards; developed in Stanford as discussed in Chapter 2. One is a fully instrumented mouthguard and the other has no instrumentation. Both mouthguards are created using the same unique dental mould taken from the participant, the non-instrumented version is the property of the participant. The non-instrumented version allows them to become comfortable with the design and feel of it prior to wearing the instrumented version. The aim is that the participants wear the non-instrumented version when training and sparring and on the day of an event it is replaced with the instrumented version.

Figure 16: An instrumented and non-instrumented mouthguard

Shown in Figure 16 on the right is the instrumented version, with the power switch on the left, printed circuit board in the centre and battery on the right. On the left of Figure 16 is the non-instrumented version, with the switch, circuit board and battery being replaced with dummy components, thus ensuring both instrumented and non-instrumented version feel exactly the same for the participant.

The mouthguards are manufactured by Opro, Hertfordshire, United Kingdom, from a custom dental mould taken from the participants. The dental impression process takes approximately 5 minutes in total and is a 5-step process, with the process detailed below in section 3.2.1.

3.2.1 Mouthguard Impression Procedure

Shown in Figure 75 below is the home impression kit supplied by Opro. The participant or the person conducting the study will carry out the impression procedure. To take a dental impression the following materials are required:

- Protective gloves
- Tape for labelling tray
- Timer
- Impression kit

Impression Kit contains:

- Impression Kit
- 2 putties
- Return bad

Figure 17: Opro home impression kit

The procedure for taking dental impressions is as follows:

1. Assemble materials required: putty, impression tray, protective gloves, tape, bag to place completed impression in, timer.
2. Put on protective gloves.
3. Place small piece of tape on the end of the impression tray to mark the ID of the participant. This number also should be written on the outside of the bag for sending to Opro.
4. Mix the putties until no streaks are visible i.e. – one colour (40 seconds).
5. Mould the impression material into the tray, ensuring complete coverage.
6. Have the participant place the impression tray into their mouth and tell them to bite down firmly. (2 ½ minutes).
7. Remove the impression tray from the participant's mouth, ensuring it is a complete impression with no gaps and that all teeth have made an impression, including molars.
8. Rinse the impression tray and allow to dry.
9. Place the impression tray into the bag to be returned to Opro.
10. Impression is now complete, clean up all materials and change gloves if taking another impression to ensure no cross contamination.

3.2.2 Mouthguard Setup Procedure

Setup and data collection from the mouthguard are achieved via Bluetooth, by way of a custom Apple Mac OS app. The app is called Bite App and was developed alongside the mouthguards.

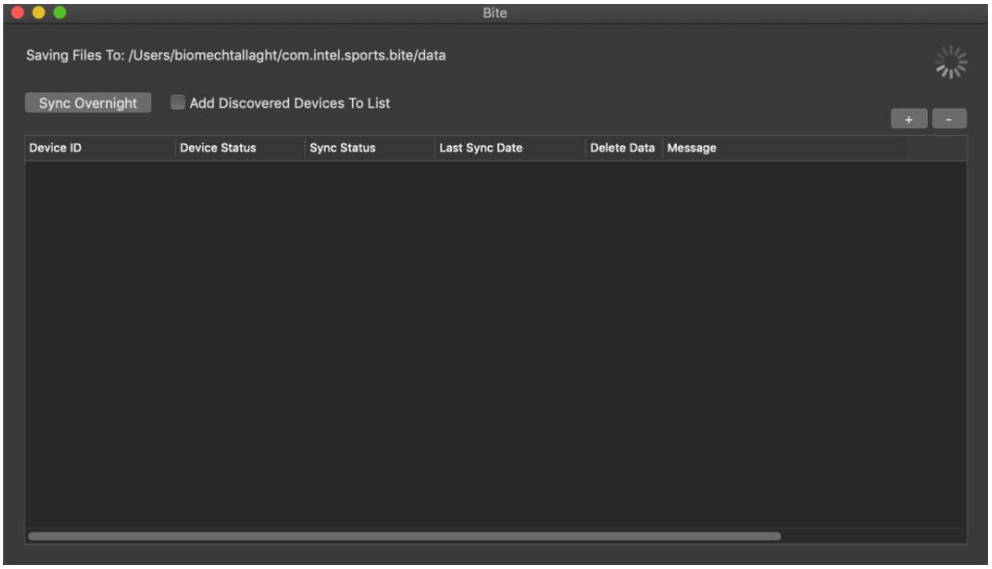

Figure 18: Bite App main interface

To setup a mouthguard, the plus in the top right of Figure 18 must be pressed. That will show all mouthguards that are powered on and in proximity, Figure 20. In order to communicate with the app, the mouthguard must be in the charging station and the blue LED must be illuminated. All mouthguards have a unique alpha-numeric device identifier; this ensures only the correct mouthguards are configured. When a mouthguard has been added it will appear in the list, as shown in Figure 21. It is imperative that the "Delete Data" box be ticked if the mouthguard had been used previously, to ensure that no unwanted data from another session is saved.

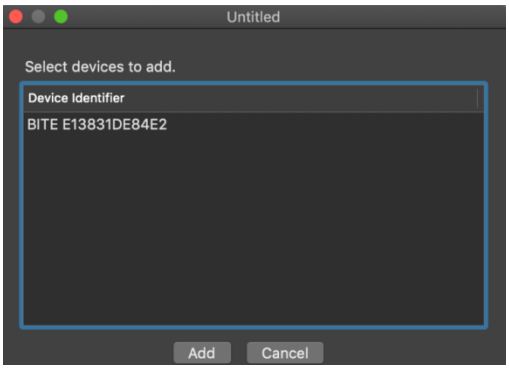

Figure 20: Adding a mouthguard in Bite App

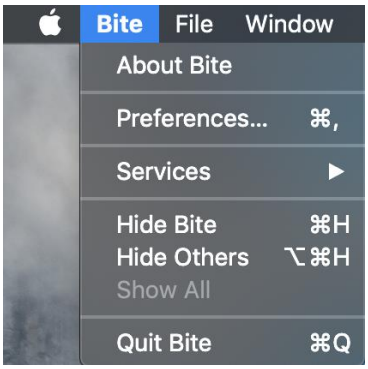

Figure 19: Setting up Bite App

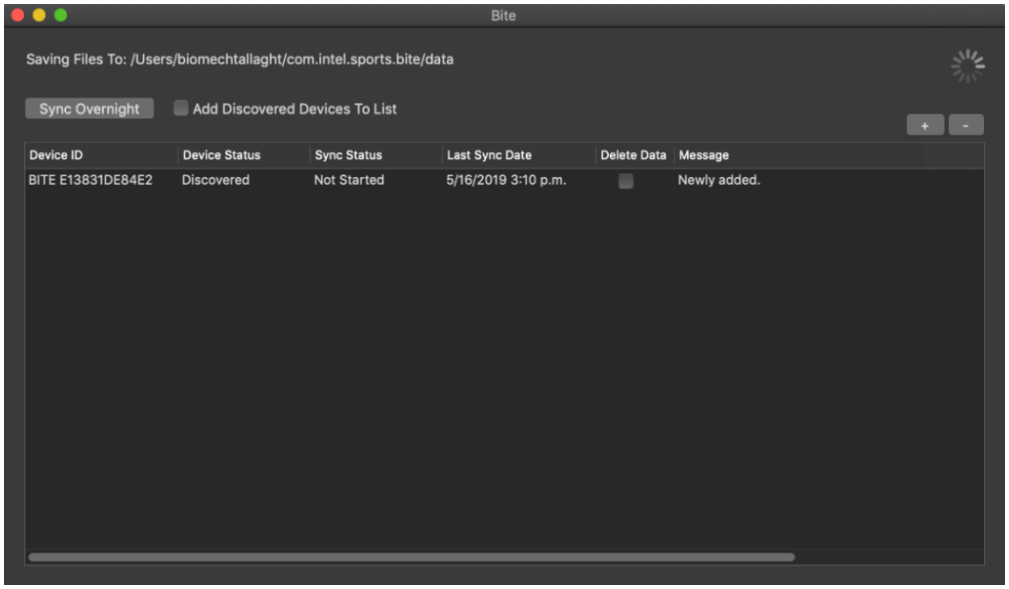

Figure 21: Mouthguard added in Bite App

When the app has discovered the mouthguard, it can be setup to collect data. This is done by selecting the Bite App in the top left and selecting preferences, shown in Figure 19. Selecting this opens a new menu, where we can set the acceleration range, Gyroscope frequency, Gyroscope range, the duration of impacts to be recorded, lower threshold for recording an impact and the time and date for the mouthguard to power on. This menu and the settings used for this study are shown in Figure 22.

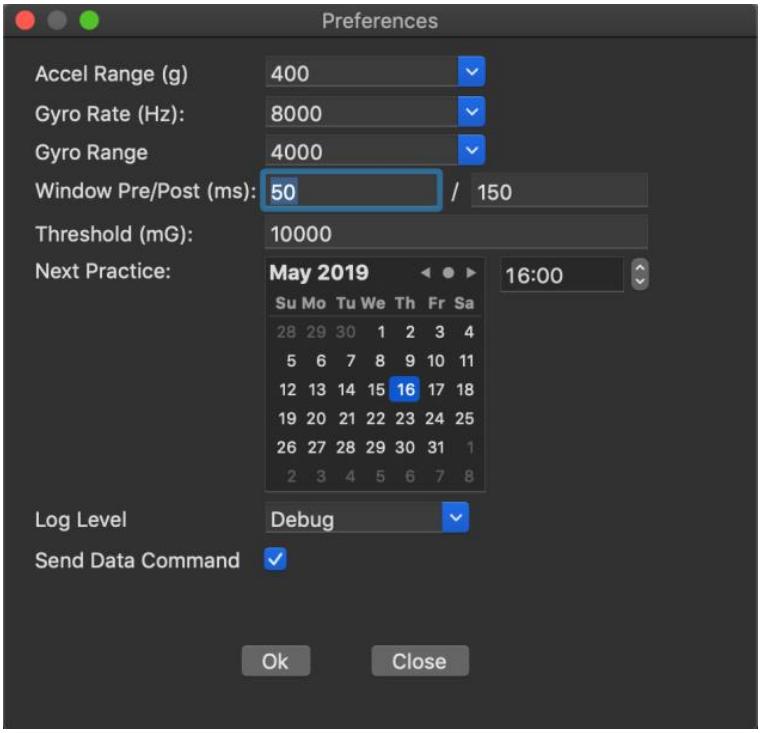

Figure 22: Bite App preferences menu

- Accel. Range (g): Is the max linear acceleration that will be recorded by the mouthguard. Default is 400g.
- Gyro rate (Hz): Is the frequency at which the gyroscope will sample data. Set to 8 KHz.
- Gyro Range: Is the maximum angular velocity that will be recorded by the mouthguard. Set to 4000 rads/s.
- Window Pre/Post (ms): Is the time, in milliseconds, the mouthguard will record before and after the impact has been received. Set to 50ms pre and 150ms post.
- Threshold (mG): The minimum linear acceleration threshold to record data. Set to 10g.
- Next practice: Is the time and date at which the mouthguard will power to collect data.

The mouthguards have 3 power modes:

1. Powered on but not setup with a time and date to record data (Green LED flashes every second)
2. Powered on and setup with a time and date to record data (Green LED flashes every 10 seconds)
3. In data recording mode (Green LED only flashes when an impact is recorded)

Turning the power on and off is achieved by way of a magnetic wand, which has to be passed by the switch embedded in the mouthguard.

3.2.3 Field Data Collection

Once the mouthguard has been setup with a time and date for a sparring session or competitive event, it can be handed over to the participant. All sparring sessions/competitive events are video recorded in 1080p. At the start of the video recording, an atomic clock showing the current time is shown on screen, this ensures all impact timestamps can be cross-referenced with the time shown on the video. An example of a typical impact recorded in a sparring session with the video timestamp visible, shown in Figure 23.

When the sparring session/competitive event is finished, the mouthguard can be collected from the participant and powered off. Prior to collecting the data from the mouthguard, it must be cleaned. The next section will cover the procedure for cleaning mouthguards so they are safe to handle.

Figure 23: Image taken from sparring session with timestamp visible

3.2.4 Procedure for Cleaning Mouthguards

Before handling used mouthguards, it is recommended that any individual that is likely to come into contact with blood and/or saliva has a Hepatitis B vaccination. This is to ensure that no blood borne pathogens can be transmitted during the handling of mouthguards.

Prior to cleaning the mouthguards, ensure there is a clean area in which they can be cleaned. The following will be needed:

- Shallow tub/basin that fits into the sink
- Small bucket
- Detergent soap
- Household bleach
- Soft bush
- Absorbent pad
- Apron/Lab coat
- Protective gloves
- Protective glasses

The procedure for cleaning mouthguards is as follows:

- Put on PPE (lab coat, protective gloves and glasses)
- Put the basin in the sink and fill part way with warm water and detergent. Fill the bucket with warm water and add 10% bleach. Have a bin nearby.
- Turn on the hood and place a new absorbent pad in the hood.
- Turn on the tap and get a small stream of warm running water.
- One at a time, open each Ziploc bag containing a mouth guard over the sink. Take out the mouth guard, rinse it under the running water, and put it into the basin with the soap water. Put the used Ziploc bag in the bin.
- Gently use the brush on the mouth guard for 10 seconds. Rinse the mouth guard under the running water and put it into the bucket of bleach solution.

- Repeat this for all the mouth guards. As you add each mouth guard give them all a swirl to make sure all the surfaces are exposed to the bleach.
- Once you have finished all the mouth guards, rinse off the gloves, empty the soap water and clean the basin and set it on the counter to dry.
- Leave the mouth guards in the bleach solution for 10 minutes (timing from the last mouth guard to be put in).
- After 10 minutes take out the mouth guards one at a time, rinse them off under running water and place them on the absorbent pad to dry. Place the mouthguards top side down so that the water runs out of the space where the teeth fit.
- You can swirl the gloves to disinfect them in the remaining bleach solution before emptying the bleach into the sink. Be careful not to splash the bleach solution as it will stain your clothes.
- Rinse out the bucket, rinse off the gloves and put them both aside to dry.
- From this point on, you can treat the mouth guards as "clean" but you should still wear gloves when handling them so as not to transfer anything from your finger to the mouth guards.
- After the mouth guards are dry each one should be put on/in a charging station. You can then start the download process.
- After charging and downloading the data, you need to prepare the mouth guards for delivery back to the participants.
- Each mouth guard should be placed in a Ziploc bag and given a spray of Listerine. Seal each bag and put them all in a large clean bag for transporting to the participants.

Figure 25: Charging station with mouthguard charging

Figure 24: Charging station empty

3.2.5 Mouthguard Data Collection

Once the mouthguards have been cleaned and are safe to handle, the data can be retrieved. This is achieved by way of the Bite App. Mouthguards must be switched on and in the charging station for the transfer of data. Figures 25 and 24 show the charging station with a mouthguard while in the charging station and when empty.

The mouthguard must now be linked to the Bite App again to retrieve the data collected. This is achieved by adding the mouthguard, when switched on, to the app as detailed in the mouthguard section previously. Once the mouthguard is linked again, the Sync Overnight button must be pressed. This will start the transfer of data. This can be seen in the list of mouthguards in the app. The number of events to be downloaded will be indicated on screen. When all events have been downloaded the process can be stopped.

Downloaded data is stored locally on the MacBook in the form of a comma separated value file (CSV). This is the raw, unprocessed data. An example of this data, with some explanations of the function of each part is shown in Figure 26.

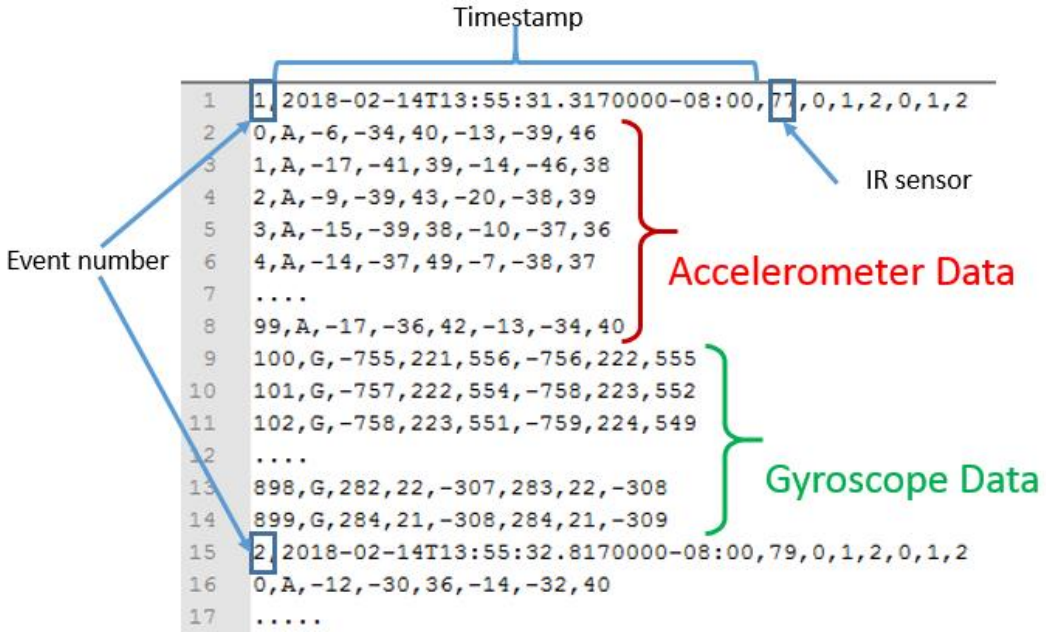

Figure 26: Raw, unprocessed data from mouthguard

This data has been filtered and differentiated. Filtering is achieved with a Butterworth CFC180 filter, while differentiation is achieved by way of a 5-point-stencil derivative for high precision. In order to format this data in a readable manner, several MATLAB programmes were created. These programmes were created by and run by the supervisor of this project. The different programmes used are:

Infrared history – produces a graphical summary of IR readings. Figure 27 shows the output from the IR History file, it is a bar chart and indicates the IR readings and the number of impacts with that value. A higher IR reading indicates the mouthguard was being worn when the impact was received, meaning that impacts recorded when the mouthguard was not worn can be easily identified.

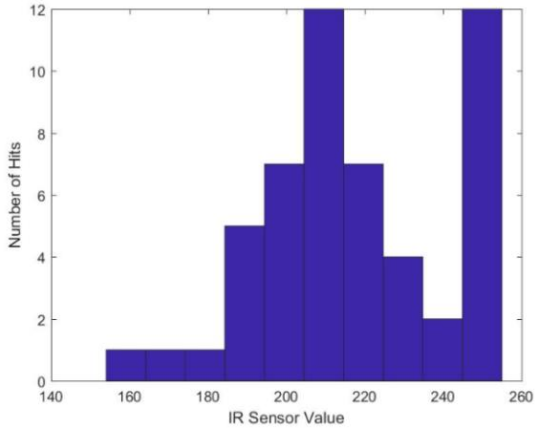

Figure 27: IR History output

Single Event – produces csv files for a single event for applying to a simulation. Figure 29 shows an excerpt from a Single event file output, the left-hand column is the time in milliseconds, with the right-hand column showing the relevant acceleration for the impact chosen. Data here has been formatted so that the units are correct and will allow for direct upload into simulation software

Range – produces an Excel file, shown in Figure 28, this gathers the data for each impact and formats it in a way that is user friendly. It categorises the impacts in terms of direction, elevation, severity and the location on the head where it was received. As well as that, it reports the max resultant linear acceleration, max resultant rotational acceleration and max resultant rotational velocity. The additional sheets in this file have the raw data for each impact recorded.

Severity is divided into 6 categories, which were defined for this study based on the data collected in the first sessions. These categories detailed below first in terms of linear acceleration and then in terms of rotational acceleration. Elevation is split in to 4 categories. While direction is split into 7 categories, with the vertical axis of the mouthguard being 0° and rotating around the head counter-clockwise.

Linear Acceleration (g):

1. Low: 10 – 30g
2. Moderate: 30 – 60g
3. Serious: 60 – 90g
4. Very Serious: 90 – 120g
5. Severe: 120 – 150g
6. Very severe: 150 – 400g

Rotational Acceleration (rads/s^2):

1. Low: 0 – 5000
2. Moderate: 5000 – 10000
3. Serious: 10000 – 15000
4. Very Serious: 15000 – 20000
5. Severe: 20000 – 25000
6. Very severe: 25000 and above

Elevation:

1. Top: The crown of the head
2. Upper: The top half of the head
3. Lower: The lower half of the head
4. Neck: The neck

Direction:

1. Front: -45° to 45°
2. Front Left: 45° to 90°
3. Left: 90° to 135°
4. Back Left: 135° to 180°
5. Back: 180° to -135°
6. Back Right: -135° to -90°
7. Right: -90° to -45°

1	BITE E452466D6516													
2	Day	Month	Year											
3	14	7	2018											
4	Threshold set to		0											
5														
6	Hit number	Hour	Minute	Sec	IR value	Max Result Linear Accel	Max Result Rotational Accel	Max Result Rot Vel	Rot Angle	Elev Angle	Impact	Sector	Elev	
7						g	rad/s/s	rad/s	Degrees	Degrees				
8	1	18	9	2	149	27.25220212	2985.768754	10.67196157	277.463985	10.71284431	Low	R	Upper	
9	2	18	20	34	156	58.28821296	5930.199408	24.94856172	216.9505719	39.19135825	Moderate	BR	Upper	
10	3	18	20	35	155	26.16035811	3096.008901	7.540171868	246.9411963	-12.16580752	Low	BR	Lower	
11	4	18	26	51	150	9.846641029	808.2367695	1.810023407	31.83403251	-6.532078433	NaN	FL	Lower	
12	5	18	34	19	154	45.31420739	4517.883378	11.0886499	12.1207512	-43.29092529	Moderate	F	Lower	
13	9	18	34	22	127	36.85772693	4005.25059	12.57224737	5.449009316	-33.10517477	Moderate	F	Lower	
14	10	18	34	24	130	15.51540189	1614.707343	4.924981557	344.2743279	-39.44666052	Low	F	Lower	
15	11	18	36	27	146	68.57422513	7011.354932	16.15566693	150.731011	37.28313776	Serious	BL	Upper	
16	12	18	37	13	181	80.89116231	7881.388727	20.62632698	115.6928959	35.55756426	Serious	BL	Upper	
17	13	18	38	31	163	61.90924671	5608.320922	12.25330377	128.3994603	34.16613006	Serious	BL	Upper	
18	14	18	42	15	172	42.75055248	4152.7396	16.51740561	91.70072876	20.31468564	Moderate	L	Upper	
19	15	18	45	25	232	8.709661659	235.4300876	5.05938155	159.1933349	81.72477337	NaN	B	Top	
20	16	18	45	26	237	10.77387952	938.4855439	4.04356081	274.5505937	24.09692914	Low	R	Upper	
21	17	18	45	58	188	67.34205116	6329.662432	21.19610935	136.9902524	49.56492691	Serious	BL	Top	
22	18	18	46	20	160	44.16913422	5118.91843	12.16396293	314.0298065	-29.2805682	Moderate	FR	Lower	
23	19	18	46	46	191	5.358308961	745.7187004	11.57636037	35.44288241	13.61610313	NaN	FL	Upper	
24	20	18	49	11	229	6.208362414	1208.426369	8.513186661	340.7952152	-18.02470926	NaN	F	Lower	
25	21	18	50	16	153	53.66002621	5697.336434	12.63015344	337.2930943	-38.7864297	Moderate	FR	Lower	
26	22	18	51	57	189	8.538820328	374.9236109	7.931255976	86.49193482	3.142944082	NaN	L	Upper	
27	23	18	52	37	231	4.778080369	571.5744308	2.364942179	73.86557897	9.493688381	NaN	L	Upper	
28	24	18	53	22	190	30.30732317	2725.512678	7.049702018	141.418858	54.928384	Moderate	BL	Top	
29	25	18	54	6	156	34.4403022	3334.222876	7.074386745	149.0329811	30.37229699	Moderate	BL	Upper	
30	26	18	59	49	241	27.56771873	1433.388199	13.60422024	63.56362569	-5.410347733	Low	FL	Lower	
31	27	19	2	23	190	71.3040455	7011.965408	22.61067712	127.2722457	46.16301093	Serious	BL	Top	
32	28	19	6	2	182	69.99346879	8096.226772	24.006959	118.3664694	38.71673904	Serious	BL	Upper	
33	29	19	9	0	175	48.06895321	4567.645504	14.02166827	146.1187422	53.18634965	Moderate	BL	Top	
34	30	19	13	17	151	55.48898903	5271.47769	11.36592845	51.7658094	-32.2548214	Moderate	FL	Lower	
35	31	19	13	20	151	48.92153313	4674.265656	9.182641962	31.97080583	-40.14198373	Moderate	FL	Lower	
36	32	19	14	0	159	40.50160681	4805.533546	21.12545824	78.15505755	-38.47942906	Moderate	L	Lower	

... | 51 | 52 | 53 | 54 | 55 | 56 | 57 | 58 | 59 | 60 | 61 | 62 | 63 | 65 | 66 | 67 | 68 | 69 | summary

Figure 28: Example of Range data output

1	-0.049	-1.56E-05
2	-0.048	-1.21E-05
3	-0.047	-1.42E-05
4	-0.046	-1.47E-05
5	-0.045	-1.63E-05
6	-0.044	-2.01E-05
7	-0.043	-2.21E-05
8	-0.042	-2.24E-05
9	-0.041	-2.28E-05
10	-0.04	-2.42E-05
11	-0.039	-2.47E-05
12	-0.038	-2.34E-05
13	-0.037	-2.32E-05
14	-0.036	-2.43E-05
15	-0.035	-2.46E-05
16	-0.034	-2.32E-05
17	-0.033	-2.16E-05
18	-0.032	-2.32E-05
19	-0.031	-2.77E-05
20	-0.03	-2.78E-05
21	-0.029	-2.15E-05
22	-0.028	-1.63E-05
23	-0.027	-1.40E-05
24	-0.026	-1.26E-05
25	-0.025	-1.14E-05
26	-0.024	-1.02E-05
27	-0.023	-8.11E-06
28	-0.022	-5.23E-06
29	-0.021	-4.05E-06
30	-0.02	-1.58E-06
31	-0.019	8.19E-06
32	-0.018	1.76E-05
33	-0.017	1.62E-05
34	-0.016	9.10E-06
35	-0.015	5.34E-06
36	-0.014	4.39E-06

RX

Figure 29: Example of Single event data output

3.2.6 Video Review

Prior to reviewing the footage, it may be necessary to add a timestamp to the recorded video footage. This is achieved with Visual MP4/MOV Time Stamp (vMTS or vMTS64), a free piece of software that allows for the timestamping of video footage [114]. The exact time of the start of the fight is recorded, an atomic clock is shown in the recorded footage and this known time is then used to timestamp the footage.

Review of video footage is conducted with Kinovea, a video player with such features as the ability to slow down footage, make measurements and annotate [115]. Designed for use in the sports industry, it is free to download and is fully open source. Videos taken during sparring/competition are loaded into the player and it allows the user to move through the footage frame by frame. Figure 30 shows an example of a confirmed impact, with the timestamp from the video shown and the corresponding impact from the mouthguard.

Figure 30: Impact viewed through Kinovea video player

Threshold set to			140										
Hit number	Hour	Minute	Sec	IR value	Max Result Linear Accel	Max Result Rotational Accel	Max Result Rot Vel	Rot Angle	Elev Angle	Impact	Sector	Elev	
44	11	40	23	209	15.59322202	775.2689841	9.000907412	8.993497863	13.86289071	Low	F	Upper	

Figure 31: Impact confirmed using Kinovea

In Figure 30, the participant wearing the mouthguard is on the right, in black and yellow shorts. As can be seen, the impact occurs at 12:40:23; it is received to the front of the face and is in the upper part of the head. This matches the data recorded by the mouthguard, shown in Figure 31. Unfortunately, the mouthguards do not take daylight savings into account, so it is up to the user to take this difference into account when reviewing footage. All impacts reported have been video confirmed in this manner.

It should be noted that video footage reviewed with Kinovea is not used to confirm any acceleration values recorded in this study, it is only used to confirm the impact time, direction, and location.

3.3 Statistical Techniques

In order to determine the best predictors for mTBI diagnoses and strain in the regions of interest, two statistical techniques will be used. The first is examining whether any single input is a good predictor for strain in the regions of interest. This has been achieved by comparing the levels of one input, peak linear acceleration for example, and graphing it against one of the outputs, MPS in the corpus callosum for example. Once the input and output have been graphed against each other, a linear trendline is added. This trendline is created using Microsoft Excel's in-built linear trendline function, an example of one of these graphs is shown in Figure 32.

The results in Figure 32 are split into 3 types; the blue diamonds are impacts from sessions that did result in a concussion diagnosis, the orange squares are from sessions that did not. The blue line indicates the linear trendline for the mTBI sessions, the orange line for the no injury sessions. A further black line is included, which demonstrates the linear relationship between input and output for all the simulated impacts. Each trendline has an r^2 value associated with it. r^2, also known as the co-efficient of determination, is a measure of how much of the variance in the output can be explained by the input. In Excel, r^2 is calculated using Equation 5.

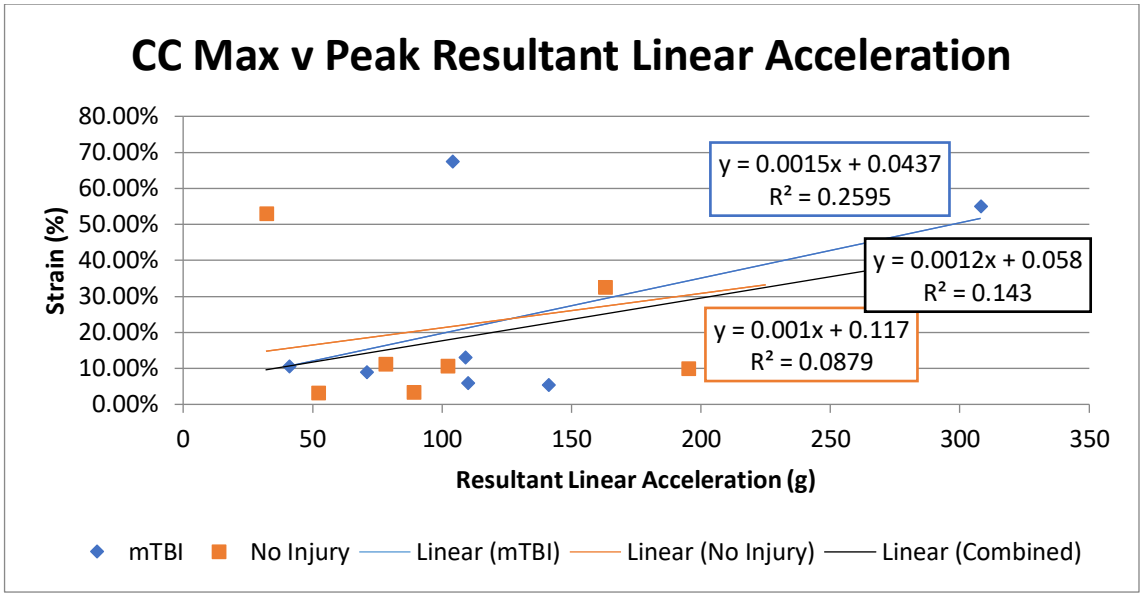

Figure 32: Example of Graph to Investigate Linear Relationship between Input and Output

Equation 5: Calculation of r^2 in Excel

$$r = \frac{\sum(x - \overline{x})\,(y - \overline{y})}{\sqrt{\sum(x - \overline{x})^2\,(y - \overline{y})^2}}$$

From Figure 32 we can see that for the combined data set, all simulated impacts, r^2 is 0.143 or 14.3%. This indicates that peak resultant linear acceleration can account for approximately 14% of the variance in MPS in the corpus callosum. This technique will be used to examine the predictive qualities of all model inputs. As this function can only take a single input into account and the fact that in this study several inputs are being examined, a more sophisticated technique will also be employed.

The 2nd statistical technique employed is a Best Subset Regression analysis. This is a type of analysis that is conducted through the Mintab, a statistical software tool developed by the State College in Pennsylvania, U.S.A. A Best Subsets regression analysis is used to create models from the chosen inputs and outputs, allows the comparison of these models and outputs some statistical values to determine which is the best model. An example of a Best Subset analysis is shown in Figure 33. The response (output) being investigated is listed at the top, while listed vertically are the predictors (inputs). Each new line shows the best model for that number of predictors, with the predictors in that model being denoted by the x, until the best model for the total number of predictors has been reached.

Response is CC Max

Vars	R-Sq	R-Sq (adj)	R-Sq (pred)	Mallows Cp	S	PLA	PLAX	PLAY	PLAZ	PRAX	PRAY	PRAZ	Duration	PnearRat	Duration	PRVal	HIP
1	31.9	27.7	17.0	-5.5	0.18851								X				
1	31.5	27.2	10.4	-5.4	0.18918			X									
2	49.0	42.2	29.9	-5.6	0.16857			X								X	
2	43.3	35.8	14.4	-4.9	0.17766			X									X
3	51.5	41.1	12.1	-4.0	0.17007		X	X									X
3	51.4	41.0	15.5	-3.9	0.17026		X	X								X	
4	54.5	40.4	13.4	-2.3	0.17108		X	X								X	X
4	54.5	40.4	19.2	-2.3	0.17109		X	X	X							X	
5	55.4	36.9	9.1	-0.4	0.17615		X	X	X							X	X
5	55.4	36.8	0.0	-0.4	0.17628	X	X		X	X						X	
6	57.8	34.9	0.0	1.3	0.17893	X	X		X	X				X		X	
6	56.7	33.1	0.0	1.4	0.18130	X			X	X		X		X		X	
7	58.3	29.1	0.0	3.2	0.18664	X	X		X	X				X	X	X	
7	58.1	28.7	0.0	3.2	0.18721	X	X		X	X	X			X		X	
8	58.7	21.9	0.0	5.2	0.19587	X	X		X	X	X			X	X	X	
8	58.5	21.7	0.0	5.2	0.19619	X	X		X	X	X	X		X		X	
9	59.3	13.5	0.0	7.1	0.20622	X	X		X	X	X	X		X	X	X	
9	59.1	13.0	0.0	7.1	0.20675	X	X		X	X	X	X		X		X	X
10	59.5	1.7	0.0	9.1	0.21984	X	X	X	X	X	X	X		X		X	X
10	59.4	1.4	0.0	9.1	0.22014	X	X		X	X	X	X	X	X	X	X	
11	59.7	0.0	0.0	11.0	0.23702	X	X	X	X	X	X	X		X	X	X	X
11	59.6	0.0	0.0	11.0	0.23715	X	X	X	X	X	X	X	X	X	X	X	
12	59.9	0.0	0.0	13.0	0.25871	X	X	X	X	X	X	X	X	X	X	X	X

Figure 33: Example of Best Subset Analysis Output

On the left, each column represents a statistical measure, they are:

- R-Sq: How well the input models the output, a general measure of goodness of fit.
- R-Sq (Adj): An adjusted R-Sq value which can take multiple predictors into account. R-Sq (adj) will continue to increase until the addition of a new predictor does not improve the model by more than chance.

- R-Sq (pred): A further adjusted R-Sq value, calculated by removing each output data point systematically, recalculating the regression equation without that data point and then determining how well it would have predicted the removed data point.
- Mallows C_p: A measure that can be used to determine the fit of the model, a value close to the number of predictors plus 1 or a small number indicates a relatively precise model.
- S: The Standard error of Regression, a measure of the average distance between the output values and the regression line. Smaller values for S are better, units are the same as the units for the response (output).

In the example shown in Figure 33, the model that would be chosen as the best would be 2 predictors, PLA Y and PRV. This model is the point at which R-Sq (adj) begins to fall and has the lowest value for S. This method of choosing the best models for prediction will be used throughout.

When data from session types, or injury types, is presented it will be shown in a Box and Whisker plot. This technique is employed as it shows the full range of the data, includes the mean, median, 1st quartile, 3rd quartile, local maximum and outliers. An example of this graph type is shown in Figure 34. The variables are defined in Table 13.

Table 13: Box and Whisker plot variable definitions

Variable	Definition
Mean	The average of all impacts
Median	50% of data is greater than this
1st Quartile	25% of data is less than this
3rd Quartile	25% of data is greater than this
Minimum	Lowest value, excluding outliers
Local Maximum	Greatest value, excluding outliers
Outlier	Greater than 3/2 times the 3rd quartile OR less than 3/2 times 1st quartile

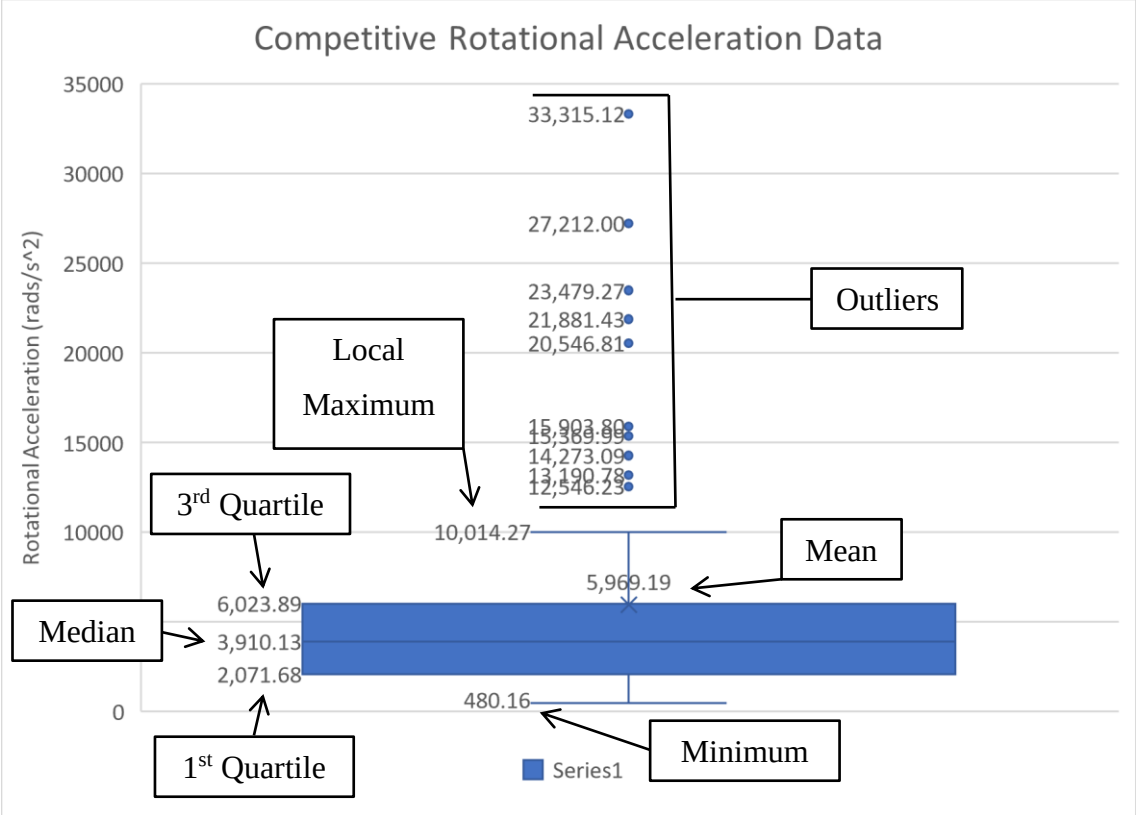

3.4 Study Design Summary

In this chapter the processes developed for manufacturing, cleaning/handling, operating and programming the mouthguards have been detailed. Further processes for collecting and reviewing data were also developed and detailed. It is these processes that ensure any impact considered for simulation has been confirmed by cross referencing the collected mouthguard data with the recorded video data. Confirmed impacts then will be examined and processed in order to output 6 DoF data for input into the FE model simulation. Simulations require inputs of linear acceleration in the x, y and z. As well as rotational acceleration in the x, y and z. All confirmed impacts have 200ms of data points for each of the 6 DoF. This process will be detailed further in the next chapter.

The statistical techniques employed have also been detailed, with the values being used to determine the best predictors being defined. These techniques will be utilised in the upcoming results chapters.

Chapter 4 Computational Setup

4.1 Introduction

LS-Dyna, was used in this study to run simulations on the GHBMC model, discussed in Chapter 2. This chapter will cover the computational setup, the loading conditions used within the solver, and the model arrangement.

Ls-Dyna is a multi-purpose programme used for finite element model simulations, it is made up of 3 sections; a pre-processing environment, an explicit solver and a post-processing environment. It has functions that are applicable in many industries including automotive, military, manufacturing and bio-engineering to name but a few. It is capable of highly non-linear and dynamic finite element analysis, allowing for dynamic boundary conditions and large deformations and is particularly suited to high speed, short duration events.

LS-PrePost is a pre and post processor that is a part of Ls-Dyna, it has been used in this study to setup simulations, i.e. - applying boundary/loading conditions, and to analyse simulation results. Some of the features available in Ls-PrePost are listed below.

Pre-processing:

- Meshing Tools – surface, solid, tool, 2d, tet, block and mesh morphing
- Metal Forming
- Roller Hemming
- Airbag folding
- Dummy positioning
- Model Checking

Post-processing:

- Results animation
- Fringe Plotting
- ASCII Plotting
- Particle/Fluid Visualisation

4.2 Virtual Machine

Simulations were run using an Amazon Web Service (AWS) virtual machine, supplied by CADFEM UK & Ireland. The instance used was a standalone Linux Cluster Head Node, using Ansys 19.0. The instance type was a c5.18xlarge with 36 cores, 144GB Ram and a 3.0GHz Intel Xeon Platinum 8124M. This instance costs approximately $3.456/Hr, in order to keep these costs at a minimum spot pricing was used. This brought the cost down to $1.24/Hr. Each simulation took approximately 2 to 3 hours to run, meaning the cost per simulation was approximately $2.48 to $3.72, depending on the total run time.

4.3 Model and Mouthguard Planes and Axes

In order to ensure mouthguard output data is in the same frame of reference as the model, the positive direction in each axis and plane was found. This was then compared to the known positive direction the mouthguards record. The model and mouthguard positive directions are detailed in the following sections. Figure 34 details the standard anatomical planes and axes [18].

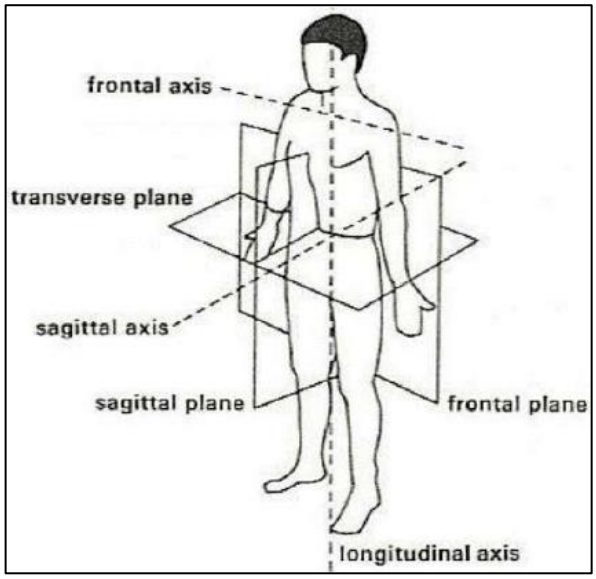

Figure 34: Anatomical regions of the human body [18]

4.3.1 Mouthguard Planes and Axes

- X axis (sagittal axis) linear positive direction: posterior to anterior
- Y axis (frontal axis) linear positive direction: right to left
- Z axis (longitudinal axis) linear positive direction: inferior to superior

4.3.2 Model Planes and Axes

- X axis (sagittal axis) linear positive direction: posterior to anterior
- Y axis (frontal axis) linear positive direction: left to right
- Z axis (longitudinal axis) linear positive direction: superior to inferior

As there is a difference in linear positive directions between the model and mouthguards, the mouthguard linear outputs in the Y and Z directions are inverted prior to applying them to the model. Positive directions of rotation are about the axes from which they are defined. i.e. – positive X rotation is clockwise about the X axis (sagittal axis) when viewing the axis in the positive linear direction. The mouthguard and model agree in the directions of positive rotation; therefore, no changes are made to these outputs.

4.4 Model Loading Conditions

The method for applying the loads to the head and neck model is as follows.

1. Define the load curves
2. Apply the loads
3. Define the Local Coordinate System
4. Define the Boundary Conditions

4.4.1 Define Load Curves

The keyword manager in LS-PrePost is used to define the data for the loads to be applied, as shown in Figure 36. From the toolbar on the right the keyword manager button is selected, the “Define” card is expanded and the “Curve” dialog box is opened. Shown in Figure 35 is the Curve dialog box.

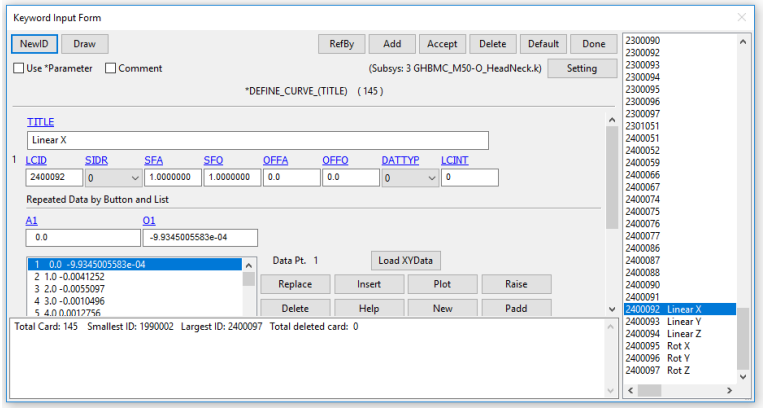

Figure 35: Curve dialog box in LS-PrePost

6 curves are added for each of the degrees of freedom that the mouthguards record; linear x, y and z and rotational x, y and z. The format for this data is comma separated values (CSV), with each data point representing a 1ms time-step. Each curve is given a unique name and load curve id (LCID), this LCID is then used in the boundary conditions to apply the load.

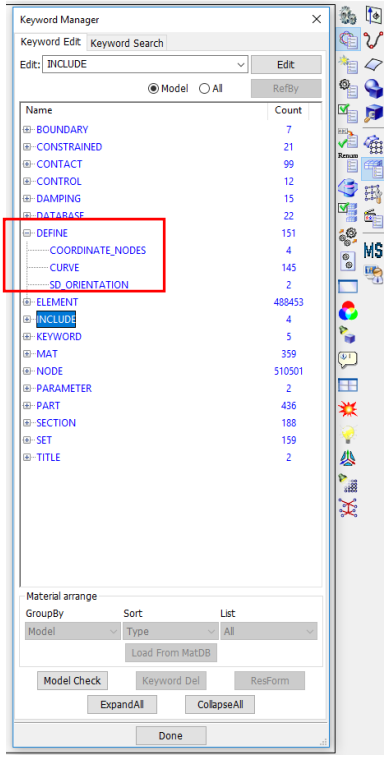

Figure 36: Keyword Manager in LS-PrePost

4.4.2 Applying the Loads

The GHBMC skull is not a rigid part, so loads cannot be applied to it directly. Therefore, an alternative method for applying loads and constraining the motion to the head CoG must be used. The method developed was:

- Head CoG is tied to the Neck Muscle Activation Plate (part id 2090001) which is a rigid part.
- Load is applied to the Neck Muscle Activation Plate using the local co-ordinate system of the head CoG node.
- *BOUNDARY_PRESCRIBED_MOTION_RIGID_LOCAL* is used to apply the loads, it uses the co-ordinate system associated with the rigid body that the loads are applied to.
- Motion of the loads is then driven about the head CoG node.

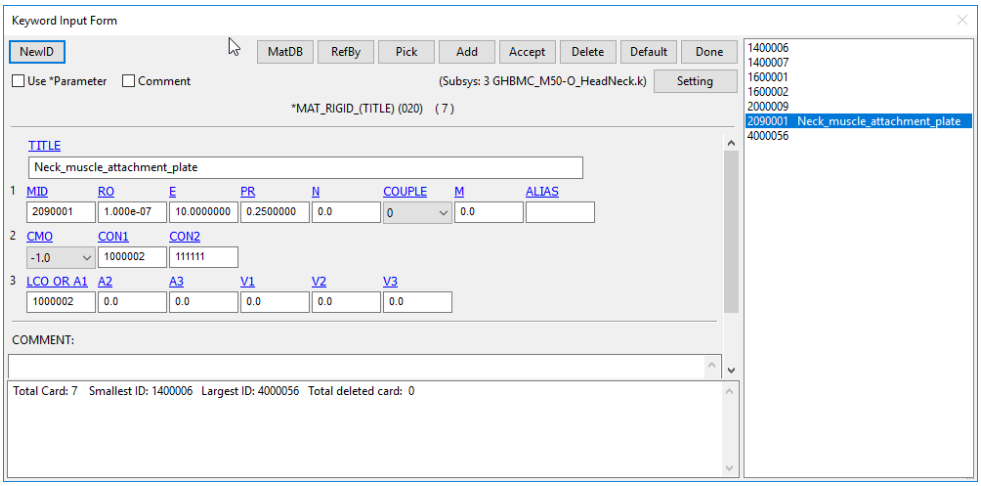

Figure 37: Mat card in LS Pre-Post

4.4.3 Defining the Local Coordinate System

Figure 37 is the LCO option, this is where the local coordinate system for the outputs can be defined. The node ID shown, 1000002, is the head CoG. CMO is set to -1.0; this tells the programme that constraints are applied in the local directions. CON1 defines the local coordinate system for which the motion will be based; again, this is the head CoG. CON2 represents the constraints on the motion, with each number representing a degree of freedom. 100000 is linear X only and 111111 is linear X, Y, Z, and rotational X, Y and Z.

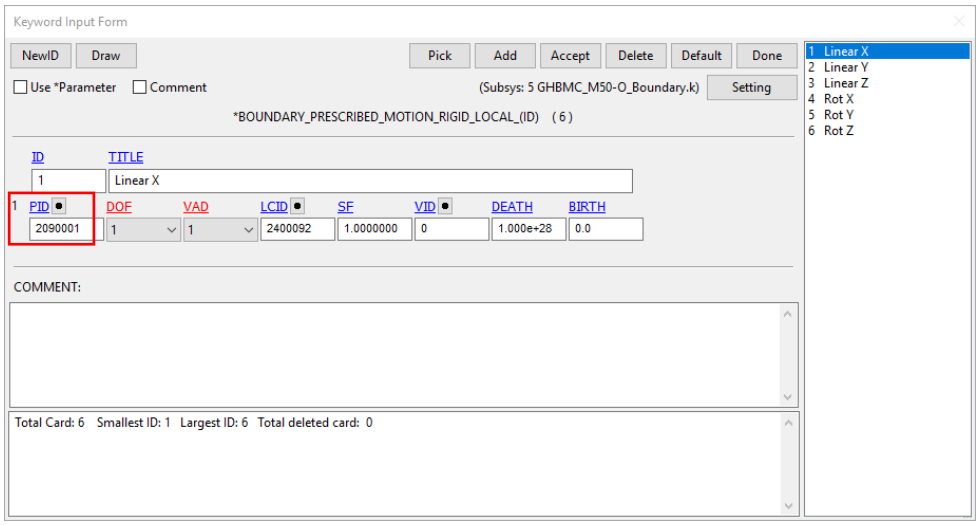

Figure 38: Boundary Keyword card in LS Pre-Post

4.4.4 Defining the Boundary Conditions

Once the coordinate system and constraints have been defined for this part, the loads in the "Boundary" keyword option can be defined. This is shown in Figure 38. The highlighted red box shows the rigid part the loads are being applied to, in this case part ID 2090001, which is the "Neck Muscle Activation Plate". DOF option defines the degree of freedom for the applied loads, for this load curve it is linear X. With linear X being 1, linear Y being 2 and so on. VAD defines whether we are applying a velocity, acceleration or displacement. With 0 being velocity, 1 being acceleration and 2 being displacement. Part ID, degree of freedom and type of load we are applying for each load curve can be defined. Once this is complete, the simulation can be run.

4.5 Running a Simulation

As discussed in the Virtual machine section above, simulations were run in a Linux based virtual machine. The setup described in the above Model Loading Conditions section is conducted on a local machine, in order to keep the cost per simulation down. Once a cluster has been created and a connection has been made the simulations can be run.

Files are copied from the local machine to the virtual machine. Then using the console commands, a simulation can be started. First the directory that the files are in must be located; in this case it is the Documents folder. An example of the console command to run a simulation is shown below.

```
lsdyna192 i=GHBMC_M50-O_Main.dyn ncpu=36 memory=100m
```

Where:
lsdyna192: specifies the LS-Dyna solver
i: is the file to run
ncpu: is the number of cores to use
memory: indicates the amount of memory allocated to run the simulation

Running this command in the console will begin the simulation. The total time of the simulation depends on the number of timesteps defined. The timestep for the output of results is 1 ms. Assuming no errors, the simulation will finish after the last timestep and will respond with “Normal Termination”. This generates several output files, which can then be transferred to the local machine for analysis.

4.6 Model Material Models

In an earlier section we discussed three separate materials model that are used in the GHBMC brain model parts; elastic, piecewise and viscoelastic. We will examine these material models and define how they calculated in this section.

Elastic Material Model

An isotropic elastic material model. The co-rotational rate of the deviatoric Cauchy stress tensor is calculated by:

$$s_{ij}^{\Delta^{n+\frac{1}{2}}} = 2G\dot{\varepsilon}'^{n+\frac{1}{2}}_{ij}$$

Equation 6: Elastic Material Model Stress Formula [116]

And the pressure by:

$$p^{n+1} = -K\ ln\ V^{n+1}$$

Equation 7: Elastic Material Model Pressure Formula [116]

Where: G is the Elastic Shear Modulus
K is the Bulk Modulus
V is the relative Volume

Viscoelastic Material Model

A classical Kelvin-Maxwell material model for viscoelastic bodies. The shear relaxation behaviour is described by Equation 1 above. A Jaumann rate of stress formulation is used:

$$s'^{\nabla}_{ij} = 2\int_0^t G(t-\tau)\,\varepsilon'_{ij}\,(\dot{\tau})dt$$

Equation 8: Viscoelastic Material Model Jaumann Rate of Stress Formula [116]

Where the prime denotes the deviatoric part of the stress rate s'^{∇}_{ij} and $\varepsilon'_{ij}$is the deviatoric stress rate.

The evolution of the stress for the Kelvin model is given by:

$$\dot{s}_{ij} + \frac{1}{\tau} s_{ij} = \left(1 + \delta_{ij}\right) G_0 \varepsilon'_{ij} + \left(1 + \delta_{ij}\right) \frac{G_\infty}{\tau} \varepsilon'_{ij}$$

Equation 9: Viscoelastic Material Model Stress Evolution Formula [116]

Where: δ_{ij} is the Kronecker delta

G_0 is the instantaneous shear modulus

G_∞ is the long-term shear modulus

τ is the decay constant

Pressure is calculated from the bulk modulus and volumetric strain:

$$p = -K\varepsilon_v$$

Equation 10: Viscoelastic Material Model Pressure Formula [116]

Where:

$$\varepsilon_v = \ln\left(\frac{V}{V_0}\right)$$

Equation 11: Viscoelastic Material Model Volumetric Strain Formula [116]

This defines the logarithmic volumetric strain. The Bandak calculation for the total strain tensor for output uses an incremental rate based on the Jaumann rate:

$$\varepsilon_{ij}^{n+1} = \varepsilon_{ij}^{n} + r_{ij}^{n} + \overset{\nabla\, n+\frac{1}{2}}{\varepsilon_{ij}} \Delta t^{n+\frac{1}{2}}$$

Equation 12: Viscoelastic Material Model Bandak Total Strain Tensor Formula [116]

Where:

$$\Delta\varepsilon_{ij}^{n+1} = \dot{\varepsilon}_{ij}^{\,n+\frac{1}{2}} \Delta t^{n+\frac{1}{2}}$$

And r_{ij}^{n} gives the rotation of the strain tensor at time $t\ t^n$ to the configuration at t^{n+1}

$$r_{ij}^{n} = \left(\varepsilon_{ip}^{n}\ \omega_{pj}^{\,n+\frac{1}{2}} + \varepsilon_{jp}^{n}\ \omega_{pi}^{\,n+\frac{1}{2}}\right) \Delta t^{n+\frac{1}{2}}$$

Piecewise Material Model

This material model gets its name piecewise due to the fact that 8 pairs of values for the Plastic Strain and Yield Stress can be defined in order to approximate a realistic non-linear stress-strain behaviour by way of a set of linear segments. It can also take strain rate effects in to account [116]. The pressure (p), deviatoric strain rate ($\dot{\varepsilon}'_{ij}$), deviatoric stress rate (s_{ij}) and volumetric strain rate ($\dot{\varepsilon}_v$) are defined in the following set of equations [116]:

$$p = -\frac{1}{3}\sigma_{ij}\delta_{ij}$$

$$\dot{\varepsilon}'_{ij} = \dot{\varepsilon}_{ij} - \frac{1}{3}\dot{\varepsilon}_v$$

$$s_{ij} = \sigma_{ij} + p\delta_{ij}$$

$$\dot{\varepsilon}_v = \dot{\varepsilon}_{ij}\delta_{ij}$$

Deviatoric stresses must satisfy the following set of equations for the yield function:

$$\phi = \frac{1}{2}s_{ij}s_{ij} - \frac{\sigma_y^2}{3} \leq 0$$

Equation 13: Piecewise Material Model Yield Function [116]

Where:

$$\sigma_y = \beta\left[\sigma_0 + f_h\left(e^p_{eff}\right)\right]$$

If the deviatoric stresses are calculated and the yield function is satisfied, then those values are accepted. Otherwise, an incremental increase in plastic strain is calculated by:

$$\Delta\varepsilon^p_{eff} = \frac{\left(\frac{3}{2}s^*_{ij}s^*_{ij}\right)^{\frac{1}{2}} - \sigma_y}{3G + E_p}$$

4.7 Computational Outputs

As discussed in earlier sections, the main FE based predictor being investigated in this study is Maximum Principal Strain (MPS). Here the method of measuring this model output will be detailed. The type of strain used in LS-PrePost is Green-St. Venant Strain, which has been discussed in earlier sections. Once a simulation has been run and finished without errors, it is then possible to examine the results. This is achieved by opening a Binary Plot file, which the software outputs upon completing a simulation. The Binary Plot file allows for many different variables to be viewed graphically, it also allows for selecting your variable and stepping through each timestep to view the calculated results. Also being investigated is Mean Adjacent Strain (MAS), which was defined in an earlier chapter. It is the mean maximum principal strain of all elements adjacent to the element in which the maximum occurred.

4.7.1 Maximum Principal Strain

Shown in Figure 39 is the first screen upon opening of a binary plot file, with 1st principal strain chosen as the variable and time at 0. Using the buttons at the bottom, it is now possible to step through the entire simulation, moving forward in increments of 1ms. Simulations will all be run for 50ms, therefore there are 50 timesteps to view for each simulation. Each region of interest will be examined across the entire simulation in order to determine the MPS in that region. The values for each will be recorded and analysed. An example of the method of examining and recording the MPS in a region will now be shown.

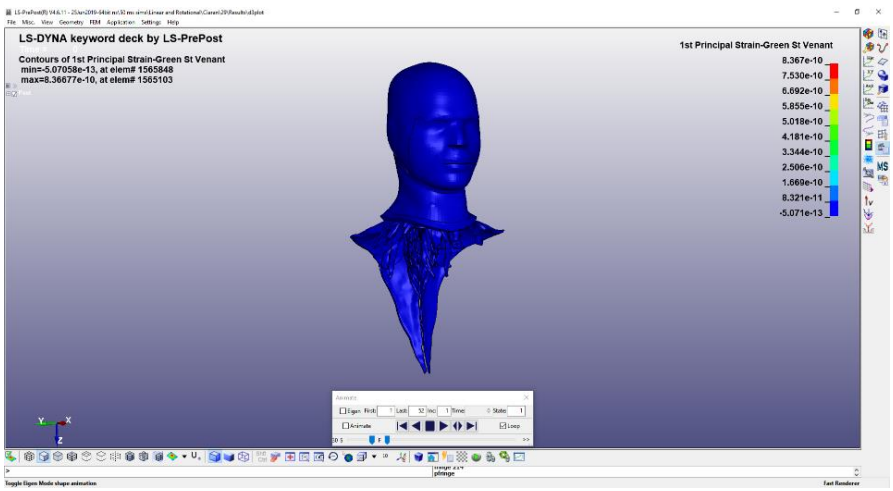

Figure 39: LS-PrePost Binary Plot

First to determine the MPS in a region, the region must be isolated. This is easily achieved using the software. Figure 40 shows an isolated Corpus Callosum, with 1st principal strain selected as the variable and time at 0.

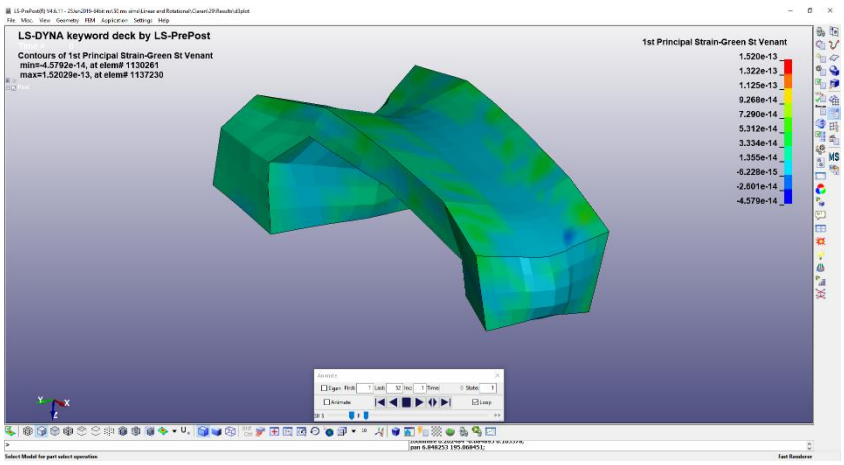

Figure 40: LS-Prepost Corpus Callosum

Now the time is advanced by 1ms and the MPS in any element in the region is shown. The simulation is then advanced through the full 50 steps and the MPS is recorded, Figure 41 shows the step at which the maximum was reached for this example. In the top right of the screen, the maximum and minimum 1st principal strain for this step is shown. The element in which the maximum was reached is indicated by the black arrow. This process is the repeated for each of the other regions of interest; midbrain, thalamus and brain stem. The MPS in each region is recorded and will be compared to the published injury thresholds in a later chapter.

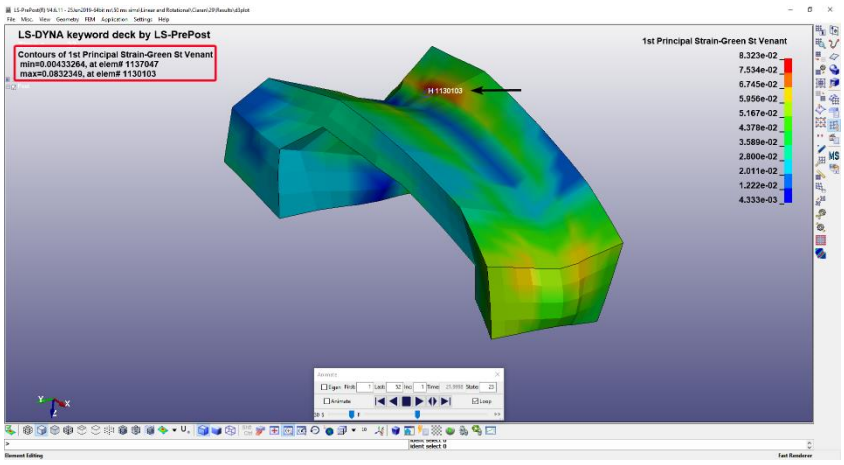

Figure 41: Ls-PrePost Corpus Callosum MPS Example

4.7.2 Mean Adjacent Strain

The process for determining the MAS for a region of interest follows on from the previous section. Once the MPS has been determined for the region, it is then possible to utilise the software to select any element adjacent to the one in which the maximum was reached. Figure 42 shows this.

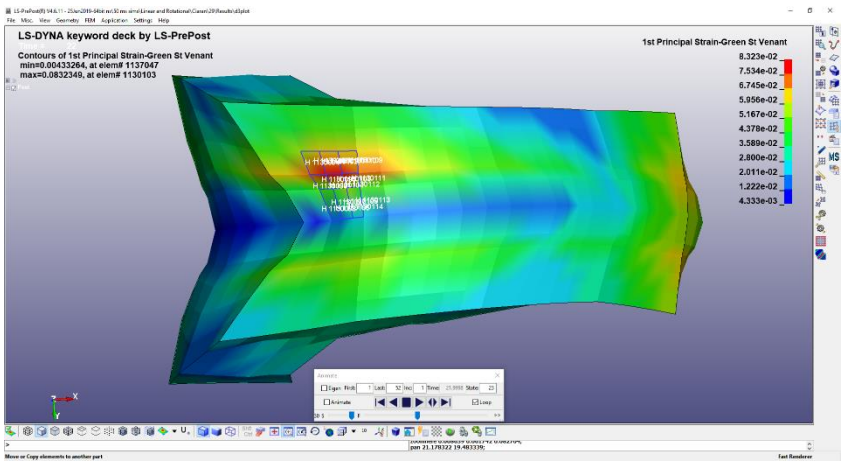

Figure 42: LS-PrePost Mean Adjacent Strain

Once the adjacent elements have been selected, it is then possible to plot and output the strain in these elements for the entire simulation. It is then important to take note of the time at which the maximum has occurred, as this is needed in order to find the values for each adjacent element at the same time. In the example shown in Figure 42, the maximum occurs at time step 23. The strain for each of the highlighted elements at time step 23 is recorded and the mean is determined. The MAS for each region will be calculated and recorded, in a later chapter it will be compared to published injury thresholds.

4.8 Computational Setup Summary

In this chapter the methods for setting up the computational simulations were detailed. This includes the virtual machine setup, run time and costs. Defining the planes and axes, as well as the direction of positive motion/rotation. The method for defining the model inputs (x, y and z linear and rotational), applying the inputs to the FE model and constraining the motion of the model were explained. The methods for calculating the FE based brain injury predictors, MPS and MAS, was also detailed. This data represents the model outputs and as such, the main variables that will be investigated in this study.

Chapter 5 Head Acceleration Results

5.1 Introduction

This chapter will report all video confirmed impacts from all sparring sessions and competitive events that were attended. Twenty-two participants in total have signed up to this study and there have been 13 sparring sessions and 8 competitive events during which data was collected. The participants will be referred to as Fighter 1, Fighter 2 etc. Fighter 1 is always the same participant; they will retain this title throughout. Ethical approval was granted by the Institute of Technology Tallaght Ethics Committee (REC-STF1-201819).

Data will be reported first by session type, as detailed below. Then sessions that resulted in an mTBI diagnosis will be compared to those that did not. Finally, the full data set will be analysed in terms of impact frequency and impact duration.

MMA Sparring

MMA Sparring sessions are typically 3 rounds of 5 minutes each and take place in an official MMA cage, in the gym where the participants train. The entire sessions were video recorded and timestamped to allow for the confirmation of any impact recorded.

Boxing Sparring

One of the participants was preparing for a boxing fight and thus 4 sessions of boxing sparring data were collected. This will be reported separately to MMA sparring sessions as the round length and number of rounds differed.

MMA Training

One participant took part in what can be best described as a long training session, as opposed to the more regimented sparring sessions described above. This training session took place over almost 2 hours and was essentially a series of training fights. This data will also be reported separately.

Competitive Events

Both professional and amateur competitive bouts took place at large MMA events. They are typically 3 rounds of 5 minutes. Although the fight may be shorter if the participant loses. Video footage is also recorded at these events, although professional video may also be available from video streaming services. It is imperative that the precise start time of the fight is known. This allows for recorded impact data to be aligned to timestamped video.

Impact direction is specified as front, right, left and back as shown in Figure 43.

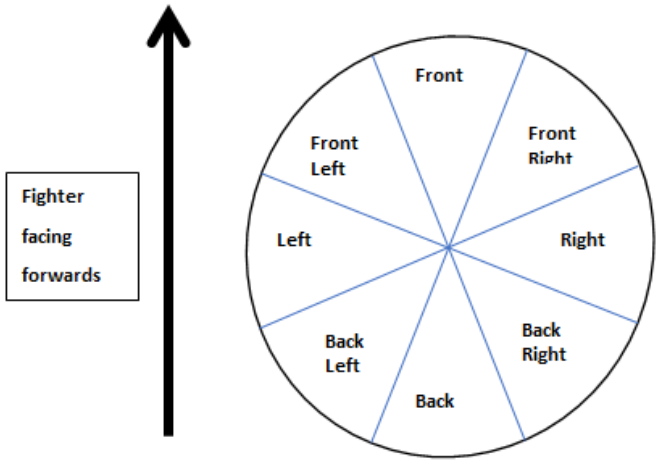

Figure 43: Sectors for Impact Directions

Table 14 summarises the sessions from which data was recorded sorted by the fighter and the session type.

Table 14: Summary of sessions attended by sorted fighter

Fighter	Competitive Bouts	MMA Sparring Sessions	MMA Training	Boxing Sparring Sessions
Fighter 1	1	0	0	0
Fighter 2	1	2	0	0
Fighter 3	2	2	0	0
Fighter 4	2	0	0	0
Fighter 5	1	2	0	0
Fighter 6	1	0	0	0
Fighter 7	0	1	0	0
Fighter 8	0	0	1	0
Fighter 9	0	1	0	0
Fighter 10	0	0	0	4
Total	8	8	1	4

5.2 Competitive Bouts

Six participants have taken part in competitive events to date, with fighters 3 and 4 taking part in 2 events each. Therefore, there are 8 competitive bouts from which data has been gathered. Professional bouts are a maximum of three 5-minute rounds, although many end before that. Table 15 details the number of impacts each fighter received during these bouts, the mean linear and rotational accelerations and standard deviations. Fighter 3 – Bout 1 received the fewest number of impacts (3), while Fighter 2 – Bout 1 received the most (18). The mean number of impacts received per competitive bout is 10.5 with a standard deviation of 4.8. Competitive events are required to have medical professionals on site at all times. Table 16 details the post-fight medical diagnoses for each of the fighters.

It is recognised that the standard deviations in these results are very large, sometimes larger than the mean. This is due to the fact that the vast majority of impacts are in the low range, but there are some very high magnitude impacts (outliers) that skew the standard deviation calculation. In order to avoid reporting these standard deviations, box and whisker plots have been employed to better represent the range of impacts received. Table 17 shows the data taken from the box and whisker plots.

Table 15: Summary of Competitive Bout Stats

Fighter	Bout	Total Confirmed Impacts	Linear Acceleration Mean (g)	Standard Deviation (g)	Rotational Acceleration Mean (rads/s^2)	Standard Deviation (rads/s^2)
Fighter 1	Bout 1	13	40.5	37.1	3729.8	4261.9
Fighter 2	Bout 1	18	61.6	67.1	4537.4	4780.2
Fighter 3	Bout 1	3	42	1.4	3173.7	816.4
Fighter 3	Bout 2	7	26.7	10.6	8738.7	7605.4
Fighter 4	Bout 1	11	26.4	8.1	2220	1028.1
Fighter 4	Bout 2	7	80	56.1	8091.5	8296.8
Fighter 5	Bout 1	15	40.2	29	11162.3	9022.1
Fighter 6	Bout 1	10	26.2	13	4167.9	2641.7

Table 16: Competitive Bouts Medical Diagnoses

Fighter	Bout	Win/Loss	Injury
Fighter 1	Bout 1	Lose	mTBI – Migraine aura for 48 hours
Fighter 2	Bout 1	Lose	mTBI – Post event symptoms of vertigo and dizziness
Fighter 3	Bout 1	Lose	mTBI – Transient loss of consciousness < 1 second. No Post-concussion syndrome (PCS)
Fighter 3	Bout 2	Win	No Injury
Fighter 4	Bout 1	Lose	mTBI – Post event/ No PCS
Fighter 4	Bout 2	Lose	No Injury
Fighter 5	Bout 1	Lose	mTBI – Post event/No PCS
Fighter 6	Bout 1	Lose	No Injury

5.2.1 Impact Severity

In Table 17 the mean rotational velocity, linear and rotational accelerations for all competitive bouts are detailed. The mean impact received in competitive bouts is 43.5g and 5969.2 rads/s^2. Only 2 fighters experienced a higher linear mean than this; Fighter 2 – Bout 1 and Fighter 4 – Bout 2. Of those diagnosed with an mTBI, only Fighter 2 – Bout 1's mean peak linear acceleration was greater than the mean for all competitive events. Three fighters; Fighter 3 – Bout 2, Fighter 4 – Bout 2 and Fighter 5 – Bout 1 had a mean rotational acceleration higher than that of the overall mean for all competitive bouts. Of these, only Fighter 5 was diagnosed with an mTBI.

Table 17: Competitive Bouts stats summary

Competitive Bouts	Mean	Median	1st Quartile	3rd Quartile	Local Maximum
Linear Acceleration (g)	43.53	31.83	19.78	44.34	81.11
Rotational Acceleration (rads/s^2)	5969.19	3910.13	2071.68	6023.89	10014.27
Rotational Velocity (rads/s)	18.22	14.65	11.55	20.64	33

Tables 18, 19 and 20 categorise the impacts for each event in terms of severity, linear and rotational acceleration, and location. A total of 86 impacts were recorded across all competitive bouts; with 45% in the "Low" linear acceleration range and 66% being in the "Low" rotational acceleration range. Just 4.7% of the linear accelerations were in the "Very Severe" range and 2.35% were in the "Very Severe" rotational acceleration range.

5.2.2 Impact Direction

It was found that front left impact direction was the location that most impacts were received (35%). This may indicate the dominant hand of the fighter's opponent. Lateral impacts, from the right and left, were the second predominant impact direction. These lateral impacts both left and right (16 from the left and right), comprised 37% of all impacts. Striking fighters in the back of the head is illegal in MMA and our results reflect this, with no impacts being recorded in that direction. Just 6% of impacts were received to the back left or right of the head. Figures 44 and 45 show the distribution for all impacts in terms of linear acceleration, rotational acceleration and location.

Table 18: Summary of Competitive Bouts sorted by Severity of Linear Acceleration

Severity - Linear Acceleration							
Fighter	**Bout**	**Low 10-30g**	**Moderate 30-60g**	**Serious 60-90g**	**Very Serious 90-120g**	**Severe 120-150g**	**Very Severe 150-400g**
Fighter 1	Bout 1	7	3	1	2	0	0
Fighter 2	Bout 1	4	9	3	0	1	1
Fighter 3	Bout 1	0	3	0	0	0	0
Fighter 3	Bout 2	3	4	0	0	0	0
Fighter 4	Bout 1	1	2	1	1	1	1
Fighter 4	Bout 2	7	4	0	0	0	0
Fighter 5	Bout 1	10	3	1	0	1	2
Fighter 6	Bout 1	7	3	0	0	0	0
Total		39	31	6	3	3	4

Table 19: Summary of Competitive Bouts sorted by Severity of Rotational Acceleration

Severity – Rotational Acceleration							
Fighter	**Bout**	**Low 0-5k rads/s^2**	**Moderate 5k-10k rads/s**	**Serious 10k-15k rads/s^2**	**Very Serious 15k-20k rads/s^2**	**Severe 20k-25k rads/s^2**	**Very Severe 25k-50k rads/s^2**
Fighter 1	Bout 1	11	0	2	0	0	0
Fighter 2	Bout 1	14	3	0	0	1	0
Fighter 3	Bout 1	3	0	0	0	0	0
Fighter 3	Bout 2	2	3	1	0	1	0
Fighter 4	Bout 1	11	0	0	0	0	0
Fighter 4	Bout 2	4	1	0	1	1	0
Fighter 5	Bout 1	5	5	2	2	1	2
Fighter 6	Bout 1	7	2	1	0	0	0
Total		57	14	6	3	4	2

Table 20: Summary of Competitive Bouts sorted by Direction of Impact

Location									
Fighter	**Bout**	**Front**	**Front Left**	**Front Right**	**Right**	**Left**	**Back**	**Back Left**	**Back Right**
Fighter 1	Bout 1	3	6	1	2	0	0	1	0
Fighter 2	Bout 1	1	9	1	2	4	0	0	1
Fighter 3	Bout 1	0	1	0	0	1	0	1	0
Fighter 3	Bout 2	1	1	1	3	1	0	0	0
Fighter 4	Bout 1	1	2	0	4	0	0	0	0
Fighter 4	Bout 1	1	0	1	3	4	0	1	1
Fighter 5	Bout 1	3	6	3	0	5	0	0	0
Fighter 6	Bout 1	2	5	0	2	1	0	0	0
Total		12	30	7	16	16	0	3	2

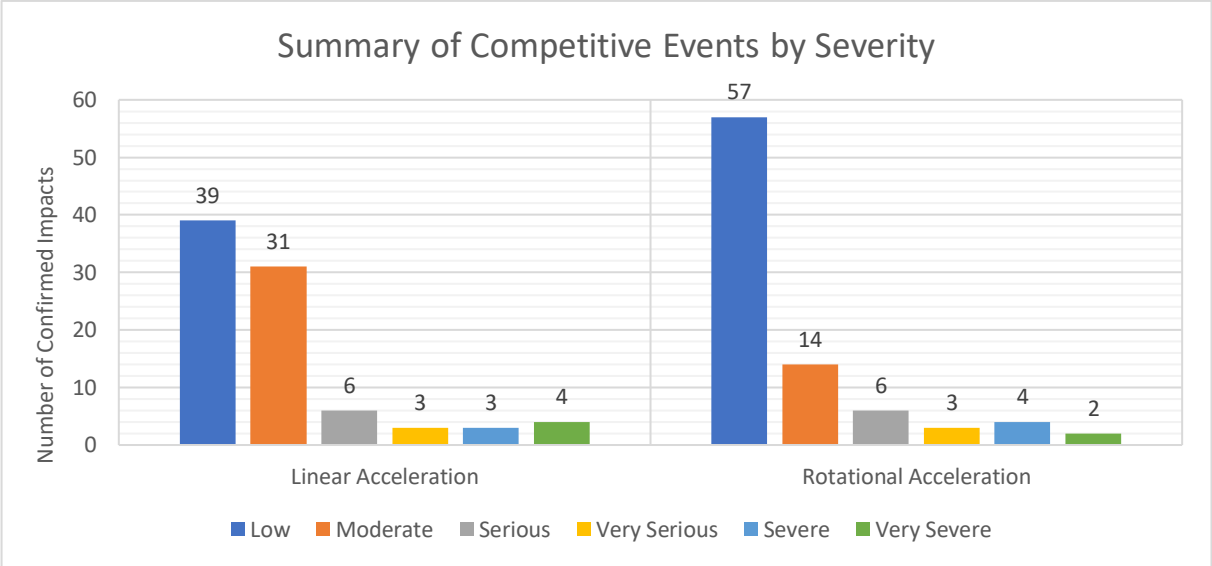

Figure 44: Summary of Competitive Bouts by Severity

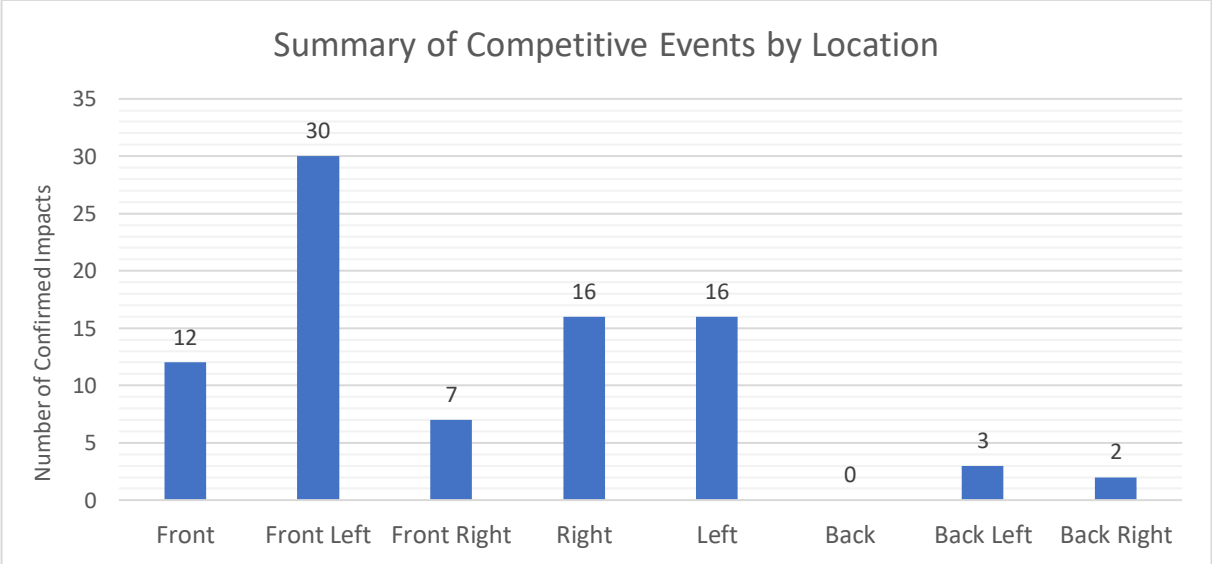

Figure 45: Summary of Competitive Bouts by Location

5.3 MMA Sparring Sessions

Five fighters took part in a total of 8 MMA sparring sessions from which data was collected. Sparring sessions are typically three 5-minute rounds. Data from the confirmed impacts in these sparring sessions is reported including: total number of impacts received, mean linear and rotational acceleration, standard deviation and mean number of impacts per sparring session. 135 confirmed head impacts occurred during MMA sparring sessions. The tables and graphs that follow detail them.

Table 21: MMA Sparring Session Stats

Fighter	Bout	Total Confirmed Impacts Per Event	Linear Acceleration Mean (g)	Standard Deviation	Rotational Acceleration Mean (rads/s^2)	Standard Deviation
Fighter 2	Session 1	16	22.8	10.3	2018.3	1314.4
Fighter 2	Session 2	18	27.5	18.5	2508.2	2070.9
Fighter 3	Session 1	12	25.2	15.1	2376.3	1476
Fighter 3	Session 2	10	26.9	21.8	2952.2	3330.1
Fighter 5	Session 1	16	23.8	15	11526.2	10872.9
Fighter 5	Session 2	15	40.5	27.1	19044	14540.7
Fighter 7	Session 1	28	21.9	12.1	1898.5	1354
Fighter 9	Session 1	20	47	56.8	4709.5	5906

Table 22: MMA Sparring Session stats summary

MMA Sparring Sessions	Mean	Median	1st Quartile	3rd Quartile	Local Maximum
Linear Acceleration (g)	29.41	20.94	14.31	30.65	53.44
Rotational Acceleration (rads/s^2)	5577.09	2150.67	1251.15	5095.36	10311.3
Rotational Velocity (rads/s)	15.52	10.75	7.32	17.55	32.54

As Table 21 shows, Fighter 3 – Session 2 received the fewest number of impacts (10). The mean number of impacts received during MMA sparring sessions was 18.75. There were 2 sessions where the fighter received more impacts than this; Fighter 7 – Session 1 and Fighter 9 – Session 1. Table 22 shows the mean linear and rotational accelerations, and rotational velocity for all impacts received during sparring sessions.

5.3.1 Impact Severity

Just 2 sparring sessions resulted in an average linear acceleration greater than that of the mean; Fighter 5 – Session 2 and Fighter 9 – Session 1. Fighter 5 – Session 1 and Session 2 also had a mean rotational acceleration greater than that of the mean for all sessions.

Tables 23, 24 and 25 detail the video confirmed impacts from each MMA sparring session, they have been categorised by severity (linear and rotational acceleration) and location respectively. Impacts defined as a low severity in terms of linear acceleration are the most common impact received, with 73% of all impacts being in this range. Just 4 impacts across all sessions are above the serious severity (90g+), representing just 3% of all impacts. Rotational acceleration is similar, with 74% of all impacts in the low severity for range. A total of 17 impacts being above the serious severity (15krads/s^2+), representing 13% of all impacts.

5.3.2 Impact Direction

When the impact direction was investigated (Table 24), it was found that 26% of all impacts were to the front left. Similar to the competitive bouts, this may only indicate the dominant hand of the fighter's opponent. Lateral impacts from the left and right sides accounted for 24% of all impacts.

Table 23: MMA Sparring Sessions Impact Severity sorted by Linear Acceleration

Severity – Linear Acceleration							
Fighter	**Session**	**Low 10-30g**	**Moderate 30-60g**	**Serious 60-90g**	**Very Serious 90-120g**	**Severe 120-150g**	**Very Severe 150-400g**
Fighter 2	Session 1	14	2	0	0	0	0
Fighter 2	Session 2	14	3	1	0	0	0
Fighter 3	Session 1	8	4	0	0	0	0
Fighter 3	Session 2	8	1	1	0	0	0
Fighter 5	Session 1	12	3	1	0	0	0
Fighter 5	Session 2	8	5	1	1	0	0
Fighter 7	Session 1	23	5	0	0	0	0
Fighter 9	Session 1	12	4	1	0	0	3
Total		99	27	5	1	0	3

Table 24: MMA Sparring Sessions Impact Severity sorted by Rotational Acceleration

Severity – Rotational Acceleration							
Fighter	**Bout**	**Low 0-5k rads/s^2**	**Moderate 5k-10k rads/s**	**Serious 10k-15k rads/s^2**	**Very Serious 15k-20k rads/s^2**	**Severe 20k-25k rads/s^2**	**Very Severe 25k-50k rads/s^2**
Fighter 2	Session 1	15	1	0	0	0	0
Fighter 2	Session 2	16	2	0	0	0	0
Fighter 3	Session 1	11	1	0	0	0	0
Fighter 3	Session 2	8	1	1	0	0	0
Fighter 5	Session 1	6	3	2	2	2	1
Fighter 5	Session 2	2	4	0	3	2	4
Fighter 7	Session 1	27	1	0	0	0	0
Fighter 9	Session 1	15	2	0	2	1	0
Total		100	15	3	7	5	5

Table 25: MMA Sparring Sessions Impact Severity sorted by Location

Location									
Fighter	**Session**	**Front**	**Front Left**	**Front Right**	**Right**	**Left**	**Back**	**Back Left**	**Back Right**
Fighter 2	Session 1	1	6	3	1	2	1	2	0
Fighter 2	Session 2	4	4	1	3	2	1	2	1
Fighter 3	Session 1	2	4	1	0	4	0	0	1
Fighter 3	Session 2	0	5	1	2	0	2	0	0
Fighter 5	Session 1	3	7	4	1	1	0	0	0
Fighter 5	Session 2	4	5	1	0	5	0	0	0
Fighter 7	Session 1	2	2	1	4	1	5	6	7
Fighter 9	Session 1	8	2	2	2	4	0	0	2
Total		24	35	14	13	19	9	10	11

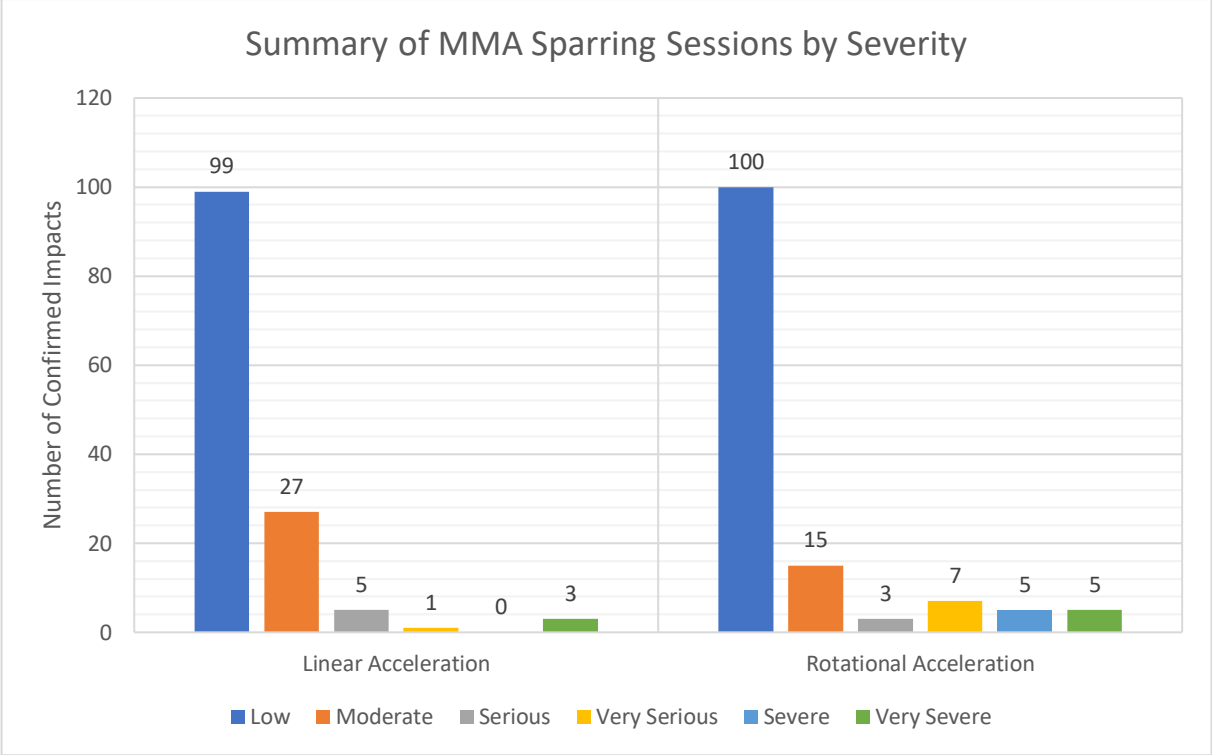

Figure 46: Summary of MMA Sparring Sessions by Severity

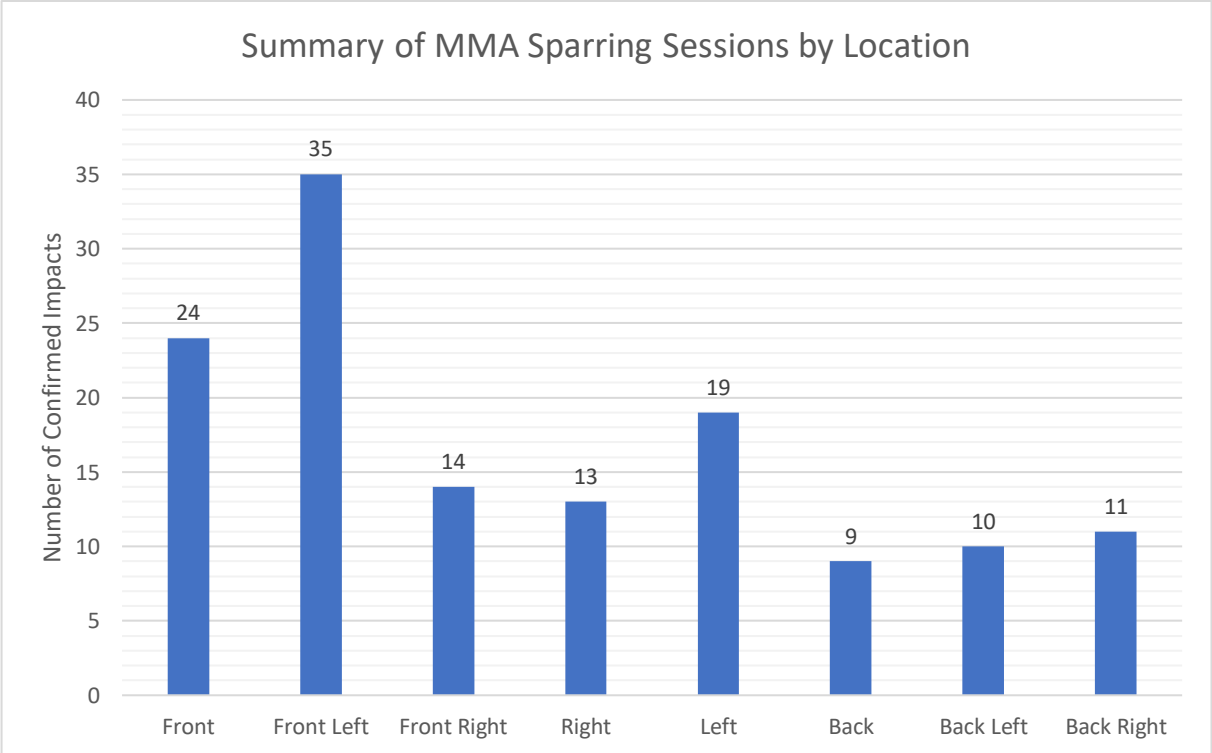

Figure 47: Summary of MMA Sparring Sessions by Location

5.4 MMA Training Sessions

As was mentioned in the introduction, Fighter 8 took part in a training session that was less regimented than those in Section 5.2. This training session took place over approximately 2 hours and was a rolling, ongoing sparring/training session with intermittent breaks. This data has been separated from the previous data as the number of impacts received here it would have skewed the means and standard deviations for the previously discussed sessions.

Table 26: MMA Training Session Data

MMA Training Sessions	Mean	Median	1st Quartile	3rd Quartile	Local Maximum
Linear Acceleration (g)	27.13	17.17	12.62	29.54	54.41
Rotational Acceleration (rads/s^2)	1960.99	1482.55	784.81	2253.01	4411.17
Rotational Velocity (rads/s)	11.57	10.96	9.6	13.29	17.59

5.4.1 Impact Severity

As shown in Table 26, this marathon training session resulted in 79 confirmed impacts for Fighter 8. The mean linear acceleration was 27.1g, this is comparable to those found in the type of session discussed in the previous section (29.4g). The number of impacts received is more than 4 times the mean received during the sessions in the previous section (18.75 impacts). The mean rotational acceleration is also comparable with the results found in the previous section.

Tables 27, 28 and 29 detail the linear and rotational accelerations severity of the impacts received by Fighter 8 in this session. 75% of all impacts are in the low linear acceleration severity range and just 2.5% are greater than 90g. The overwhelming majority of these impacts fall into the low rotational acceleration severity range (94%). None of the impacts recorded was greater than 10k rads/s^2.

5.4.2 Impact Direction

Similar to the data in Section 5.2, front left was the location at which most impacts were received (44%). Lateral impacts from the left and right sides accounted for 22% of all impacts.

Table 27: MMA Training Session Fighter 8 Impact Severity sorted by Linear Acceleration

Severity – Linear Acceleration							
Fighter	**Session**	**Low 10-30g**	**Moderate 30-60g**	**Serious 60-90g**	**Very Serious 90-120g**	**Severe 120-150g**	**Very Severe 150-400g**
Fighter 8	Session 1	59	16	2	1	0	1

Table 28: MMA Training Session Fighter 8 Impact Severity sorted by Rotational Acceleration

Severity – Rotational Acceleration							
Fighter	**Session**	**Low 0-5k rads/s^2**	**Moderate 5k-10k rads/s**	**Serious 10k-15k rads/s^2**	**Very Serious 15k-20k rads/s^2**	**Severe 20k-25k rads/s^2**	**Very Severe 25k-50k rads/s^2**
Fighter 8	Session 1	74	5	0	0	0	0

Table 29: MMA Training Session Fighter 8 Impact Severity sorted by Location

Location									
Fighter	**Session**	**Front**	**Front Left**	**Front Right**	**Right**	**Left**	**Back**	**Back Left**	**Back Right**
Fighter 8	Session 1	15	35	7	11	6	0	2	3

5.5 Boxing Sparring Sessions

Fighter 10 was preparing for a professional boxing event, so we have separated these results in order to ensure that the data presented is comparable. Boxing sparring typically is in the format of 2-minute rounds, with the number of rounds varying depending on how close to a competitive event the session is. As boxing is a sport where only punching is involved, as opposed to the multi-discipline MMA, the gloves worn are substantially larger. MMA gloves are typically 4oz (approximately 113g), with very little padding. While boxing gloves can be up to 18oz (approximately 510g), with the size depending on the weight class of the fighter, they come with a considerable amount of padding. Four boxing sparring sessions were studied; the data from these is detailed below.

Table 30: Boxing Sparring Session Fighter 10 Data

Fighter	Bout	Total Confirmed Impacts	Linear Acceleration Mean (g)	Standard Deviation	Rotational Acceleration Mean (rads/s^2)	Standard Deviation
Fighter 10	Session 1	30	18.1	6.4	6619.1	5038.5
Fighter 10	Session 2	36	20.3	10.3	5064.6	4837.3
Fighter 10	Session 3	36	16.9	9.6	5596.4	6697.4
Fighter 10	Session 4	34	65.0	72.6	6790.4	7363.0

5.5.1 Impact Severity

Table 30 details the number of impacts and the average impacts received per session. The mean number of impacts received is greater than that of MMA sparring sessions as only punching is allowed in boxing. The mean linear and rotational impact for boxing sparring sessions is comparable to those recorded in MMA sparring sessions, with a mean of 30.1g and 5979.8 rads/s^2 across all these sessions. The mean impact received in session 4 was considerably higher than those recorded in any other session, the opponent for session 4 was an internationally recognised boxer. The mean impact data received across all boxing sessions is detailed in Table 31.

Table 31: Boxing Sparring Session Fighter 10 Data

Boxing Sparring Sessions	Mean	Median	1st Quartile	3rd Quartile	Local Maximum
Linear Acceleration (g)	30.1	18.92	12.67	28.75	52.45
Rotational Acceleration (rads/s^2)	5979.79	4140.52	2597.84	6877.88	13045.94
Rotational Velocity (rads/s)	19.55	17.1	13.39	23.03	36.97

The linear acceleration, rotational acceleration and location are detailed in Tables 32, 33 and 34. Table 32 shows that 76% of impacts were in the Low severity range, and just 4% of all impacts were in the very serious range or higher (90g+). 59% of all impacts were in the low severity rotational acceleration range, with just 6% of all impacts being the very serious range or higher (15k rads/s^2+).

5.5.2 Impact Direction

Most impacts during the boxing sparring sessions were lateral impacts, both from the left and right (50%). 31% of all impacts were directly to the front of the face.

Table 32: Boxing Sparring Session Impact Severity sorted by Linear Acceleration

Severity – Linear Acceleration							
Fighter	**Session**	**Low 10-30g**	**Moderate 30-60g**	**Serious 60-90g**	**Very Serious 90-120g**	**Severe 120-150g**	**Very Severe 150-400g**
Fighter 10	Session 1	29	1	0	0	0	0
Fighter 10	Session 2	30	6	0	0	0	0
Fighter 10	Session 3	33	3	0	0	0	0
Fighter 10	Session 4	12	13	2	3	0	4
Total		104	23	2	3	0	4

Table 33: Boxing Sparring Session Impact Severity sorted by Rotational Acceleration

Severity – Rotational Acceleration							
Fighter	**Session**	**Low 0-5k rads/s^2**	**Moderate 5k-10k rads/s**	**Serious 10k-15k rads/s^2**	**Very Serious 15k-20k rads/s^2**	**Severe 20k-25k rads/s^2**	**Very Severe 25k-50k rads/s^2**
Fighter 10	Session 1	14	9	5	1	1	0
Fighter 10	Session 2	26	5	3	0	2	0
Fighter 10	Session 3	21	12	2	0	0	1
Fighter 10	Session 4	19	10	2	0	2	1
Total		80	36	12	1	5	2

Table 34: Boxing Sparring Session Impact Severity sorted by Location

Location									
Fighter	**Session**	**Front**	**Front Left**	**Front Right**	**Right**	**Left**	**Back**	**Back Left**	**Back Right**
Fighter 10	Session 1	11	4	1	11	1	1	0	1
Fighter 10	Session 2	4	5	2	17	5	0	2	1
Fighter 10	Session 3	8	9	6	12	0	0	0	1
Fighter 10	Session 4	19	5	3	3	3	0	0	1
Total		42	23	12	43	9	1	2	4

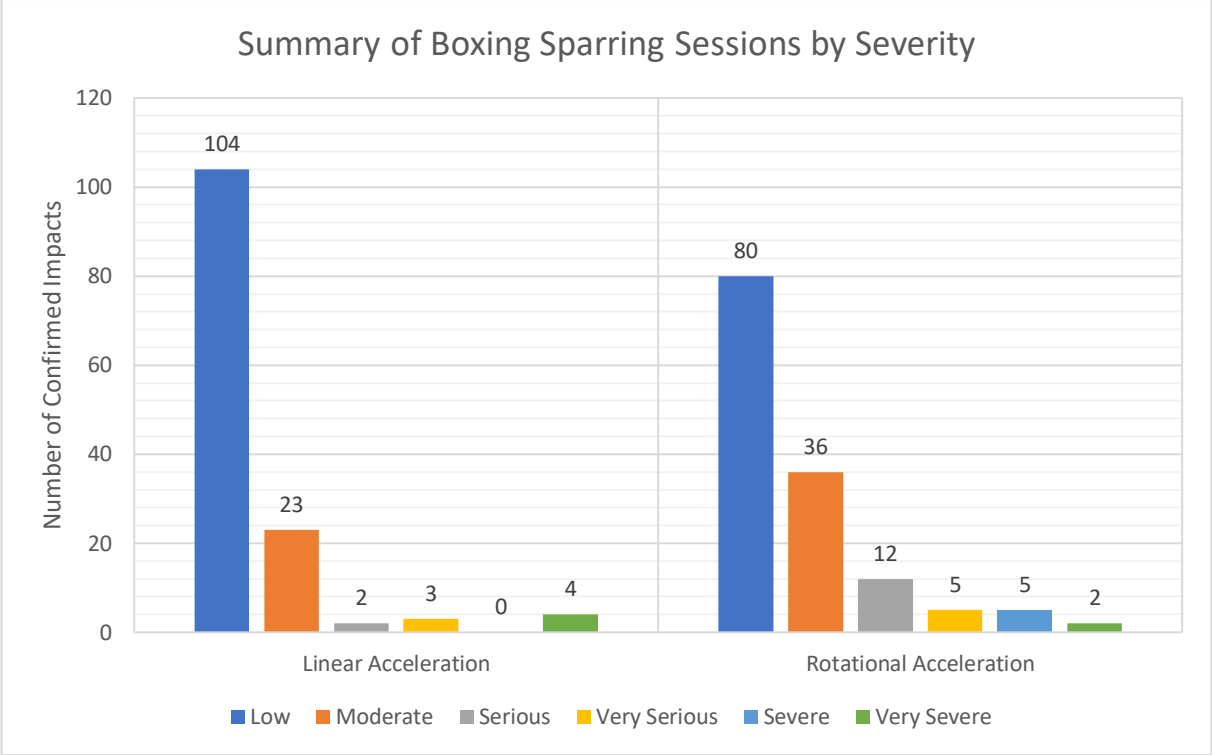

Figure 48: Summary of Boxing Sparring Sessions by Linear Acceleration

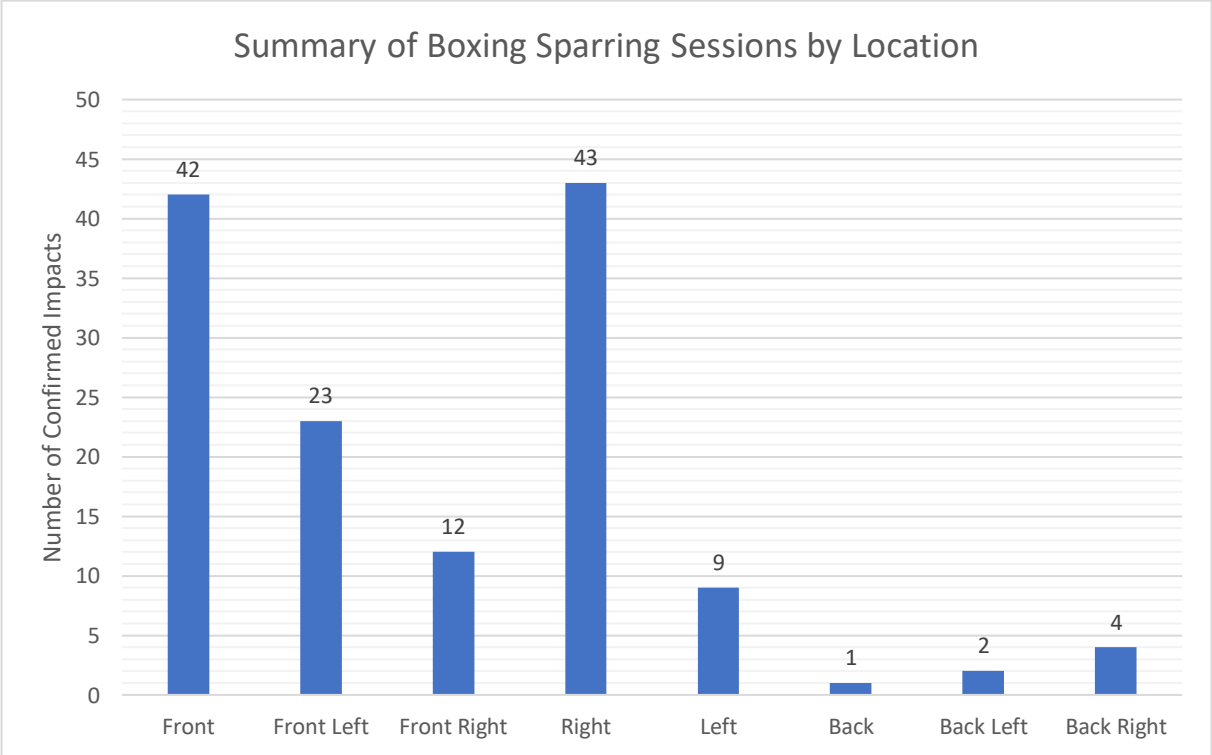

Figure 49: Summary of Boxing Sparring Sessions by Location

5.6 Summary of Results by Type

Tables 17, 22, 26 and 30 summarise the stats for each type of session from which data was recorded. The following set of graphs and tables summarise the data for each session type. Table summarises the number of impacts received in each session and any relevant injury diagnosis. There was no medical professional present for any sparring or training session, therefore there is no diagnosis available for these sessions. Table 35 details the mean, median, 1st quartile, 3rd quartile and local maximum PLA, PRA and PRV for each session type.

This study has found that the PLA for competitive events are 49% greater than those recorded in out of competition sessions. When the mean PRA and PRV of the out of competition bouts and competitive events are compared, there is an increase of 21.4% and 12.35% respectively. These increases are as expected as the level of performance of the opponent is likely to be greater in a competitive event than when compared to a sparring session. Figures 48-50 show the range of impacts for each session type, in terms of rotational velocity, linear and rotational acceleration.

Out of competition data is examined first, followed by competition data. Boxing sparring sessions resulted in the greatest number confirmed impacts, despite only having 4 sessions from which to collect data. This is to be expected as boxing only involves punching, with the vast majority of punches being aimed at the head. The mean number of impacts received per boxing sparring session is 34 and the 4th of these sessions resulted in the single highest out of competition mean impact, at 80g. As was discussed in the previous section, 5.4, this large difference in the mean impact can be accounted for by the fact that the opponent from this session was an internationally recognised professional boxer. The mean linear acceleration across all of these sessions is comparable to that recorded in both the MMA training data and the MMA sparring data; 30.1g for boxing sparring, 29.4g for MMA sparring and 27.1g for MMA training.

Table 35: Summary of number of impacts received and injury cases

Session Type	Fighter	Bout	Total Confirmed Impacts	Injury
Competitive Bouts	Fighter 2	Bout 1	18	mTBI
	Fighter 1	Bout 1	13	mTBI
	Fighter 5	Bout 1	15	mTBI
	Fighter 4	Bout 1	11	mTBI
	Fighter 6	Bout 1	10	No Injury
	Fighter 3	Bout 2	7	No Injury
	Fighter 4	Bout 2	7	No Injury
	Fighter 3	Bout 1	3	mTBI
MMA Sparring Sessions	Fighter 2	Session 1	16	N/A
	Fighter 2	Session 2	18	N/A
	Fighter 3	Session 1	12	N/A
	Fighter 3	Session 2	10	N/A
	Fighter 5	Session 1	16	N/A
	Fighter 5	Session 2	15	N/A
	Fighter 7	Session 1	28	N/A
	Fighter 9	Session 1	20	N/A
MMA Training Sessions	Fighter 8	Session 1	79	N/A
Boxing Sparring Sessions	Fighter 10	Session 1	30	N/A
	Fighter 10	Session 2	36	N/A
	Fighter 10	Session 3	36	N/A
	Fighter 10	Session 4	34	N/A

Table 36: Summary of Data by Session Type

Data Type	Session Type	Mean	Median	1st Quartile	3rd Quartile	Local Maximum
Linear Acceleration (g)	Competitive Bouts	43.53	31.83	19.78	44.34	81.11
	MMA Sparring Sessions	29.41	20.94	14.31	30.65	53.44
	MMA Training Sessions	27.13	17.17	12.62	29.54	54.41
	Boxing Sparring Sessions	30.1	18.92	12.67	28.75	52.45
Rotational Acceleration (rads/s^2)	Competitive Bouts	5969.19	3910.13	2071.68	6023.89	10014.27
	MMA Sparring Sessions	5577.09	2150.67	1251.15	5095.36	10311.3
	MMA Training Sessions	1960.99	1482.55	784.81	2253.01	4411.17
	Boxing Sparring Sessions	5979.79	4140.52	2597.84	6877.88	13045.94
Rotational Velocity (rads/s)	Competitive Bouts	18.22	14.65	11.55	20.64	33
	MMA Sparring Sessions	15.52	10.75	7.32	17.55	32.54
	MMA Training Sessions	11.57	10.96	9.6	13.29	17.59
	Boxing Sparring Sessions	19.55	17.1	13.39	23.03	36.97

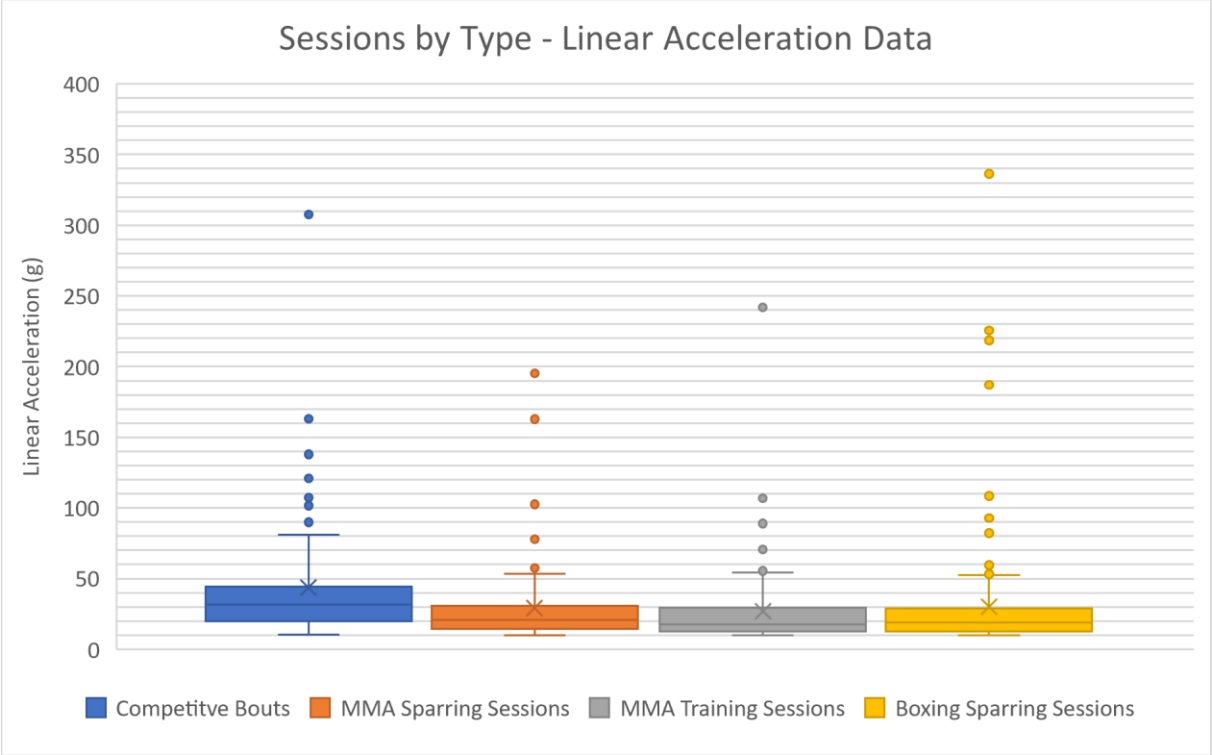

Figure 50: Summary of Sessions by Type - Linear Acceleration

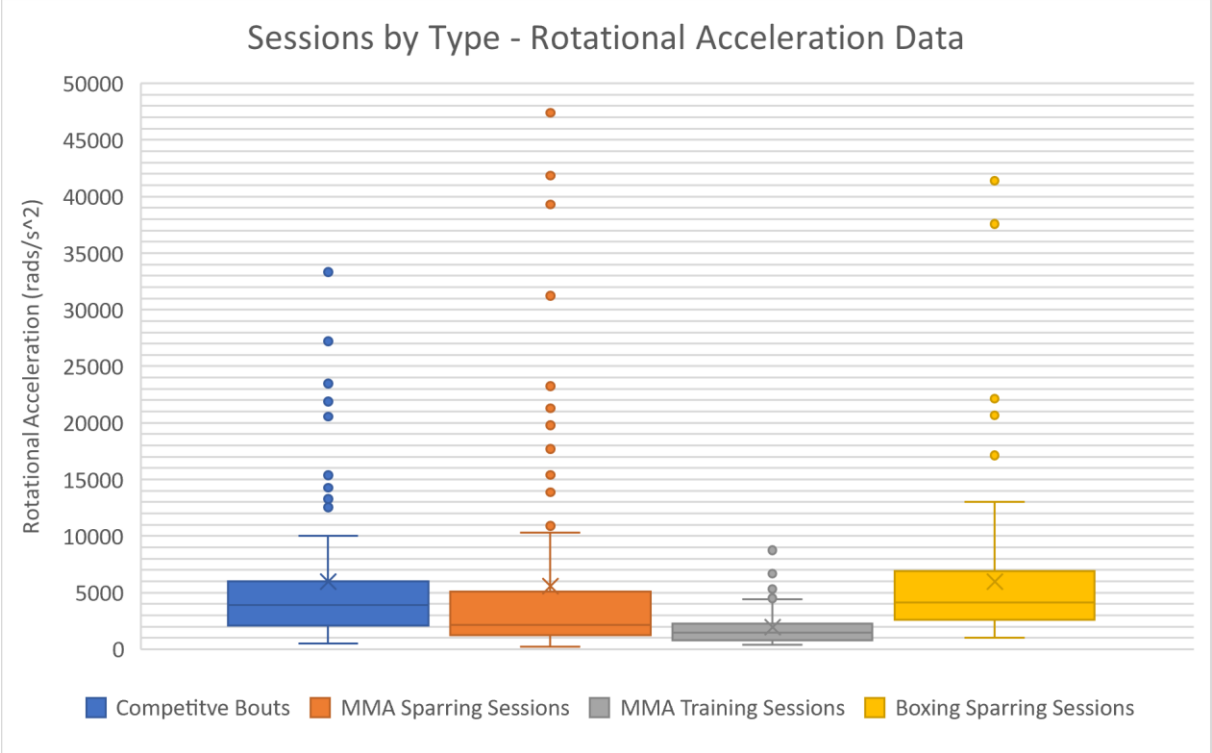

Figure 51: Summary of Sessions by Type - Rotational Acceleration

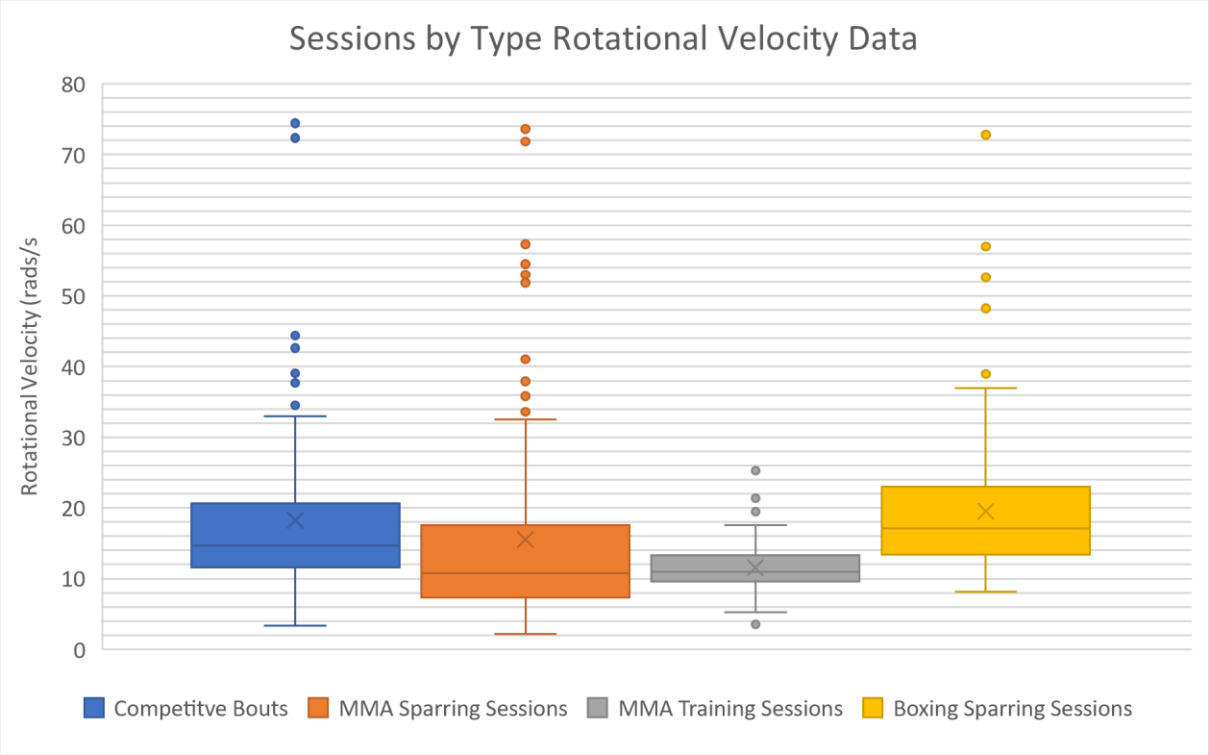

Figure 52: Summary of Sessions by Type - Rotational Velocity

The rotational mean impact data from the boxing sparring sessions is comparable to the MMA sparring and competition mean, approximately 5980 rads/s^2 for boxing, 5577 rads/s^2 for MMA sparring and 5969 rads/s^2 for MMA competition. MMA sparring sessions resulted an average of half the number of head impacts recorded when compared to boxing. In MMA sparring sessions fighters received between 10 and 28 impacts per session, with a mean of 18.75 impacts per session.

Fighter 7 – Session 1 had the lowest linear acceleration mean of 21.9g. Fighter 9 – Session 1 had the largest, at 47g. The mean for all of these sessions (29.4g) is detailed in Table 32. Again Fighter 7 – Session 1 had the lowest rotational mean acceleration impact, at 1899 rads/s^2. The highest recorded rotational mean acceleration across all data recorded was for Fighter 5 – Session 2, at 19044 rads/s^2. This rotational mean acceleration is alarmingly high and is at odds with almost all other data recorded. Fighter 5 has had some issues with the fit of the mouthguard and as such this could be a contributing factor for the relatively high impact data recorded. This is will be discussed further in Chapter 7.

In the single MMA training data set, which took place over 2 hours, the number of impacts recorded was 79. This is over 4 times the mean number of impacts recorded in all training sessions, 18.75. This number of impacts in the single session is very large when compared to all other sessions recorded and highlights the need for a better understanding of the potential cumulative effect of many non-injurious impacts in a short timeframe. While the number of impacts was far higher than any other session, the mean linear acceleration impact is comparable to other out of competition sessions, at 27.1g. While the mean rotational impact was far lower than those recorded for other out of competition sessions; at 1961 rads/s^2 for MMA training, compared to 5577 rads/s^2 for MMA sparring. Across the entire out of competition sessions no TBI's were recorded, although it should be noted that no medical professional was present at any of these sessions. This means that any symptoms would have to be self-reported at a later time. As was discussed in the early chapter 2.3.3, self-reporting of injuries is a serious concern with studies showing as many as 45% of injuries going unreported [24].

A total of 84 impacts were recorded during competitive bouts across 8 events. Fighters received between 3 and 18 impacts with a mean linear head acceleration of 43.5g. A mean of 10.5 impacts per competitive bout was recorded, which is lower than all those recorded in training sessions. This mean linear acceleration mean is 61%, 48% and 43% larger than MMA training, MMA sparring and boxing sparring respectively. The largest mean linear acceleration was recorded in a competitive bout, Fighter 4 – Bout 2 of 80g from 7 impacts received. The highest mean rotational impact received was once again Fighter 5 – Bout 1. Some probable causes for the unusually high magnitudes recorded from this participant will be discussed in the upcoming Chapter 7.

5.7 Data Analysis

All impacts from any session which resulted in a concussive diagnosis were compared to those from all sessions that did not result in a concussive diagnosis. Table 37 summaries these findings. An increase of 47% was found in PLA for impacts in a session that resulted in a concussion diagnosis, a 13.5% increase in PRA and a 3.7% increase in PRV.

Figures 53 and 54 summarise the data from all sessions, in terms of severity and location. A similar trend is apparent when examining the impacts in terms of severity, approximately 60% of all impacts recorded were in the Low severity range for both linear and rotational acceleration.

Front left was again the most common impact location, 25% of all impacts. With the lateral impacts when combined being the next most common, 27% of all impacts recorded.

Table 37: Summary of Mean Impact Data for all Session Types

Data Type	Session Type	Mean	Median	1st Quartile	3rd Quartile	Local Maximum
Linear Acceleration (g)	All Sessions	32	20.78	13.62	34.26	62.18
	mTBI Sessions	44.1	32.02	19.82	44.34	81.11
	No Injury	29.99	19.9	13.15	31.26	58.08
Rot Acceleration (rads/s^2)	All Sessions	5124.83	2805.21	1503.82	5443.77	11151.88
	mTBI Sessions	5707.41	3536.3	1953.09	5645.35	7795.04
	No Injury	5028.25	2751.45	1444.94	5397.77	11151.88
Rot Velocity (rads/s)	All Sessions	16.6	13.39	10.1	19.6	33.62
	mTBI Sessions	17.11	13.52	11.34	18.68	26.16
	No Injury	16.51	13.3	10.06	19.62	33.62

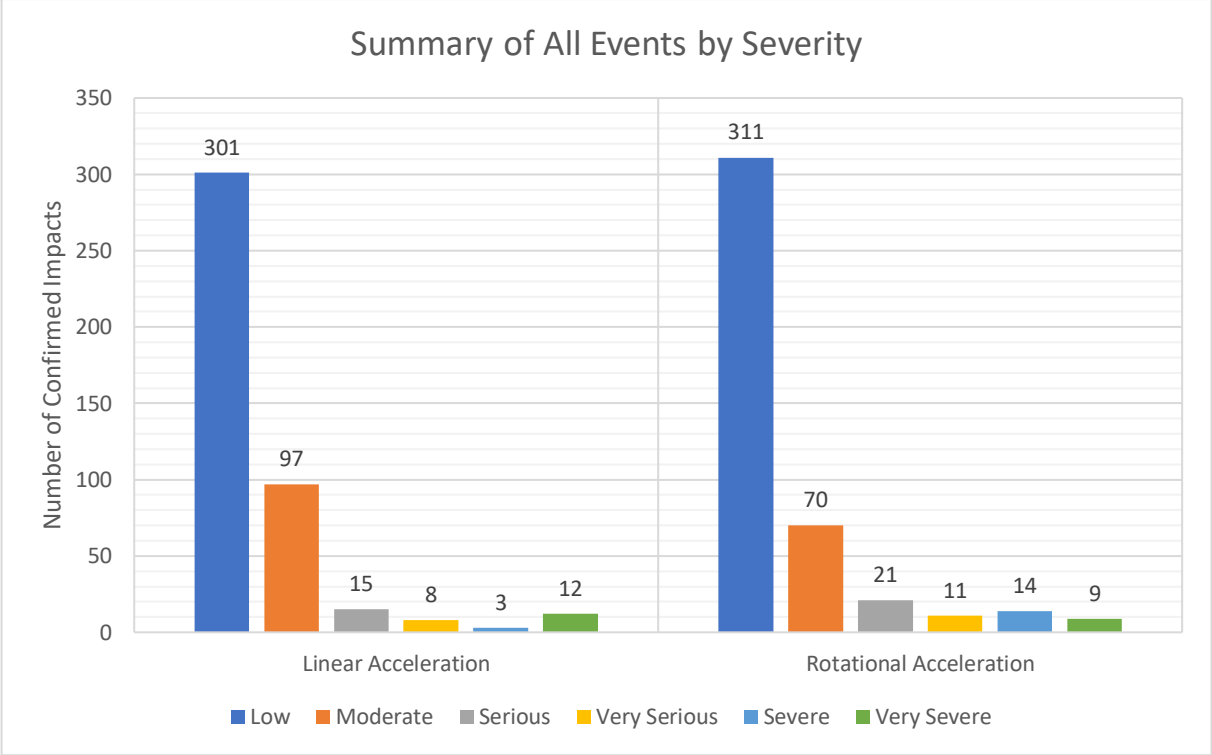

Figure 53: Summary of All Events by Severity

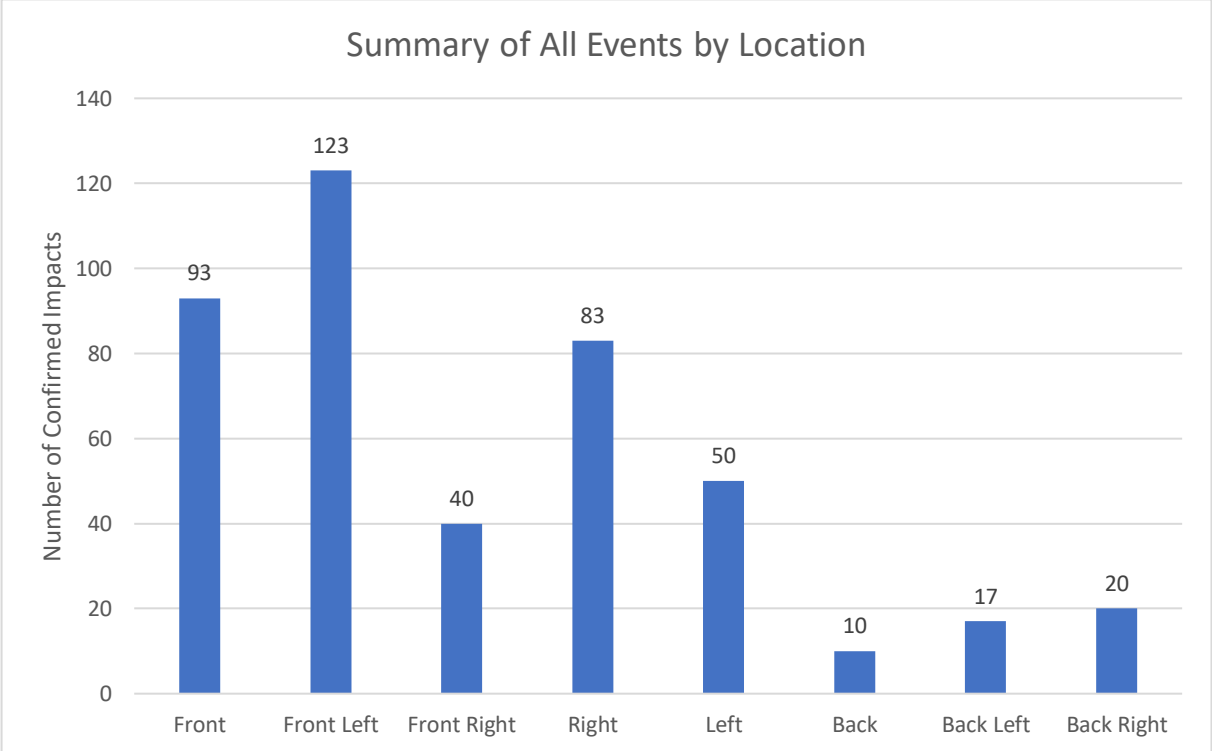

Figure 54: Summary of All Events by Location

5.7.1 Impact Frequency

There are some differences in total time spent participating in an event, as competitive events may end before the maximum time due to a referee stoppage. Thus, the frequency of impacts received will be examined. Impacts per minute is calculated as the total number of impacts in a session/bout divided by the total time the session/bout lasted for. Table 38 details these findings.

Table 38: Impacts/Minute received by Event

Fighter	Event Type	Impacts/minute	Injury	
Fighter 1 – Bout 1	Competitive Event	0.87	mTBI	
Fighter 2 – Bout 1	Competitive Event	1.3	mTBI	
Fighter 3 – Bout 1	Competitive Event	1.66	mTBI	
Fighter 3 – Bout 2	Competitive Event	1.07	No Injury	
Fighter 4 – Bout 1	Competitive Event	0.96	mTBI	
Fighter 4 – Bout 2	Competitive Event	3.95	No Injury	
Fighter 5 – Bout 1	Competitive Event	3.89	mTBI	
Fighter 6 – Bout 1	Competitive Event	0.67	No Injury	Mean = 1.80
Fighter 2 – Session 1	MMA Sparring	1.33	No Injury	
Fighter 2 – Session 2	MMA Sparring	1.2	No Injury	
Fighter 3 – Session 1	MMA Sparring	1	No Injury	
Fighter 3 – Session 2	MMA Sparring	0.66	No Injury	
Fighter 5 – Session 1	MMA Sparring	1.07	No Injury	
Fighter 5 – Session 2	MMA Sparring	1	No Injury	
Fighter 7 – Session 1	MMA Sparring	2.33	No Injury	
Fighter 9 – Session 1	MMA Sparring	2.22	No Injury	
Fighter 8 – Session 1	MMA Training	1.33	No Injury	Mean = 1.35
Fighter 10 – Session 1	Boxing Sparring	2	No Injury	
Fighter 10 – Session 2	Boxing Sparring	2.4	No Injury	
Fighter 10 – Session 3	Boxing Sparring	2	No Injury	
Fighter 10 – Session 4	Boxing Sparring	2.43	No Injury	

5.7.2 Impact Duration

The duration of the linear acceleration of an impact has been defined as the time in milliseconds (ms) that the PLA is greater than 10g, i.e. the time for the PLA to first go above 10g and then return below 10g. The rotational acceleration duration is defined as the time in ms that the PRA is greater than 1000 rads/s^2, i.e. the time for the PRA to first go above 1000 rads/s^2 and then return below 1000 rads/s^2. Examples of each method are shown in Figures 53 and 54, PLA duration in Figure 55 is 20ms and PRA duration in Figure 56 is 18ms.

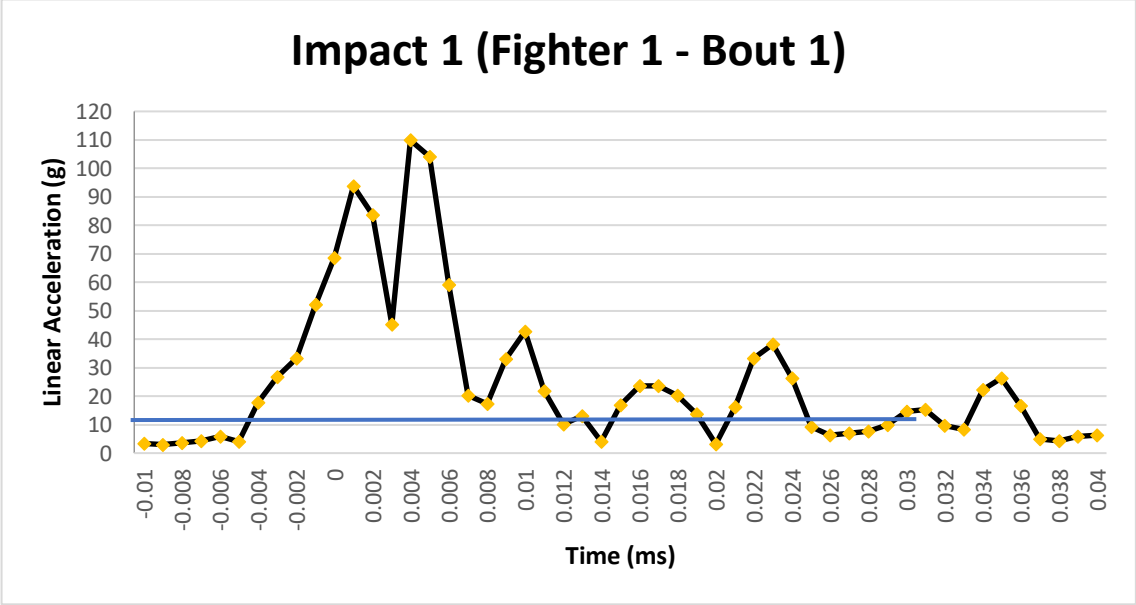

Figure 55: Example of calculating linear acceleration duration

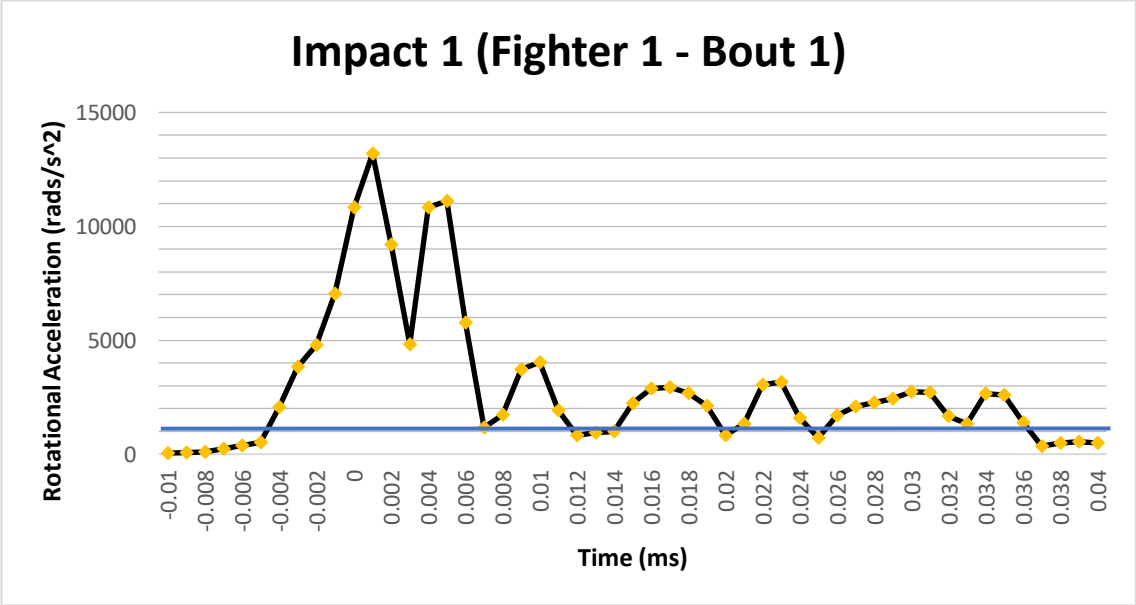

Figure 56: Example of calculating rotational acceleration duration

Using the method as described above, Table 39 was created detailing the duration of simulated impacts in terms of both linear and rotational acceleration duration. And from this Figure 57 was created. It indicates a potential link between a longer duration and an increased probability of an mTBI diagnosis. This will be discussed further in the upcoming Discussion chapter.

Table 39: Linear and rotational acceleration durations

Fighter/Session	Linear Acceleration Duration (ms)	Rotational Acceleration Duration (ms)	Injury
Impact 1 (Competition: Fighter 1 – Bout 1)	20	18	mTBI
Impact 2 (Competition: Fighter 2 – Bout 1)	19	31	mTBI
Impact 3 (Competition: Fighter 3 – Bout 1)	16	11	mTBI
Impact 4 (Competition: Fighter 3- Bout 2)	8	17	No Injury
Impact 5 (Competition: Fighter 4 – Bout 1)	26	25	mTBI
Impact 6 (Competition: Fighter 4 – Bout 2)	12	33	No Injury
Impact 7 (Competition: Fighter 5 – Bout 1)	10	32	mTBI
Impact 8 (Competition: Fighter 6 – Bout 1)	9	13	No Injury
Impact 9 (Competition: Fighter 5 – Bout 1)	10	15	mTBI
Impact 10 (Competition: Fighter 5 – Bout 1)	11	31	mTBI
Impact 11 (Sparring/Training: Fighter 8 – Session 1)	8	10	No Injury
Impact 12 (Sparring/Training: Fighter 9 – Session 1)	5	5	No Injury
Impact 13 (Sparring/Training: Fighter 3 – Session 2)	7	7	No Injury
Impact 14 (Sparring/Training: Fighter 8 – Session 1)	9	9	No Injury
Impact 15 (Sparring/Training: Fighter 9 – Session 1)	15	15	No Injury
Impact 16 (Sparring/Training: Fighter 9 – Session 1)	15	15	No Injury
Impact 17 (Sparring/Training: Fighter 5 – Session 2)	10	10	No Injury
Impact 18 (Sparring/Training: Fighter 10 – Session 4)	14	19	No Injury

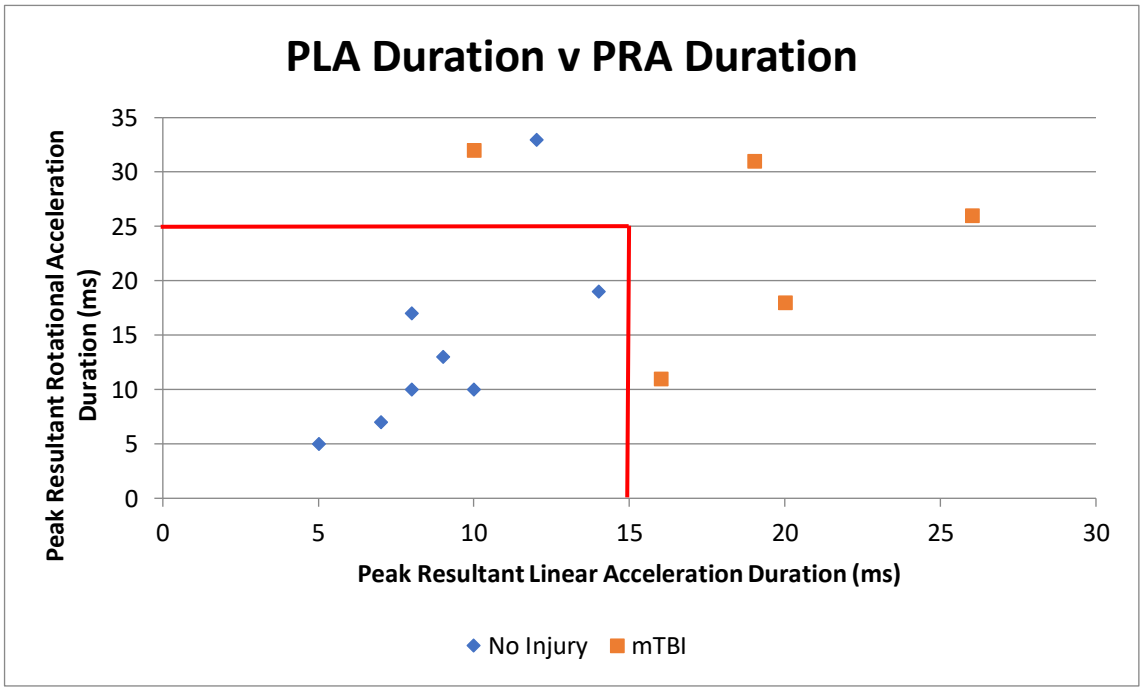

Figure 57: Linear Acceleration Duration v Rotational Acceleration Duration

5.7.3 Head Impact Power

As was discussed in the earlier section, 2.6.4 Head Impact Power, HIP was calculated for each of the simulated impacts. Equation 4 shows how these values were reached.

$$HIP = \underbrace{C_1 a_x \int a_x dt + C_2 a_y \int a_y dt + C_3 a_z \int a_z dt}_{\text{Linear Contribution}} + \underbrace{C_4 a_x \int a_x dt + C_5 a_y \int a_y dt + C_6 a_z \int a_z dt}_{\text{Rotational Contribution}}$$

Equation 4: Head Impact Power Equation [88]

The C_n coefficients represent approximations of the mass and the moment of inertia for a 50th percentile human head [89]. a_x,a_y, a_z are the linear and rotational components.

Where: $C_1, C_2, C_3 = 4.5kg$

$C_4 = 0.016Nms^{-2}$

$C_5 = 0.024Nms^{-2}$

$C_6 = 0.022Nms^{-2}$

Table 40 shows the values for HIP for each of the simulated impacts in kW. The largest HIP score was Impact 2, Fighter 2 – Bout 1, 60.8kW. This was an in-competition bout and was the impact with the largest PLA, 308g. This bout did result in an mTBI diagnosis. The second largest HIP score was found in Impact 7, Fighter 5 – Bout 1, 41.2kW. As with Impact 1, this impact was from an in-competition bout and the participant was diagnosed with an mTBI. The largest value for HIP in a session that did not result in an mTBI diagnosis was Fighter 4 – Bout 2, 35.9kW.

When the mean values for mTBI and No Injury are calculated, it was found that the mean for a session/bout that did result in an mTBI diagnosis was 22.7kW. And those taken from a session/bout that did not result in an mTBI diagnosis was 12.7kW. This represents a 78.7% increase. Newman *et al.* proposed a threshold of 12.8kW for a 50% probability of an mTBI diagnosis, 9 impacts from 7 sessions/bouts in this study exceeded this threshold [89]. Three of the participants in those sessions/bouts were diagnosed with an mTBI.

These results will be investigated as predictors for strain in the regions of interest for this study. HIP scores will be plotted against strain values recorded during the simulations and any possible linear relationships will be determined. This will be conducted in the upcoming section, 6.4 Data Analysis.

Table 40: HIP results for simulated impacts

Impact Number	Fighter/Bout	Head Impact Power (kW)	Injury Case
1	Fighter 1 - Bout 1	16.6	mTBI
2	Fighter 2 - Bout 1	60.8	mTBI
3	Fighter 3 - Bout 1	3.9	mTBI
4	Fighter 3 - Bout 2	6.4	No Injury
5	Fighter 4 - Bout 1	9.8	mTBI
6	Fighter 4 - Bout 2	35.9	No Injury
7	Fighter 5 - Bout 1	41.2	mTBI
8	Fighter 6 - Bout 1	1.2	No Injury
9	Fighter 5 - Bout 1	18.0	mTBI
10	Fighter 5 - Bout 1	8.5	mTBI
11	Fighter 8 - Session 1	1.2	No Injury
12	Fighter 9 - Session 1	15.2	No Injury
13	Fighter 3 - Session 2	3.1	No Injury
14	Fighter 8 - Session 1	2.9	No Injury
15	Fighter 9 - Session 1	10.0	No Injury
16	Fighter 9 - Session 1	13.1	No Injury
17	Fighter 5 - Session 2	18.7	No Injury
18	Fighter 10 - Session 4	31.7	No Injury

Chapter 6 Computational Results

6.1 Introduction

This chapter reports the results from simulations of individual head impacts, focusing on the brain regions and published thresholds as discussed in section 2.6. Simulations were undertaken using the method described in Chapter 4.

Confirmed impacts with the highest rotational accelerations were chosen to simulate, 50ms was simulated to fully capture each impact. Maximum principal strain for each of the regions has been compared to published injury thresholds. Table 41 reports these thresholds. The maximum principal strain is the maximum strain that is found in any element, at any time during the simulation.

Table 41: Published Threshold for likelihood of a Concussion [6]

Brain region	Mean Strain for No Injury	50% Probability for Concussion	Mean Strain for Concussion
Corpus Callosum	12% (0.12)	15% (0.15)	31% (0.31)
Thalamus	10% (0.10)	13% (0.13)	26% (0.26)
Midbrain	13% (0.13)	15% (0.15)	25% (0.25)
Brain Stem	12% (0.12)	14% (0.14)	21% (0.21)

To avoid reporting high peak strains for individual elements, a parameter we have named Mean Adjacent Strain (MAS) has been used. Mean adjacent strain was determined by first finding the max principal strain in an element, in the region being investigated, and the time at which it occurs. Then all adjacent elements are selected and the strain values are plotted for the entire simulation time. The mean is calculated for all those elements at the time when the maximum occurred. This was used as the maximum principal strain in a single element is not representative of how strain would occur in the brain. The method for calculating MAS has been described in more detail in the earlier section, 4.7.2 Mean Adjacent Strain.

Figures 58-62 show an example of the strain as reported in the FE model software and represents how the simulation results will be presented.

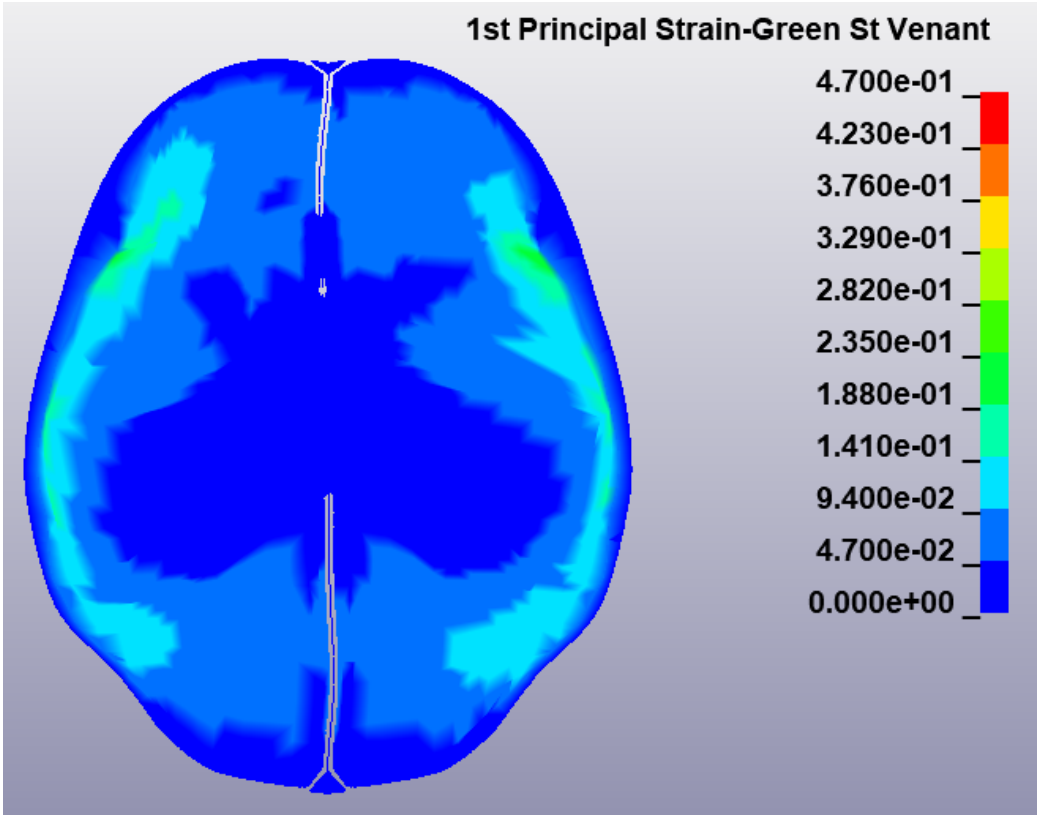

Figure 58: Impact 15 (Fighter 9- Session 1) Transverse Brian Slice (165g and 15994 rads/s^2)

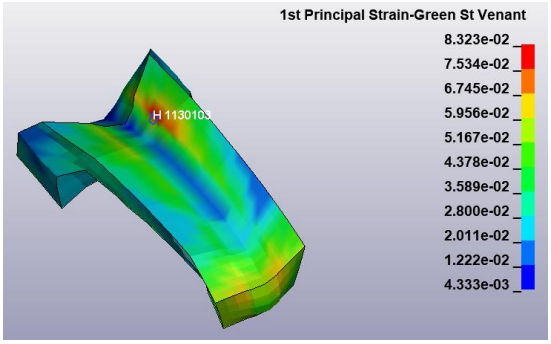

Figure 59: Impact 15 Corpus Callosum strain (MPS 8.3%)

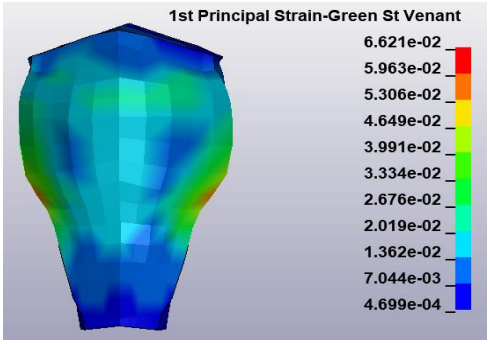

Figure 60: Impact 15 Brainstem strain (MPS 6.6%)

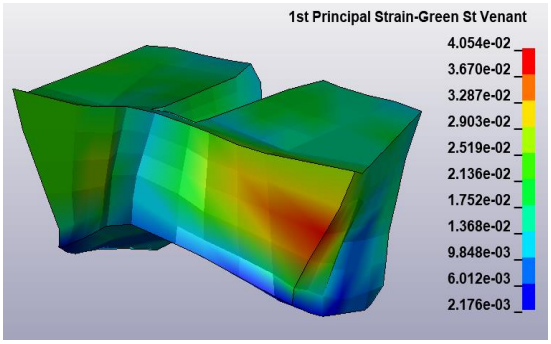

Figure 61: Impact 15 Midbrain strain (MPS 4.05%)

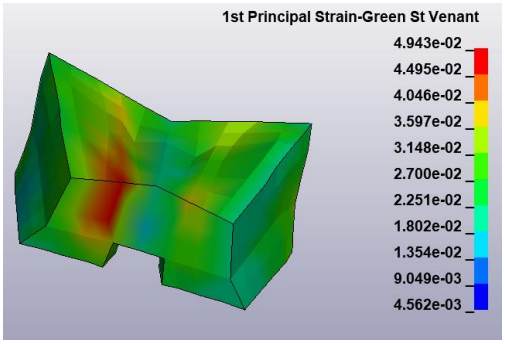

Figure 62: Impact 15 Thalamus strain (MPS 3.2%)

6.2 Competitive Bouts

To date 6 of the participants have taken part in competitive bouts, both professional and elite amateur. Some of the participants have taken part in more than one event, resulting in a total of 8 competitive bouts from 6 participants. Ten impacts with the highest rotational acceleration were selected from these bouts to simulate. Details of these impacts are shown in Table 42. Mouthguard output acceleration data used for each of these simulated impacts can be found in Appendix 5. Table 43 details the strain results for each of the simulations, both the max principle strain and the mean adjacent strain in the regions of interest are reported.

Five of these events resulted in a concussive diagnosis; Fighter 1 – Bout 1, Fighter 2- Bout 1, Fighter 3 – Bout 1, Fighter 4 – Bout 1 and Fighter 5 – Bout 1. Of those diagnosed with a concussion just Fighter 2 and Fighter 5's simulated impacts resulted in strain levels greater than the published thresholds. Both of these impacts resulted in strain levels greater than the mean strain for a concussion in the corpus callosum, thalamus and brain stem. Furthermore, the levels of strain found in the mid brain also exceeded that of the mean strain for a 50% probability for a concussion. Fighter 5 – Bout 1 also received 2 impacts that resulted in large rotational accelerations, neither of these impacts resulted in levels of strain that exceeded the published thresholds; although they may have contributed to the diagnosis.

The cumulative effect of sub-concussive head impacts is unclear at this time, with conflicting reports in the literature. Some studies indicate there is no effect [91] [117]. While others report that there is an effect [118] [119]. Fighter 3 – Bout 1 and Fighter 4 – Bout 1's results may provide potential evidence of the effect of cumulative sub-concussive impacts. Each of these bouts largest impacts not resulting in strain that exceeded the thresholds but did result in a concussive diagnosis. In contrast to this; Fighter 3 – Bout 2 and Fighter 4 – Bout 2's impacts with the largest rotational accelerations did result in strain that exceeded the thresholds but they were not diagnosed with an mTBI. These results highlight the need for further research into the potential cumulative effects of repeated sub concussive impacts.

Table 42: Competitive Bout Impact Data

	Fighter 1 – Bout 1	**Fighter 2 - Bout 1**	**Fighter 3 - Bout 1**	**Fighter 3 - Bout 2**	**Fighter 4 - Bout 1**	**Fighter 4 - Bout 2**	**Fighter 5 - Bout 1**	**Fighter 6 - Bout 1**	**Fighter 5 - Bout 1**	**Fighter 5 - Bout 1**
Impact Number	1	2	3	4	5	6	7	8	9	10
Peak Resultant Linear Acceleration (g)	110	308	41	32	141	163	109	52	104	71
Linear Acceleration Duration (ms)	20	19	16	8	26	12	10	9	10	11
Peak Linear Acceleration X (g)	83	224	30	12	110	90	84	17	27	51
Peak Linear Acceleration Y (g)	39	115	31	14	55	16	6	7	103	52
Peak Linear Acceleration Z (g)	72	232	15	29	106	148	95	52	27	13
Peak Resultant Rotational Acceleration (rads/s^2)	13191	21881	2906	23479	13609	23757	33315	10014	27212	15984
Rotational Acceleration Duration (ms)	18	31	11	17	25	33	32	13	15	31
Peak Rotational Acceleration X (rads/s^2)	4579	8713	1711	17594	4817	6522	1774	2771	8778	12139
Peak Rotational Acceleration Y (rads/s^2)	13097	9853	1870	15332	12719	21268	33305	10004	25192	14105
Peak Rotational Acceleration Z (rads/s^2)	1852	19918	2542	4441	4440	15565	5548	830	10877	9962
Peak Rotational Velocity (rads/s)	45.3	37.7	15.6	39	20.4	74.4	72.3	10.7	42.6	28.4
Direction	F	FR	FL	F	BL	F	F	L	L	FL
Sim Duration (ms)	50	50	50	50	50	50	50	50	50	50
Head Impact Power (kW)	16.6	60.8	3.9	6.4	9.8	35.9	41.2	1.2	18.0	8.5

(Simulation input data for each of the impacts can be found in Appendix 5)

Table 43: Summary of Simulation Results for Competitive Bouts

Region	Fighter 1 – Bout 1	Fighter 2 – Bout 1	Fighter 3 – Bout 1	Fighter 3 – Bout 2	Fighter 4 – Bout 1	Fighter 4 – Bout 2	Fighter 5 – Bout 1	Fighter 6 – Bout 1	Fighter 5 – Bout 1	Fighter 5 – Bout 1
Impact Number	1	2	3	4	5	6	7	8	9	10
CC MPS	6.00%	55.00%	10.50%	53.00%	5.30%	32.50%	13.00%	3.30%	67.50%	9.00%
CC MAS	3.05%	23.00%	4.70%	20.00%	2.73%	13.60%	6.50%	1.47%	26.95%	4.40%
Thalamus MPS	3.20%	32.00%	6.60%	29.00%	2.50%	18.00%	7.70%	2.12%	37.50%	5.20%
Thalamus MAS	2.60%	20.00%	4.10%	17.00%	2.10%	11.10%	6.45%	1.73%	23.45%	4.50%
Midbrain MPS	2.40%	21.00%	3.70%	10.50%	2.90%	10.50%	5.00%	1.25%	15.90%	6.40%
Midbrain MAS	2.14%	15.50%	3.40%	8.15%	2.20%	9.00%	4.60%	1.14%	9.40%	4.70%
Brainstem MPS	3.20%	31.40%	3.80%	11.00%	3.80%	17.00%	6.50%	2.00%	26.80%	7.80%
Brainstem MAS	1.00%	9.00%	1.18%	3.30%	1.15%	4.70%	2.00%	0.60%	7.25%	2.60%
Injury	mTBI 48 hour symptoms: migraine aura	mTBI Post Event Symptoms: vertigo and dizziness	mTBI Transient LOC < 1 sec, no PCS	No Injury	mTBI Post Event, no PCS	No Injury	mTBI Post Event, no PCS	No Injury	mTBI Post Event, no PCS	mTBI Post Event, no PCS

Legend	
Mean Strain for No Injury	
50% Probability for Concussion	
Mean Strain for Concussion	

6.3 Sparring/Training Sessions

To date 7 of the participants have taken part in training sessions from which data was gathered. These include MMA sparring, boxing sparring and MMA training sessions. Some of the participants have taken part in more than one event, giving a total of 13 out of competition sessions from 7 participants. From this data 8 impacts with the highest rotational acceleration were selected to be simulated. Details of these impacts are shown in Table 44. Mouthguard output acceleration data for each of these impacts can be found in the Appendix 6. Table 45 details the strain results from each of the simulations, reporting both the max principle strain and the mean adjacent strain in the regions of interest.

None of the out of competition sessions resulted in a concussive diagnosis, as was discussed previously, the fact that there was no medical professional present may be a factor. The impacts that were simulated from these sessions had linear accelerations ranging from 70g to 225g and rotational accelerations ranging from 6679rads/s^2 to 47407 rads/s^s. The largest of the rotational accelerations occurred in Fighter 5 - Session 2, this acceleration was the highest single magnitude of all impacts recorded. And as was discussed in the previous section there is some concern about the validity of these unusually large magnitudes. It will also be discussed further in Chapter 7.

Impact 18 from Fighter 10 – Session 4 was the only impact that resulted in strain greater than the published thresholds. This impact had the largest peak linear acceleration in X, Y and Z, the second largest peak rotational acceleration. The levels of strain found from the simulation of this impact were greater than the thresholds for MPS in the corpus callosum and in the thalamus. The mean adjacent strain levels were greater than the thresholds for 50% probability of concussion in the corpus callosum, thalamus and brain stem. The fighter reported no symptoms to the knowledge of the writer, so it can only be assumed that no injury occurred. Although none of these impacts resulted in a concussive diagnosis, the levels of strain recorded are similar to those recorded from the competitive bouts.

Table 44: Sparring/Training Session Impact Data

	Fighter 8 - Session 1	**Fighter 9 - Session 1**	**Fighter 3 - Session 2**	**Fighter 8 - Session 1**	**Fighter 9 - Session 1**	**Fighter 9 - Session 1**	**Fighter 5 - Session 2**	**Fighter 10 - Session 4**
Impact Number	11	12	13	14	15	16	17	18
Peak Resultant Linear Acceleration (g)	89	195	78	70	165	162	102	225
Linear Acceleration Duration (ms)	8	5	7	9	15	15	10	14
Peak Linear Acceleration X (g)	46	160	11	50	122	121	57	167
Peak Linear Acceleration Y (g)	33	57	77	27	25	32	42	81
Peak Linear Acceleration Z (g)	69	131	10	44	112	108	90	151
Peak Resultant Rotational Acceleration (rads/s^2)	8732	21297	10311	6679	15994	15483	47407	22762
Rotational Acceleration Duration (ms)	10	5	7	9	15	15	10	19
Peak Rotational Acceleration X (rads/s^2)	2139	5834	10290	3546	4262	3863	33995	15169
Peak Rotational Acceleration Y (rads/s^2)	8189	20103	2120	5672	15742	14955	35255	20971
Peak Rotational Acceleration Z (rads/s^2)	3007	3926	1487	803	3284	1753	14467	7299
Peak Rotational Velocity (rads/s)	9.6	36.1	25.6	11..2	38.3	35.8	53	52.6
Direction	FR	F	R	FR	F	F	FL	F
Sim Duration (ms)	50	50	50	50	50	50	50	50
Head Impact Power (kW)	1.2	15.2	3.1	2.9	10.0	13.1	18.7	31.7

(Simulation input data for each of the impacts can be found in Appendix 6)

Table 45: Summary of Simulation Results for Sparring/Training Sessions

Region	Fighter 8 - Session 1	Fighter 9 - Session 1	Fighter 3 - Session 2	Fighter 8 - Session 1	Fighter 9 - Session 1	Fighter 9 - Session 1	Fighter 5 - Session 4	Fighter 10 - Session 4
Impact Number	11	12	13	14	15	16	17	18
CC MPS	3.40%	10.00%	11.20%	1.40%	8.30%	8.30%	10.70%	59.00%
CC MAS	1.70%	4.80%	5.40%	0.70%	4.23%	4.18%	5.50%	23.40%
Thalamus MPS	2.10%	6.00%	6.30%	0.73%	4.95%	4.60%	6.00%	34.50%
Thalamus MAS	1.70%	5.20%	3.90%	0.65%	4.30%	2.90%	5.96%	21.60%
Midbrain MPS	1.60%	3.90%	4.20%	0.63%	4.05%	3.30%	9.80%	13.90%
Midbrain MAS	1.23%	3.60%	3.77%	0.46%	3.00%	2.90%	6.20%	8.60%
Brainstem MPS	2.40%	7.10%	5.50%	1.00%	6.60%	4.30%	10.20%	19.60%
Brainstem MAS	0.74%	2.10%	1.64%	0.30%	1.93%	1.30%	3.50%	5.70%
Injury	No Injury	No Injury	No Injury	No Injury	No Injury	No Injury	No Injury	No Injury

Legend	
Mean Strain for No Injury	
50% Probability for Concussion	
Mean Strain for Concussion	

6.4 Data Analysis

MPS and MAS in the corpus callosum, thalamus, midbrain and brain stem have been recorded and compared to published thresholds. The levels of strain recorded in these regions have been plotted against a range of recorded and derived data in order to determine whether there is a linear trend. Complete tables and plots which detail the relationships that were found are available in Appendix 7 and 8 respectively. Also included is an analysis of HIP as a predictor for strain in the regions of interest, along with investigating HIP as a predictor for mTBI. As with MPS and MAS, HIP values have been plotted against strain in the regions of interest to determine whether there is a linear relationship between the two. The result of this investigation is shown in Table 46, in the form MPS (MAS). Complete plots for this data is available in Appendix 9.

Table 46: Summary of HIP vs strain in brain regions results

Brain Region	TBI Cases	No Injury Cases	All Cases
Corpus Callosum	0.2427 (0.2744)	0.3345 (0.3847)	0.2834 (0.3262)
Thalamus	0.2635 (0.2865)	0.3469 (0.4008)	0.3003 (0.3383)
Midbrain	0.4482 (0.5808)	0.6008 (0.6123)	0.5245 (0.6087)
Brain Stem	0.4025 (0.4266)	0.7209 (0.7714)	0.5409 (0.5562)

HIP performed the best when predicting the strain in the Midbrain, R^2 = 0.5245 and 0.6087 for MPS and MAS respectively. The predictive qualities of HIP ranged from 0.2834 for MPS in the corpus callosum to 0.6087 for MAS in the midbrain. Table 47 below shows that this represents the 2nd best single predictor examined in this study. With only PRA about the Z-axis outperforming HIP, with R^2 = 0.7245 and 0.7053 for strain in the midbrain and brain stem respectively. HIP performs similarly to the kinematic predictors in the corpus callosum and the thalamus, R^2 = 0.3262 and 0.3383 for HIP v corpus callosum and thalamus respectively. While, PLA in the Y-axis and PRA about the Z-axis resulted in R^2 between 0.3424 and 0.3682 for the corpus callosum and thalamus.

The strain in each brain region for the five events which resulted in a concussive injury, Fighter 1 – Bout 1, Fighter 2 – Bout 1, Fighter 3 – Bout 1, Fighter 4 – Bout 1 and Fighter 5 – Bout 1 is reported in the following sets of images (Figures 63 - 83). In the case where several impacts from the same event were simulated, the impact that resulted in

the largest strain will be reported. Also reported is the strain distribution in the entire brain.

The scale in the transverse slices of the brain maximum is set to 47% equal to the published threshold for grey matter [6]. For the images of each region, the scale is set to the default. For the images of each region the default scale is set to the maximum found in the region. All these events resulted in a concussive injury, although just Impact 2 and Impact 9 (Figures 68 - 72 and 83 - 87) resulted in strain greater than the published thresholds in any of the brain regions. These impacts have resulted in the largest distribution of strain throughout the entire brain.

The best predictors for strain for each of these regions investigated in this study based on the simulation results will be examined. i.e. the best linear relationship found between strain in the region and a recorded acceleration. For example: Peak Linear Acceleration in the X axis vs MPS in the corpus callosum. Table 46 details the relationships that were determined when all simulation results were plotted. R^2 for MPS and MAS in each region is reported in the form MPS (MAS).

Table 47: Summary of Single Best Predictor for Strain in each Brain Region

Brain region	**Linear Acceleration**		**Rotational Acceleration**	
	Axis	**R^2**	**Axis**	**R^2**
Corpus Callosum	Y	0.3146 (0.341)	Z	0.3195 (0.3577)
Thalamus	Y	0.3262 (0.3424)	Z	0.3242 (0.3682)
Midbrain	Y	0.4351 (0.3469)	Z	0.6992 (0.7245)
Brain Stem	Y	0.4954 (0.493)	Z	0.6659 (0.7053)

Utilising the new metric proposed in this study, MAS, has improved the prediction of almost all variables examined. The differences ranged from; a small decrease in R^2 for PLA in the Y-axis v midbrain and brain stem, to large increases in R^2 for HIP v Midbrain strain (16% increase).

Further statistical analysis was conducted in order to determine if any combination of the inputs proved to be a better predictor of strain in a region, this analysis was a Best Subset Regression analysis. The predictors that were tested are: peak resultant linear acceleration, peak resultant rotational acceleration, peak linear acceleration X, peak linear acceleration Y, peak linear acceleration Z, peak rotational acceleration X, peak rotational acceleration Y, peak rotational acceleration Z, linear acceleration duration, rotational acceleration duration, HIP and peak resultant rotational velocity. These predictors were used as free predictors for the analysis and the responses were: MPS and MAS in the corpus callosum, thalamus, mid brain and brain stem. The results of these analyses follow in Table 47. Data is reported in the form MPS (MAS) for each region. These results will be discussed in the next chapter, Chapter 7 Discussion.

Table 48: Results of best subset regression analysis

Region	**Number of Variables**	**Variables**	**R^2**	**R^2 (adj)**	**R^2 (pred)**	**Mallow's Cp**	**S**
Corpus Callosum	2	PLA Y PRV	0.49 (0.541)	0.422 (0.48)	0.299 (0.37)	-5.6 (-5.7)	0.16857 (0.062)
Thalamus	2	PLA Y PRV	0.5 (0.553)	0.434 (0.493)	0.316 (0.388)	-5.6 (-5.6)	0.0944 (0.053)
Midbrain	2	PLA Y PRA Z	0.792 (0.771)	0.764 (0.741)	0.722 (0.674)	-5.0 (-3.3)	0.028 (0.02)
Brain Stem	2	PLA Y PRA Z	0.799 (0.828)	0.772 (0.805)	0.707 (0.759)	-4.4 (-4.7)	0.042 (0.011)

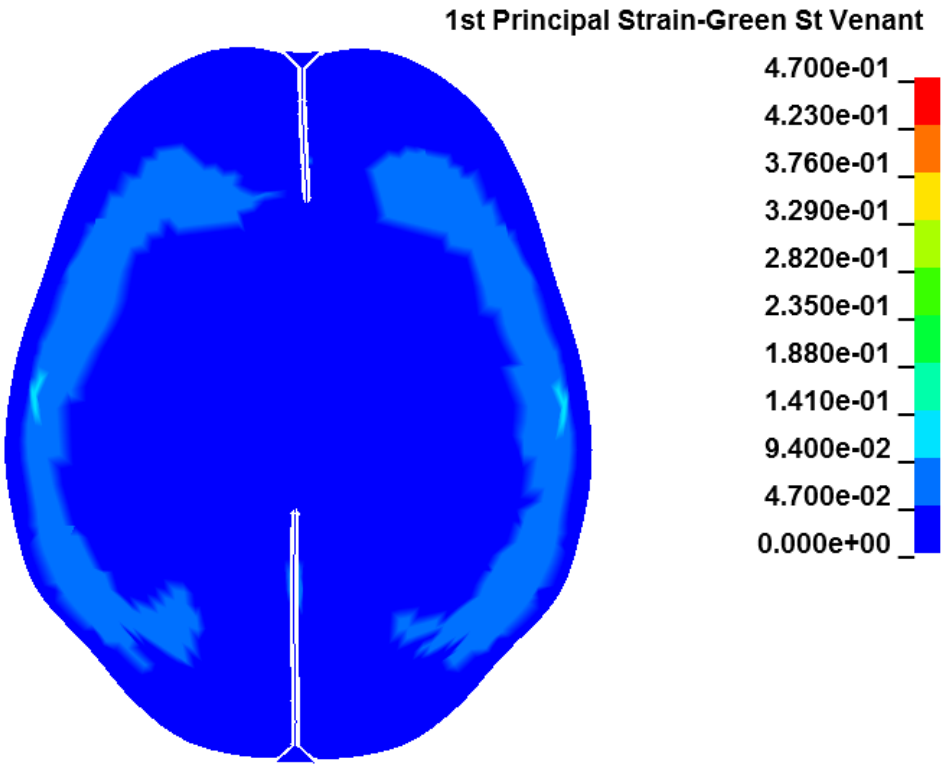

Figure 63: Impact 1 (Fighter 1 - Bout 1) Transverse brain slice (110g and 13,191 rads/s^2)

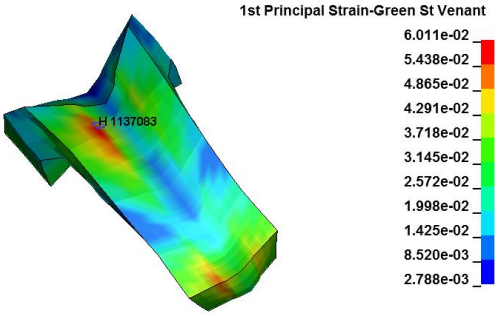

Figure 64: Impact 1 Corpus Callosum strain (MPS 6%)

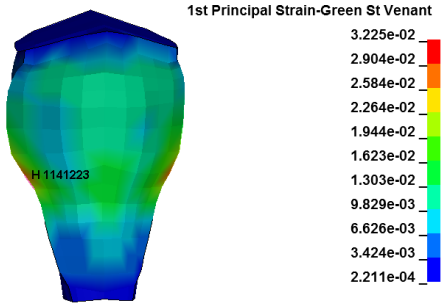

Figure 65: Impact 1 Brainstem strain (MPS 3.2%)

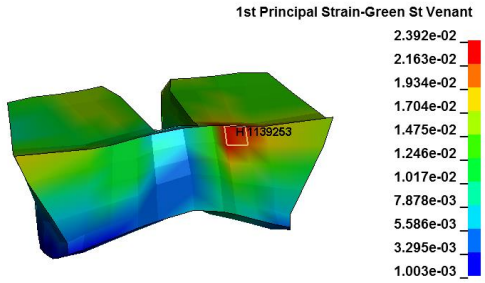

Figure 66: Impact 1 Midbrain strain (MPS 2.4%)

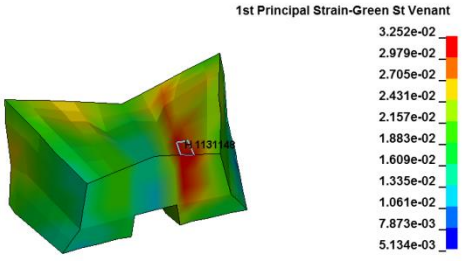

Figure 67: Impact 1 Thalamus strain (MPS 3.2%)

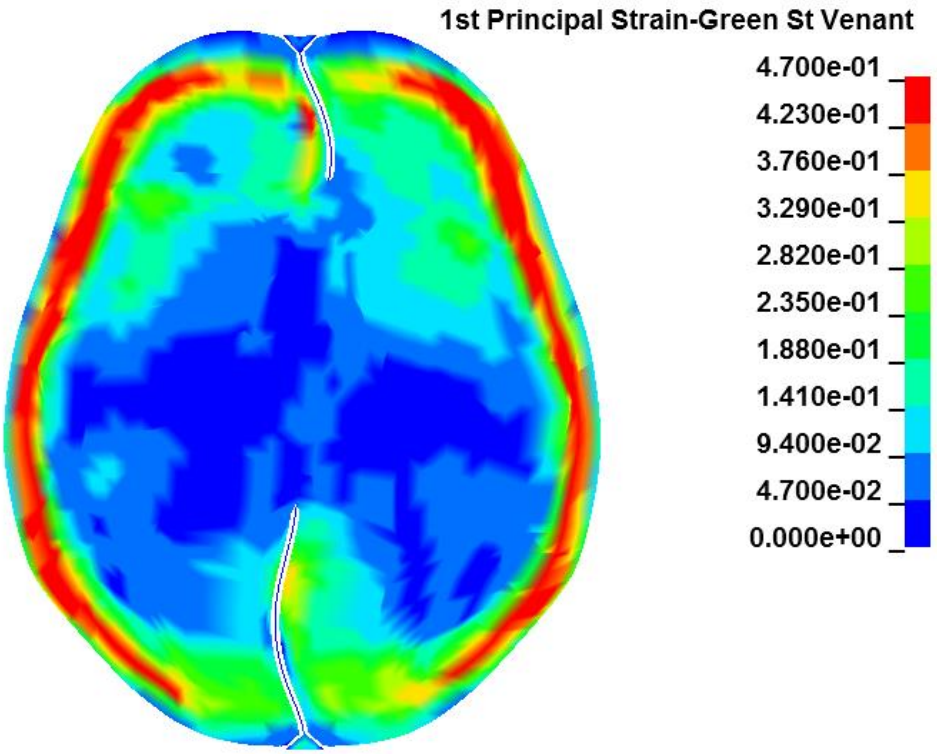

Figure 68: Impact 2 (Fighter 2 - Bout 1) Transverse brain slice (308g and 21,881 rads/s^2)

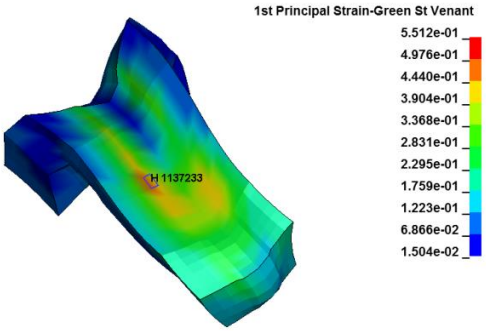

Figure 69: Impact 2 Corpus Callosum strain (MPS 53%)

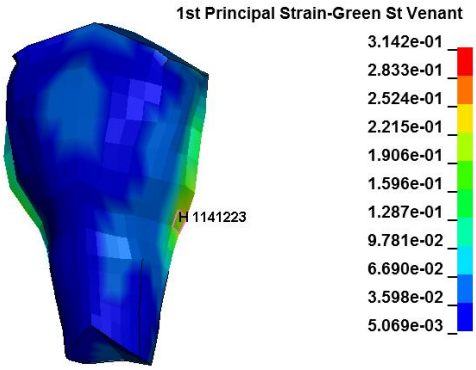

Figure 70: Impact 2 Brainstem strain (MPS 31.4%)

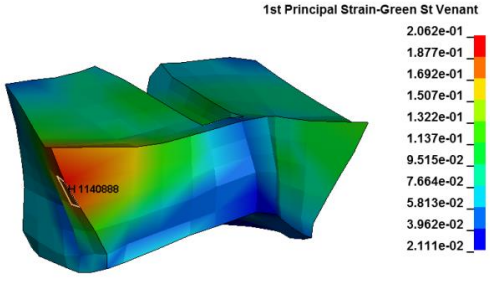

Figure 71: Impact 2 Midbrain strain (MPS 21%)

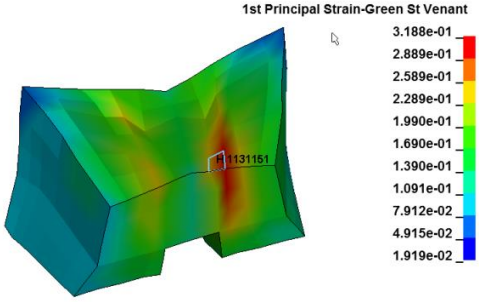

Figure 72: Impact 2 Thalamus strain (MPS 32%)

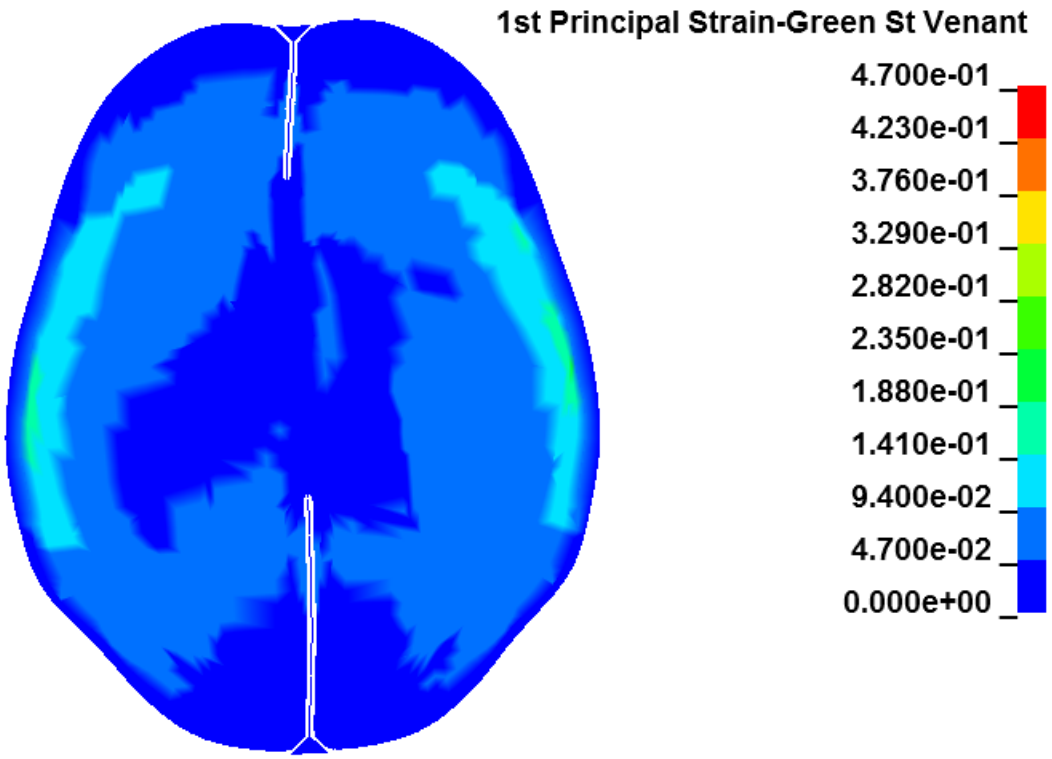

Figure 73: Impact 3 (Fighter 3 - Bout 1) Transverse brain slice (41g and 2906 rads/s^2)

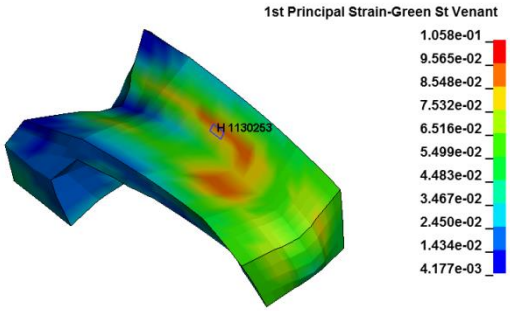

Figure 74: Impact 3 Corpus Callosum strain (MPS 10.5%)

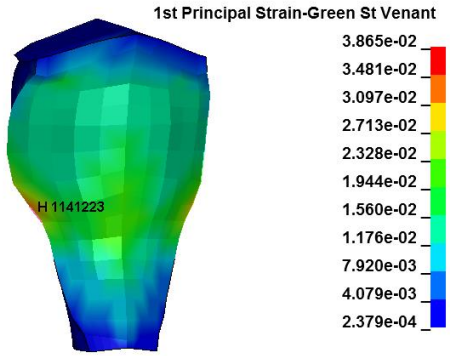

Figure 75: Impact 3 Brainstem strain (MPS 3.8%)

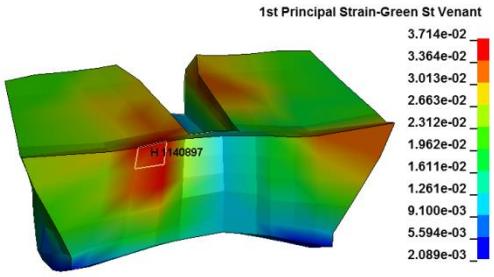

Figure 76: Impact 3 Midbrain strain (MPS 3.7%)

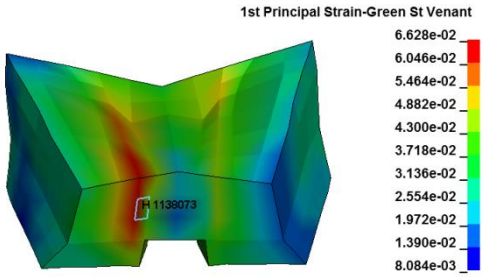

Figure 77: Impact 3 Thalamus strain (MPS 6.6%)

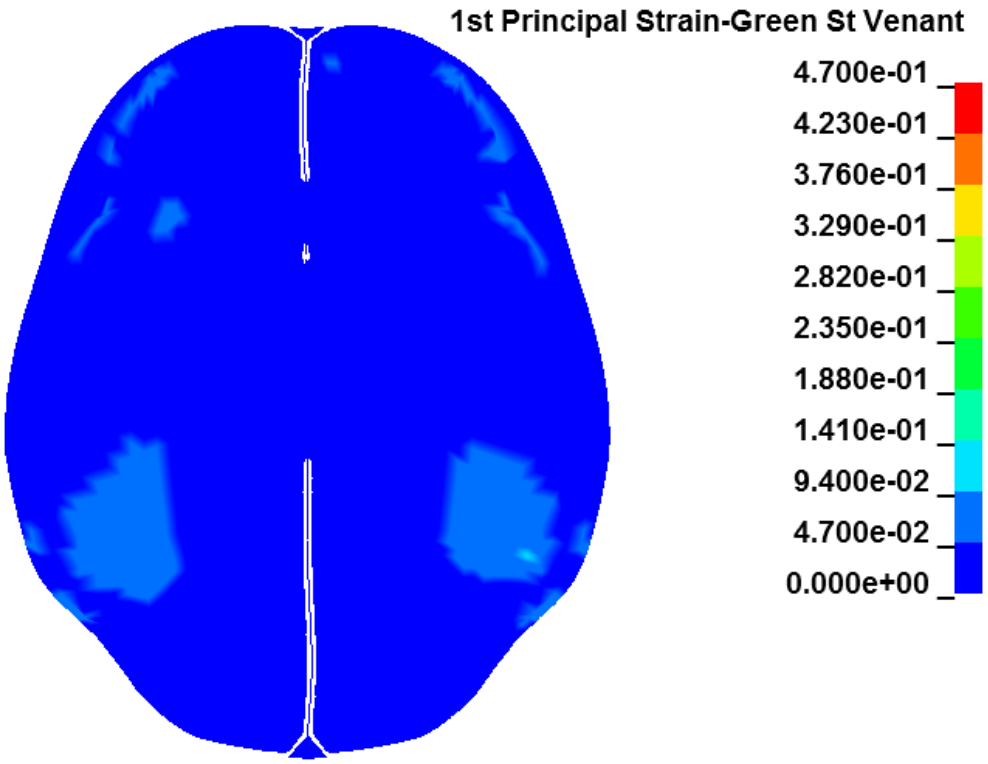

Figure 78: Impact 5 (Fighter 4 - Bout 1) Transverse brain slice (141g and 13609 rads/s^2)

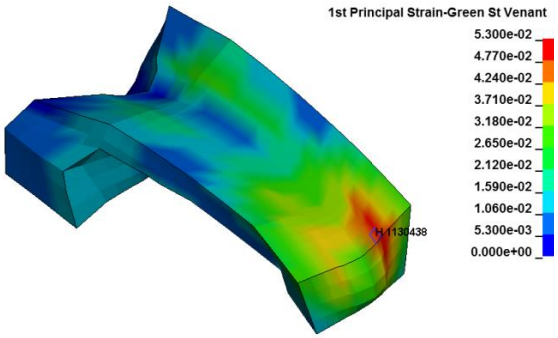

Figure 79: Impact 5 Corpus Callosum strain (MPS 5.3%)

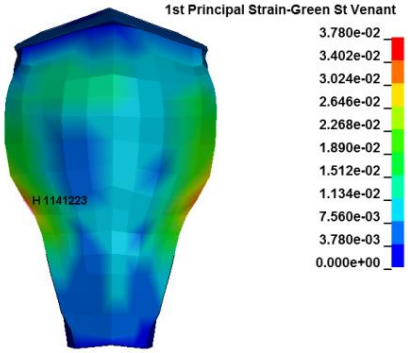

Figure 80: Impact 5 Brainstem strain (MPS 3.8%)

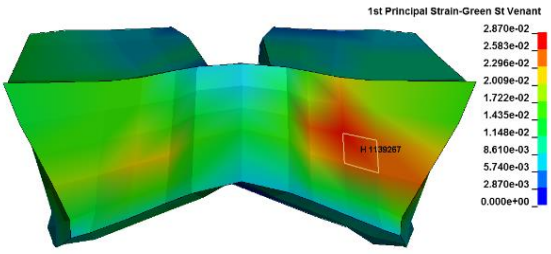

Figure 81: Impact 5 Midbrain strain (MPS 2.87%)

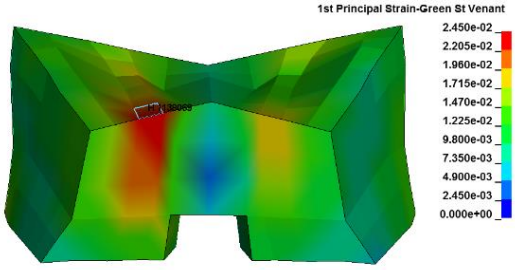

Figure 82: Impact 5: Thalamus strain (MPS 2.45%)

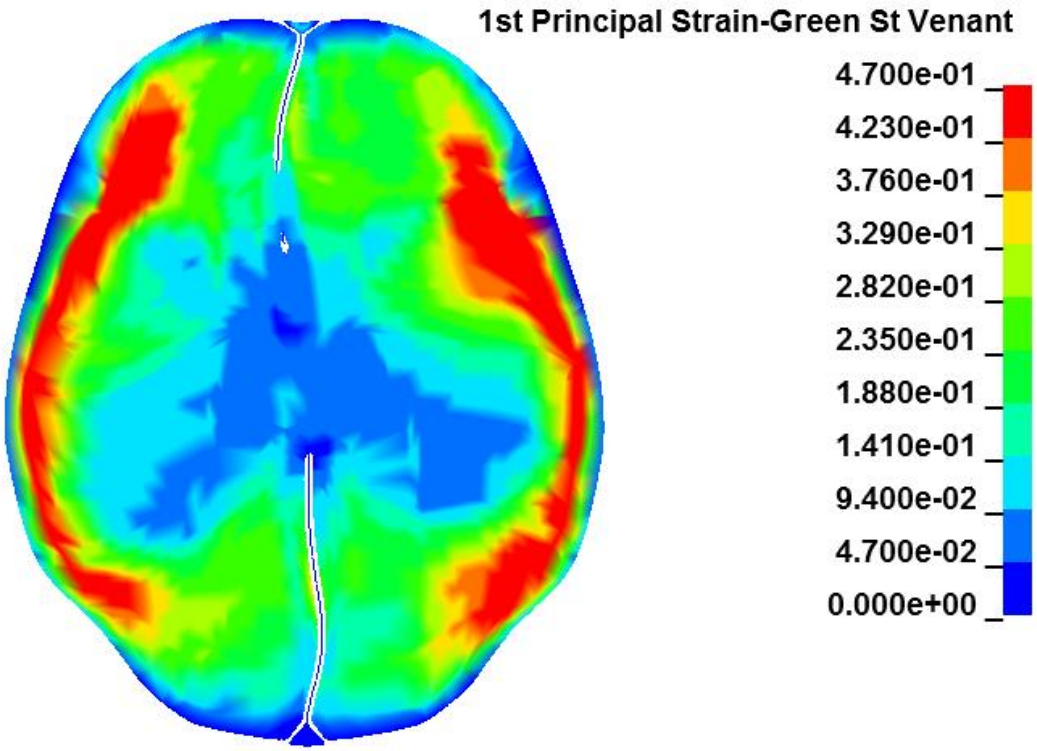

Figure 83: Impact 9 (Fighter 5 - Bout 1) Transverse brain slice (104g and 27212 rads/s^2)

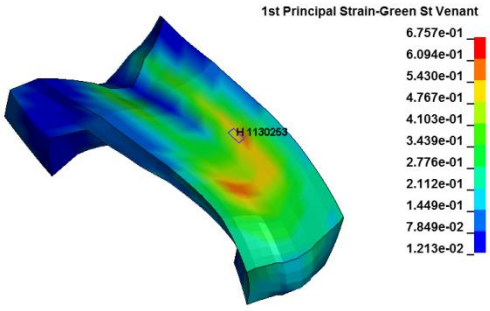

Figure 84: Impact 9 Corpus Callosum strain (MPS 67.5%)

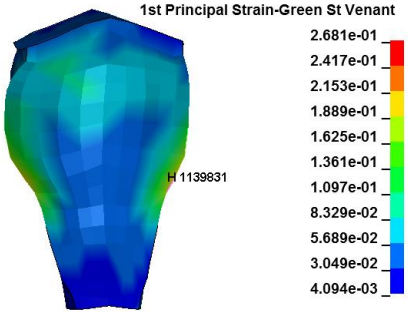

Figure 85: Impact 9 Brain stem strain (MPS 26.8%)

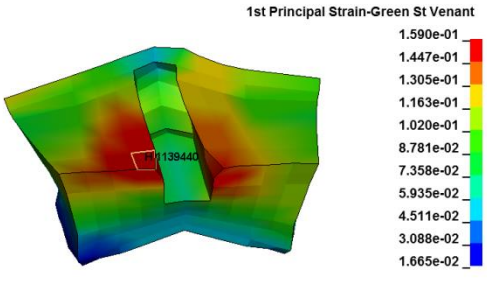

Figure 86: Impact 9 Midbrain strain (MPS 15.9%)

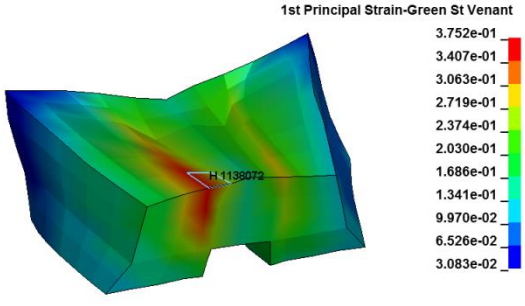

Figure 87: Impact 9 Thalamus strain (MPS 37.5%)

Chapter 7 Discussion

The purpose of this study was to measure and simulate *in vivo* head impacts in MMA with an instrumented mouthguard developed in Stanford University, California [120]. A total of 434 *in vivo* impacts were recorded. All impacts have been confirmed by comparing timestamped video footage of each session against the timestamp on the mouthguards data record. Further confirmation was achieved by ensuring the direction of the impact data matches the direction that the mouthguard recorded.

Data from a total of 434 impacts were recorded across 4 distinct types of combat sports sessions; MMA sparring, boxing sparring, MMA training and competitive MMA events. The majority of impacts fall into the "Low" linear acceleration range (69.36%), those in the "Very Serious" range or higher represent a very small percentage of all impacts (5.3%). Similarly, the majority of the rotational accelerations are in the "Low" range (71.66%) and those in the "Very Serious" range or higher are also a small percentage of the total (7.83%). Impacts recorded in the "Very Severe" linear range (2.77%), > 150g, are recognised as being unusually high and there are 3 possible reasons for this. It is possible that the mouthguard fit is not ideal and when an impact is received the mouthguard moves slightly while in the participants mouth. This could result in very high acceleration values. It is also possible when an impact is received the lower jaw comes into contact with the mouthguard, again this may result in very high acceleration values. The final and most likely reason for these very high accelerations is that the mouthguard takes a direct impact, resulting in large spikes in the accelerations recorded. Confirming or rejecting this outside of a laboratory setting is problematic, as the quality of video footage is not always high enough to clearly see where exactly the impact occurs. This is due, in part, to the fact that the impacts duration is short and could take place in as few as 2 video frames. In order to confirm or reject these impacts several camera angles of each fight would be required, using high resolution and frame rate cameras. Impacts recorded > 150g have been confirmed in the way described in the introduction to this section and as such they are treated as true impacts.

The impacts in the "Very Serious" rotational acceleration range, > 25000 rads/s^2, are treated the same as above. They have been confirmed in the method described in a previous section but it is possible that they too have recorded very high accelerations due to a direct mouthguard impact, an ill-fitted mouthguard or an impact from the lower jaw. The Stanford mouthguard has been validated for American Football impacts but it is not

validated for MMA impacts [121]. Validation for these kinds of impacts is on-going but is as yet unpublished.

When the direction of the impacts is examined, the most common location is “Front Left” (28.3%), i.e. the front left of the fighter’s face. Following that is impacts received directly to the “Front” of the face of the fighter (21.42%). Combined impacts from the “Left” and “Right” represent a large portion of the total impacts (30.65%). Impacts received directly to the rear of the head are illegal in both MMA and boxing and as expected these impacts represent a very small percentage of the total (2.3%).

When the frequency of the impacts is examined for competitive events, it was found that the fighter that received the lowest frequency was uninjured (Fighter 6 – Bout 1). Fighter 5 – Bout 1 had the highest frequency of all the participants that were diagnosed with a concussive injury (3.89), while the highest frequency of all events (Fighter 4 – Bout 2) at 3.95 was not diagnosed with a concussive injury. The mean impacts/minute for each event type has been calculated and indicates that competitive events result in the average rate increasing by 0.45 impacts/min. This represents an increase of 37% when compared to MMA Sparring and MMA Training events types. Although these means differ by 37%, when the range for each session type is examined (competitive events 0.67 to 3.95 and out of competition events 0.66 to 2.33) it is found that impact frequency is not a good predictor of injury.

The sessions from the Boxing Sparring events have not been included when calculating the mean for each event type as it was in a different sport which only allows for punches to the head and body. Meaning the increased frequency at which they received head impacts is to be expected and as such is not comparable to MMA data. When the participants that took part in competitive events are ranked by the total number of impacts received, four of the top five are participants who were diagnosed with a concussive injury; this is shown in Table 39. Fighter 3 – Bout 1 received just 3 impacts which were all in the “Moderate” severity range with a high impact frequency, all others that received more than 10 impacts in their bout were diagnosed with a concussive injury.

Four of the five participants that were diagnosed with a concussive injury have the longest durations. Table 40 details the impact durations recorded. Simulation input data for these

impacts can be found in Appendices 6 and 7. The only participant who was diagnosed with a concussive injury but did not have a longer linear acceleration duration, Fighter 5 – Bout 1 (Impacts 7, 9 and 10), did have two impacts with the longest rotational acceleration duration. A plot of linear acceleration duration vs rotational acceleration duration is shown in Figure 50. This would indicate that duration of the impact, as well as PLA and PRA are important factors to take into account when attempting to predict the likelihood of a concussive injury being diagnosed. This agrees with a study conducted by Gilchrist *et al.*, who found that the magnitude of PLA and PRA required to cause a concussive injury decreases as the impact duration increases [87].

As it is not always possible to associate a single impact to a diagnosis, the linear and rotational acceleration duration for the impact which resulted in the largest rotational acceleration in a session was plotted (Figure 57). It shows that all the impacts with a PLA duration greater than 15ms resulted in a concussive diagnosis for the participants. It also shows that three of the four impacts with a PRA duration greater than 25ms resulted in a concussive diagnosis. This may indicate an increased likelihood of a concussive injury for impacts with a PLA duration greater than 15ms or PRA duration greater than 25ms. In total of the six impacts that exceeded these durations, five of those resulted in a concussive diagnosis for the participant.

When the results from this study are compared to the literature, Duhaime and Beckwith reported a mean PRA of 3620 rad/s^2 and 4253 rad/s^2 respectively for impacts that could be directly linked to an concussion [45] [122]. This study has found that in MMA the PRA is considerably higher, 5707 rad/s^2 for mTBI and 5028 rads/s^2 for no injury. The studies by Duhaime and Beckwith were conducted in American Football and Ice Hockey and as such the higher magnitudes of PRA in MMA are expected as the majority of impacts are due to direct head impacts, as opposed to collision-based impacts in American Football and Ice Hockey. Broglio reported that a PLA of greater than 96.1g and PRA of greater than 5582.3 rads/s^2 increasing the probability of a concussion in high school American Football players [90]. These rotational acceleration magnitudes are similar to those found in this study.

In a further study Beckwith reported a 50th percentile impact PLA of 20.5g and PRA of 1400 rads/s^2 and 95th percentile PLA of 62.7g and PRA of 4378 rads/s^2 [92]. In this study the 50th percentile impact was found to have a PLA of 20.78g and PRA of 2805.2 rads/s^2 and the 95th percentile PLA of 90.6g and PRA of 20579.47 rads/s^2. The 50th percentile impact PLA is very similar to that found by Beckwith, the 50th percentile PRA is considerably higher. The 95th percentile impact PLA and PRA are also considerably higher than those found by Beckwith. This can be explained by the difference in the types of impacts received in the different sports, MMA impacts are direct head impacts and as such larger magnitudes would be expected. Using the same data set as Beckwith, Rowson found that concussive impacts had a mean PRA of 5022 rads/s^2 and a PRV of 22.3 rads/s [41]. These are similar to those found in this study.

To summarise, these head acceleration results indicate that the best predictors for a concussive injury are impact duration (both PLA duration and PRA duration), which has also been found in other studies [87] [123]. Furthermore, given that the magnitudes of PLA and PRA were the main difference between those that were diagnosed with a concussive injury and those that were not, this indicates that there may be thresholds for PLA and PRA in sub-concussive impacts. It also indicates that there may be a cumulative effect of sub-concussive impacts. This due to the fact that the concussed and non-concussed groups received a similar impact frequency, while those that received more impacts total were more likely to be diagnosed with a concussive injury.

When examining the simulation results overall, it was found that the best single predictor for strain across all of the variables examined was PRA about the Z axis when plotted against MAS in the midbrain, $R^2 = 0.7245$. None of the kinematic inputs were found to be a good predictor for concussion. When HIP was investigated as a predictor for mTBI, it was compared to the study by Newman *et al.* [89]. Newman found that a HIP value of 12.8kW represented a 50% probability of an mTBI. In this study, nine simulated impacts exceeded this threshold and 3 of those resulted in an mTBI (33%). Given the small sample size, this is not unexpected. The mean HIP values for simulated impacts from a session that did result in an mTBI were 78% greater than the impacts that were received in a session that did not (22.7kW and 12.7kW respectively).

HIP was shown to be the 2nd best single predictor for strain in all brain regions investigated. It performed as well as, or better than, any of the kinematic based strain predictors. R^2 values for HIP found in this study ranged from 0.2834 – 0.5409 for MPS and 0.3262 – 0.6087 for MAS. As with the kinematic based predictors, the worst prediction was found in the corpus callosum and the best was in the brain stem for MPS and midbrain for MAS. Only PRA about the Z-axis outperformed HIP as a predictor for strain.

The results from the set of best subset regression analyses indicate that using an additional predictor for each region shows an improvement over using a single predictor. As R^2 (adj) will be reported as it is an adjusted value that takes the number of predictors into account. R^2 (adj) for each region shows an increase when compared to R^2 from the single predictors' tests. In the corpus callosum an increase from 0.3577 for MAS and PRA about the Z axis to 0.48 when PLA in the Y axis and PRV. The same 2 predictors improve the predictions for the thalamus, going from 0.362 for a single predictor to 0.493 for 2 predictors. When the results for the midbrain and brain stem are compared, it indicates that PLA in the Y axis and PRA in about the Z axis show an improvement when compared to a single predictor. The midbrain increases from 0.7245 for a single predictor to 0.764 for 2 predictors and brain stem from 0.7053 for a single predictor to 0.805 for 2 predictors. Although HIP was the 2nd best predictor for strain investigated in this study, it was not a part of one of the best subsets in this statistical analysis.

Mean adjacent strain was proposed as an alternative metric in this study and it has shown some encouraging results. Sixteen different relationships were examined in this study; PLA, PRA, HIP, PRV and duration were compared to MPS and MAS in the brain regions of interest. In all but three of these examinations, MAS saw an improvement in the prediction of strain. Just one of these three saw a substantial reduction, (20%, 0.4351 for MPS and 0.3469 for MAS). This was found in the relationship between PLA in the Y-axis and strain in the midbrain. All other relationships examined saw an improvement in the predictions, with an average of 6.43% increase. The largest increase was found when HIP and strain in the midbrain (16%) were examined.

To summarise, these results indicate that the best predictors for strain is PLA in the Y axis and PRA about the Z axis across all regions. With HIP being the 2nd best single predictor examined across all regions. Whereas, when the corpus callosum and thalamus are examined it can be seen that the addition of PRV to PLA in the Y axis improves the predictions for strain. In the midbrain and brain stem the combining PLA in the Y axis and PRA about the Z axis improves the predictions for strain. PLA in the Y axis being a good predictor across all regions indicates that impacts received laterally result in increased levels of strain in the brain, similar to that found in other studies that examined impact direction as a predictor for strain [70] [124] [32] [125].

Chapter 8 Conclusion

This study's purpose was to measure and simulate *in vivo* head impacts in MMA, 434 *in vivo* MMA head impacts were recorded and 18 impacts with the largest rotational accelerations were simulated. Several kinematic based inputs have been examined in order to determine if they are a good predictor for strain and concussion diagnosis. This study found that some of the kinematic based inputs are reasonable predictors for strain in certain regions of the brain, with PRA about the Z axis and PLA about the Y axis being the best single predictors for strain in the regions examined in this study. When combined, these 2 predictors provide an improved prediction in the midbrain and brain stem. When combined PRV and PLA in the Y axis improve the prediction for strain in the corpus callosum and thalamus. PLA in the Y axis has been shown to be a good predictor for strain in all brain regions investigated, indicating that these regions are particularly sensitive to lateral impacts. Although, these kinematic based inputs do not appear to be good predictors for a concussion diagnosis.

Five concussions were recorded in this study, of those five cases, just two of the simulated impacts resulted in strains greater than the published thresholds. There are many factors that may influence the probability of a person being diagnosed with a concussion; linear acceleration magnitude, rotational acceleration magnitude, impact direction, impact duration, concussion history, number of impacts received and gender among others [87] [85] [88] [118] [119] [126] [127] [80]. Only when all of these factors can be addressed, can the full picture be seen. Overall it can be stated that the participants who were diagnosed with a concussive injury received more impacts per minute (37%), increased mean PLA (47%), increased mean PRA (13%), a small increase in mean PRV (3.7%) and longer impact durations when compared to those that were not diagnosed with a concussive injury. Impact duration (both PLA and PRA) have been shown to be the best predictor for a concussive diagnosis, eight of the simulated impacts had durations greater than 15ms for PLA or 25ms for PRA and seven of these resulted in a concussive diagnosis. Of the five events that resulted in a concussive diagnosis, four of those participants received the most impacts in competitive events; this would indicate that there is a cumulative effect of multiple sub-concussive impacts that increases the likelihood of a concussive diagnosis.

The magnitudes of rotational acceleration found in this study for concussed participants are similar to those found in other sports, PRA and PRV of 5707 rads/s^2 and 17.11 rads/s in this study and PRA and PRV of 5022 rads/s^2 and 22.3 rads/s in collegiate American Football [41]. The 50th percentile impact in this study was found to be very similar to the 50th percentile impact found in collegiate American Football and Ice Hockey, 20.5g for American Football and Ice Hockey and 20.78g in this study [92].

The human tolerance to short duration, high magnitude impacts in unhelmeted sports remains unknown, but the data in this study is important to help understand the magnitude and variation of these tolerances. This study shows that not only the peak resultant acceleration magnitude of the impacts is an important factor but it is also necessary to examine the direction from which it was received, the number of impacts received, the impact duration and the profile of the component parts of the impacts in order to best predict the probability of a concussive diagnosis. The number of fighters and events in this study is limited, but the study is on-going.

8.1 Limitations

There are several limitations to this study that need to be addressed. The GHBMC is a partially validated human body model. It has been validated for displacement [60] but has not been validated for strain. Furthermore the model itself is a 50^{th} percentile model, which is based on a person who fit some dozen anthropomorphic measures [61]. This means the model is unlikely to accurately represent the mass, volume or response of the brain of any of the participants and as such is an approximation. Some of the materials properties of this model could also be improved, for example the modelling of the CSF as a fluid, rather than as a solid as it currently is. A recent study into the mechanical behaviour of the dura matter in the meninges, with a porcine brain, has shown the dura has regional differences in thickness and is not homogenously stiff. Furthermore the dura matter and sagittal sinus were shown to have anisotropic behaviour [128]. The addition of these material properties to FE models could improve the overall response and behaviour.

The Stanford mouthguards also have some limitations. These devices have been validated for American Football impacts but have not been validated for MMA impacts, which are typically much shorter durations and higher magnitudes than those found in helmeted sports [121]. The higher magnitude impacts recorded in this study, > 150g and/or > 25krads/s^2, are unusually high and may be due to three possible reasons. Firstly, the mouthguard itself may not fit correctly. Meaning that an impact may result in the mouthguard moving in the participant's mouth, this could result in excessive acceleration data. Secondly, the lower jaw state has been shown to play an important role in the accurate recording of accelerations [55]. And as such, if the lower jaw impacts the mouthguard when an impact is received it could also result in excessive acceleration. Lastly, and the most likely cause, is that the mouthguard itself takes a direct impact. Confirming or reject this can be extremely problematic outside of laboratory setting. When sessions are recorded for video, the short duration impacts are over in a very small number of frames and there is just one angle of the session. This means it is very difficult to see exactly where the impact occurs. Validation for the short duration, high magnitude impacts is ongoing but is as yet unpublished.

When confirming impacts through video footage they often need to be timestamped with external software. The best effort is made when ensuring that all timestamps and impact locations are matching, although this is not always possible due to poor angles and/or video quality. Any impacts that cannot be seen clearly or their direction cannot be confirmed, are not treated as true impacts. Therefore, it is possible that some real impacts have been missed.

Furthermore, as was discussed previously medical professionals attend all competitive events and the participants are examined and diagnosed post fight. Unfortunately, SCAT5 tests were not carried out by the medical professionals at any event to date. Therefore, the ability to correlate the severity of symptoms or the change in function is severely limited. SCAT5 tests have begun with the participants for future events, with the recent introduction of a physiotherapist to the research group.

8.2 Future Work and Recommendations

Based on the development of this study's design and results, there are several areas that future work that can investigate and improve upon. Firstly, increase the participant count. Increasing the number of participants would greatly increase the amount of opportunities to collect data and in turn increase the overall number of recorded impacts. Doing so will only improve the quality of any further conclusions drawn.

In relation to the dental moulding process, this study found that up to 50% of moulds were rejected by the manufacturer due to them being low quality impressions. Many of the participants were also quite uncomfortable with the impression process. This could be improved upon by utilising 3-d dental scanning technology. It is less invasive than taking an imprint of the teeth and would reduce the possibility that opportunities to collect data may be missed due to low quality impressions.

As discussed in the previous section, the Stanford mouthguard is as yet unvalidated for MMA impacts. Conducting validation studies into short duration, high magnitude impacts will be essential to the future of work in this area. Also discussed in the previous section, obtaining high quality video of events was problematic. Further studies using this study design could investigate obtaining several angles of high-quality video at an event. Doing so would also increase the accuracy of confirmed impacts, as all impacts cannot be confirmed through footage from a single, fixed angle video.

In this study 434 confirmed impacts were recorded and 18 were simulated. Increasing the number of simulated impacts would help to better understand which kinematic inputs have the largest influence on strain in the brain. Developing a system where all confirmed impacts are formatted as simulation files by Matlab once processed and then a further system for running batches of simulations at once would greatly increase the efficiency of the study. And as such, would greatly improve the knowledge base and predictive qualities of research in this field.

In order to minimise the computational cost of simulations in this study, 50ms of the full 200ms data for each impact was used. Future work with this data set could, in conjunction with the previous recommendation, examine the full 200ms of data for each simulation. This would be to ensure that the complete response from any confirmed impact could be examined in full.

The falx and tentorium have been highlighted by research as potential areas of interest in mTBI research. They have been shown to potentially influence the level of strains in the corpus callosum and brain stem recorded in simulated impacts [129]. The falx was not included in this study as in the GHBMC model, it is a 2-d part made of shell elements. Introducing this topic would require investigating a different type of strain due, which was outside of the scope in this study. The tentorium is not included in the GHBMC model at all. It would be an interesting area of future research with this data set.

The orientation of axons in the white matter has been highlighted by recent studies as an important factor in the prediction mTBI [130]. It was not possible to investigate this area of research as the GHBMC model is isotropic and does not account for axonal direction. A potential area of future work would be to investigate anisotropic material models and apply them to the white matter parts of the brain model.

This study focused on MMA exclusively, it could be opened up to other sports. Rugby Union, American Football, Rugby League, Boxing, Ice Hockey and Lacrosse are some other sports that have been studied previously, mainly through recreating impacts as discussed earlier in this study. Collecting *in vivo* data from these sports and comparing them to the data collected from MMA, would better inform this field of research to understand what the potentially most dangerous or injurious impacts would be. As each different sport would have a different impact profile, duration, magnitude, as well as different concussion incident rates.

References

[1] J. A. Langlois *et al.*, "Traumatic Brain Injury in the United States: Emergency Department Visits, Hospitalizations, and Deaths," *J. Sci. Med. Sport*, vol. 21, no. 5, pp. 1004–1007, 2018, doi: 10.1016/j.jsams.2018.03.011.

[2] C. A. Taylor, J. M. Bell, M. J. Breiding, and L. Xu, "Traumatic Brain Injury–Related Emergency Department Visits, Hospitalizations, and Deaths — United States, 2007 and 2013," *Centers Dis. Control Prev. Morbitity Mortal. Wkly. Rep.*, vol. 66, no. 9, pp. 1–16, 2017, doi: 10.15585/mmwr.ss6609a1.

[3] W. H. Meeuwisse *et al.*, "The Berlin 2016 process: a summary of methodology for the 5th International Consensus Conference on Concussion in Sport," *Br. J. Sports Med.*, p. bjsports-2017-097569, 2017, doi: 10.1136/bjsports-2017-097569.

[4] V. G. Coronado *et al.*, "Trends in Sports- and Recreation-Related Traumatic Brain Injuries Treated in US Emergency Departments," *J. Head Trauma Rehabil.*, vol. 30, no. 3, pp. 185–197, 2015, doi: 10.1097/HTR.0000000000000156.

[5] A. Delouche *et al.*, "Diffusion MRI: Pitfalls, literature review and future directions of research in mild traumatic brain injury," *Eur. J. Radiol.*, vol. 85, no. 1, pp. 25–30, 2016, doi: 10.1016/j.ejrad.2015.11.004.

[6] D. Patton, A. McIntosh, and S. Kleiven, "The Biomechanical Determinants of Concussion: Finite Element Simulations to," *J. Appl. Biomech.*, pp. 721–730, 2013, doi: 10.1123/jab.2014-0223.

[7] S. Kleiven, "Predictors for traumatic brain injuries evaluated through accident reconstructions," *Stapp Car Crash J.*, vol. 51, no. November 2007, pp. 81–114, 2007, doi: 2007-22-0003 [pii].

[8] D. C. Viano, I. R. Casson, E. J. Pellman, L. Zhang, A. I. King, and K. H. Yang, "Concussion in professional football: Brain responses by finite element analysis: Part 9," *Neurosurgery*, vol. 57, no. 5, pp. 891–915, 2005, doi: 10.1227/01.NEU.0000186950.54075.3B.

[9] M. G. Hutchison, D. W. Lawrence, M. D. Cusimano, and T. A. Schweizer, "Head Trauma in Mixed Martial Arts," *Am. J. Sports Med.*, vol. 42, no. 6, pp. 1352–1358, 2014, doi: 10.1177/0363546514526151.

[10] G. J. Buse, "No holds barred sport fighting: A 10 year review of mixed martial arts competition," *Br. J. Sports Med.*, vol. 40, no. 2, pp. 169–172, 2006, doi:

10.1136/bjsm.2005.021295.

[11] D. King, P. A. Hume, M. Brughelli, and C. Gissane, “Instrumented mouthguard acceleration analyses for head impacts in amateur rugby union players over a season of matches,” *Am. J. Sports Med.*, vol. 43, no. 3, pp. 614–624, 2015, doi: 10.1177/0363546514560876.

[12] D. King, P. Hume, C. Gissane, and T. Clark, “Head Impacts in a Junior Rugby League Team Measured with Wireless sensor X patch,” vol. 19, no. January, pp. 13–23, 2017, doi: 10.3171/2016.7.PEDS1684.

[13] E. McCuen *et al.*, “Collegiate women’s soccer players suffer greater cumulative head impacts than their high school counterparts,” *J. Biomech.*, vol. 48, no. 13, pp. 3729–3732, 2015, doi: 10.1016/j.jbiomech.2015.08.003.

[14] F. H. Martini, J. L. Nath, and E. F. Bartholomew, *Fundamentals of Anatomy and Physiology*, 10th ed. Pearson, 2015.

[15] Karolinska Institue, “Atlas: Corpus Callosum. Central Nervous System - Visual Perspectives.” http://cnsvp.stanford.edu/atlas/corpus_callosum.html (accessed Sep. 11, 2019).

[16] “Meninges: Function and Layers.” https://www.thoughtco.com/brain-anatomy-meninges-4018883 (accessed Sep. 11, 2019).

[17] P. Johns, *Clinical Neuroscience*. Elsevier Ltd, 2014.

[18] T. Poluyi, “Control System Development for Six Degree of Freedom Spine Simulator,” 2014.

[19] D. H. Daneshvar, D. O. Riley, C. J. Nowinski, A. C. McKee, R. A. Stern, and R. C. Cantu, “Long-Term Consequences: Effects on Normal Development Profile After Concussion,” *Phys. Med. Rehabil. Clin. N. Am.*, vol. 22, no. 4, pp. 683–700, 2011, doi: 10.1016/j.pmr.2011.08.009.

[20] R. C. W. Hall, R. C. W. Hall, and M. J. Chapman, “Definition, diagnosis, and forensic implications of postconcussional syndrome,” *Psychosomatics*, vol. 46, no. 3, pp. 195–202, 2005, doi: 10.1176/appi.psy.46.3.195.

[21] A. Sterr, K. A. Herron, C. Hayward, and D. Montaldi, “Are mild head injuries as mild as we think? Neurobehavioral concomitants of chronic post-concussion syndrome,” *BMC Neurol.*, vol. 6, pp. 1–10, 2006, doi: 10.1186/1471-2377-6-7.

[22] S. C. Rose, A. N. Fischer, and G. L. Heyer, “How long is too long? The lack of consensus regarding the post-concussion syndrome diagnosis,” *Brain Inj.*, vol. 29, no. 7–8, pp. 798–803, Jul. 2015, doi: 10.3109/02699052.2015.1004756.

[23] R. J. Echemendia *et al.*, “The Sport Concussion Assessment Tool 5th Edition (SCAT5),” *Br. J. Sports Med.*, vol. 5, no. 2, p. bjsports-2017-097506, 2017, doi: 10.1136/bjsports-2017-097506.

[24] M. McCrea, T. Hammeke, G. Olsen, P. Leo, and K. Guskiewicz, “Unreported Concussion in High School Football Players: Implications for Prevention,” *Clin. J. Sport Med.*, vol. 14, no. 1, pp. 13–17, 2004, doi: 10.1097/00042752-200401000-00003.

[25] C. R. Moon, Donald W., Beedle, Charles W., Kovacic, “Peak head acceleration of athletes during competition - football,” *Med. Sci. Sports*, vol. Vol 3, no. Spring, p. pp 44-50, 1971.

[26] M. WE., “Calibration and Utilization of an Instrumented Football Helmet for the Monitoring of Impact Accelerations,” The Pennsylvania State University, 1983.

[27] R. S. Naunheim, J. Standeven, C. Richter, and L. M. Lewis, “Comparison of impact data in hockey, football, and soccer,” *J. Trauma*, vol. 48, no. 5, pp. 938–941, 2000, doi: 10.1097/00005373-200005000-00020.

[28] B. R. Cummiskey, “Characterization and evaluation of head impact sensors and varsity football helmets,” 2015.

[29] D. A. Patton, “A Review of Instrumented Equipment to Investigate Head Impacts in Sport,” *Appl. Bionics Biomech.*, vol. 2016, 2016, doi: 10.1155/2016/7049743.

[30] G. P. Siegmund, S. J. Bonin, J. F. Luck, and C. R. D. Bass, “Validation of a Skin-Mounted Sensor for Measuring In-Vivo Head Impacts,” *Int. Res. Counc. Biomech. Inj.*, pp. 182–183, 2015.

[31] D. Nevins, L. Smith, and J. Kensrud, “Laboratory evaluation of wireless head impact sensor,” *Procedia Eng.*, vol. 112, pp. 175–179, 2015, doi: 10.1016/j.proeng.2015.07.195.

[32] A. S. McIntosh, D. A. Patton, B. Fréchède, P. A. Pierré, E. Ferry, and T. Barthels, “The biomechanics of concussion in unhelmeted football players in Australia: A case-control study,” *BMJ Open*, vol. 4, no. 5, pp. 1–10, 2014, doi: 10.1136/bmjopen-2014-005078.

[33] D. King, C. Gissane, M. Brughelli, P. A. Hume, and J. Harawira, “Sport-related concussions in New Zealand: A review of 10years of Accident Compensation Corporation moderate to severe claims and costs,” *J. Sci. Med. Sport*, vol. 17, no. 3, pp. 250–255, 2014, doi: 10.1016/j.jsams.2013.05.007.

[34] R. Greenwald, J. Chu, and J. Crisco, “Head Impact Telemetry System (HITS) for

measurement of head acceleration in the field," *Proc. Am. Soc. Biomech. Annu. Meet.*, 2003, [Online]. Available: https://asbweb.org/conferences/2003/pdfs/203.pdf.

[35] S. M. Duma and S. Rowson, "The Biomechanics of Concussion: 60 Years of Experimental Research," 2014, pp. 115–137.

[36] S. M. Duma *et al.*, "Analysis of real-time head accelerations in collegiate football players," *Clin. J. Sport Med.*, vol. 15, no. 1, pp. 3–8, 2005, doi: 10.1097/00042752-200501000-00002.

[37] J. J. Crisco, "An Algorithm for Estimating Acceleration Magnitude and Impact Location Using Multiple Nonorthogonal Single-Axis Accelerometers," *J. Biomech. Eng.*, vol. 126, no. 6, p. 849, 2005, doi: 10.1115/1.1824135.

[38] S. Duma *et al.*, "Measuring real time head accelerations in collegiate football players," *Am. Soc. Biomech.*, no. May 2014, pp. 3–5, 2004.

[39] J. R. Funk, S. M. Duma, S. J. Manoogian, and S. Rowson, "Biomechanical risk estimates for mild traumatic brain injury," *Annu. Proc. / Assoc. Adv. Automot. Med. Adv. Automot. Med.*, vol. 51, pp. 343–361, 2007.

[40] J. P. Mihalik, D. R. Bell, S. W. Marshall, and K. M. Guskiewicz, "Measurements of head impacts in collegiate football players: an investigation of positional and event type differences," *Neurosurgery*, vol. 61, no. 6, pp. 1229–1235, 2007, doi: 10.1227/01.NEU.0000280147.37163.30.

[41] S. Rowson, J. G. Beckwith, J. J. Chu, D. S. Leonard, R. M. Greenwald, and S. M. Duma, "A six degree of freedom head acceleration measurement device for use in football," *J. Appl. Biomech.*, vol. 27, no. 1, pp. 8–14, 2011, doi: 10.1123/jab.27.1.8.

[42] J. G. Beckwith, R. M. Greenwald, and J. J. Chu, "Measuring head kinematics in football: Correlation between the head impact telemetry system and hybrid III headform," *Ann. Biomed. Eng.*, vol. 40, no. 1, pp. 237–248, 2012, doi: 10.1007/s10439-011-0422-2.

[43] S. Rowson, G. Brolinson, M. Goforth, D. Dietter, and S. Duma, "Linear and Angular Head Acceleration Measurements in Collegiate Football," *J. Biomech. Eng.*, vol. 131, no. 6, p. 061016, 2009, doi: 10.1115/1.3130454.

[44] R. Jadischke, D. C. Viano, N. Dau, A. I. King, and J. McCarthy, "On the accuracy of the head impact telemetry (hit) system used in football helmets," *J. Biomech.*, vol. 46, no. 13, pp. 2310–2315, 2013, doi: 10.1016/j.jbiomech.2013.05.030.

[45] J. G. Beckwith *et al.*, "Head Impact Exposure Sustained by Football Players on

Days of Diagnosed Concussion," vol. 45, no. 4, pp. 737–746, 2014, doi: 10.1249/MSS.0b013e3182792ed7.Head.

[46] S. Rowson and S. M. Duma, "Brain injury prediction: Assessing the combined probability of concussion using linear and rotational head acceleration," *Ann. Biomed. Eng.*, vol. 41, no. 5, pp. 873–882, 2013, doi: 10.1007/s10439-012-0731-0.

[47] J. G. Beckwith, J. J. Chu, and R. M. Greenwald, "Validation of a noninvasive system for measuring head acceleration for use during boxing competition," *J. Appl. Biomech.*, vol. 23, no. 3, pp. 238–244, 2007, doi: 10.1123/jab.23.3.238.

[48] S. Rowson *et al.*, "Rotational head kinematics in football impacts: An injury risk function for concussion," *Ann. Biomed. Eng.*, vol. 40, no. 1, pp. 1–13, 2012, doi: 10.1007/s10439-011-0392-4.

[49] M. Higgins, P. D. Halstead, L. Snyder-Mackler, and D. Barlow, "Measurement of impact acceleration: Mouthpiece accelerometer versus helmet accelerometer," *J. Athl. Train.*, vol. 42, no. 1, pp. 5–10, 2007.

[50] B. J. Paris AJ, Antonini KR, "Accelerations of the Head During Soccer Ball Heading," in *Accelerations of the head during soccer ball heading. InProceedings of the ASME Summer Bioengineering Conference*, 2010, p. (pp. 815-816).

[51] T. M. Kara, J. A. Delsignore, J. M. Brock, J. Lund, and A. J. Paris, "Evaluation of an Instrumented Mouthguard to Measure the Accelerations of the Head due to Soccer Ball Heading," *Proc 12th Pan-American Congr. Appl. Mech.*, pp. 2–6, 2012.

[52] A. Bartsch and S. Samorezov, "Cleveland Clinic intelligent mouthguard: a new technology to accurately measure head impact in athletes and soldiers," *Proc. SPIE 8723, Sens. Technol. Glob. Heal. Mil. Med. Environ. Monit. III*, vol. 8723, p. 87230N, 2013, doi: 10.1117/12.2027366.

[53] A. Bartsch, S. Samorezov, E. Benzel, V. Miele, and D. Brett, "Validation of an ' Intelligent Mouthguard ' single event head impact dosimeter," *Stapp Car Crash J.*, vol. 58, no. November, pp. 1–28, 2014.

[54] D. A. B. C. Camarillo *et al.*, "An instrumented mouthguard for measuring linear and angular head impact kinematics in american football," *Ann. Biomed. Eng.*, vol. 41, no. 9, pp. 1939–1949, 2013, doi: 10.1007/s10439-013-0801-y.

[55] C. Kuo *et al.*, "Effect of the mandible on mouthguard measurements of head kinematics," *J. Biomech.*, vol. 49, no. 9, pp. 1845–1853, 2016, doi:

10.1016/j.jbiomech.2016.04.017.

[56] L. C. Wu *et al.*, “Bandwidth and sample rate requirements for wearable head impact sensors,” *J. Biomech.*, vol. 49, no. 13, pp. 2918–2924, 2016, doi: 10.1016/j.jbiomech.2016.07.004.

[57] C. H. Hardy and P. V. Marcal, “Elastic Analysis of a Skull,” 1971.

[58] A. M. Nahum, R. Smith, and C. C. Ward, “Intracranial Pressure Dynamics During Head Impact,” in *21st Stapp Car Crash Conferneceeece*, 1977, vol. 1, doi: 10.4271/770922.

[59] X. Trosseille, C. Tarriére, F. Lavaste, F. Guillon, and A. Domont, “Development of a F.E.M. of the Human Head According to a Specific Test Protocol,” in *36th Stapp Car Crash Conference*, 1992, vol. 1, doi: 10.4271/922527.

[60] H. Mao *et al.*, “Development of a Finite Element Human Head Model Partially Validated With Thirty Five Experimental Cases,” *J. Biomech. Eng.*, vol. 135, no. 11, p. 111002, 2013, doi: 10.1115/1.4025101.

[61] F. S. Gayzik, D. P. Moreno, C. P. Geer, S. D. Wuertzer, R. S. Martin, and J. D. Stitzel, “Development of a full body CAD dataset for computational modeling: A multi-modality approach,” *Ann. Biomed. Eng.*, vol. 39, no. 10, pp. 2568–2583, 2011, doi: 10.1007/s10439-011-0359-5.

[62] L. S. A. Talebanpour, “A Comparison between Simulated and Measured Human Brain Response under Mild Acceleration,” in *IRCOBI Conference 2017*, 2017, pp. 674–676.

[63] W. N. Hardy *et al.*, “A Study of the Response of the Human Cadaver Head to Impact,” *Stapp Car Crash J.*, vol. 51, no. October, pp. 17–80, 2007, doi: 10.1016/j.bbi.2008.05.010.

[64] W. N. Hardy, C. D. Foster, M. J. Mason, K. H. Yang, A. King, and S. Tashman, “Investigation of Head Injury Mechanisms Using Neutral Density Technology and High-Speed Biplanar X-Ray,” *SAE Tech. Pap. Ser.*, vol. 45, no. November, 2001, doi: 10.4271/2001-22-0016.

[65] M. C. H. Dodgson, “Colloidal structure of brain,” *Biorheology*, vol. 1, no. 1, pp. 21–30, 1962, doi: 10.3233/BIR-1962-1104.

[66] J. H. Galford, James E. McElhaney, “A viscoelastic study of scalp, brain, and dura,” *J. Biomech.*, vol. 3, no. 2, pp. 211–221, 1970, doi: 10.1016/0021-9290(70)90007-2.

[67] D. C. VIANO and P. LOVSUND, “Biomechanics of Brain and Spinal-Cord Injury:

Analysis of Neuropathologic and Neurophysiology Experiments," *J. Crash Prev. Inj. Control*, vol. 1, no. 1, pp. 35–43, 1999, doi: 10.1080/10286589908915739.

[68] E. G. Takhounts, R. H. Eppinger, J. Q. Campbell, R. E. Tannous, E. D. Power, and L. S. Shook, "On the Development of the SIMon Finite Element Head Model.," *Stapp Car Crash J.*, vol. 47, no. October, pp. 107–33, 2003, [Online]. Available: http://www.ncbi.nlm.nih.gov/pubmed/17096247.

[69] A. Oeur, B. T. Hoshizaki, and M. D. Gilchrist, "The Influence of Impact Angle on the Dynamic Response of a Hybrid III Headform and Brain Tissue Deformation," *Mech. Concussion Sport.*, pp. 56–69, 2014, doi: 10.1520/STP155220120160.

[70] L. Zhang, K. H. Yang, and A. I. King, "Comparison of Brain Responses Between Frontal and Lateral Impacts by Finite Element Modeling," *J. Neurotrauma*, vol. 18, no. 1, pp. 21–30, 2001, doi: 10.1089/089771501750055749.

[71] L. E. Bilston, *Brain Tissue Mechanical Properties*. Springer, 2011.

[72] S. Chatelin, A. Constantinesco, and R. Willinger, "Fifty years of brain tissue mechanical testing: From in vitro to in vivo investigations," *Biorheology*, vol. 47, no. 5–6, pp. 255–276, 2010, doi: 10.3233/BIR-2010-0576.

[73] J. L. Wood, "Dynamic response of human cranial bone," *J. Biomech.*, vol. 4, no. 1, pp. 1–12, 1971, doi: 10.1016/0021-9290(71)90010-8.

[74] J. H. McElhaney, J. L. Fogle, J. W. Melvin, R. R. Haynes, V. L. Roberts, and N. M. Alem, "Mechanical properties of cranial bone," *J. Biomech.*, vol. 3, no. 5, 1970, doi: 10.1016/0021-9290(70)90059-X.

[75] I. T. B. Melvin, J. W., P. M. Fuller, "The mechanical properties of the diploë layer in the human skull.," *SESA Spring Meet.*, vol. May, 1970.

[76] D. B. Hans Delye, Jan Goffin, Peter Verschueren, Jos Vander Sloten, Georges Van der Perre, Herwig Alaerts, Ignaas Verpoest, "Biomechanical Properties of the Superior Sagittal Sinus-Bridging Vein Complex," *Stapp Car Crash J.*, vol. 50, pp. 398–410, 2006, doi: 10.4271/2006-22-0024.

[77] N. YOGANANDAN *et al.*, "Biomechanics of skull fracture.," *J. Neurotrauma*, vol. 12, no. 4, pp. 659–668, 1995, doi: 10.1089/neu.1995.12.659.

[78] V. R. Hodgson, L. M. Thomas, and S. W. Greenberg, "Fracture Behavior of the Skull Frontal Bone Against Cylindrical Surfaces," *SAE Tech. Pap. 700909*, 1970.

[79] G. W. Nyquist, J. M. Cavanaugh, S. J. Goldberg, and A. I. King, "Facial Impact Tolerance and Response," *SAE Tech. Pap. 861896*, vol. 1, 1986, doi: 10.4271/861896.

[80] D. “L” Allsop, C. Y. Warner, M. G. Wille, D. C. Schneider, and A. M. Nahum, “Facial Impact Response — A Comparison of the Hybrid III Dummy and Human Cadaver,” *SAE Tech. Pap. Ser.*, vol. 1, 1988, doi: 10.4271/881719.

[81] A. M. Nahum and R. W. Smith, “An Experimental Model for Closed Head Impact Injury,” *SAE Tech. Pap. Ser.*, vol. 1, 1976, doi: 10.4271/760825.

[82] S. Kleiven and W. N. Hardy, “Correlation of an FE Model of the Human Head with Local Brain Motion--Consequences for Injury Prediction,” *Stapp Car Crash J.*, vol. 46, no. September, pp. 123–144, 2002, doi: 2002-22-0007 [pii].

[83] T. J. Horgan and M. D. Gilchrist, “The creation of three-dimensional finite element models for simulating head impact biomechanics,” *Int. J. Crashworthiness*, vol. 8, no. 4, pp. 353–366, 2003.

[84] D. R. Namjoshi *et al.*, “Towards clinical management of traumatic brain injury: a review of models and mechanisms from a biomechanical perspective,” *Dis. Model. Mech.*, vol. 6, no. 6, pp. 1325–1338, 2013, doi: 10.1242/dmm.011320.

[85] Charles W. Gadd, “Use of a weighted-impulse criterion for estimating injury hazard,” in *10th Stapp Car Crash Conference*, 1966, doi: https://doi.org/10.4271/660793.

[86] T. . Hodgson, “Effect of long-duration impact on head,” *SAE Tech. Pap.*, 1972.

[87] A. Post, T. Blaine Hoshizaki, M. D. Gilchrist, and M. D. Cusimano, “Peak linear and rotational acceleration magnitude and duration effects on maximum principal strain in the corpus callosum for sport impacts,” *J. Biomech.*, vol. 61, pp. 183–192, 2017, doi: 10.1016/j.jbiomech.2017.07.013.

[88] J. A. Newman *et al.*, “A new biomechanical assessment of mild traumatic brain injury, part 2: results and conclusions,” *Proc. 2000 Int. Conf. Biomech. Impact*, pp. 223–233, 2000.

[89] J. A. Newman and N. Shewchenko, “A Proposed New Biomechanical Head Injury Assessment Function - The Maximum Power Index,” *SAE Tech. Pap.*, vol. 2000-Novem, no. November, 2000, doi: 10.4271/2000-01-SC16.

[90] S. Broglio, B. Schnebel, and J. Sosnoff, “The Biomechanical Properties of Concussions in High School Football,” *Med. Sci. ...*, vol. 42, no. 11, pp. 2064–2071, 2010, doi: 10.1249/MSS.0b013e3181dd9156.The.

[91] J. T. Eckner, M. Sabin, J. S. Kutcher, and S. P. Broglio, “No Evidence for a Cumulative Impact Effect on Concussion Injury Threshold,” *J. Neurotrauma*, vol. 28, no. 10, pp. 2079–2090, Aug. 2011, doi: 10.1089/neu.2011.1910.

[92] J. G. Beckwith *et al.*, “Head impact exposure in collegiate football players,” *J. Biomech.*, vol. 44, no. 15, pp. 2673–2678, 2011, doi: 10.1016/j.jbiomech.2011.08.003.

[93] L. Zhang, K. H. Yang, and A. I. King, “A Proposed Injury Threshold for Mild Traumatic Brain Injury,” *J. Biomech. Eng.*, vol. 126, no. 2, p. 226, 2004, doi: 10.1115/1.1691446.

[94] A. H. S. Holbourn, “Mechanics of Head Injuries,” *Lancet*, vol. 242, no. 6267, pp. 438–441, 1943, doi: 10.1016/S0140-6736(00)87453-X.

[95] J. S. Pudenz, R.H., Sheldon, C.H. and Restarski, “The Lucite Calvarium: A Method for Direct Observation of the Brain. I. The Surgical and Lucite Processing Techniques,” *J. Neurosurg.*, vol. 3, pp. 487–505, 1946.

[96] L. T. VR Hodgson, ES Gurdjian, “Experimental skull deformation and brain displacement demonstrated by flash x-ray technique,” *J. Neurosurg.*, 1966.

[97] A. N. Shatsky, S. A., Evans, D. E., Miller, F., & Martins, “Shatsky, Stanley A., et al. "High-speed angiography of experimental head injury,” *J. Neurosurg.*, vol. 41, no. 5, pp. 523–530, 1974.

[98] F. Trosseille, X., Tarriére, C., Lavaste, F., Guillon, “Development of a F.E.M. of the Human Head According to a Specific Test Protocol,” in *Stapp Car Crash Conference*, 1992, p. 19.

[99] A. C. Bain and D. F. Meaney, “Tissue-Level Thresholds for Axonal Damage in an Experimental Model of Central Nervous System White Matter Injury,” *J. Biomech. Eng.*, vol. 122, no. 6, p. 615, 2000, doi: 10.1115/1.1324667.

[100] E. G. Takhounts *et al.*, “Investigation of traumatic brain injuries using the next generation of simulated injury monitor (SIMon) finite element head model,” *Stapp Car Crash J.*, vol. 52, no. November, pp. 1–31, 2008, doi: 2008-22-0001 [pii].

[101] F. Hernandez *et al.*, “Six Degree-of-Freedom Measurements of Human Mild Traumatic Brain Injury,” *Ann. Biomed. Eng.*, vol. 43, no. 8, pp. 1918–1934, 2015, doi: 10.1007/s10439-014-1212-4.

[102] A. S. McIntosh, P. McCrory, and J. Comerford, “The dynamics of concussive head impacts in rugby and Australian rules football,” *Med. Sci. Sports Exerc.*, vol. 32, no. 12, pp. 1980–1984, 2000, doi: 10.1097/00005768-200012000-00002.

[103] B. Fréchède and A. S. McIntosh, “Numerical reconstruction of real-life concussive football impacts,” *Med. Sci. Sports Exerc.*, vol. 41, no. 2, pp. 390–398, 2009, doi: 10.1249/MSS.0b013e318186b1c5.

[104] E. J. Pellman *et al.*, “Concussion in Professional Football: Location and Direction of Helmet Impacts - Part 2,” *Neurosurgery*, vol. 53, no. 6, pp. 1328–1341, 2003, doi: 10.1227/01.NEU.0000093499.20604.21.

[105] G. J. Buse *et al.*, “Injuries Sustained by the Mixed Martial Arts Athlete,” *Br. J. Sports Med.*, vol. 21, no. 2, pp. 64–69, 2017, doi: 10.1177/1941738116664860.

[106] T. Keown, “The kid gloves come on,” *espn.com*, 2012. http://www.espn.com/mma/story/_/id/8766646/future-mma-kids-crazy-rayfield-espn-magazine (accessed May 14, 2019).

[107] “IMMAF,” 2019. https://immaf.org/sport (accessed May 14, 2019).

[108] “Safe MMA.” https://safemma.org/ (accessed May 14, 2019).

[109] “Code Blue.” http://codeblue.ie/ (accessed May 14, 2019).

[110] G. H. Bledsoe, E. B. Hsu, G. Grabowski, J. D. Brill, and G. Li, “Combat Sports Special Issue Incidence of Injury in Professional Mixed Martial Arts Competitions,” ©*Journal Sport. Sci. Med.*, pp. 136–142, 2006, [Online]. Available: http://www.jssm.org.

[111] D. Karpman, S; Reid, P; Phillips, L; Qin, Z; Gross, “Combative Sports Injuries: An Edmonton Retrospective,” *Clin. J. Sport Med.*, vol. 26, no. 4, pp. 332–334, 2016, doi: 10.1097/JSM.0000000000000235.

[112] C. J. Heath and J. L. Callahan, “Self-reported concussion symptoms and training routines in mixed martial arts athletes,” *Res. Sport. Med.*, vol. 21, no. 3, pp. 195–203, 2013, doi: 10.1080/15438627.2013.792082.

[113] K. M. Ngai, F. Levy, and E. B. Hsu, “Injury trends in sanctioned mixed martial arts competition: A 5-year review from 2002 to 2007,” *Br. J. Sports Med.*, vol. 42, no. 8, pp. 686–689, 2008, doi: 10.1136/bjsm.2007.044891.

[114] “Visual MP4/MOV Time Stamp (vMTS or vMTS64),” 2014. https://www.dts8888.com/index.htm.

[115] J. Charmant, “Kinovea,” 2019. https://www.kinovea.org/ (accessed Aug. 28, 2019).

[116] L. S. T. C. (LSTC), *LS DYNA Theory Manual*, vol. 11261. LIVERMORE SOFTWARE TECHNOLOGY CORPORATION (LSTC), 2019.

[117] T. Caplan, Bruce; Bogner, Jennifer; Brenner, Lisa; Belanger, Heather G.; Vanderploeg, Rodney D.; McAllister, “Subconcussive Blows to the Head: A Formative Review of Short-term Clinical Outcomes,” *J. Head Trauma Rehabil.*, vol. Volume 31, no. Number 3, pp. 159-166(8), 2016, doi:

https://doi.org/10.1097/HTR.0000000000000138.

[118] E. M. Davenport *et al.*, “Subconcussive impacts and imaging findings over a season of contact sports,” *Concussion*, vol. 1, no. 4, p. CNC19, 2016, doi: 10.2217/cnc-2016-0003.

[119] M. D. Julian E. Bailes, M. D. Anthony L. Petraglia, and P. D. Bennet I. Omalu, M.D. M.B.A., M.P.H. Eric Nauman, Ph.D.Thomas Talavage, “Role of subconcussion in repetitive mild traumatic brain injury,” *J Neurosurg*, vol. 119, no. November, pp. 1235–1245, 2013.

[120] D. G. David B. Camarillo, Pete B. Shull, James Mattson, Rebecca Shultz, “An Instrumented Mouthguard for Measuring Linear and Angular Head Impact Kinematics in American Football,” *Ann Biomed Eng.*, vol. 41, no. 9, pp. 1939–1949, 2013, doi: 10.1038/jid.2014.371.

[121] L. C. Wu, L. Zarnescu, V. Nangia, B. Cam, and D. B. Camarillo, “A Head Impact Detection System Using SVM Classification and Proximity Sensing in an Instrumented Mouthguard,” vol. 9294, no. c, pp. 1–11, 2014, doi: 10.1109/TBME.2014.2320153.

[122] M. D. Ann-Christine Duhaime *et al.*, “Spectrum of acute clinical characteristics of diagnosed concussions in college athletes wearing instrumented helmets,” *J. Neurosurg.*, vol. 117, no. December, pp. 1092–1099, 2012.

[123] J. Michio Clark, A. Post, T. Blaine Hoshizaki, and M. D. Gilchrist, “Distribution of brain strain in the cerebrum for laboratory impacts to ice hockey goaltender masks,” *J. Biomech. Eng.*, vol. 140, no. 12, 2018, doi: 10.1115/1.4040605.

[124] C. Deck, N. Bourdet, F. Meyer, and R. Willinger, “Protection performance of bicycle helmets,” *J. Safety Res.*, vol. 71, pp. 67–77, 2019, doi: 10.1016/j.jsr.2019.09.003.

[125] T. A. Gennarelli, L. E. Thibault, G. Tomei, R. Wiser, D. Graham, and J. Adams, “Directional Dependence of Axonal Brain Injury due to Centroidal and Non-Centroidal Acceleration,” in *SAE Technical Paper*, 1987, doi: 10.4271/872197.

[126] A. C. Colvin, J. Mullen, M. R. Lovell, R. V. West, M. W. Collins, and M. Groh, “The role of concussion history and gender in recovery from soccer-related concussion,” *Am. J. Sports Med.*, vol. 37, no. 9, pp. 1699–1704, 2009, doi: 10.1177/0363546509332497.

[127] A. E. Lincoln, S. V. Caswell, J. L. Almquist, R. E. Dunn, J. B. Norris, and R. Y. Hinton, “Trends in concussion incidence in high school sports: A prospective 11-

year study," *Am. J. Sports Med.*, vol. 39, no. 5, pp. 958–963, 2011, doi: 10.1177/0363546510392326.

[128] D. R. Walsh *et al.*, "Regional mechanical and biochemical properties of the porcine cortical meninges," *Acta Biomater.*, vol. 80, no. 2018, pp. 237–246, 2018, doi: 10.1016/j.actbio.2018.09.004.

[129] J. Ho, Z. Zhou, X. Li, and S. Kleiven, "The peculiar properties of the falx and tentorium in brain injury biomechanics," *J. Biomech.*, vol. 60, pp. 243–247, 2017, doi: https://doi.org/10.1016/j.jbiomech.2017.06.023.

[130] C. Giordano, S. Zappalà, and S. Kleiven, "Anisotropic finite element models for brain injury prediction: the sensitivity of axonal strain to white matter tract inter-subject variability," *Biomech. Model. Mechanobiol.*, vol. 16, no. 4, pp. 1269–1293, 2017, doi: 10.1007/s10237-017-0887-5.

Appendices

Appendix 1

SCAT5

Full document available at:

https://bjsm.bmj.com/content/bjsports/early/2017/04/26/bjsports-2017-097506SCAT5.full.pdf

BJSM Online First, published on April 26, 2017 as 10.1136/bjsports-2017-097506SCAT5
To download a clean version of the SCAT tools please visit the journal online (http://dx.doi.org/10.1136/bjsports-2017-097506SCAT5)

SCAT5© SPORT CONCUSSION ASSESSMENT TOOL – 5TH EDITION
DEVELOPED BY THE CONCUSSION IN SPORT GROUP
FOR USE BY MEDICAL PROFESSIONALS ONLY

supported by

Patient details

Name: _____

DOB: _____

Address: _____

ID number: _____

Examiner: _____

Date of Injury: _____ Time: _____

WHAT IS THE SCAT5?

The SCAT5 is a standardized tool for evaluating concussions designed for use by physicians and licensed healthcare professionals[1]. The SCAT5 cannot be performed correctly in less than 10 minutes.

If you are not a physician or licensed healthcare professional, please use the Concussion Recognition Tool 5 (CRT5). The SCAT5 is to be used for evaluating athletes aged 13 years and older. For children aged 12 years or younger, please use the Child SCAT5.

Preseason SCAT5 baseline testing can be useful for interpreting post-injury test scores, but is not required for that purpose. Detailed instructions for use of the SCAT5 are provided on page 7. Please read through these instructions carefully before testing the athlete. Brief verbal instructions for each test are given in italics. The only equipment required for the tester is a watch or timer.

Recognise and Remove

A head impact by either a direct blow or indirect transmission of force can be associated with a serious and potentially fatal brain injury. If there are significant concerns, including any of the red flags listed in Box 1, then activation of emergency procedures and urgent transport to the nearest hospital should be arranged.

Key points

- Any athlete with suspected concussion should be REMOVED FROM PLAY, medically assessed and monitored for deterioration. No athlete diagnosed with concussion should be returned to play on the day of injury.
- If an athlete is suspected of having a concussion and medical personnel are not immediately available, the athlete should be referred to a medical facility for urgent assessment.
- Athletes with suspected concussion should not drink alcohol, use recreational drugs and should not drive a motor vehicle until cleared to do so by a medical professional.
- Concussion signs and symptoms evolve over time and it is important to consider repeat evaluation in the assessment of concussion.
- The diagnosis of a concussion is a clinical judgment, made by a medical professional. The SCAT5 should NOT be used by itself to make, or exclude, the diagnosis of concussion. An athlete may have a concussion even if their SCAT5 is "normal".

Remember:

- The basic principles of first aid (danger, response, airway, breathing, circulation) should be followed.
- Do not attempt to move the athlete (other than that required for airway management) unless trained to do so.
- Assessment for a spinal cord injury is a critical part of the initial on-field assessment.
- Do not remove a helmet or any other equipment unless trained to do so safely.

Appendix 2

IMMAF Unified Rules of Amateur Mixed Martial Arts

Full document available at:

http://www.immaf.org/wp-content/uploads/2015/08/IMMAF-Unified-Amateur-3x3-Rule-Set_15.11.15.pdf

IMMAF UNIFIED AMATEUR MIXED MARTIAL ARTS RULES

SCOPE:

IMMAF Amateur Mixed Martial Arts [MMA] competition shall provide young participants new to the sport of MMA the necessary experience to progress through to a possible career within the sport. The sole ethos of Amateur MMA is to provide the safest possible environment for combatants to train and gain the required experience and knowledge under directed pathways allowing them to compete under the confines of the rules set out within this document.

It is recognized by the International Mixed Martial Arts Federation [IMMAF] that codes and legislation may differ from country to country and region to region: This can be reflected in the resultant documentation and rules sets from the member countries. IMMAF Amateur tournaments will be held in different countries and local variations to rules shall be reflected in the IMMAF Amateur Mixed Martial Arts rules for and disseminated prior to each competition. IMMAF strives for, in conjunction with setting hitherto unparalleled safety standards, a unified and aesthetically common identity of the sport of Mixed Martial Arts for amateur competition.

1) **DEFINITION:**

"Mixed martial arts" means competition involving the use, subject to any applicable limitations set forth in these Unified Rules, of a combination of techniques from different disciplines of the martial arts, including, without limitation, grappling, kicking and striking.

2) **JURISDICTION:**

The Referee shall remain the sole arbiter of a contest.

All contests and exhibitions of mixed martial arts must be conducted under the supervision and authority of the commission.

3) **ROUNDS:**

A) Each non-championship mixed martial arts contest is to be for 3 rounds, each round no more than 3 minutes duration, with a rest period of 1 minute between each round.

1

Unified Rules of Mixed Martial Arts

Full document available at:

https://www.dca.ca.gov/csac/forms_pubs/publications/unified_rules_2017.pdf

1st Vice President
Brian Dunn
1313 Farnam St.
Omaha, NE 68102
(402) 595-1624
Brian.dunn@nebraska.gov

Secretary
Joe Walsh
100 East Grand Ave.
Des Moines, IA. 50319
(515)281-8067
Walsh.iac@outlook.com

2nd Vice President
Greg Alvarez
1106 Clayton Lane
Austin, TX 78723
(512) 659-5034
Greg.alvarez@tdlr.texas.gov

President
Michael Mazzulli
Dept.of Athletics,1 Mohegan Blvd.
Uncasville, CT 06382
(860) 862-7583
mmazzulli@moheganmail.com

Treasurer
Lydia Robertson
P.O. Box 17304
Little Rock, AR 72222
(501) 837-4948
Lydia.abc@sbcglobal.net

On December 16, 2016 the California Athletic Commission authorized and approved the revised Unified Rules of MMA as adopted by the Association of Boxing Commissions and Combative in August 2016. The rules became effective January 1st, 2017. The authority to authorize and approve these rules is below.

Title 16 California Code of Regulations section 533.

Championship Matches and Exhibitions.

Recognizing that different forms of martial arts exist, notwithstanding any rule in this division to the contrary, the commission may, in its discretion, authorize alternate rules or provisions from time to time for full contact martial arts championships and exhibitions so long as the safety and welfare of the contestants and the public are not jeopardized.

Note: Authority cited: Sections 18611 and 18763, Business and Professions Code. Reference: Sections 18640 and 18765, Business and Professions Code.

The Unified Rules Of Mixed Martial Arts

Scoring:

The 10 point must system is defined as follows:

All bouts will be evaluated and scored by three judges. The 10-Point Must System will be the standard system of scoring a bout. Under the 10-Point Must Scoring System, 10 points must be awarded to the winner of the round and nine points or less must be awarded to the loser, except for an even round, which is scored (10-10).

**** as of 2017 Unified Rules ****

Appendix 3

Study Consent Form

Technological University of Dublin

Olldcsoil Teicneolaíochta Bhaile Átha Cliath

Department of Mechanical Engineering

Participant Information Sheet and Consent Form

Research title:
The investigation of head impacts in Sport

Why is this study being performed?

The primary aim of this project is to measure the severity and rate of head impacts in sport. Participants will be asked to wear a mouthguard with embedded sensors, they will be individually molded from dental impressions. When the mouthguards have been fabricated, they will be tested for comfort and fit, and if necessary modified. Head linear and rotational acceleration will be measured by the devices during events. The data collected will be used primarily as input data to a simulation model of the brain; to aid in the understanding of the biomechanics of the brain during impact. Your participation in this study is entirely voluntary.

Why have I been chosen?

Your invitation to participate is based on you having met the criteria.

- Active sports participant

Suitable candidates will not fall into any of the categories mentioned below:

- suffer from any physical or mental impairment.

What is required for participation?

Prior to an event or training session instrumented mouthguards will be switched with the un-instrumented mouthguard. Following a competition or training session the mouthguards will be taken for a time to download the data from them. Participation in the study will not affect performance or selection. All mouthguards are molded from dental impressions and are therefore individual fitted to participants.

Video

We will use video of the event (video recorded or taken from online sources such as YouTube) to correlate data from the mouthguard device with observed head impacts.

Who will have access to your information?

The researchers, research partners and the supervisors on the project will have access to all of the data. The information will be stored on a computer. In addition to the accelerometer data, any incidents during an event, the date and time, and location of the event will also be recorded. It is intended that the data will be analysed and condensed and may be used in a scientific publication or conference presentation. It will not be possible to identify individual participants in any presented or published data.

Anonymised data will also be stored on FITBIR (United States Federal Interagency Traumatic Brain Injury Research Informatics System). This is a US database that allows researchers to analyse head impacts across a range of sports. This information is important in studying the rate and severity of head impacts in sport and it will not be possible through this system to trace the data back to individual participants.

What will happen to the results:

The anonymised data will be keep on FITBIR indefinitely. Data at ITT Dublin will be retained for a minimum of 5 years (as required by the data protection policy) in a secure computer location only accessible by the researchers and supervisors.

How will the results be disseminated?

Results will be disseminated through Journal Publications and conference proceedings. The identities of individuals will not be included.

Will you receive any compensation?

No

Risks:

The risks associated with this study are irritation from wearing the instrumented mouthguard. The mouthguard device used in the proposed study is made of the same material as mouthguards currently worn in sports. The device used in this study serves the same function as typical mouth guards of protecting the teeth and will be manufactured by OPRO who are the main manufacturers of mouthguards for many sports. With electronics situated in the mouth, there may be a heightened probability for device breakage and component short circuiting. These may cause heating, and chemical/electrical irritation. An allergic reaction to the material is possible and might also cause irritation. We view this risk as low due to the thick hypoallergenic ethylene vinyl acetate bi-layer encompassing electronics, the low total power of the battery used (3.7V, 30mAh), that all electronics and battery will be fully hermetically sealed as a moisture and dielectric barrier. Please notify us if you experience any adverse effects.

PARTICIPANT CONSENT FORM

With permission, this form has been based on that produced by the RCSI Research Ethics Committee

Study title: **The investigation of head impacts in Sport**

I have read and understood the **Information Leaflet** about this research project. The information has been fully explained to me and I have been able to ask questions, all of which have been answered to my satisfaction.	**Yes** ☐	**No** ☐
I understand that I don't have to take part in this study and that I can opt out at any time. I understand that I don't have to give a reason for opting out and I understand that opting out won't affect my future medical care.	**Yes** ☐	**No** ☐
I am aware of the potential risks, benefits and alternatives of this research study.	**Yes** ☐	**No** ☐
I give permission for researchers to look at my medical records to get information. I have been assured that information about me will be kept private and confidential.	**Yes** ☐	**No** ☐
I have been given a copy of the Information Leaflet and this completed consent form for my records.	**Yes** ☐	**No** ☐
I consent to take part in this research study having been fully informed of the risks, benefits and alternatives.	**Yes** ☐	**No** ☐
I give informed explicit consent to have my data processed as part of this research study.	**Yes** ☐	**No** ☐
I consent to be contacted by researchers as part of this research study.	**Yes** ☐	**No** ☐

Participant Name (Block Capitals)	Participant Signature	Date

To be completed by the Principal Investigator or nominee.

I, the undersigned, have taken the time to fully explain to the above participant the nature and purpose of this study in a way that they could understand. I have explained the risks involved as well as the possible benefits. I have invited them to ask questions on any aspect of the study that concerned them.

----------Name (Block Capitals) | Qualifications * | Signature | Date

* If the nominee is a student researcher studying at the Institute of Technology Tallaght, please write the name of the programme in place of the qualifications in the above declaration

Appendix 4

Mouthguards Raw Data

Competitive Bouts

Fighter 1 Bout 1

	Max Result Linear Accel (g)	Max Result Rotational Accel (rads/s^2)	Max Result Rot Vel (rads/s)	Rot Angle (°)	Elev Angle (°)	Impact	Sector	Elev
Fighter 1 - Bout 1	89.88	4385.98	12.51	275.02	9.56	Serious	R	Upper
	107.37	12546.23	35.01	117.21	24.38	Very Serious	BL	Upper
	42.55	4458.08	11.37	40.52	-31.14	Moderate	FL	Lower
	11.11	746.39	11.92	291.87	8.93	Low	R	Upper
	37.11	2709.43	12.95	49.00	10.29	Moderate	FL	Upper
	14.70	728.48	6.09	61.10	-3.23	Low	FL	Lower
	25.25	3094.85	13.40	315.10	-26.59	Low	FR	Lower
	13.10	1904.84	8.22	338.78	-31.79	Low	F	Lower
	109.88	13190.78	45.34	15.83	-40.97	Very Serious	F	Lower
	11.51	480.16	4.38	35.74	-4.21	Low	FL	Lower
	15.36	1240.00	7.16	49.34	3.59	Low	FL	Upper
	35.76	1942.94	18.06	66.88	0.07	Moderate	FL	Upper
	12.75	1059.16	3.34	350.27	-3.35	Low	F	Lower

Fighter 2 Bout 1

	Max Result Linear Accel (g)	Max Result Rotational Accel (rads/s^2)	Max Result Rot Vel (rads/s)	Rot Angle (°)	Elev Angle (°)	Impact	Sector	Elev
Fighter 2 - Bout 1	31.69	1983.53	13.17	24.76	-17.71	Moderate	FL	Lower
	49.96	4107.37	13.40	24.50	-27.99	Moderate	FL	Lower
	49.00	6527.42	23.61	272.20	10.76	Moderate	R	Upper
	17.54	1120.42	14.51	40.17	-6.34	Low	FL	Lower
	32.08	2152.40	10.41	71.77	-22.20	Moderate	L	Lower
	307.65	21881.43	37.70	336.67	-37.70	Very Severe	FR	Lower
	120.84	7795.04	28.53	62.59	1.46	Severe	FL	Upper
	25.91	2305.84	15.61	80.38	-15.24	Low	L	Lower
	72.79	6987.49	17.18	14.31	-43.00	Serious	F	Lower

	38.35	3672.11	7.87	46.59	-4.72	Moderate	FL	Lower
	42.54	2577.95	8.46	227.90	-40.93	Moderate	BR	Lower
	15.13	986.96	5.40	58.73	-4.77	Low	FL	Lower
	44.62	4813.19	14.79	260.79	24.63	Moderate	R	Upper
	30.80	2046.91	13.65	67.56	-24.82	Moderate	L	Lower
	16.52	930.38	6.07	55.64	-28.96	Low	FL	Lower
	81.11	4185.67	17.67	72.59	3.15	Serious	L	Upper
	52.48	4197.76	11.34	37.26	-5.18	Moderate	FL	Lower
	79.13	3400.48	11.88	61.46	-17.50	Serious	FL	Lower

Fighter 3

Bout 1

	Max Result Linear Accel (g)	Max Result Rotational Accel (rads/s^2)	Max Result Rot Vel (rads/s)	Rot Angle (°)	Elev Angle (°)	Impact	Sector	Elev
Fighter 3 - Bout 1	40.92	2524.68	16.43	69.42	-41.45	Moderate	L	Lower
	41.48	2906.15	15.55	43.64	-1.67	Moderate	FL	Lower
	43.50	4090.38	15.60	128.91	31.01	Moderate	BL	Upper

Bout 2

	Max Result Linear Accel (g)	Max Result Rotational Accel (rads/s^2)	Max Result Rot Vel (rads/s)	Rot Angle (°)	Elev Angle (°)	Impact	Sector	Elev
Fighter 3 - Bout 2	20.99	5430.82	15.25	267.19	-0.97	Low	R	Lower
	31.69	23479.27	39.05	4.71	68.49	Moderate	F	Top
	17.34	14273.09	19.12	284.90	-41.33	Low	R	Lower
	10.68	1538.03	8.00	334.38	23.70	Low	FR	Upper
	40.66	6704.79	20.22	69.76	-9.24	Moderate	L	Lower
	30.09	5949.25	21.41	254.46	-3.10	Moderate	R	Lower
	35.10	3795.80	21.24	59.83	-9.46	Moderate	FL	Lower

Fighter 4

Bout 1

	Max Result Linear Accel (g)	Max Result Rotational Accel (rads/s^2)	Max Result Rot Vel (rads/s)	Rot Angle (°)	Elev Angle (°)	Impact	Sector	Elev
Fighter 4 - Bout 1	17.11	1859.39	10.84	120.22	-11.82	Low	BL	Lower
	27.36	2645.28	12.20	220.32	-2.41	Low	BR	Lower
	33.44	4930.53	17.12	82.91	-1.03	Moderate	L	Lower
	32.40	1775.34	8.71	257.22	-58.69	Moderate	R	Neck
	23.89	1794.14	12.60	70.81	-4.59	Low	L	Lower
	19.19	1242.61	11.74	261.07	-6.12	Low	R	Lower
	26.87	2340.07	8.31	89.92	-4.38	Low	L	Lower
	19.47	1611.71	6.66	101.14	-10.92	Low	L	Lower
	16.33	1216.70	12.30	350.67	-1.96	Low	F	Lower
	31.96	2618.48	16.33	285.74	9.32	Moderate	R	Upper
	41.93	2385.81	16.93	297.16	4.75	Moderate	FR	Upper

Bout 2

	Max Result Linear Accel (g)	Max Result Rotational Accel (rads/s^2)	Max Result Rot Vel (rads/s)	Rot Angle (°)	Elev Angle (°)	Impact	Sector	Elev
Fighter 4 - Bout 2	137.95	15369.99	44.40	272.33	10.04	Severe	R	Upper
	101.63	4086.47	20.27	55.12	-18.73	Very Serious	FL	Lower
	60.01	3721.35	17.33	284.18	17.31	Serious	R	Upper
	163.01	23757.35	74.44	2.99	-61.54	Very Severe	F	Neck
	54.53	5406.82	20.78	275.14	-1.25	Moderate	R	Lower
	10.37	1239.18	7.04	25.43	-30.59	Low	FL	Lower
	32.64	3059.36	12.33	284.70	-5.89	Moderate	R	Lower

Fighter 5 Bout 1

	Max Result Linear Accel (g)	Max Result Rotational Accel (rads/s^2)	Max Result Rot Vel (rads/s)	Rot Angle (°)	Elev Angle (°)	Impact	Sector	Elev
Fighter 5 - Bout 1	108.80	33315.12	72.34	5.03	-60.36	Very Severe	F	Neck
	37.53	6048.77	20.92	73.37	-4.08	Moderate	L	Lower
	26.17	15903.80	32.63	41.87	-79.96	Low	FL	Neck
	38.94	13289.73	34.51	72.61	10.31	Moderate	L	Upper
	27.17	4044.44	18.89	298.20	-13.01	Low	FR	Lower
	24.77	5563.90	20.13	299.77	-9.74	Low	FR	Lower
	17.27	5435.42	14.16	24.76	-17.38	Low	FL	Lower
	21.24	4207.10	13.31	311.26	-21.36	Low	FR	Lower
	14.86	4024.46	13.04	32.86	7.83	Low	FL	Upper
	17.13	20546.81	29.16	343.44	-15.77	Low	F	Lower
	104.35	27212.00	42.61	84.59	-5.75	Very Severe	L	Lower
	20.88	14673.17	16.53	352.77	-33.21	Low	F	Lower
	59.67	6081.34	21.56	81.32	1.22	Serious	L	Upper
	70.66	15984.03	28.36	47.37	4.51	Severe	FL	Upper
	37.54	5672.50	9.11	65.86	-16.67	Moderate	FL	Lower
	29.44	4591.39	19.75	77.61	-10.79	Low	L	Lower
	27.61	3164.55	11.58	55.40	-6.46	Low	FL	Lower

Fighter 6 Bout 1

	Max Result Linear Accel (g)	Max Result Rotational Accel (rads/s^2)	Max Result Rot Vel (rads/s)	Rot Angle (°)	Elev Angle (°)	Impact	Sector	Elev
Fighter 6 - Bout 1	32.93	6591.34	33.00	62.44	-14.06	Moderate	FL	Lower
	17.10	1802.98	11.23	61.50	-11.44	Low	FL	Lower
	51.98	10014.27	10.68	79.82	83.53	Moderate	L	Top
	26.03	4430.64	11.54	33.11	-54.36	Low	FL	Neck
	20.72	2481.67	13.58	345.05	-31.48	Low	F	Lower
	42.00	5869.50	20.76	46.61	-25.08	Moderate	FL	Lower
	11.90	1790.34	12.02	286.05	-14.87	Low	R	Lower
	11.04	2145.96	12.72	32.77	-36.72	Low	FL	Lower
	22.84	3381.19	22.30	11.70	-44.54	Low	F	Lower
	25.94	3171.39	17.23	280.84	1.61	Low	R	Upper

Sparring Sessions

Fighter 2
Session 1

	Max Result Linear Accel (g)	Max Result Rotational Accel (rads/s^2)	Max Result Rot Vel (rads/s)	Rot Angle (°)	Elev Angle (°)	Impact	Sector	Elev
Fighter 2 - Session 1	23.52	1609.66	9.15	294.04	-17.88	Low	FR	Lower
	20.36	1273.95	8.30	46.83	-0.61	Low	FL	Lower
	53.15	5638.49	11.90	37.06	-26.95	Moderate	FL	Lower
	36.42	3312.85	9.32	348.14	-30.72	Moderate	F	Lower
	24.23	3497.41	9.77	313.69	-32.93	Low	FR	Lower
	27.67	2256.13	8.09	279.21	2.83	Low	R	Upper
	22.40	1109.82	5.31	65.15	5.32	Low	FL	Upper
	15.70	1105.37	5.89	65.05	6.73	Low	FL	Upper
	23.79	1110.90	5.73	135.33	-28.63	Low	BL	Lower
	17.77	1182.58	6.99	171.62	-15.92	Low	B	Lower
	20.72	1395.10	5.07	62.70	-2.09	Low	FL	Lower
	12.83	2631.92	19.62	328.97	-25.11	Low	FR	Lower
	11.90	772.89	4.09	144.40	-18.69	Low	BL	Lower
	16.33	1317.26	6.78	61.09	-5.14	Low	FL	Lower
	12.95	995.87	5.37	87.83	22.60	Low	L	Upper
	24.29	3082.75	6.46	89.77	-0.67	Low	L	Lower

Session 2

	Max Result Linear Accel (g)	Max Result Rotational Accel (rads/s^2)	Max Result Rot Vel (rads/s)	Rot Angle (°)	Elev Angle (°)	Impact	Sector	Elev
Fighter 2 - Session 2	58.08	6685.63	26.97	1.99	-40.26	Moderate	F	Lower
	80.44	8425.89	16.87	4.10	-45.01	Serious	F	Neck
	18.36	1249.98	5.21	280.11	8.65	Low	R	Upper
	27.66	2492.70	13.89	134.28	-10.54	Low	BL	Lower
	13.34	986.66	4.29	36.14	-15.68	Low	FL	Lower
	10.37	702.40	5.81	285.23	2.26	Low	R	Upper
	16.76	1405.74	6.84	54.81	-7.38	Low	FL	Lower
	20.06	2488.90	7.79	295.69	-34.42	Low	FR	Lower

	14.91	1518.33	9.69	43.27	-27.07	Low	FL	Lower
	47.15	4256.33	16.67	274.63	12.63	Moderate	R	Upper
	27.07	1512.02	15.30	68.67	-2.16	Low	L	Lower
	16.10	1308.79	6.22	342.44	5.02	Low	F	Upper
	24.81	2602.59	6.46	9.13	-22.17	Low	F	Lower
	25.57	2963.49	17.78	68.68	14.49	Low	L	Upper
	42.93	2821.78	12.98	239.18	-30.12	Moderate	BR	Lower
	13.08	1581.28	12.71	127.31	-15.88	Low	BL	Lower
	15.04	686.55	4.96	184.82	-6.44	Low	B	Lower
	23.13	1458.92	6.91	41.24	-5.77	Low	FL	Lower

Fighter 3

Session 1

	Max Result Linear Accel (g)	Max Result Rotational Accel (rads/s^2)	Max Result Rot Vel (rads/s)	Rot Angle (°)	Elev Angle (°)	Impact	Sector	Elev
Fighter 3 - Session 1	14.32	1407.63	6.20	314.46	21.79	Low	FR	Upper
	32.57	2484.35	13.24	243.53	6.42	Moderate	BR	Upper
	19.34	1810.95	11.77	40.19	-33.47	Low	FL	Lower
	26.04	2083.79	8.43	58.54	11.84	Low	FL	Upper
	23.43	2000.60	12.30	68.51	-12.97	Low	L	Lower
	13.89	1500.83	11.44	61.49	-4.92	Low	FL	Lower
	10.56	1504.82	9.72	88.59	-14.16	Low	L	Lower
	59.34	3390.18	13.67	74.11	-10.97	Moderate	L	Lower
	12.38	814.71	8.99	17.69	-3.33	Low	F	Lower
	30.63	5847.99	41.02	45.68	9.54	Moderate	FL	Upper
	46.25	4416.69	7.43	338.98	-33.19	Moderate	F	Lower
	13.29	1253.58	12.15	73.69	-14.74	Low	L	Lower

Session 2

	Max Result Linear Accel (g)	Max Result Rotational Accel (rads/s^2)	Max Result Rot Vel (rads/s)	Rot Angle (°)	Elev Angle (°)	Impact	Sector	Elev
Fighter 3 - Session 2	14.38	1201.48	6.57	268.74	0.73	Low	R	Upper
	23.13	3144.24	5.91	24.33	-37.45	Low	FL	Lower
	15.82	857.82	8.58	304.00	7.00	Low	FR	Upper
	10.31	970.04	10.98	45.33	-4.04	Low	FL	Lower
	53.44	7722.22	33.62	59.30	-16.33	Moderate	FL	Lower
	11.47	1212.32	10.44	180.93	-3.25	Low	B	Lower
	77.89	10311.30	25.60	275.09	-3.94	Serious	R	Lower
	16.94	990.04	12.90	49.33	-4.86	Low	FL	Lower
	27.91	2150.67	9.83	47.52	-8.00	Low	FL	Lower
	18.01	961.98	6.40	165.48	10.09	Low	B	Upper

Fighter 5
Session 1

	Max Result Linear Accel (g)	Max Result Rotational Accel (rads/s^2)	Max Result Rot Vel (rads/s)	Rot Angle (°)	Elev Angle (°)	Impact	Sector	Elev
Fighter 5 - Session 1	13.14	2140.53	16.48	60.76	-4.62	Low	FL	Lower
	14.30	5167.60	15.16	309.60	14.37	Low	FR	Upper
	14.82	4867.77	11.95	307.00	-5.35	Low	FR	Lower
	42.73	13863.32	23.25	356.14	74.88	Moderate	F	Top
	28.38	21492.29	34.06	299.92	-88.67	Low	FR	Neck
	11.44	3726.81	28.77	51.60	-8.27	Low	FL	Lower
	11.39	3285.05	7.29	38.24	-2.53	Low	FL	Lower
	60.81	41843.69	73.61	283.91	-65.59	Serious	R	Neck
	17.21	1595.11	12.42	66.37	-3.20	Low	FL	Lower
	10.04	2030.94	6.55	67.16	-6.62	Low	FL	Lower
	25.79	19784.09	28.18	337.09	-34.97	Low	FR	Lower
	21.28	15568.71	32.54	70.59	71.10	Low	L	Top
	10.17	8795.83	18.41	45.29	-31.26	Low	FL	Lower
	21.13	10894.08	14.19	356.70	-34.39	Low	F	Lower
	30.67	6117.63	27.67	63.11	-6.88	Moderate	FL	Lower
	47.11	23245.34	31.16	351.50	54.64	Moderate	F	Top

Session 2

	Max Result Linear Accel (g)	Max Result Rotational Accel (rads/s^2)	Max Result Rot Vel (rads/s)	Rot Angle (°)	Elev Angle (°)	Impact	Sector	Elev
Fighter 5 - Session 2	14.76	1824.44	7.09	67.69	-3.91	Low	L	Lower
	52.73	15406.37	34.40	62.06	-18.08	Moderate	FL	Lower
	15.48	2500.26	7.73	69.75	0.67	Low	L	Upper
	26.74	15508.80	29.59	12.75	75.03	Low	F	Top
	102.58	47406.96	53.01	46.93	-61.69	Very Serious	FL	Neck
	83.28	39561.61	57.31	348.42	77.31	Serious	F	Top
	19.42	17684.82	28.93	23.57	-61.22	Low	FL	Neck
	58.95	31226.29	51.87	97.70	78.16	Moderate	L	Top
	14.40	7429.99	10.37	297.41	24.32	Low	FR	Upper
	57.58	7000.59	11.53	2.70	2.11	Moderate	F	Upper
	20.08	6043.53	9.98	109.55	-33.83	Low	L	Lower
	52.23	39312.17	54.50	17.06	65.21	Moderate	F	Top
	17.57	9116.81	18.23	57.60	-20.34	Low	FL	Lower
	29.63	23727.09	71.83	36.23	-55.89	Low	FL	Neck
	41.62	21910.21	37.90	80.62	82.82	Moderate	L	Top

Fighter 7

Session 1

	Max Result Linear Accel (g)	Max Result Rotational Accel (rads/s^2)	Max Result Rot Vel (rads/s)	Rot Angle (°)	Elev Angle (°)	Impact	Sector	Elev
Fighter 7 - Session 1	30.11	3613.54	12.27	155.69	37.38	Moderate	BL	Upper
	12.23	1036.67	11.27	237.01	-9.09	Low	BR	Lower
	11.92	861.41	11.07	238.69	1.29	Low	BR	Upper
	10.73	844.13	10.75	246.90	-0.19	Low	BR	Lower
	13.99	1252.33	6.15	340.85	-31.81	Low	F	Lower
	11.91	560.50	6.94	191.20	0.88	Low	B	Upper
	21.00	1341.63	7.40	117.94	13.04	Low	BL	Upper
	15.52	1445.67	8.59	219.47	-11.94	Low	BR	Lower
	21.96	1071.13	21.36	277.28	-4.97	Low	R	Lower
	49.40	5206.73	9.46	24.28	-40.01	Moderate	FL	Lower
	29.79	2174.02	9.04	136.16	10.11	Low	BL	Upper
	19.82	1208.62	9.80	234.13	-3.74	Low	BR	Lower
	48.75	4533.03	8.82	318.13	-40.45	Moderate	FR	Lower
	39.88	3221.76	15.05	270.92	-6.69	Moderate	R	Lower
	49.97	4859.89	21.69	233.31	24.11	Moderate	BR	Upper
	13.09	1521.31	10.10	245.73	9.18	Low	BR	Upper
	29.09	3563.75	12.19	21.69	-24.91	Low	F	Lower
	18.18	838.19	7.11	106.09	4.43	Low	L	Upper
	25.48	2558.96	4.94	60.99	-19.37	Low	FL	Lower
	12.01	247.24	2.13	175.77	-77.74	Low	B	Neck
	11.86	1416.20	7.36	291.29	15.11	Low	R	Upper
	20.94	2001.87	4.14	138.95	33.54	Low	BL	Upper
	17.28	1300.57	8.78	269.06	-3.12	Low	R	Lower
	14.06	1444.69	4.39	135.40	-3.85	Low	BL	Lower
	10.81	838.44	9.42	166.34	-57.43	Low	B	Neck
	17.83	741.92	5.92	173.06	-25.63	Low	B	Lower
	11.05	1122.41	26.85	181.71	60.61	Low	B	Top
	24.79	2331.93	4.92	119.04	27.56	Low	BL	Upper

Fighter 9

Session 1

	Max Result Linear Accel (g)	Max Result Rotational Accel (rads/s^2)	Max Result Rot Vel (rads/s)	Rot Angle (°)	Elev Angle (°)	Impact	Sector	Elev
Fighter 9 - Session 1	165.14	15994.05	38.27	357.04	-42.54	Very Severe	F	Lower
	17.61	2594.50	14.94	224.11	-41.38	Low	BR	Lower
	34.48	2765.96	21.12	57.93	-3.56	Moderate	FL	Lower
	10.83	1188.63	12.10	330.40	-17.59	Low	FR	Lower
	10.49	703.36	8.63	345.66	23.48	Low	F	Upper
	15.59	775.27	9.00	8.99	13.86	Low	F	Upper
	162.80	15483.06	35.83	352.49	-41.57	Very Severe	F	Lower
	10.28	914.20	6.55	244.50	-21.38	Low	BR	Lower
	47.33	4114.80	14.90	8.91	-36.16	Moderate	F	Lower
	12.33	1681.44	8.49	333.66	-17.11	Low	FR	Lower
	45.84	5023.12	17.31	258.39	30.03	Moderate	R	Upper
	195.14	21297.25	36.08	19.54	-29.55	Very Severe	F	Lower
	58.49	7765.76	29.99	7.47	-39.19	Serious	F	Lower
	31.69	4051.64	18.73	25.12	-49.40	Moderate	FL	Neck
	14.92	1796.13	12.94	286.41	-15.99	Low	R	Lower
	11.04	729.13	10.29	71.28	20.06	Low	L	Upper
	26.15	2097.00	14.01	350.32	6.76	Low	F	Upper
	25.72	2295.18	11.05	80.26	21.38	Low	L	Upper
	21.89	1237.14	8.87	69.88	-9.66	Low	L	Lower
	21.48	1682.55	10.29	86.13	0.37	Low	L	Upper

MMA Training Sessions

Fighter 8

	Max Result Linear Accel (g)	Max Result Rotational Accel (rads/s^2)	Max Result Rot Vel (rads/s)	Rot Angle (°)	Elev Angle (°)	Impact	Sector	Elev
Fighter 8	15.49	861.31	10.01	36.51	-32.52	Low	FL	Lower
	17.71	1403.89	10.48	6.66	-41.38	Low	F	Lower
	10.66	475.56	9.62	41.66	-15.67	Low	FL	Lower
	11.87	626.65	9.97	48.29	-9.70	Low	FL	Lower
	11.56	632.41	10.32	44.26	-12.44	Low	FL	Lower
	13.15	556.71	11.59	40.18	-17.57	Low	FL	Lower
	12.82	569.60	9.07	23.31	-29.06	Low	FL	Lower
	12.15	560.42	11.41	23.25	-22.15	Low	FL	Lower
	11.76	642.38	8.67	28.03	-22.83	Low	FL	Lower
	12.35	724.42	9.55	38.83	-19.02	Low	FL	Lower
	13.04	830.24	11.71	53.77	-13.79	Low	FL	Lower
	13.56	632.26	11.65	36.16	-21.66	Low	FL	Lower
	12.86	770.75	6.38	35.88	-14.18	Low	FL	Lower
	13.94	770.56	11.23	51.59	-13.36	Low	FL	Lower
	58.95	4315.13	11.04	35.12	-39.20	Moderate	FL	Lower
	39.41	3597.46	10.40	88.41	-0.16	Moderate	L	Lower
	13.41	1230.73	13.03	19.37	-26.34	Low	F	Lower
	11.49	520.88	8.69	10.95	-33.69	Low	F	Lower
	13.56	923.18	12.56	25.89	-18.02	Low	FL	Lower
	13.35	991.02	10.83	33.60	-29.08	Low	FL	Lower
	11.38	509.13	9.38	19.56	-31.24	Low	F	Lower
	11.87	605.13	9.81	38.36	-25.94	Low	FL	Lower
	13.15	655.85	11.52	29.27	-21.38	Low	FL	Lower
	12.12	392.12	7.59	35.68	-17.30	Low	FL	Lower
	12.09	721.46	11.47	43.98	-17.81	Low	FL	Lower
	23.36	4710.47	9.26	93.07	2.59	Low	L	Upper
	12.43	546.34	10.68	32.90	-17.49	Low	FL	Lower
	22.92	3096.33	10.53	278.45	-5.03	Low	R	Lower
	12.34	932.24	12.26	59.19	-6.45	Low	FL	Lower

	17.11	1086.28	10.96	37.77	-21.30	Low	FL	Lower
	34.21	3429.60	10.13	33.07	-38.55	Moderate	FL	Lower
	17.95	1351.36	7.04	335.43	-39.41	Low	FR	Lower
	10.06	696.10	3.87	12.90	-36.37	Low	F	Lower
	13.47	872.70	3.51	68.56	-5.89	Low	L	Lower
	55.43	3613.56	25.26	63.48	-14.92	Moderate	FL	Lower
	22.98	1322.29	9.74	51.57	-14.47	Low	FL	Lower
	10.03	1102.41	7.73	281.02	-1.44	Low	R	Lower
	26.49	2007.77	9.49	345.32	-33.97	Low	F	Lower
	12.01	2261.49	14.06	246.84	10.03	Low	BR	Upper
	24.96	1997.78	19.71	61.52	-13.19	Low	FL	Lower
	17.57	1715.18	13.46	264.24	12.36	Low	R	Upper
	21.73	1353.02	5.28	267.49	-16.00	Low	R	Lower
	24.91	1482.55	15.39	62.68	-14.07	Low	FL	Lower
	28.69	2244.53	11.47	359.02	-25.33	Low	F	Lower
	17.18	714.59	10.85	31.13	-15.26	Low	FL	Lower
	89.08	8732.03	9.59	324.82	-50.49	Serious	FR	Neck
	26.61	3283.16	10.41	355.54	-32.82	Low	F	Lower
	20.54	1700.16	15.36	62.77	-17.94	Low	FL	Lower
	34.23	3186.70	15.55	38.40	-29.58	Moderate	FL	Lower
	70.74	6678.94	11.20	334.51	-38.66	Serious	FR	Lower
	15.07	2221.96	16.36	68.48	-4.94	Low	L	Lower
	26.99	2865.70	15.93	237.56	30.92	Low	BR	Upper
	41.96	5069.00	15.64	42.74	-31.11	Moderate	FL	Lower
	44.47	1801.18	11.84	346.42	-18.35	Moderate	F	Lower
	106.85	4489.91	16.31	274.56	26.01	Very Serious	R	Upper
	13.62	1024.25	8.81	130.03	20.20	Low	BL	Upper
	57.43	5468.81	21.38	91.87	-1.85	Moderate	L	Lower
	43.04	3554.21	7.90	336.70	-32.77	Moderate	FR	Lower
	30.40	3269.03	11.27	207.60	3.00	Moderate	BR	Upper
	40.31	2240.73	14.88	357.74	-20.94	Moderate	F	Lower
	17.22	1847.32	17.59	269.97	10.27	Low	R	Upper
	11.14	1052.97	8.42	313.66	-6.37	Low	FR	Lower
	18.67	1201.53	11.17	272.89	-4.56	Low	R	Lower

	35.04	2027.71	10.66	2.71	-11.03	Moderate	F	Lower
	11.95	1440.51	10.05	259.85	-40.89	Low	R	Lower
	18.62	1966.45	6.09	323.01	-26.73	Low	FR	Lower
	45.15	4411.17	14.12	6.32	-34.58	Moderate	F	Lower
	14.46	798.87	10.10	349.97	-32.62	Low	F	Lower
	32.03	1867.90	10.80	270.29	13.14	Moderate	R	Upper
	17.79	2027.18	8.72	42.12	-9.94	Low	FL	Lower
	54.41	5313.76	17.19	140.53	11.24	Moderate	BL	Upper
	20.08	1432.36	11.36	346.56	-8.37	Low	F	Lower
	241.79	1600.29	13.13	14.87	-33.13	Very Severe	F	Lower
	11.10	1931.41	13.69	281.65	7.39	Low	R	Upper
	19.66	1584.85	15.04	321.52	-35.52	Low	FR	Lower
	25.75	2389.61	14.23	274.32	0.37	Low	R	Upper
	25.13	1598.21	19.49	53.05	-24.73	Low	FL	Lower
	11.49	1800.61	10.28	81.75	10.92	Low	L	Upper
	31.05	1983.57	11.16	51.68	-26.49	Moderate	FL	Lower

Boxing Sparring Sessions

Fighter 10 Session 1

	Max Result Linear Accel (g)	Max Result Rotational Accel (rads/s^2)	Max Result Rot Vel (rads/s)	Rot Angle (°)	Elev Angle (°)	Impact	Sector	Elev
Fighter 10 - Session 1	11.54	1334.34	12.22	49.42	-4.08	Low	FL	Lower
	28.22	2746.04	11.79	74.76	-5.80	Low	L	Lower
	14.64	6365.88	13.35	290.94	12.63	Low	R	Upper
	11.20	3704.67	9.03	186.60	59.30	Low	B	Top
	27.07	3298.46	17.71	279.95	2.76	Low	R	Upper
	22.21	11151.88	17.06	56.85	-18.01	Low	FL	Lower
	11.59	1447.07	15.73	275.39	-13.60	Low	R	Lower
	15.52	2886.57	20.25	266.29	57.10	Low	R	Top
	13.65	4272.88	17.14	64.57	-0.32	Low	FL	Lower
	11.97	5003.24	17.31	14.34	5.66	Low	F	Upper
	19.21	7792.05	13.18	2.68	-34.77	Low	F	Lower
	10.59	4001.45	12.12	287.14	-11.83	Low	R	Lower
	20.91	6891.48	15.44	340.73	-8.59	Low	F	Lower
	20.12	13045.94	27.30	357.90	-47.99	Low	F	Neck
	19.98	12163.29	28.25	5.97	-49.72	Low	F	Neck
	33.60	22443.84	31.07	338.77	-78.11	Moderate	F	Neck
	22.78	12913.65	20.14	275.41	-44.15	Low	R	Lower
	13.59	2112.99	23.20	282.85	10.87	Low	R	Upper
	12.10	9655.72	23.40	10.92	-58.09	Low	F	Neck
	26.26	6760.50	25.77	273.91	15.59	Low	R	Upper
	10.34	4446.31	13.24	352.78	-38.61	Low	F	Lower
	18.21	5370.63	16.82	283.55	0.28	Low	R	Upper
	13.63	2366.54	9.63	357.12	-28.07	Low	F	Lower
	16.18	6658.83	18.89	311.26	-48.40	Low	FR	Neck
	13.41	2358.45	15.76	238.27	-3.99	Low	BR	Lower
	28.89	5523.19	23.36	284.47	-7.51	Low	R	Lower
	18.91	2032.77	10.31	66.46	-2.31	Low	FL	Lower
	16.20	2530.68	11.91	264.72	11.19	Low	R	Upper
	13.94	10171.14	25.26	357.34	-61.00	Low	F	Neck
	26.73	17122.39	27.37	356.48	-67.08	Low	F	Neck

Session 2

	Max Result Linear Accel (g)	Max Result Rotational Accel (rads/s^2)	Max Result Rot Vel (rads/s)	Rot Angle (°)	Elev Angle (°)	Impact	Sector	Elev
Fighter 10 - Session 2	21.69	3285.18	32.00	264.62	11.52	Low	R	Upper
	12.52	4089.98	13.39	268.78	8.89	Low	R	Upper
	16.19	4520.91	10.76	281.59	-22.28	Low	R	Lower
	22.86	11093.61	29.15	25.86	-52.94	Low	FL	Neck
	21.01	2741.26	13.84	76.43	-11.04	Low	L	Lower
	26.89	12473.84	34.51	357.31	67.13	Low	F	Top
	12.08	2418.77	15.33	68.67	-9.11	Low	L	Lower
	13.14	2595.52	10.14	212.44	59.65	Low	BR	Top
	17.10	2656.95	28.03	271.91	-7.74	Low	R	Lower
	10.44	2219.81	10.88	341.58	-36.20	Low	F	Lower
	20.60	4394.56	12.29	96.94	3.61	Low	L	Upper
	51.98	6097.87	36.75	263.40	12.52	Moderate	R	Upper
	18.94	3061.03	18.59	285.63	-14.01	Low	R	Lower
	11.93	4221.77	14.56	63.48	-10.83	Low	FL	Lower
	14.17	3510.66	18.86	289.58	-14.16	Low	R	Lower
	19.99	5933.80	18.48	263.93	20.27	Low	R	Upper
	19.57	2875.07	19.93	48.62	-13.92	Low	FL	Lower
	13.75	7128.64	10.65	15.44	-59.37	Low	F	Neck
	12.63	5817.83	28.17	130.62	-26.49	Low	BL	Lower
	44.94	4493.27	26.37	274.72	8.08	Moderate	R	Upper
	20.13	2247.89	24.75	61.38	-4.09	Low	FL	Lower
	11.07	5152.62	19.15	316.42	69.20	Low	FR	Top
	16.02	2373.12	12.37	284.30	32.27	Low	R	Upper
	22.39	2323.39	16.57	271.62	-0.82	Low	R	Lower
	11.12	1423.93	10.10	277.81	-10.85	Low	R	Lower
	31.92	2756.85	11.13	271.54	6.58	Moderate	R	Upper
	20.93	2309.38	13.21	69.59	-4.87	Low	L	Lower
	40.75	10236.85	30.26	289.62	5.43	Moderate	R	Upper
	14.62	2239.49	20.76	254.02	-7.22	Low	R	Lower
	15.52	3187.65	11.68	125.27	11.65	Low	BL	Upper

34.36	22611.90	26.60	297.81	-29.13	Moderate	FR	Lower
12.36	1422.32	14.33	276.56	-0.57	Low	R	Lower
12.77	3105.99	10.59	67.29	-0.36	Low	FL	Lower
12.40	2831.90	18.81	84.92	-60.71	Low	L	Neck
37.67	20677.46	48.25	357.24	-49.30	Moderate	F	Neck
15.28	1793.63	17.69	268.07	1.94	Low	R	Upper

Session 3

	Max Result Linear Accel (g)	Max Result Rotational Accel (rads/s^2)	Max Result Rot Vel (rads/s)	Rot Angle (°)	Elev Angle (°)	Impact	Sector	Elev
Fighter 10 - Session 3	10.67	2594.85	12.03	29.59	-31.23	Low	FL	Lower
	10.60	1429.23	14.75	288.79	-4.85	Low	R	Lower
	17.46	2805.09	11.61	297.33	16.00	Low	FR	Upper
	13.03	3621.67	15.63	275.75	-24.02	Low	R	Lower
	32.14	6837.07	35.07	265.72	0.70	Moderate	R	Upper
	13.85	8219.58	25.00	31.35	-40.52	Low	FL	Lower
	10.79	2004.24	19.35	276.15	-7.37	Low	R	Lower
	11.09	1157.00	15.13	256.10	5.83	Low	R	Upper
	12.07	7203.83	20.57	347.66	-64.62	Low	F	Neck
	10.13	2516.86	15.49	32.53	-27.41	Low	FL	Lower
	11.68	7720.05	22.55	347.12	-69.03	Low	F	Neck
	23.87	10052.77	19.55	224.78	73.05	Low	BR	Top
	20.47	2570.13	18.16	45.76	-7.01	Low	FL	Lower
	10.22	7517.59	14.49	357.95	-37.75	Low	F	Lower
	12.90	2604.80	10.40	51.03	-15.62	Low	FL	Lower
	13.71	5206.67	21.40	38.56	-26.13	Low	FL	Lower
	19.44	1886.67	11.24	251.27	9.82	Low	R	Upper
	10.30	7239.28	15.83	330.80	-59.43	Low	FR	Neck
	31.33	3593.56	21.08	284.40	3.43	Moderate	R	Upper
	59.62	41398.47	72.78	317.62	-54.80	Moderate	FR	Neck
	20.36	3185.71	32.43	57.39	-9.94	Low	FL	Lower
	10.03	4191.06	16.51	348.00	-43.49	Low	F	Lower
	22.08	2840.57	15.76	58.29	-16.18	Low	FL	Lower
	10.32	5236.91	19.11	339.56	1.49	Low	F	Upper
	10.39	5330.68	13.98	7.83	-35.59	Low	F	Lower
	27.21	3344.70	19.10	276.30	0.59	Low	R	Upper
	24.95	6753.20	13.40	290.84	-16.21	Low	R	Lower
	19.06	2352.85	15.54	265.17	-10.84	Low	R	Lower
	10.62	6287.61	18.08	321.79	-12.34	Low	FR	Lower
	18.74	2310.93	10.20	250.97	16.08	Low	R	Upper

	11.94	1030.84	8.14	265.22	6.26	Low	R	Upper
	11.76	4550.52	11.07	342.60	32.48	Low	F	Upper
	15.63	9552.70	11.82	341.36	-70.73	Low	F	Neck
	13.97	2759.13	13.11	33.79	82.31	Low	FL	Top
	14.25	11138.26	15.11	331.81	-41.40	Low	FR	Lower
	11.57	2424.09	12.97	292.66	-14.16	Low	FR	Lower

Session 4

	Max Result Linear Accel (g)	Max Result Rotational Accel (rads/s^2)	Max Result Rot Vel (rads/s)	Rot Angle (°)	Elev Angle (°)	Impact	Sector	Elev
Fighter 10 - Session 4	15.83	1639.07	14.06	262.40	-42.56	Low	R	Lower
	20.84	3484.47	19.21	43.42	-21.85	Low	FL	Lower
	25.12	2805.32	15.51	346.79	-8.38	Low	F	Lower
	13.61	2047.59	14.23	343.44	-10.54	Low	F	Lower
	20.45	2676.45	19.59	352.58	-13.19	Low	F	Lower
	82.22	8686.76	23.05	341.05	-43.49	Serious	F	Lower
	51.83	5471.97	21.67	100.23	-0.92	Moderate	L	Lower
	55.20	4824.69	22.96	5.83	-43.35	Moderate	F	Lower
	30.21	2626.58	20.21	66.90	-14.50	Moderate	FL	Lower
	39.99	5790.75	36.97	8.95	-13.89	Moderate	F	Lower
	52.45	5626.52	23.56	359.91	-18.70	Moderate	F	Lower
	18.48	2868.81	9.73	349.14	-8.05	Low	F	Lower
	53.21	5551.31	24.20	345.83	-42.73	Moderate	F	Lower
	108.58	9994.08	21.32	338.20	-46.91	Very Serious	F	Neck
	97.14	10634.80	27.25	347.40	-43.31	Very Serious	F	Lower
	39.00	4873.39	21.92	31.12	-29.02	Moderate	FL	Lower
	336.29	37580.16	57.00	327.20	-37.35	Very Severe	FR	Lower
	187.08	9828.00	15.37	251.65	0.12	Very Severe	R	Upper
	43.32	4630.38	15.26	347.24	-28.34	Moderate	F	Lower
	225.64	22761.69	52.63	356.17	-41.95	Very Severe	F	Lower
	43.36	3499.76	14.31	95.53	-9.86	Moderate	L	Lower
	14.80	1957.16	13.78	337.95	-24.12	Low	F	Lower
	218.65	22145.83	38.97	358.30	-42.41	Very Severe	F	Lower
	33.17	3103.19	15.89	338.07	-25.25	Moderate	F	Lower

	29.42	3858.51	25.76	23.98	-30.62	Low	FL	Lower
	22.02	2930.56	15.38	80.88	-3.44	Low	L	Lower
	28.36	2863.83	21.12	44.45	-23.95	Low	FL	Lower
	11.60	1425.07	13.17	297.38	-7.86	Low	FR	Lower
	62.18	7291.52	20.34	5.36	-38.95	Serious	F	Lower
	35.04	4891.04	13.87	262.02	16.51	Moderate	R	Upper
	45.23	5138.20	20.05	246.72	-1.48	Moderate	BR	Lower
	10.63	1438.58	14.19	9.33	-16.38	Low	F	Lower
	46.38	5184.73	15.29	316.84	-34.84	Moderate	FR	Lower
	92.76	10753.55	30.04	5.95	-52.21	Very Serious	F	Neck

Appendix 5

Simulation Data – Competitive Bouts

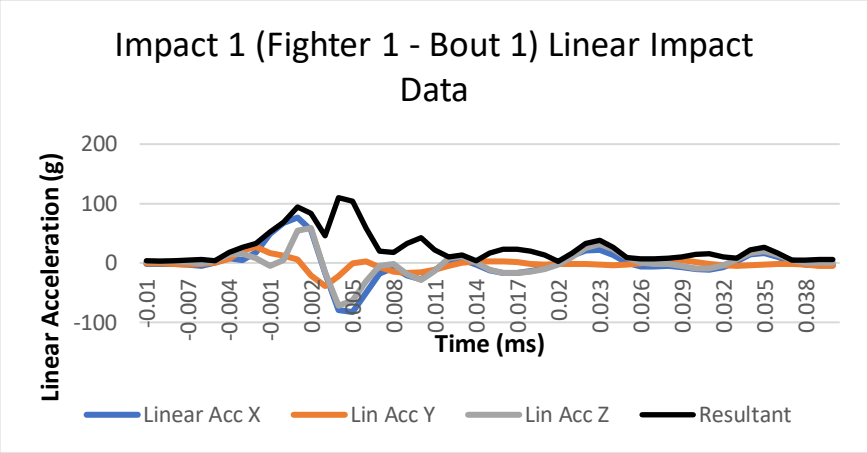

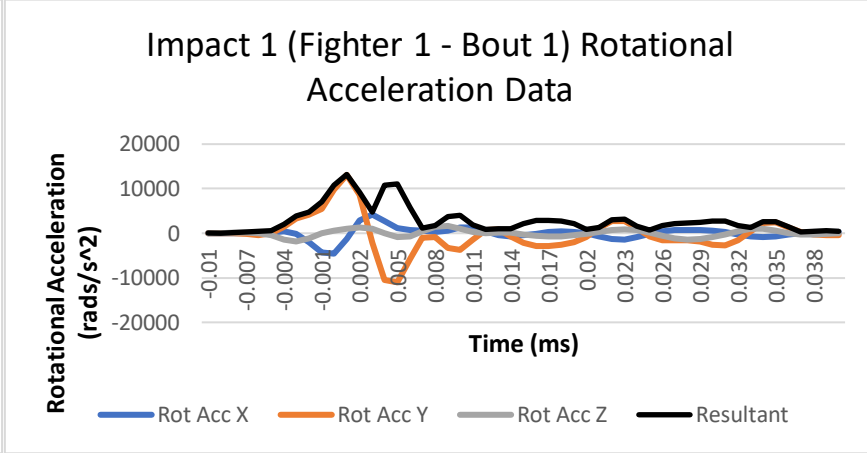

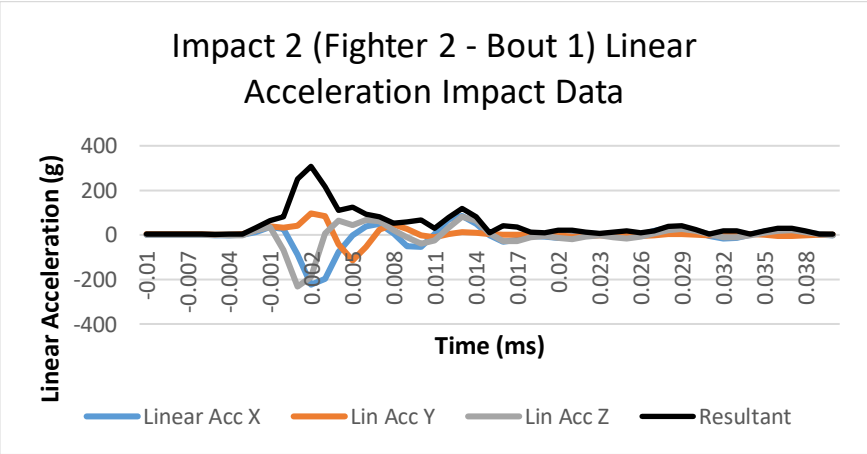

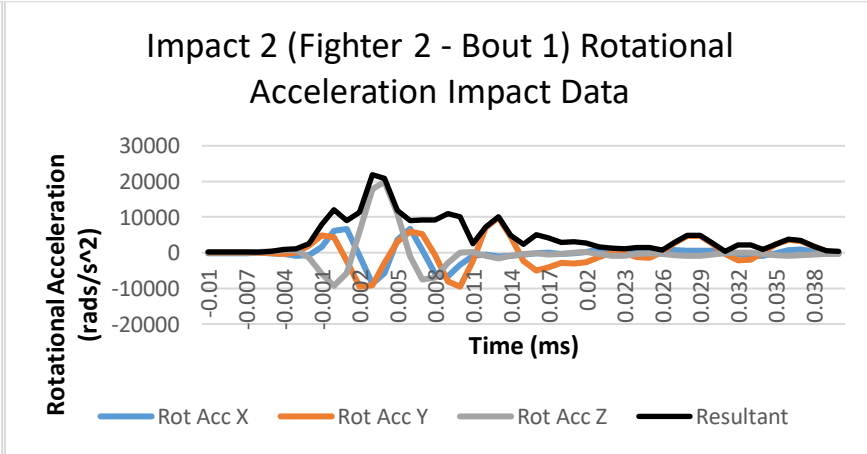

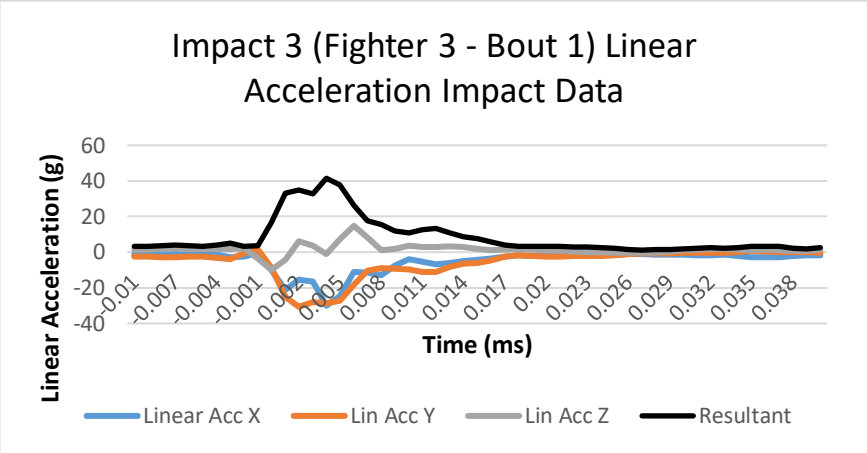
Impact 3 (Fighter 3 - Bout 1) Linear Acceleration Impact Data
Linear Acceleration (g)
60
40
20
0
-20
-40
-0.01
-0.007
-0.004
-0.001
0.002
0.005
0.008
0.011
0.014
0.017
0.02
0.023
0.026
0.029
0.032
0.035
0.038
Time (ms)
Linear Acc X
Lin Acc Y
Lin Acc Z
Resultant

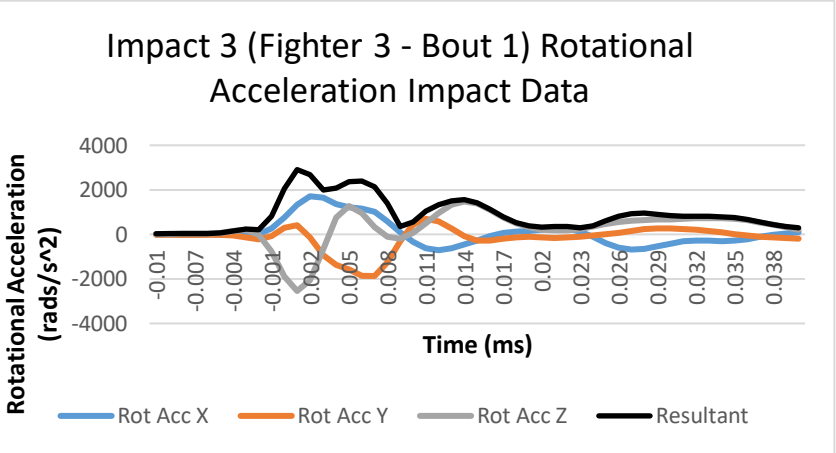
Impact 3 (Fighter 3 - Bout 1) Rotational Acceleration Impact Data
Rotational Acceleration (rads/s^2)
4000
2000
0
-2000
-4000
-0.01
-0.007
-0.004
-0.001
0.002
0.005
0.008
0.011
0.014
0.017
0.02
0.023
0.026
0.029
0.032
0.035
0.038
Time (ms)
Rot Acc X
Rot Acc Y
Rot Acc Z
Resultant

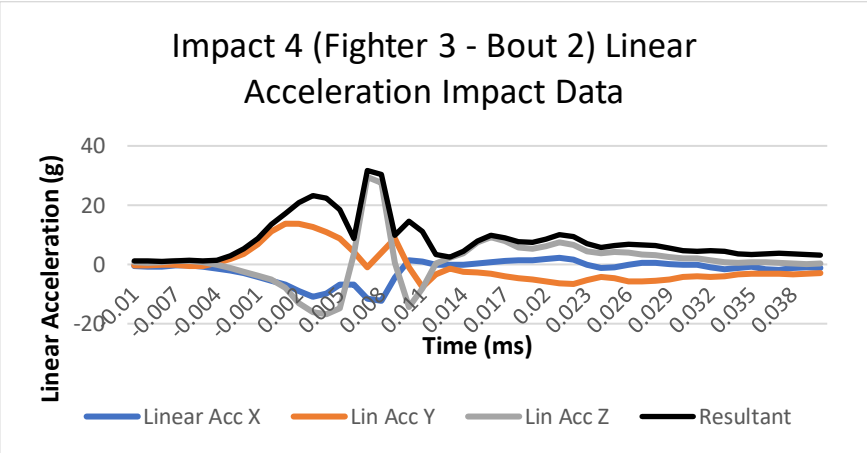
Impact 4 (Fighter 3 - Bout 2) Linear Acceleration Impact Data
Linear Acceleration (g)
40
20
0
-20
-0.01
-0.007
-0.004
-0.001
0.002
0.005
0.008
0.011
0.014
0.017
0.02
0.023
0.026
0.029
0.032
0.035
0.038
Time (ms)
Linear Acc X
Lin Acc Y
Lin Acc Z
Resultant

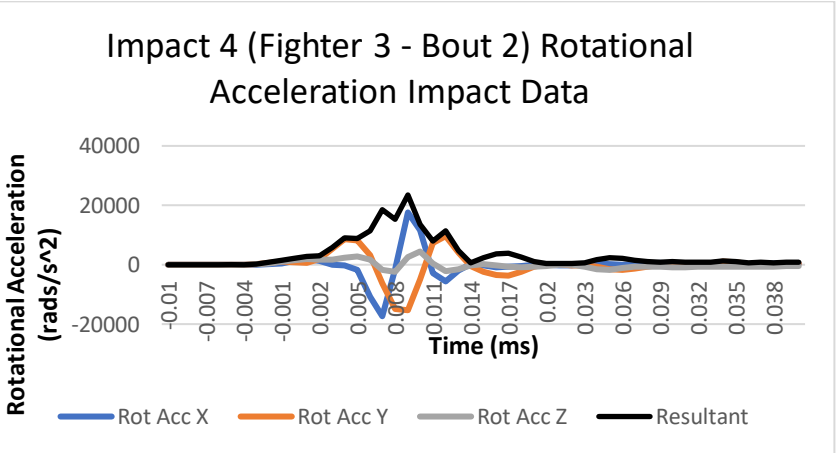
Impact 4 (Fighter 3 - Bout 2) Rotational Acceleration Impact Data
Rotational Acceleration (rads/s^2)
40000
20000
0
-20000
-0.01
-0.007
-0.004
-0.001
0.002
0.005
0.008
0.011
0.014
0.017
0.02
0.023
0.026
0.029
0.032
0.035
0.038
Time (ms)
Rot Acc X
Rot Acc Y
Rot Acc Z
Resultant

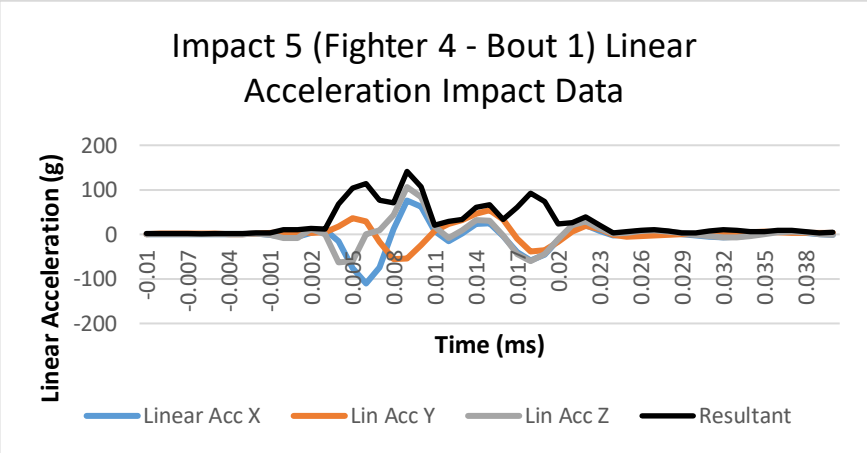
Impact 5 (Fighter 4 - Bout 1) Linear Acceleration Impact Data
Linear Acceleration (g)
200
100
0
-100
-200
-0.01
-0.007
-0.004
-0.001
0.002
0.005
0.008
0.011
0.014
0.017
0.02
0.023
0.026
0.029
0.032
0.035
0.038
Time (ms)
Linear Acc X
Lin Acc Y
Lin Acc Z
Resultant

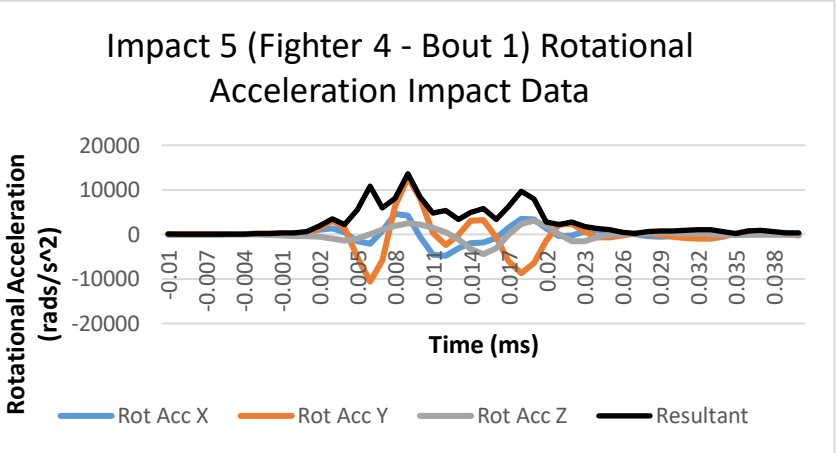
Impact 5 (Fighter 4 - Bout 1) Rotational Acceleration Impact Data
Rotational Acceleration (rads/s^2)
20000
10000
0
-10000
-20000
-0.01
-0.007
-0.004
-0.001
0.002
0.005
0.008
0.011
0.014
0.017
0.02
0.023
0.026
0.029
0.032
0.035
0.038
Time (ms)
Rot Acc X
Rot Acc Y
Rot Acc Z
Resultant

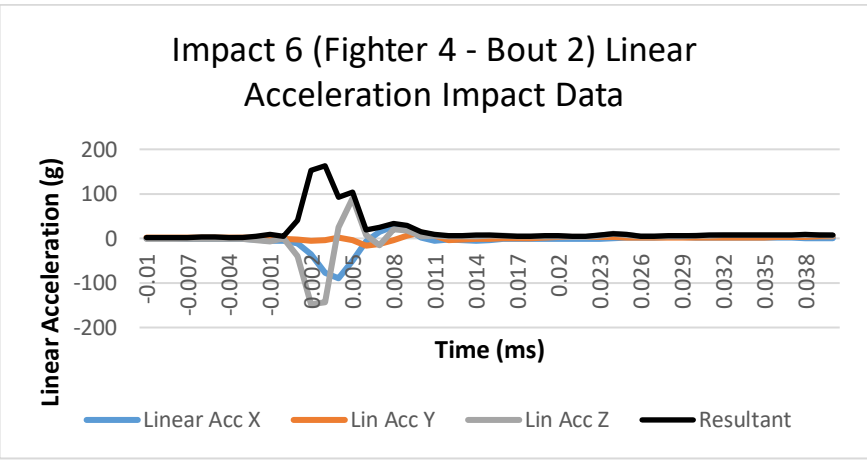
Impact 6 (Fighter 4 - Bout 2) Linear Acceleration Impact Data
Linear Acceleration (g)
200
100
0
-100
-200
-0.01
-0.007
-0.004
-0.001
0.002
0.005
0.008
0.011
0.014
0.017
0.02
0.023
0.026
0.029
0.032
0.035
0.038
Time (ms)
Linear Acc X
Lin Acc Y
Lin Acc Z
Resultant

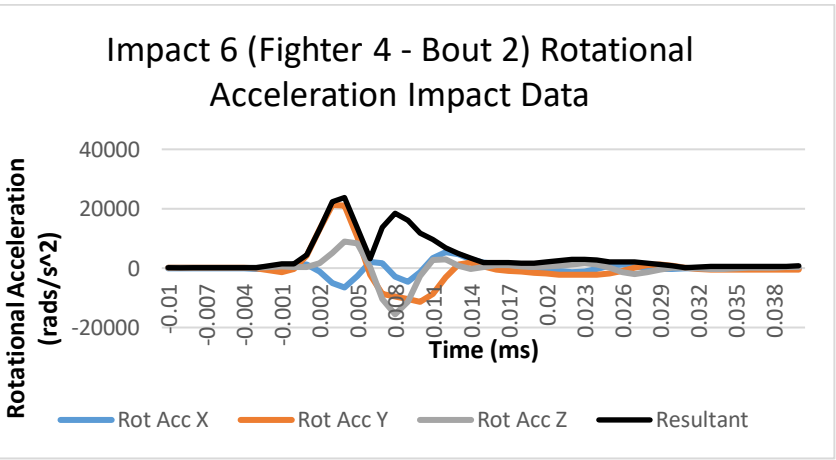
Impact 6 (Fighter 4 - Bout 2) Rotational Acceleration Impact Data
Rotational Acceleration (rads/s^2)
40000
20000
0
-20000
-0.01
-0.007
-0.004
-0.001
0.002
0.005
0.008
0.011
0.014
0.017
0.02
0.023
0.026
0.029
0.032
0.035
0.038
Time (ms)
Rot Acc X
Rot Acc Y
Rot Acc Z
Resultant

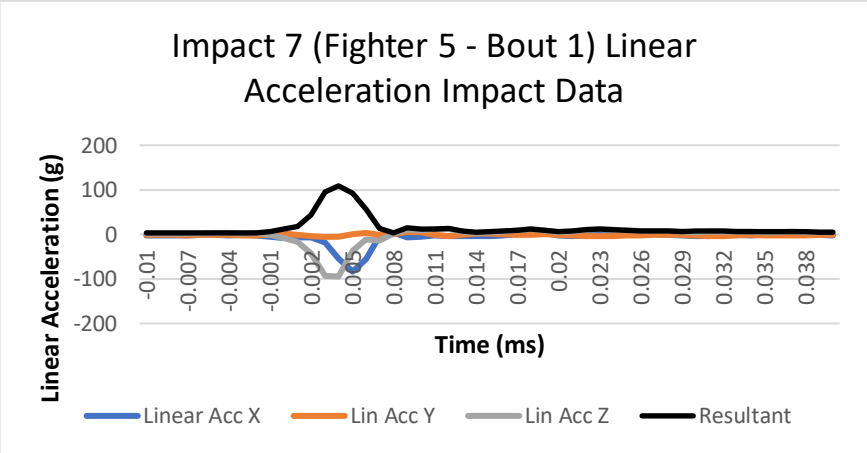
Impact 7 (Fighter 5 - Bout 1) Linear Acceleration Impact Data
Linear Acceleration (g)
200
100
0
-100
-200
-0.01
-0.007
-0.004
-0.001
0.002
0.005
0.008
0.011
0.014
0.017
0.02
0.023
0.026
0.029
0.032
0.035
0.038
Time (ms)
Linear Acc X
Lin Acc Y
Lin Acc Z
Resultant

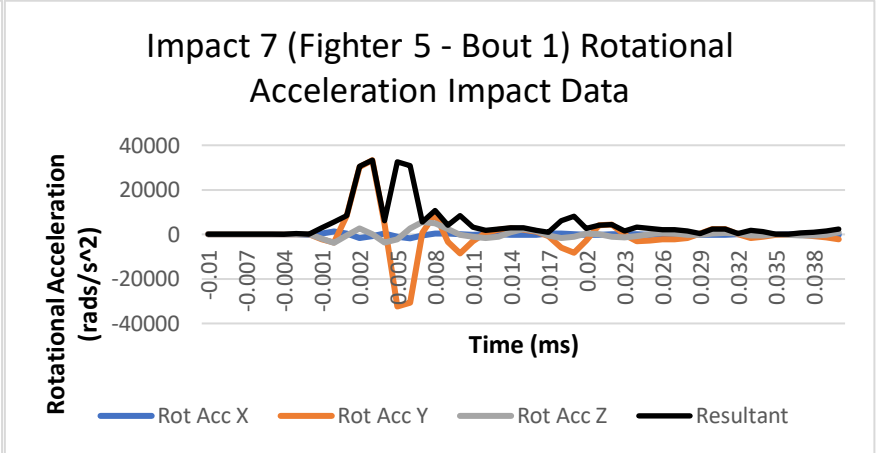
Impact 7 (Fighter 5 - Bout 1) Rotational Acceleration Impact Data
Rotational Acceleration (rads/s^2)
40000
20000
0
-20000
-40000
-0.01
-0.007
-0.004
-0.001
0.002
0.005
0.008
0.011
0.014
0.017
0.02
0.023
0.026
0.029
0.032
0.035
0.038
Time (ms)
Rot Acc X
Rot Acc Y
Rot Acc Z
Resultant

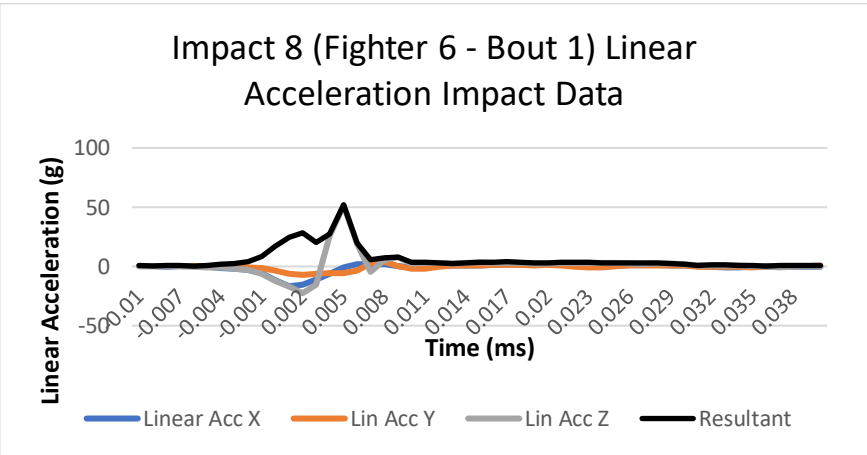
Impact 8 (Fighter 6 - Bout 1) Linear Acceleration Impact Data
Linear Acceleration (g)
100
50
0
-50
-0.01
-0.007
-0.004
-0.001
0.002
0.005
0.008
0.011
0.014
0.017
0.02
0.023
0.026
0.029
0.032
0.035
0.038
Time (ms)
Linear Acc X
Lin Acc Y
Lin Acc Z
Resultant

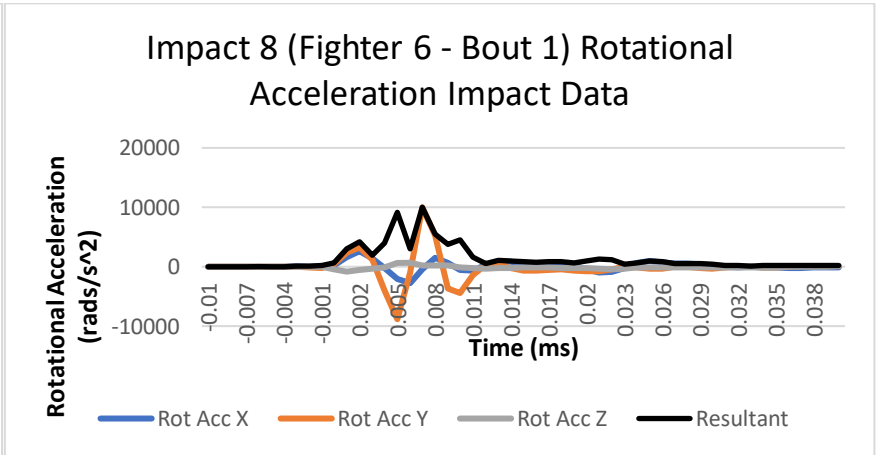
Impact 8 (Fighter 6 - Bout 1) Rotational Acceleration Impact Data
Rotational Acceleration (rads/s^2)
20000
10000
0
-10000
-0.01
-0.007
-0.004
-0.001
0.002
0.005
0.008
0.011
0.014
0.017
0.02
0.023
0.026
0.029
0.032
0.035
0.038
Time (ms)
Rot Acc X
Rot Acc Y
Rot Acc Z
Resultant

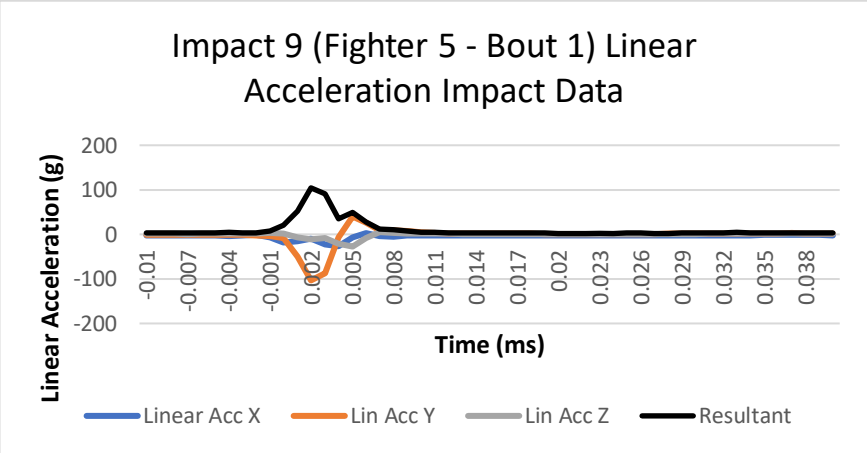
Impact 9 (Fighter 5 - Bout 1) Linear Acceleration Impact Data
Linear Acceleration (g)
200
100
0
-100
-200
-0.01
-0.007
-0.004
-0.001
0.002
0.005
0.008
0.011
0.014
0.017
0.02
0.023
0.026
0.029
0.032
0.035
0.038
Time (ms)
Linear Acc X
Lin Acc Y
Lin Acc Z
Resultant

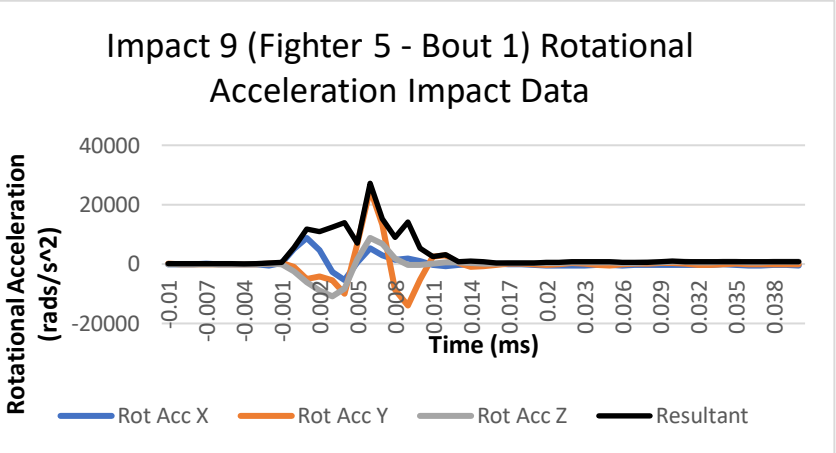
Impact 9 (Fighter 5 - Bout 1) Rotational Acceleration Impact Data
Rotational Acceleration (rads/s^2)
40000
20000
0
-20000
-0.01
-0.007
-0.004
-0.001
0.002
0.005
0.008
0.011
0.014
0.017
0.02
0.023
0.026
0.029
0.032
0.035
0.038
Time (ms)
Rot Acc X
Rot Acc Y
Rot Acc Z
Resultant

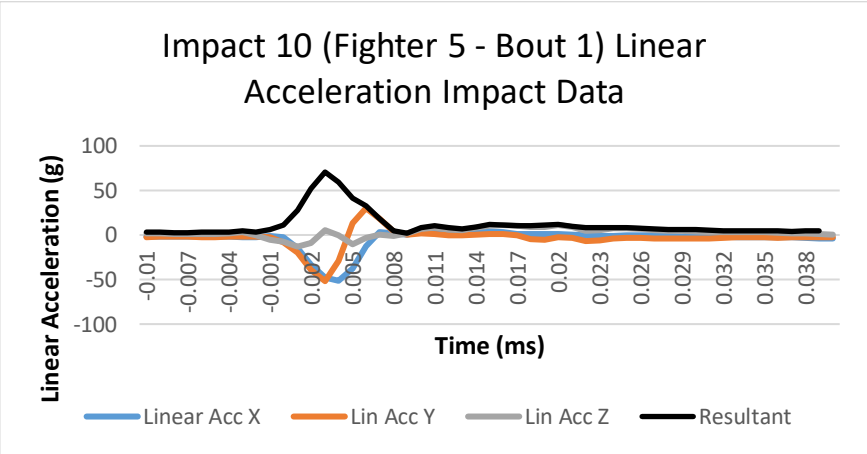
Impact 10 (Fighter 5 - Bout 1) Linear Acceleration Impact Data
Linear Acceleration (g)
100
50
0
-50
-100
-0.01
-0.007
-0.004
-0.001
0.002
0.005
0.008
0.011
0.014
0.017
0.02
0.023
0.026
0.029
0.032
0.035
0.038
Time (ms)
Linear Acc X
Lin Acc Y
Lin Acc Z
Resultant

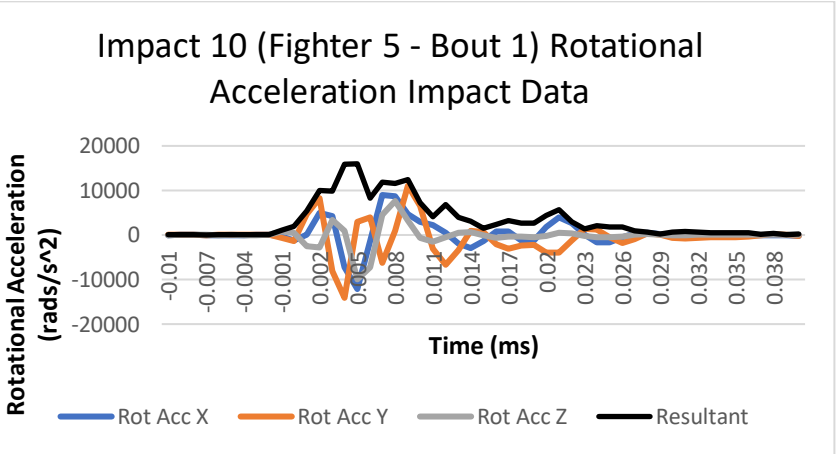
Impact 10 (Fighter 5 - Bout 1) Rotational Acceleration Impact Data
Rotational Acceleration (rads/s^2)
20000
10000
0
-10000
-20000
-0.01
-0.007
-0.004
-0.001
0.002
0.005
0.008
0.011
0.014
0.017
0.02
0.023
0.026
0.029
0.032
0.035
0.038
Time (ms)
Rot Acc X
Rot Acc Y
Rot Acc Z
Resultant

Appendix 6

Simulation Data – MMA Sparring Sessions/MMA Training/Boxing Sparring

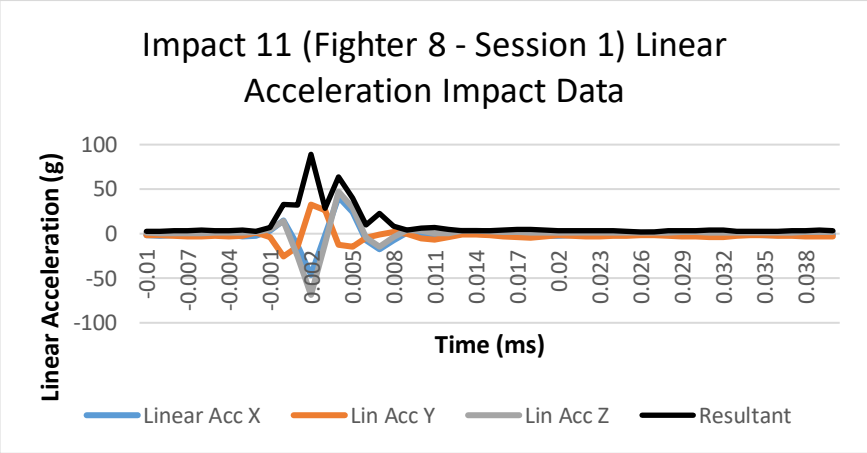

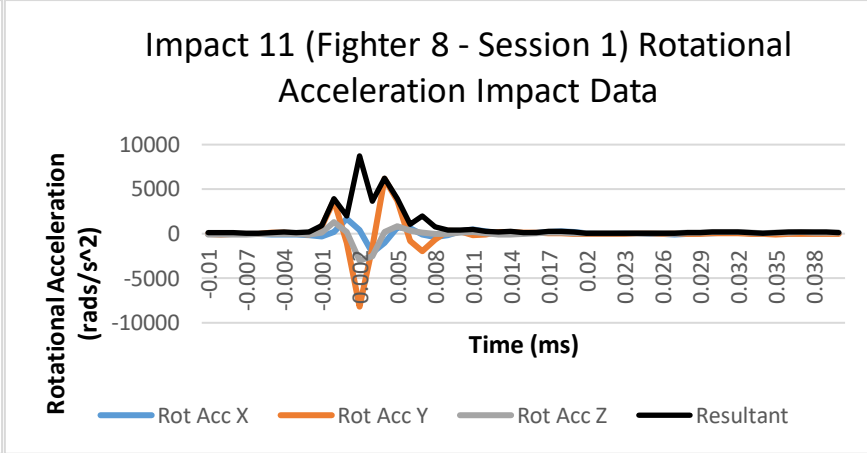

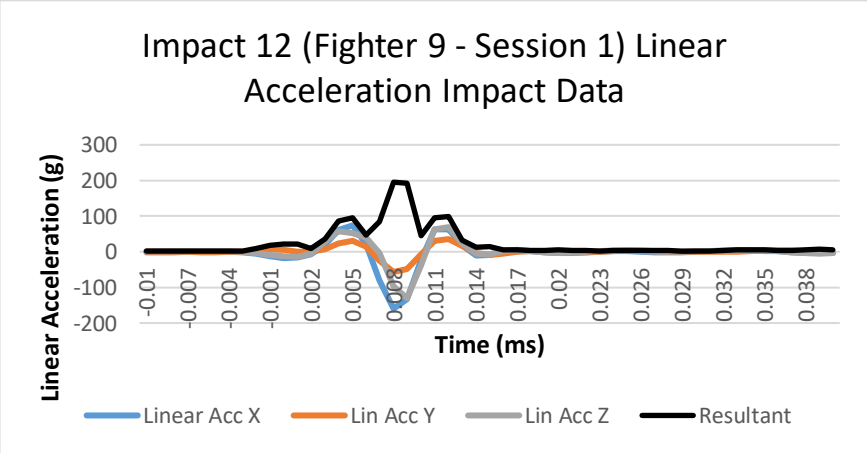

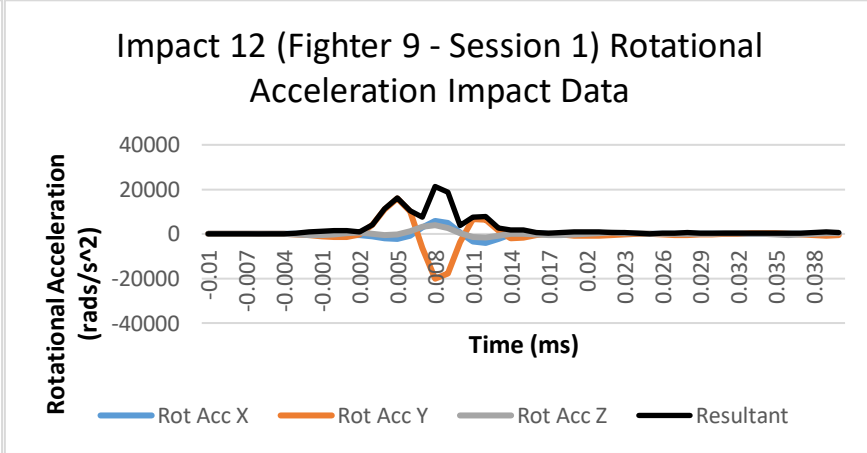

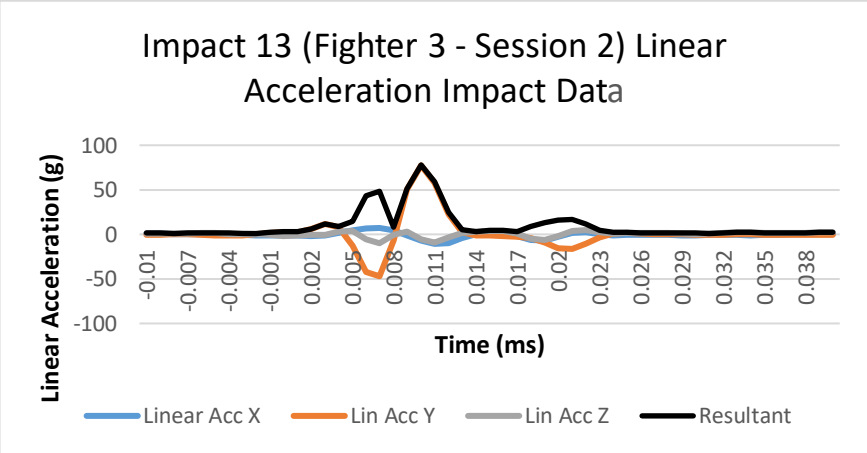
Impact 13 (Fighter 3 - Session 2) Linear Acceleration Impact Data
Linear Acceleration (g)
100
50
0
-50
-100
-0.01
-0.007
-0.004
-0.001
0.002
0.005
0.008
0.011
0.014
0.017
0.02
0.023
0.026
0.029
0.032
0.035
0.038
Time (ms)
Linear Acc X
Lin Acc Y
Lin Acc Z
Resultant

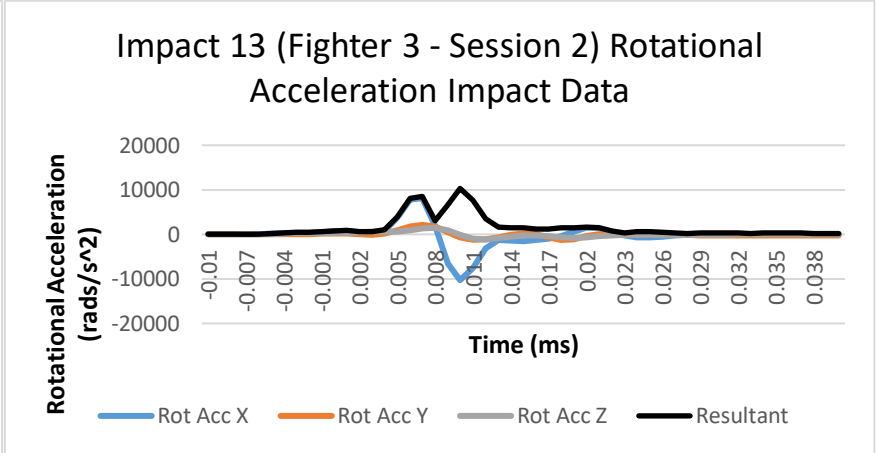
Impact 13 (Fighter 3 - Session 2) Rotational Acceleration Impact Data
Rotational Acceleration (rads/s^2)
20000
10000
0
-10000
-20000
-0.01
-0.007
-0.004
-0.001
0.002
0.005
0.008
0.011
0.014
0.017
0.02
0.023
0.026
0.029
0.032
0.035
0.038
Time (ms)
Rot Acc X
Rot Acc Y
Rot Acc Z
Resultant

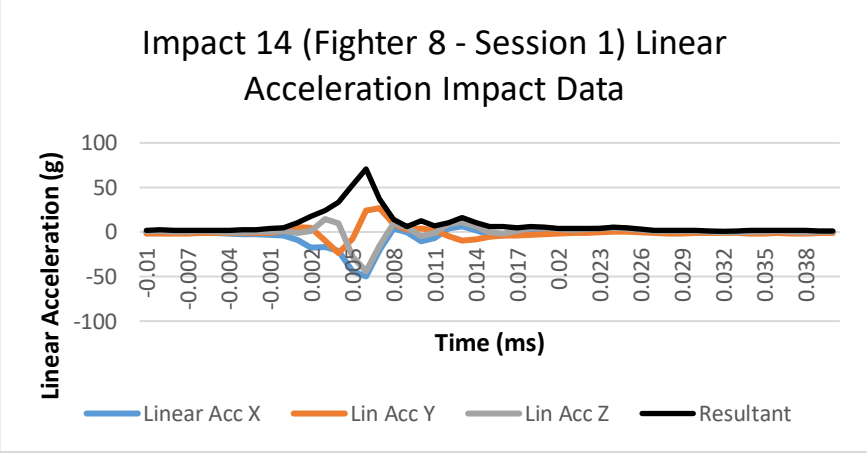
Impact 14 (Fighter 8 - Session 1) Linear Acceleration Impact Data
Linear Acceleration (g)
100
50
0
-50
-100
-0.01
-0.007
-0.004
-0.001
0.002
0.005
0.008
0.011
0.014
0.017
0.02
0.023
0.026
0.029
0.032
0.035
0.038
Time (ms)
Linear Acc X
Lin Acc Y
Lin Acc Z
Resultant

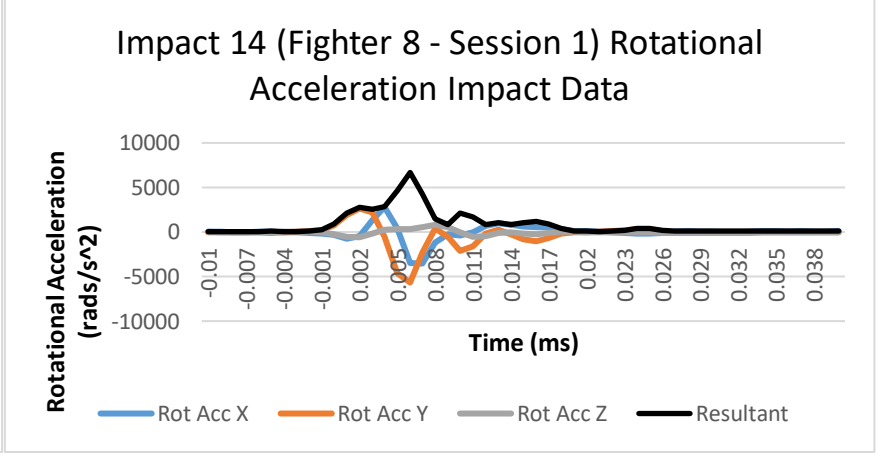
Impact 14 (Fighter 8 - Session 1) Rotational Acceleration Impact Data
Rotational Acceleration (rads/s^2)
10000
5000
0
-5000
-10000
-0.01
-0.007
-0.004
-0.001
0.002
0.005
0.008
0.011
0.014
0.017
0.02
0.023
0.026
0.029
0.032
0.035
0.038
Time (ms)
Rot Acc X
Rot Acc Y
Rot Acc Z
Resultant

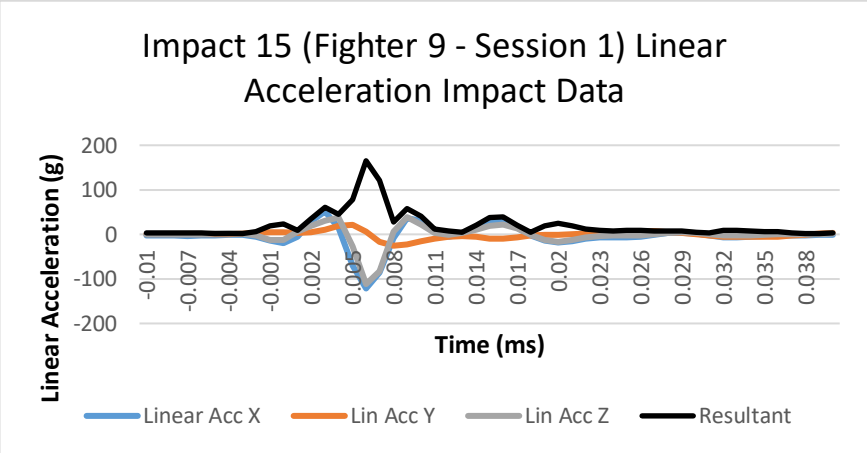
Impact 15 (Fighter 9 - Session 1) Linear Acceleration Impact Data
Linear Acceleration (g)
200
100
0
-100
-200
-0.01
-0.007
-0.004
-0.001
0.002
0.005
0.008
0.011
0.014
0.017
0.02
0.023
0.026
0.029
0.032
0.035
0.038
Time (ms)
Linear Acc X
Lin Acc Y
Lin Acc Z
Resultant

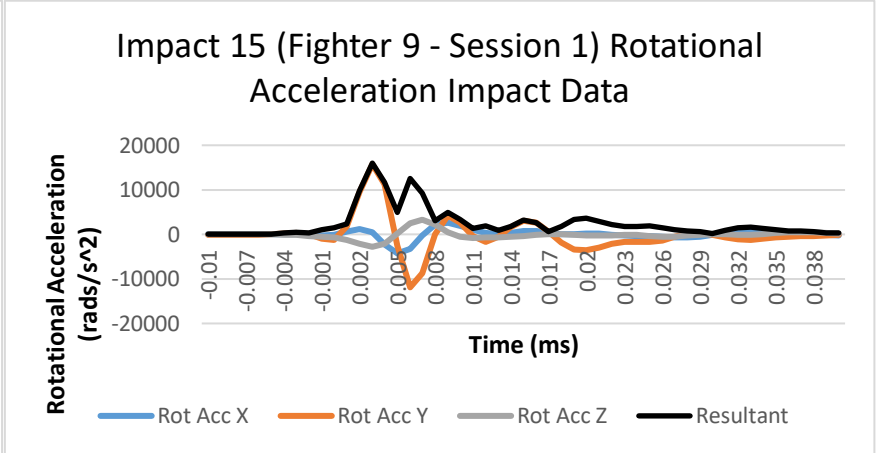
Impact 15 (Fighter 9 - Session 1) Rotational Acceleration Impact Data
Rotational Acceleration (rads/s^2)
20000
10000
0
-10000
-20000
-0.01
-0.007
-0.004
-0.001
0.002
0.005
0.008
0.011
0.014
0.017
0.02
0.023
0.026
0.029
0.032
0.035
0.038
Time (ms)
Rot Acc X
Rot Acc Y
Rot Acc Z
Resultant

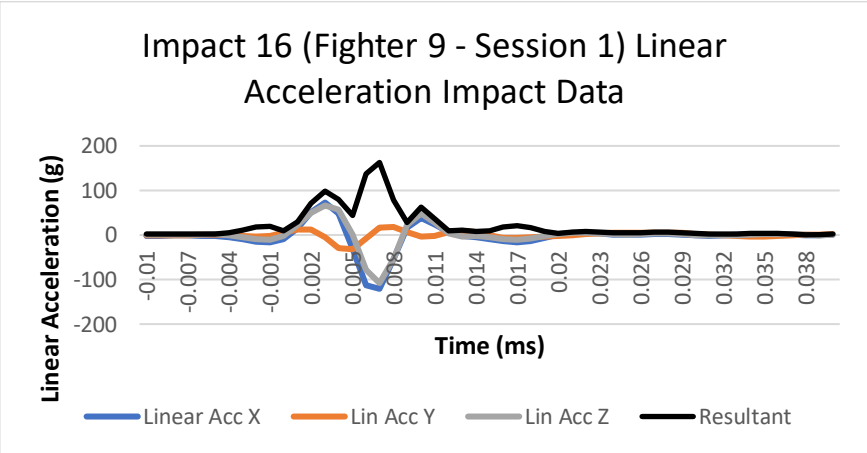
Impact 16 (Fighter 9 - Session 1) Linear Acceleration Impact Data
Linear Acceleration (g)
200
100
0
-100
-200
-0.01
-0.007
-0.004
-0.001
0.002
0.005
0.008
0.011
0.014
0.017
0.02
0.023
0.026
0.029
0.032
0.035
0.038
Time (ms)
Linear Acc X
Lin Acc Y
Lin Acc Z
Resultant

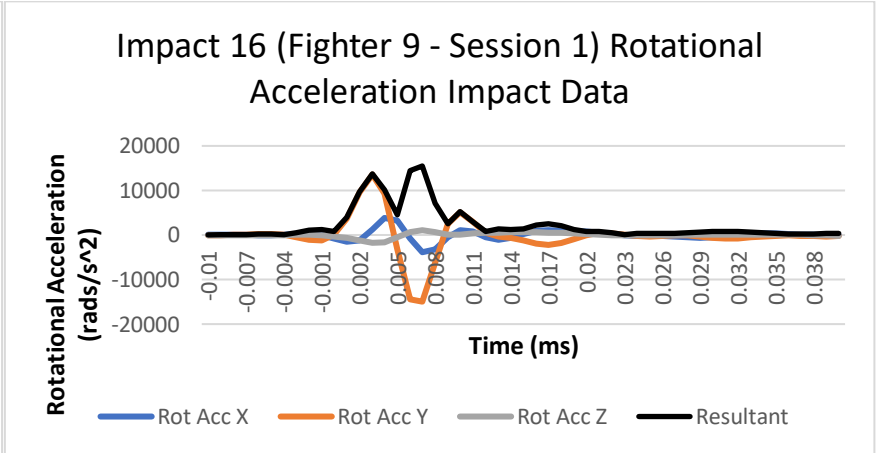
Impact 16 (Fighter 9 - Session 1) Rotational Acceleration Impact Data
Rotational Acceleration (rads/s^2)
20000
10000
0
-10000
-20000
-0.01
-0.007
-0.004
-0.001
0.002
0.005
0.008
0.011
0.014
0.017
0.02
0.023
0.026
0.029
0.032
0.035
0.038
Time (ms)
Rot Acc X
Rot Acc Y
Rot Acc Z
Resultant

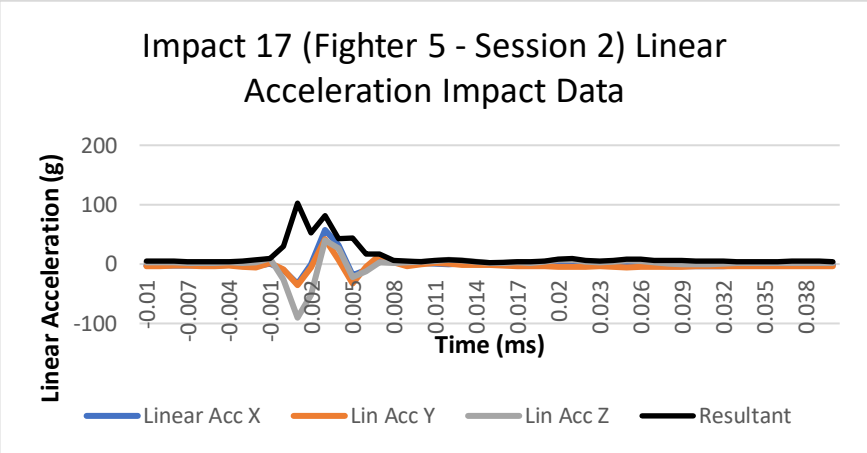
Impact 17 (Fighter 5 - Session 2) Linear Acceleration Impact Data
Linear Acceleration (g)
200
100
0
-100
-0.01
-0.007
-0.004
-0.001
0.002
0.005
0.008
0.011
0.014
0.017
0.02
0.023
0.026
0.029
0.032
0.035
0.038
Time (ms)
Linear Acc X
Lin Acc Y
Lin Acc Z
Resultant

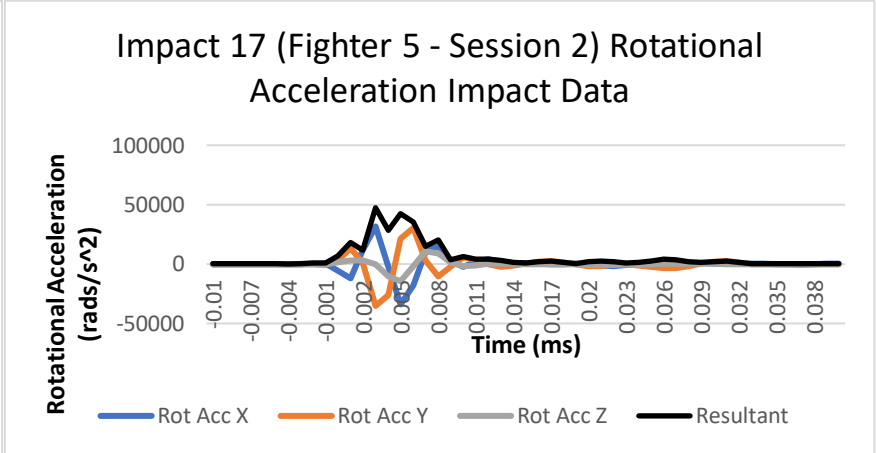
Impact 17 (Fighter 5 - Session 2) Rotational Acceleration Impact Data
Rotational Acceleration (rads/s^2)
100000
50000
0
-50000
-0.01
-0.007
-0.004
-0.001
0.002
0.005
0.008
0.011
0.014
0.017
0.02
0.023
0.026
0.029
0.032
0.035
0.038
Time (ms)
Rot Acc X
Rot Acc Y
Rot Acc Z
Resultant

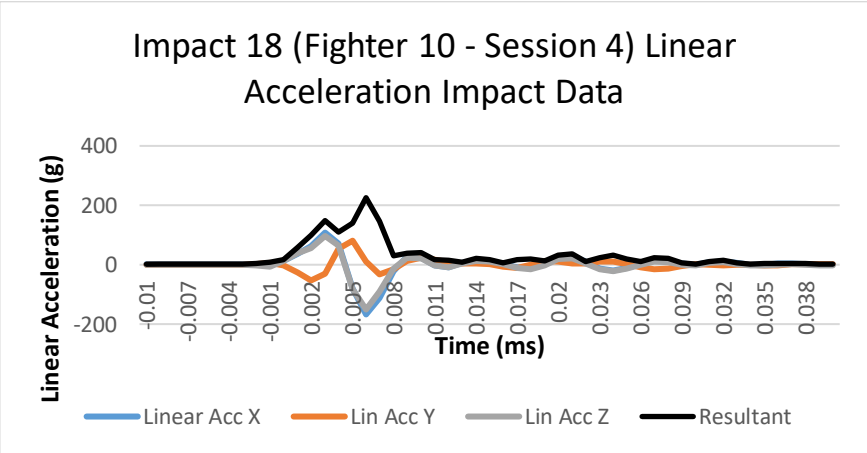
Impact 18 (Fighter 10 - Session 4) Linear Acceleration Impact Data
Linear Acceleration (g)
400
200
0
-200
-0.01
-0.007
-0.004
-0.001
0.002
0.005
0.008
0.011
0.014
0.017
0.02
0.023
0.026
0.029
0.032
0.035
0.038
Time (ms)
Linear Acc X
Lin Acc Y
Lin Acc Z
Resultant

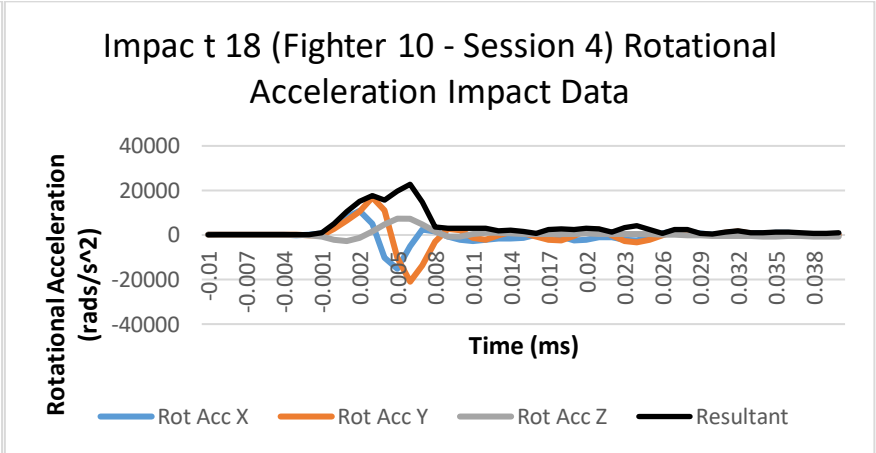
Impac t 18 (Fighter 10 - Session 4) Rotational Acceleration Impact Data
Rotational Acceleration (rads/s^2)
40000
20000
0
-20000
-40000
-0.01
-0.007
-0.004
-0.001
0.002
0.005
0.008
0.011
0.014
0.017
0.02
0.023
0.026
0.029
0.032
0.035
0.038
Time (ms)
Rot Acc X
Rot Acc Y
Rot Acc Z
Resultant

Appendix 7

Linear Relationships

The following tables report the R^2 values for all kinematic variables when plotted against strain in each of the regions of interest. Also reported is the R^2 values for strains against HIP. Appendix 8 reports all the graphs from which these values were found. There are 3 data sets being examined; mTBI cases, no injury cases and combined.

Linear Acceleration

Region v Measured Acceleration	Linear		
	TBI Cases	**No Injury Cases**	**All Cases**
CC Max v Peak Resultant Linear Acceleration	0.2595	0.0573	0.143
CC Max v Peak Linear Acceleration X	0.0617	0.0432	0.0548
CC Max v Peak Linear Acceleration Y	0.7175	0.0436	0.3146
CC Max v Peak Linear Acceleration Z	0.0991	0.0731	0.0808
CC Mean v Peak Resultant Linear Acceleration	0.2819	0.0807	0.1704
CC Mean v Peak Linear Acceleration X	0.0751	0.0586	0.0702
CC Mean v Peak Linear Acceleration Y	0.7103	0.0585	0.341
CC Mean v Peak Linear Acceleration Z	0.116	0.0957	0.0989
Thalamus Max v Peak Resultant Linear Acceleration	0.274	0.0714	0.159
Thalamus Max v Peak Linear Acceleration X	0.0712	0.0551	0.066
Thalamus Max v Peak Linear Acceleration Y	0.7132	0.0553	0.3262
Thalamus Max v Peak Linear Acceleration Z	0.1102	0.085	0.0917
Thalamus Mean v Peak Resultant Linear Acceleration	0.2729	0.1037	0.1811
Thalamus Mean v Peak Linear Acceleration X	0.0709	0.0844	0.0819
Thalamus Mean v Peak Linear Acceleration Y	0.6855	0.0736	0.3424
Thalamus Mean v Peak Linear Acceleration Z	0.1107	0.1232	0.1078
Midbrain Max v Peak Resultant Linear Acceleration	0.5163	0.1221	0.3042
Midbrain Max v Peak Linear Acceleration X	0.2653	0.0725	0.161
Midbrain Max v Peak Linear Acceleration Y	0.7761	0.0743	0.4351
Midbrain Max v Peak Linear Acceleration Z	0.2893	0.1841	0.2233
Midbrain Mean v Peak Resultant Linear Acceleration	0.6176	0.1026	0.329
Midbrain Mean v Peak Linear Acceleration X	0.3858	0.0503	0.1874
Midbrain Mean v Peak Linear Acceleration Y	0.6707	0.0348	0.3469
Midbrain Mean v Peak Linear Acceleration Z	0.4064	0.17	0.2737
Brain Stem Max v Peak Resultant Linear Acceleration	0.4721	0.2849	0.3715
Brain Stem Max v Peak Linear Acceleration X	0.2158	0.1854	0.1945
Brain Stem Max v Peak Linear Acceleration Y	0.7996	0.0914	0.4954
Brain Stem Max v Peak Linear Acceleration Z	0.2491	0.3637	0.2561
Brain Stem Mean v Peak Resultant Linear Acceleration	0.4965	0.2617	0.3747
Brain Stem Mean v Peak Linear Acceleration X	0.2411	0.1711	0.2029
Brain Stem Mean v Peak Linear Acceleration Y	0.7929	0.102	0.493
Brain Stem Mean v Peak Linear Acceleration Z	0.2682	0.3406	0.2638

Rotational Acceleration

Region v Measured Acceleration	Rotational		
	TBI Cases	No Injury Cases	All Cases
CC Max v Peak Resultant Rotational Acceleration	0.1074	0.2316	0.1427
CC Max v Peak Rotational Acceleration X	0.1875	0.1389	0.0933
CC Max v Peak Rotational Acceleration Y	0.0473	0.092	0.0692
CC Max v Peak Rotational Acceleration Z	0.5663	0.14	0.3195
CC Mean v Peak Resultant Rotational Acceleration	0.25	0.1309	0.1627
CC Mean v Peak Rotational Acceleration X	0.1857	0.1552	0.0963
CC Mean v Peak Rotational Acceleration Y	0.0521	0.115	0.0813
CC Mean v Peak Rotational Acceleration Z	0.5915	0.1699	0.3577
Thalamus Max v Peak Resultant Rotational Acceleration	0.2268	0.1045	0.1392
Thalamus Max v Peak Rotational Acceleration X	0.1821	0.1346	0.09
Thalamus Max v Peak Rotational Acceleration Y	0.0414	0.0939	0.0667
Thalamus Max v Peak Rotational Acceleration Z	0.5874	0.1363	0.3242
Thalamus Mean v Peak Resultant Rotational Acceleration	0.2764	0.1638	0.1923
Thalamus Mean v Peak Rotational Acceleration X	0.1927	0.1845	0.1137
Thalamus Mean v Peak Rotational Acceleration Y	0.065	0.1565	0.1075
Thalamus Mean v Peak Rotational Acceleration Z	0.6031	0.1817	0.3682
Midbrain Max v Peak Resultant Rotational Acceleration	0.1949	0.4787	0.2866
Midbrain Max v Peak Rotational Acceleration X	0.2901	0.4434	0.2042
Midbrain Max v Peak Rotational Acceleration Y	0.007	0.4228	0.119
Midbrain Max v Peak Rotational Acceleration Z	0.87	0.5223	0.6992
Midbrain Mean v Peak Resultant Rotational Acceleration	0.1783	0.4127	0.2559
Midbrain Mean v Peak Rotational Acceleration X	0.2253	0.3299	0.1522
Midbrain Mean v Peak Rotational Acceleration Y	0.0014	0.3529	0.0906
Midbrain Mean v Peak Rotational Acceleration Z	0.9035	0.5423	0.7245
Brain Stem Max v Peak Resultant Rotational Acceleration	0.2199	0.3277	0.2142
Brain Stem Max v Peak Rotational Acceleration X	0.2796	0.2166	0.0932
Brain Stem Max v Peak Rotational Acceleration Y	0.0173	0.3586	0.0991
Brain Stem Max v Peak Rotational Acceleration Z	0.806	0.531	0.6659
Brain Stem Mean v Peak Resultant Rotational Acceleration	0.2166	0.4148	0.2497
Brain Stem Mean v Peak Rotational Acceleration X	0.3024	0.3028	0.1301
Brain Stem Mean v Peak Rotational Acceleration Y	0.014	0.4292	0.1145
Brain Stem Mean v Peak Rotational Acceleration Z	0.8472	0.5679	0.7053
CC Max v Peak Rotational Velocity	0.0239	0.3475	0.166
CC Mean Adjacent v Peak Rotational Velocity	0.0309	0.4007	0.1896
Thalamus Max v Peak Rotational Velocity	0.024	0.3437	0.1646
Thalamus Mean Adjacent v Peak Rotational Velocity	0.041	0.3961	0.1999
Midbrain Max v Peak Rotational Velocity	0.012	0.6891	0.2238
Midbrain Mean Adjacent v Peak Rotational Velocity	0.018	0.7702	0.2652
Brain Stem Max v Peak Rotational Velocity	0.0171	0.7715	0.2075
Brain Stem Mean Adjacent v Peak Rotational Velocity	0.0164	0.7753	0.2185

Region compared with HIP	TBI Cases	No Injury Cases	All Cases
CC Max	0.2427	0.3345	0.2834
CC Mean Adjacent	0.2744	0.3847	0.3262
Thalamus Max	0.2635	0.3469	0.3003
Thalamus Mean Adjacent0.	0.2865	0.4008	0.3383
Midbrain Max	0..4482	0.6008	0.5245
Midbrain Mean Adjacent	0.5808	0.6123	0.6087
Brain Stem Max	0.4025	0.7209	0.5409
Brain Stem Mean Adjacent	0.4266	0.7714	0.5562

Appendix 8

Graphs of Accelerations/Velocities against strain in brain regions

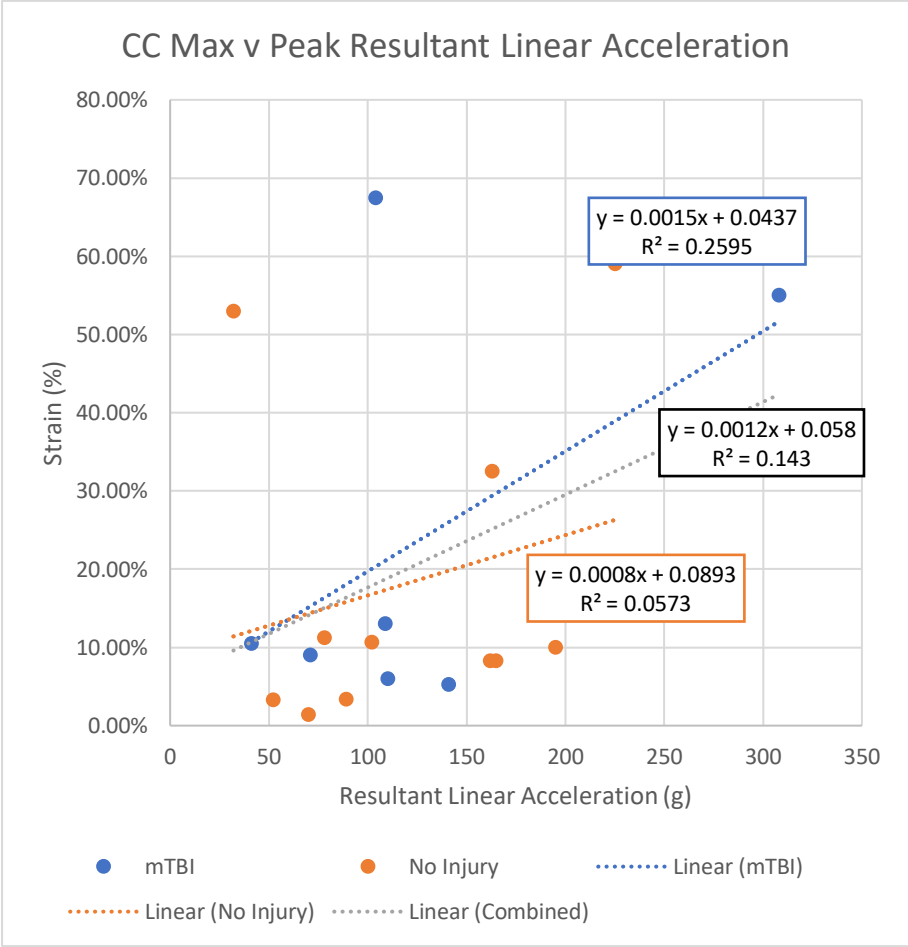

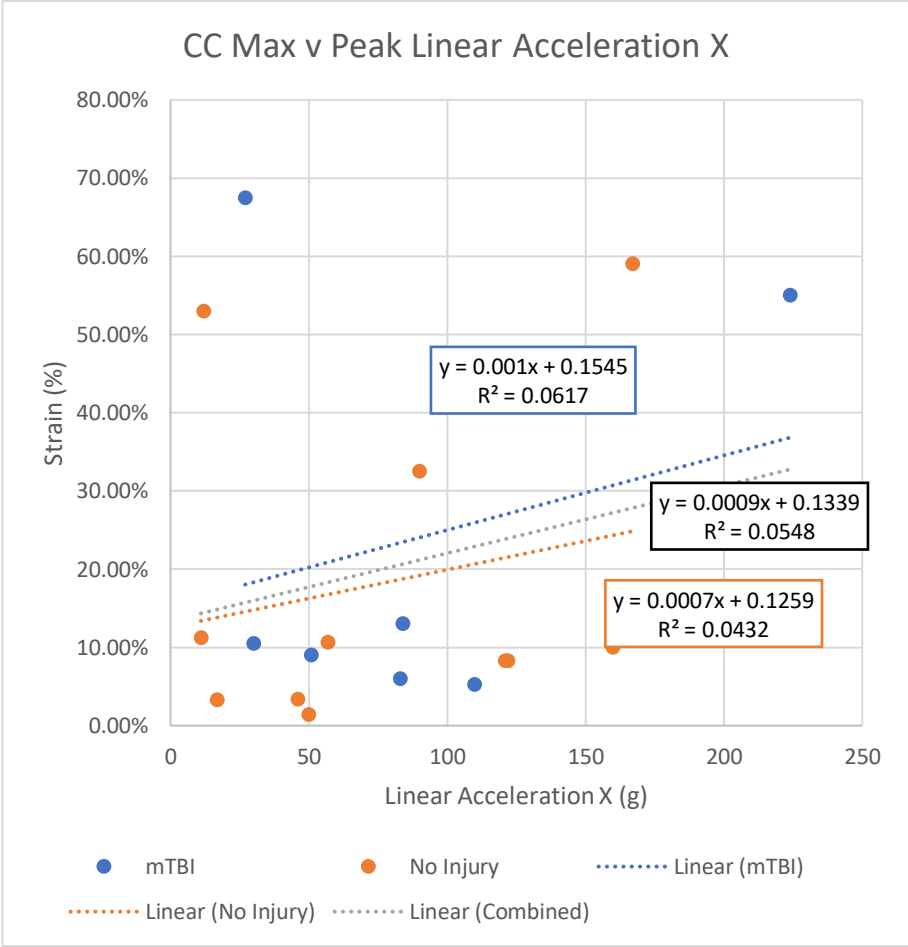

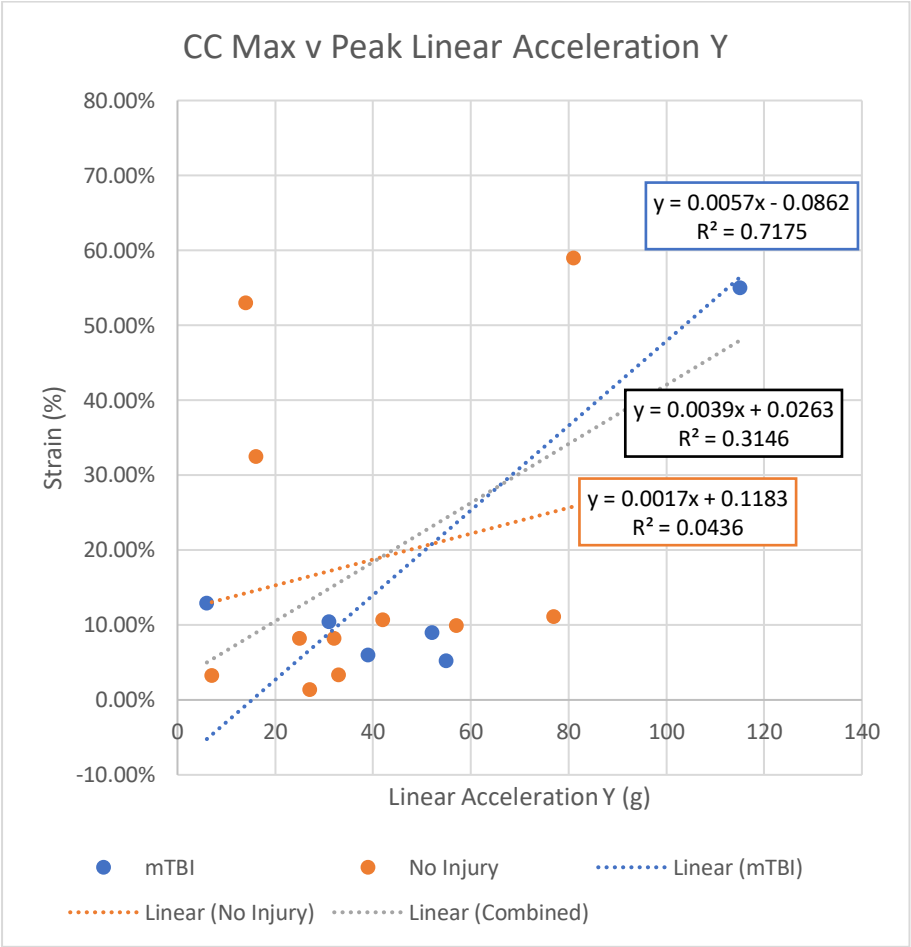
CC Max v Peak Linear Acceleration Y
80.00%
70.00%
60.00%
50.00%
40.00%
30.00%
20.00%
10.00%
0.00%
-10.00%
Strain (%)
0
20
40
60
80
100
120
140
Linear Acceleration Y (g)
y = 0.0057x - 0.0862
R² = 0.7175
y = 0.0039x + 0.0263
R² = 0.3146
y = 0.0017x + 0.1183
R² = 0.0436
mTBI
No Injury
Linear (mTBI)
Linear (No Injury)
Linear (Combined)

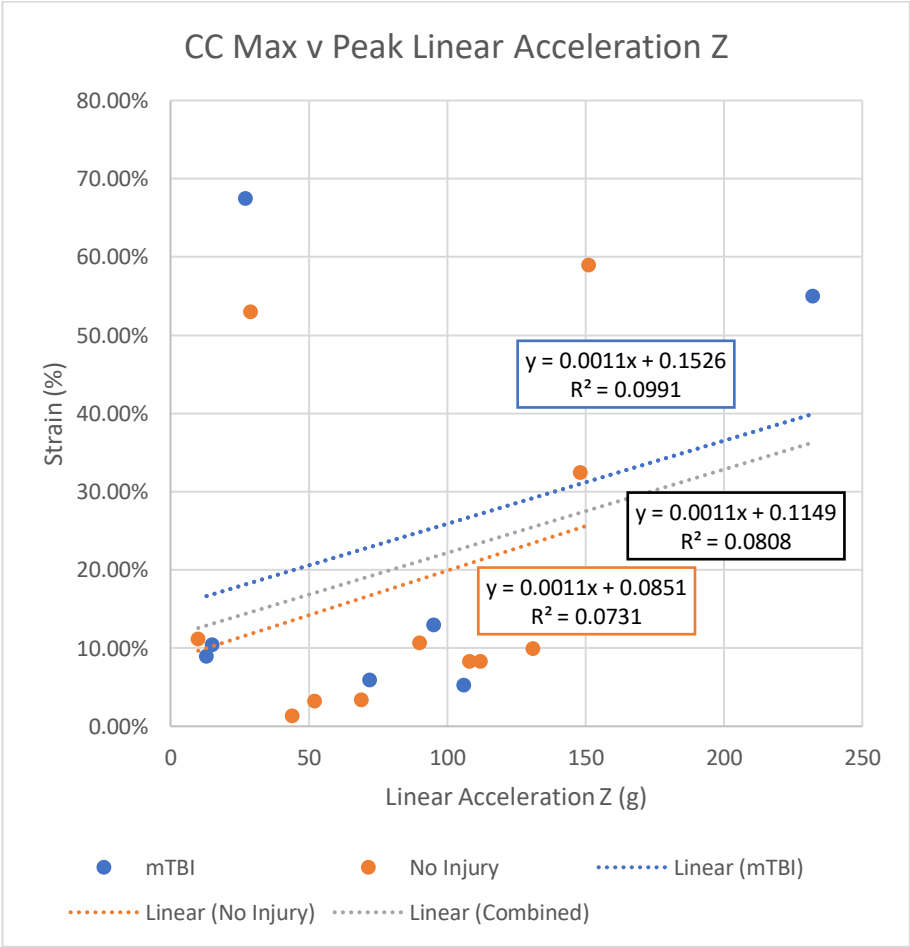
CC Max v Peak Linear Acceleration Z
80.00%
70.00%
60.00%
50.00%
40.00%
30.00%
20.00%
10.00%
0.00%
Strain (%)
0
50
100
150
200
250
Linear Acceleration Z (g)
y = 0.0011x + 0.1526
R² = 0.0991
y = 0.0011x + 0.1149
R² = 0.0808
y = 0.0011x + 0.0851
R² = 0.0731
mTBI
No Injury
Linear (mTBI)
Linear (No Injury)
Linear (Combined)

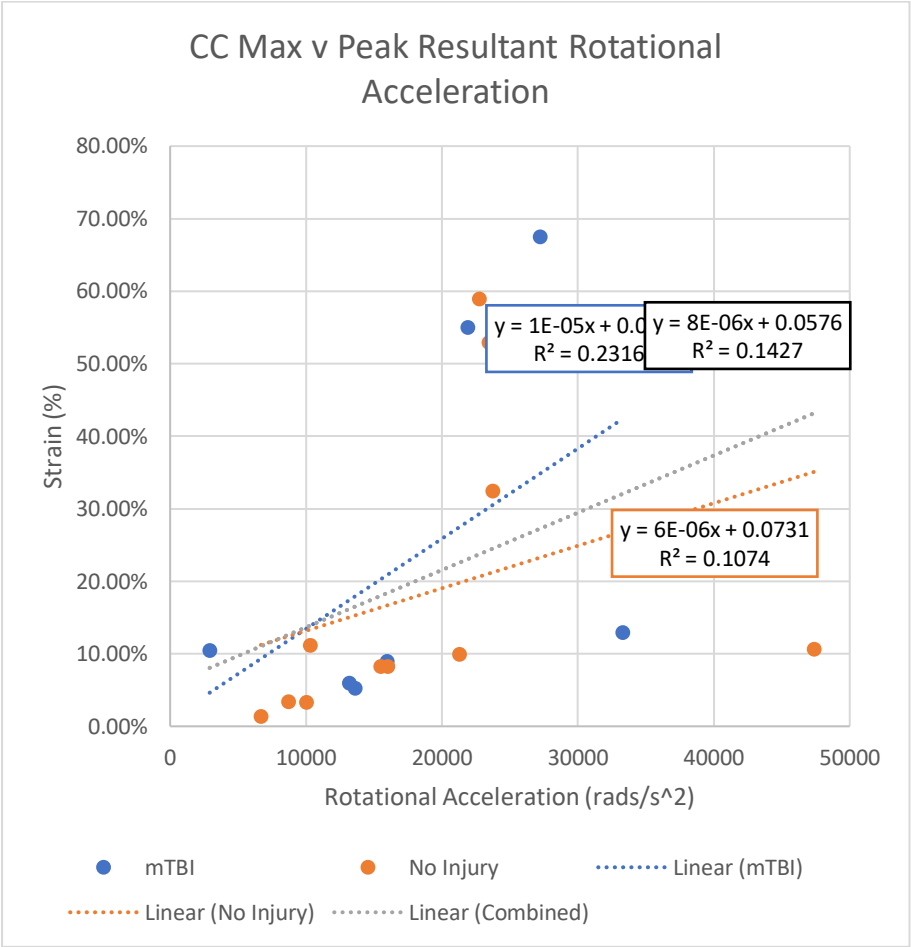
CC Max v Peak Resultant Rotational Acceleration
80.00%
70.00%
60.00%
50.00%
40.00%
30.00%
20.00%
10.00%
0.00%
Strain (%)
0
10000
20000
30000
40000
50000
Rotational Acceleration (rads/s^2)
y = 1E-05x + 0.0
R² = 0.2316
y = 8E-06x + 0.0576
R² = 0.1427
y = 6E-06x + 0.0731
R² = 0.1074
mTBI
No Injury
Linear (mTBI)
Linear (No Injury)
Linear (Combined)

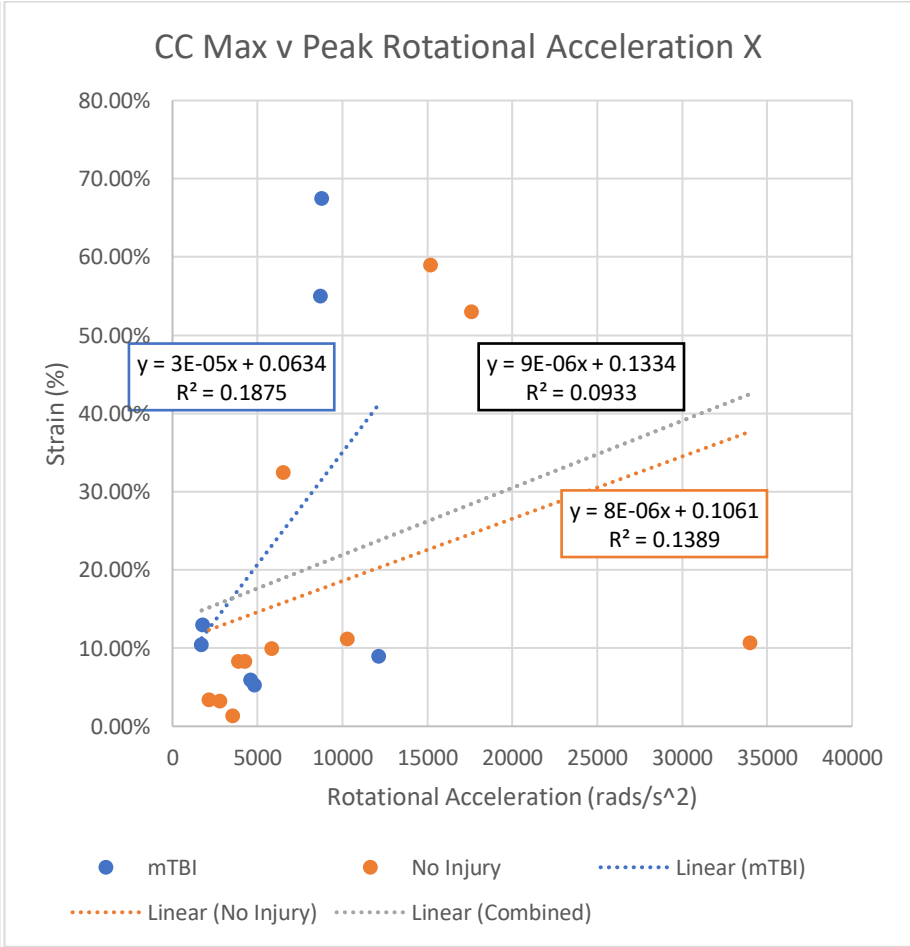
CC Max v Peak Rotational Acceleration X
80.00%
70.00%
60.00%
50.00%
40.00%
30.00%
20.00%
10.00%
0.00%
Strain (%)
0
5000
10000
15000
20000
25000
30000
35000
40000
Rotational Acceleration (rads/s^2)
y = 3E-05x + 0.0634
R² = 0.1875
y = 9E-06x + 0.1334
R² = 0.0933
y = 8E-06x + 0.1061
R² = 0.1389
mTBI
No Injury
Linear (mTBI)
Linear (No Injury)
Linear (Combined)

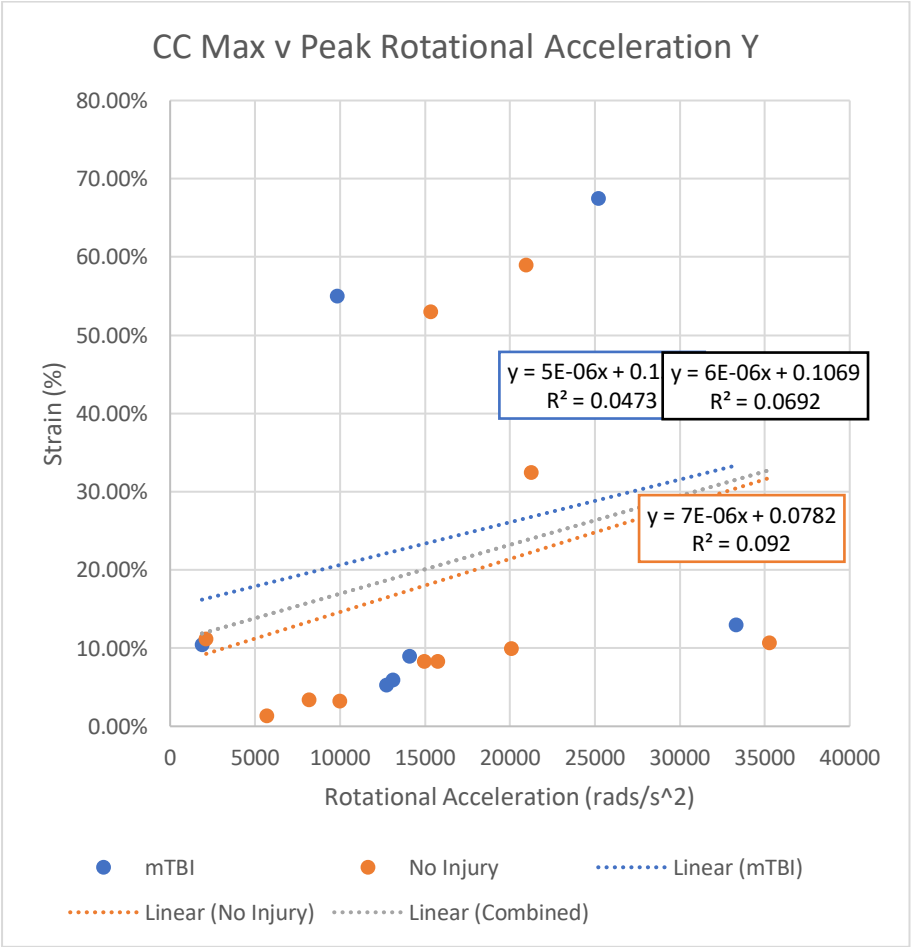
CC Max v Peak Rotational Acceleration Y
80.00%
70.00%
60.00%
50.00%
40.00%
30.00%
20.00%
10.00%
0.00%
Strain (%)
0
5000
10000
15000
20000
25000
30000
35000
40000
Rotational Acceleration (rads/s^2)
y = 5E-06x + 0.1
R² = 0.0473
y = 6E-06x + 0.1069
R² = 0.0692
y = 7E-06x + 0.0782
R² = 0.092
mTBI
No Injury
Linear (mTBI)
Linear (No Injury)
Linear (Combined)

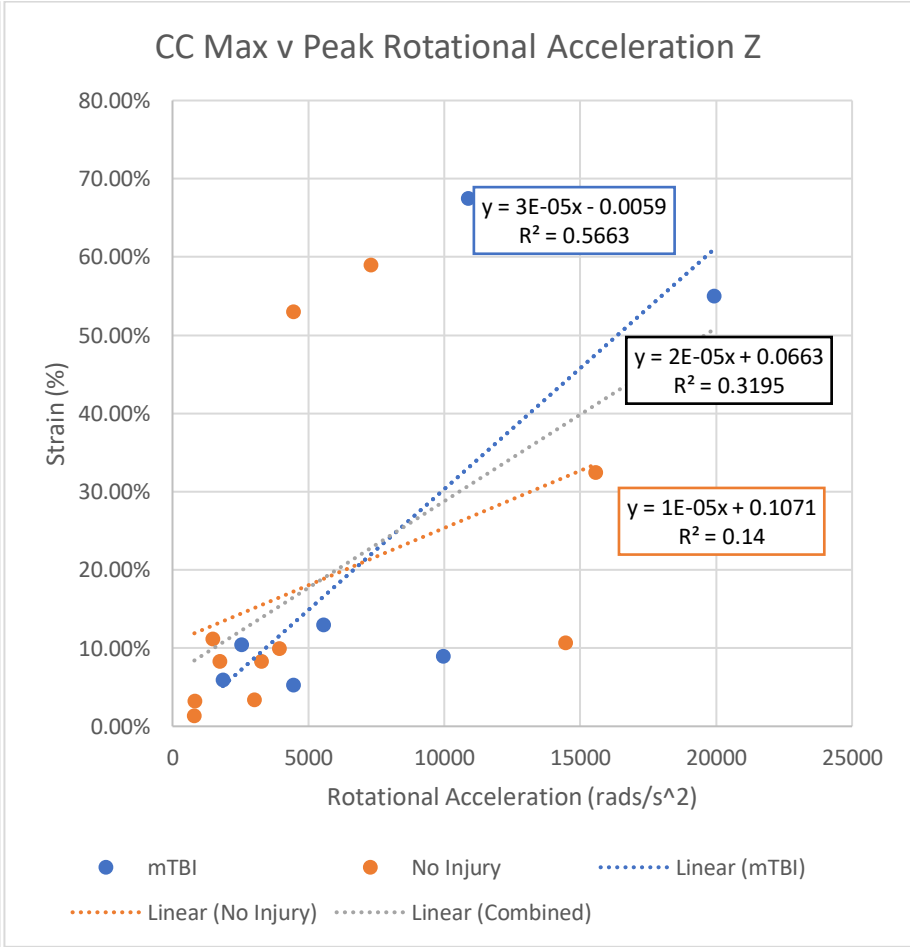
CC Max v Peak Rotational Acceleration Z
80.00%
70.00%
60.00%
50.00%
40.00%
30.00%
20.00%
10.00%
0.00%
Strain (%)
0
5000
10000
15000
20000
25000
Rotational Acceleration (rads/s^2)
y = 3E-05x - 0.0059
R² = 0.5663
y = 2E-05x + 0.0663
R² = 0.3195
y = 1E-05x + 0.1071
R² = 0.14
mTBI
No Injury
Linear (mTBI)
Linear (No Injury)
Linear (Combined)

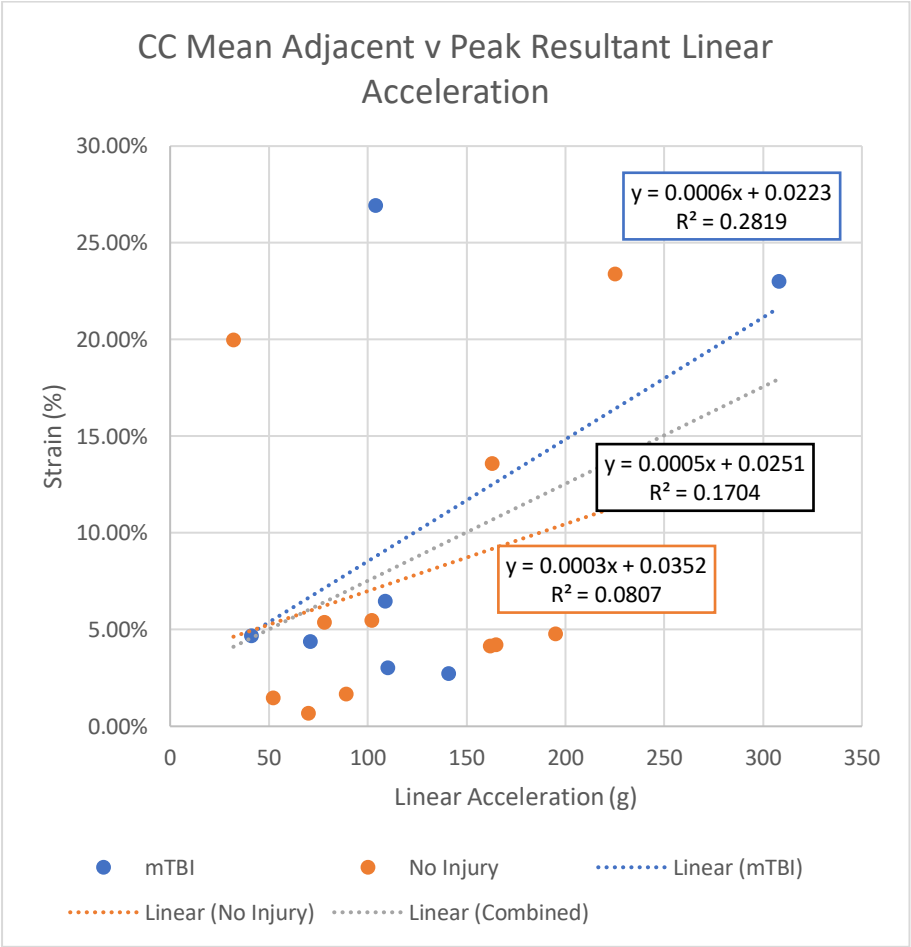
CC Mean Adjacent v Peak Resultant Linear Acceleration
30.00%
25.00%
20.00%
15.00%
10.00%
5.00%
0.00%
Strain (%)
0
50
100
150
200
250
300
350
Linear Acceleration (g)
y = 0.0006x + 0.0223
R² = 0.2819
y = 0.0005x + 0.0251
R² = 0.1704
y = 0.0003x + 0.0352
R² = 0.0807
mTBI
No Injury
Linear (mTBI)
Linear (No Injury)
Linear (Combined)

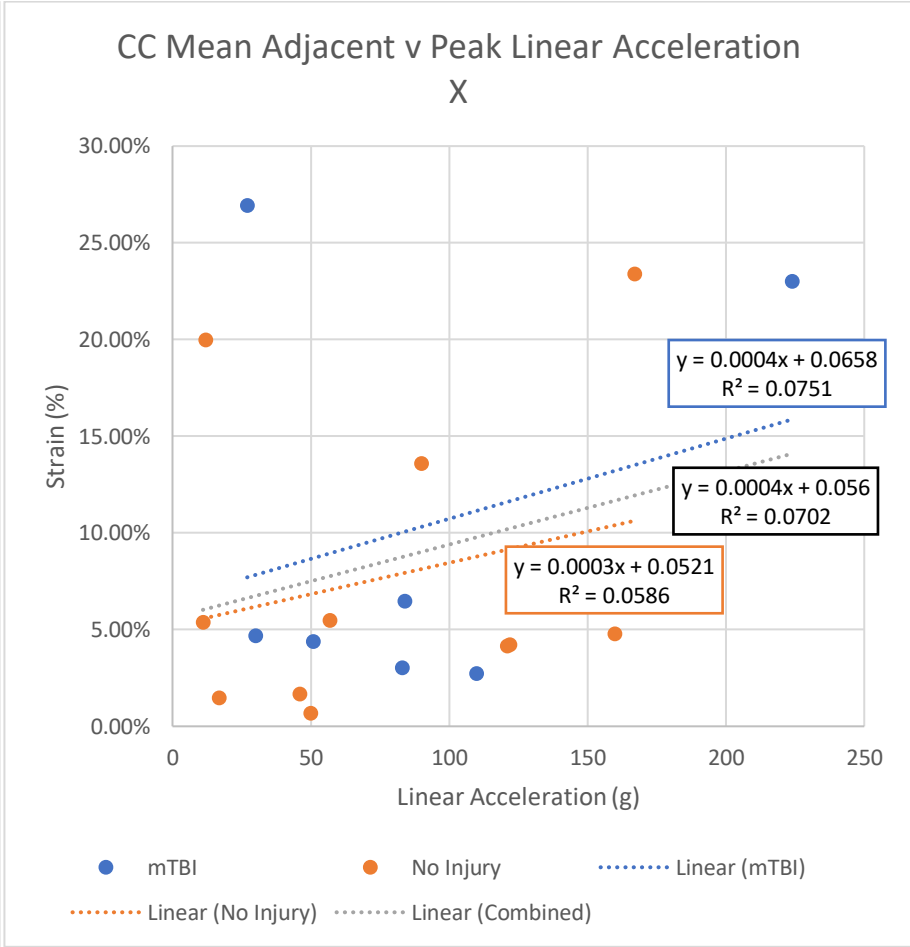
CC Mean Adjacent v Peak Linear Acceleration X
30.00%
25.00%
20.00%
15.00%
10.00%
5.00%
0.00%
Strain (%)
0
50
100
150
200
250
Linear Acceleration (g)
y = 0.0004x + 0.0658
R² = 0.0751
y = 0.0004x + 0.056
R² = 0.0702
y = 0.0003x + 0.0521
R² = 0.0586
mTBI
No Injury
Linear (mTBI)
Linear (No Injury)
Linear (Combined)

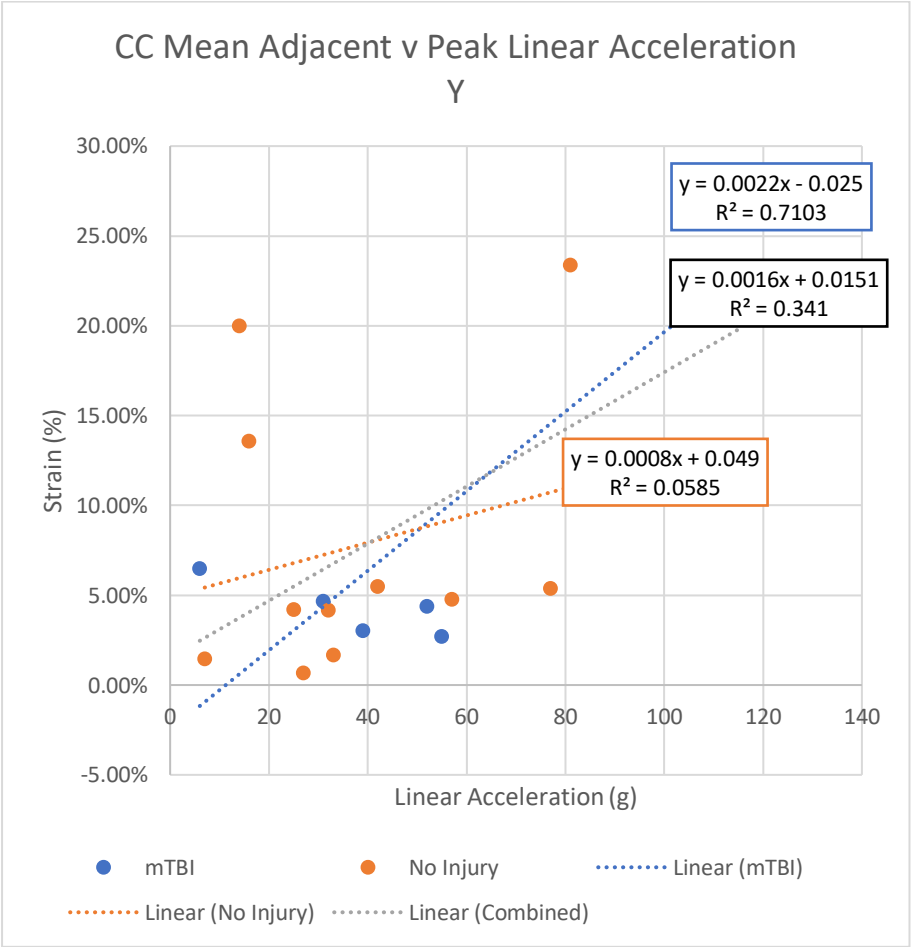
CC Mean Adjacent v Peak Linear Acceleration
Y
30.00%
25.00%
20.00%
15.00%
10.00%
5.00%
0.00%
-5.00%
Strain (%)
0
20
40
60
80
100
120
140
Linear Acceleration (g)
y = 0.0022x - 0.025
R² = 0.7103
y = 0.0016x + 0.0151
R² = 0.341
y = 0.0008x + 0.049
R² = 0.0585
mTBI
No Injury
Linear (mTBI)
Linear (No Injury)
Linear (Combined)

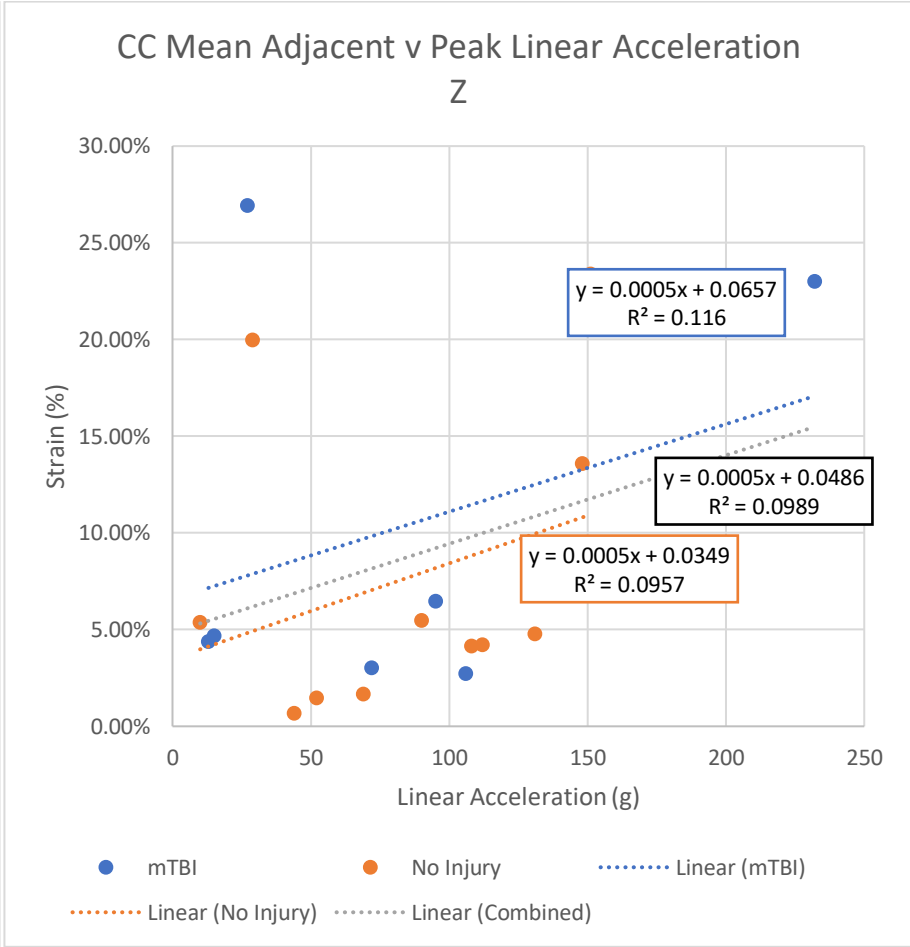
CC Mean Adjacent v Peak Linear Acceleration
Z
30.00%
25.00%
20.00%
15.00%
10.00%
5.00%
0.00%
Strain (%)
0
50
100
150
200
250
Linear Acceleration (g)
y = 0.0005x + 0.0657
R² = 0.116
y = 0.0005x + 0.0486
R² = 0.0989
y = 0.0005x + 0.0349
R² = 0.0957
mTBI
No Injury
Linear (mTBI)
Linear (No Injury)
Linear (Combined)

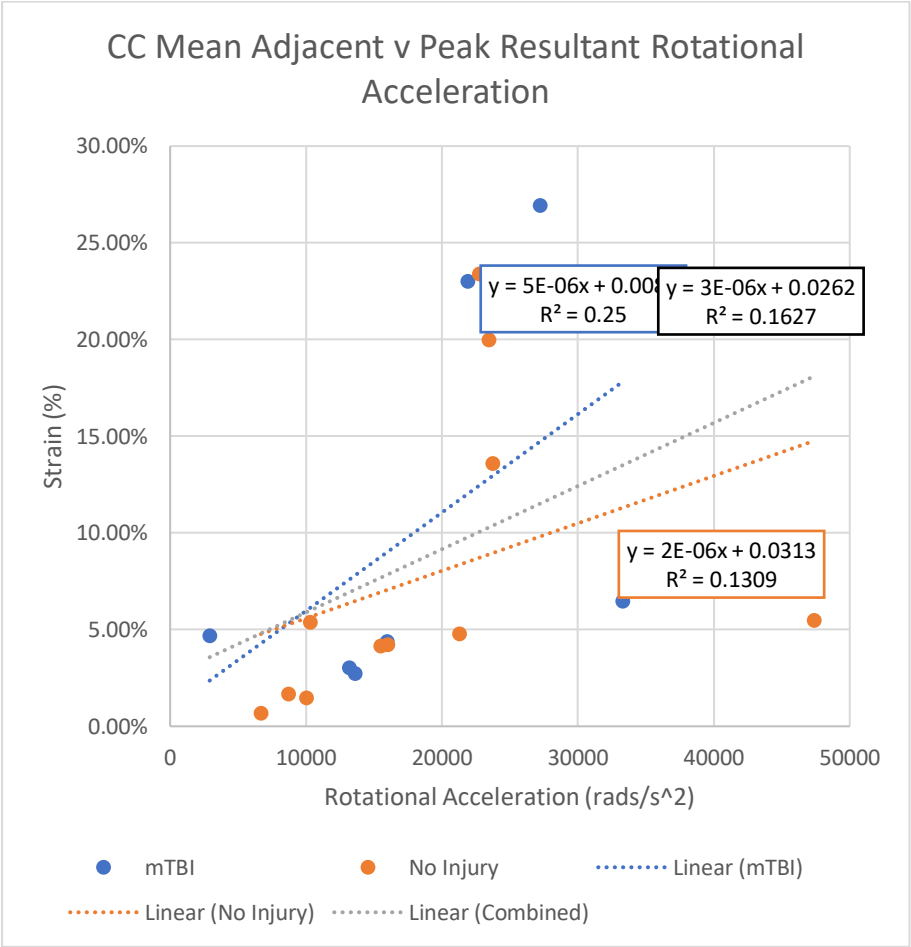
CC Mean Adjacent v Peak Resultant Rotational Acceleration
30.00%
25.00%
20.00%
15.00%
10.00%
5.00%
0.00%
Strain (%)
0
10000
20000
30000
40000
50000
Rotational Acceleration (rads/s^2)
y = 5E-06x + 0.00
R² = 0.25
y = 3E-06x + 0.0262
R² = 0.1627
y = 2E-06x + 0.0313
R² = 0.1309
mTBI
No Injury
Linear (mTBI)
Linear (No Injury)
Linear (Combined)

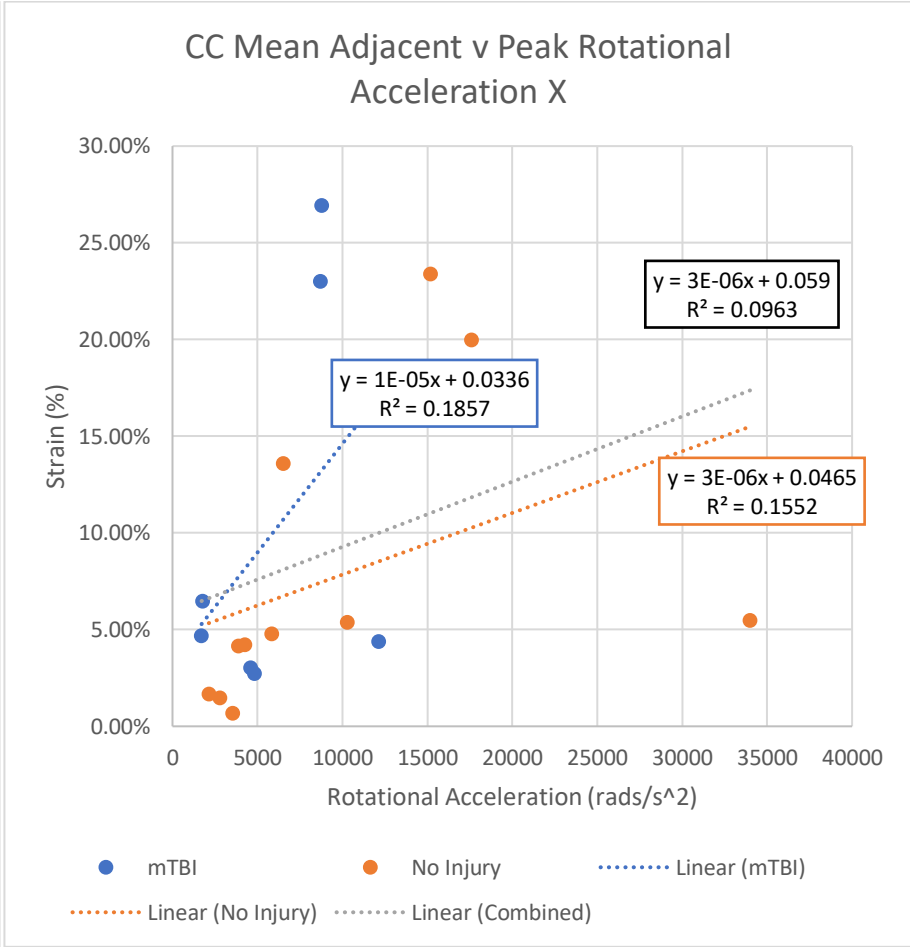
CC Mean Adjacent v Peak Rotational Acceleration X
30.00%
25.00%
20.00%
15.00%
10.00%
5.00%
0.00%
Strain (%)
0
5000
10000
15000
20000
25000
30000
35000
40000
Rotational Acceleration (rads/s^2)
y = 3E-06x + 0.059
R² = 0.0963
y = 1E-05x + 0.0336
R² = 0.1857
y = 3E-06x + 0.0465
R² = 0.1552
mTBI
No Injury
Linear (mTBI)
Linear (No Injury)
Linear (Combined)

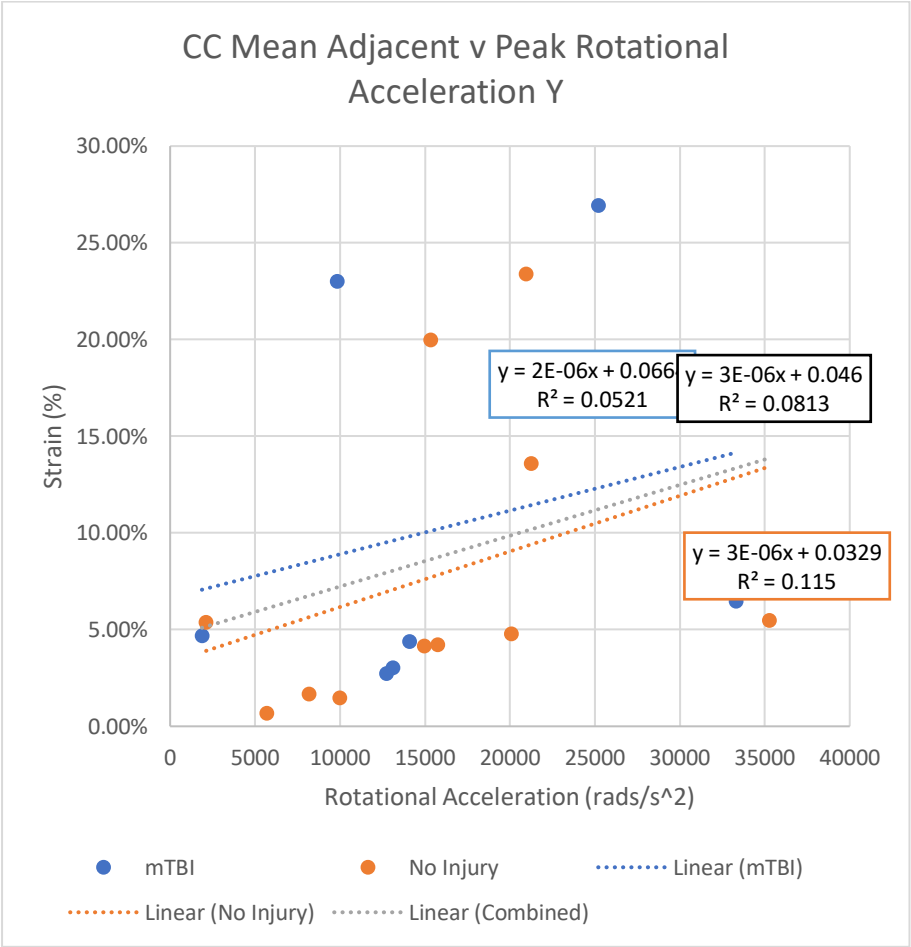
CC Mean Adjacent v Peak Rotational Acceleration Y
30.00%
25.00%
20.00%
15.00%
10.00%
5.00%
0.00%
Strain (%)
0
5000
10000
15000
20000
25000
30000
35000
40000
Rotational Acceleration (rads/s^2)
y = 2E-06x + 0.066
R² = 0.0521
y = 3E-06x + 0.046
R² = 0.0813
y = 3E-06x + 0.0329
R² = 0.115
mTBI
No Injury
Linear (mTBI)
Linear (No Injury)
Linear (Combined)

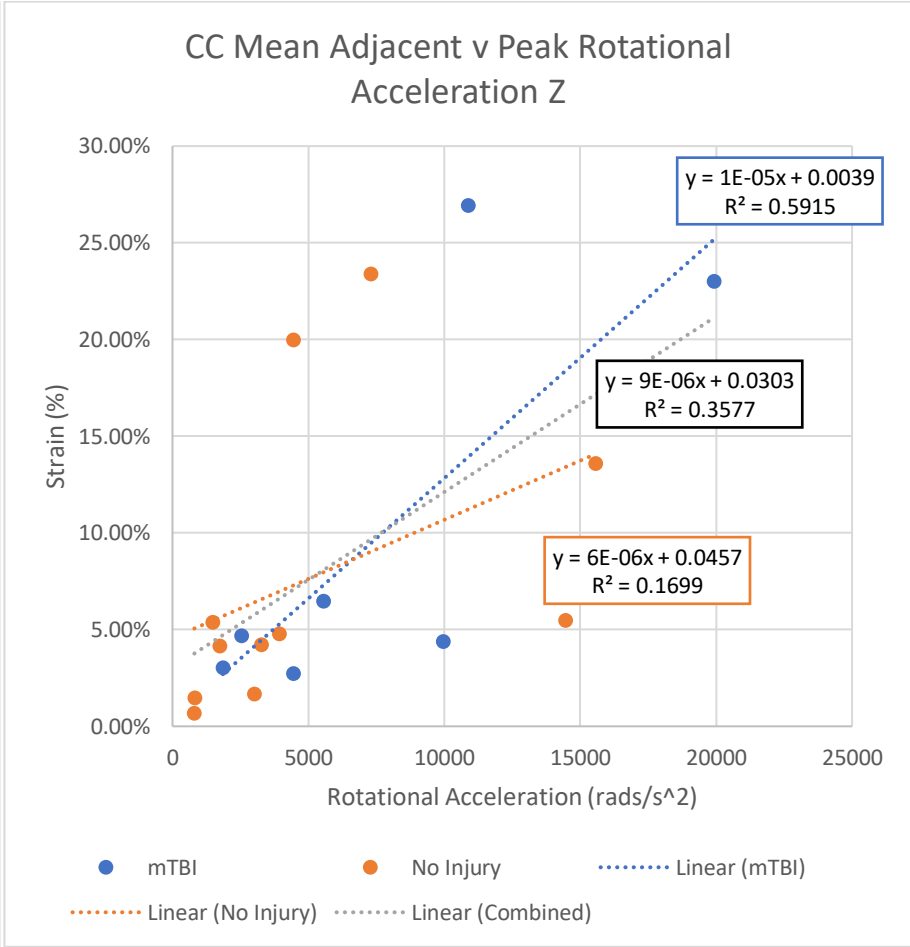
CC Mean Adjacent v Peak Rotational Acceleration Z
30.00%
25.00%
20.00%
15.00%
10.00%
5.00%
0.00%
Strain (%)
0
5000
10000
15000
20000
25000
Rotational Acceleration (rads/s^2)
y = 1E-05x + 0.0039
R² = 0.5915
y = 9E-06x + 0.0303
R² = 0.3577
y = 6E-06x + 0.0457
R² = 0.1699
mTBI
No Injury
Linear (mTBI)
Linear (No Injury)
Linear (Combined)

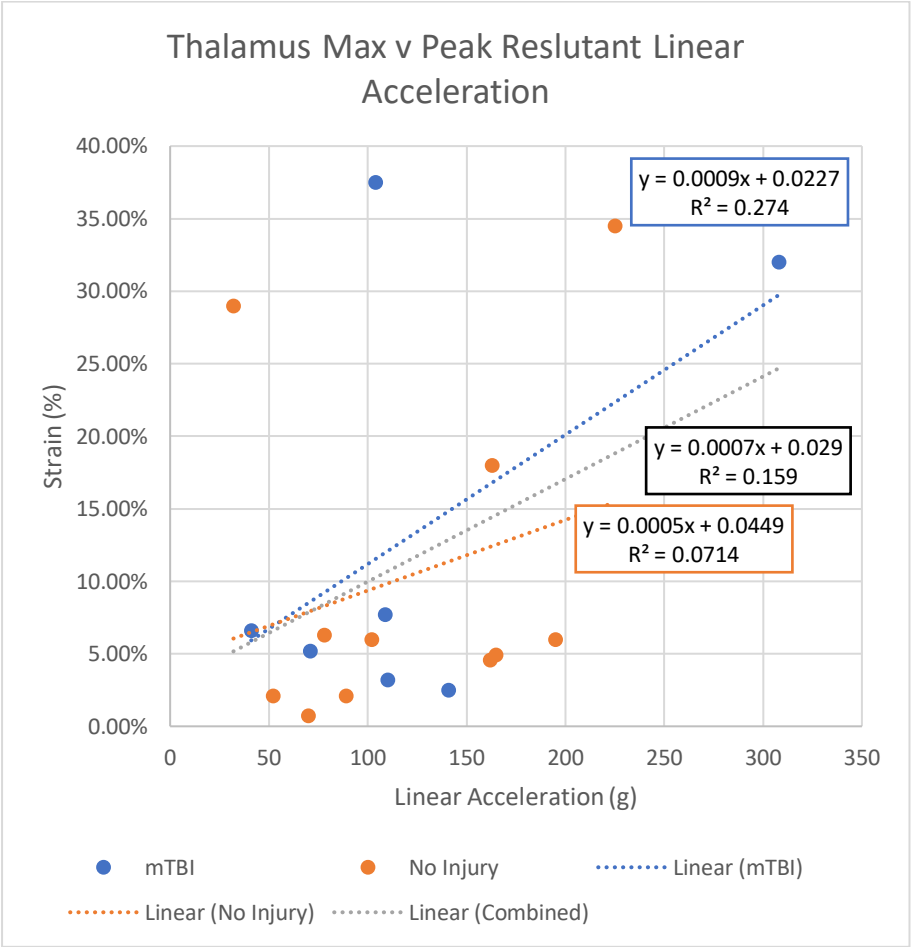
Thalamus Max v Peak Reslutant Linear Acceleration
40.00%
35.00%
30.00%
25.00%
20.00%
15.00%
10.00%
5.00%
0.00%
Strain (%)
0
50
100
150
200
250
300
350
Linear Acceleration (g)
y = 0.0009x + 0.0227
R² = 0.274
y = 0.0007x + 0.029
R² = 0.159
y = 0.0005x + 0.0449
R² = 0.0714
mTBI
No Injury
Linear (mTBI)
Linear (No Injury)
Linear (Combined)

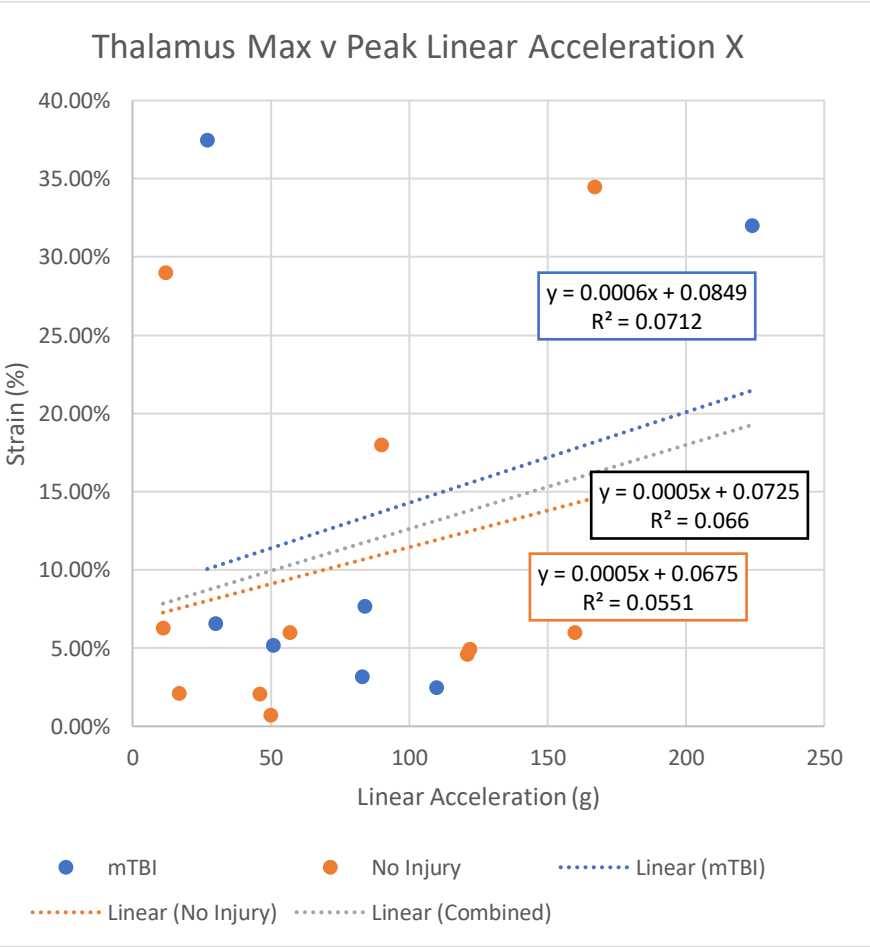
Thalamus Max v Peak Linear Acceleration X
40.00%
35.00%
30.00%
25.00%
20.00%
15.00%
10.00%
5.00%
0.00%
Strain (%)
0
50
100
150
200
250
Linear Acceleration (g)
y = 0.0006x + 0.0849
R² = 0.0712
y = 0.0005x + 0.0725
R² = 0.066
y = 0.0005x + 0.0675
R² = 0.0551
mTBI
No Injury
Linear (mTBI)
Linear (No Injury)
Linear (Combined)

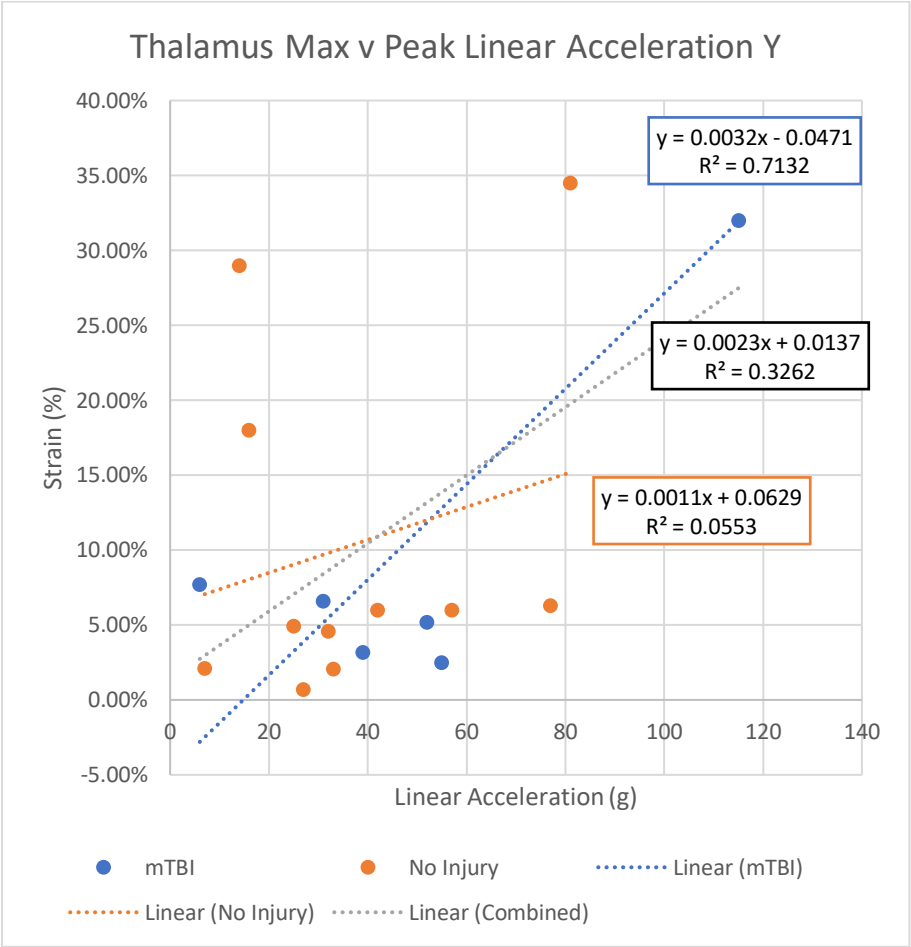
Thalamus Max v Peak Linear Acceleration Y
y = 0.0032x - 0.0471
R² = 0.7132
y = 0.0023x + 0.0137
R² = 0.3262
y = 0.0011x + 0.0629
R² = 0.0553
Strain (%)
Linear Acceleration (g)
mTBI
No Injury
Linear (mTBI)
Linear (No Injury)
Linear (Combined)

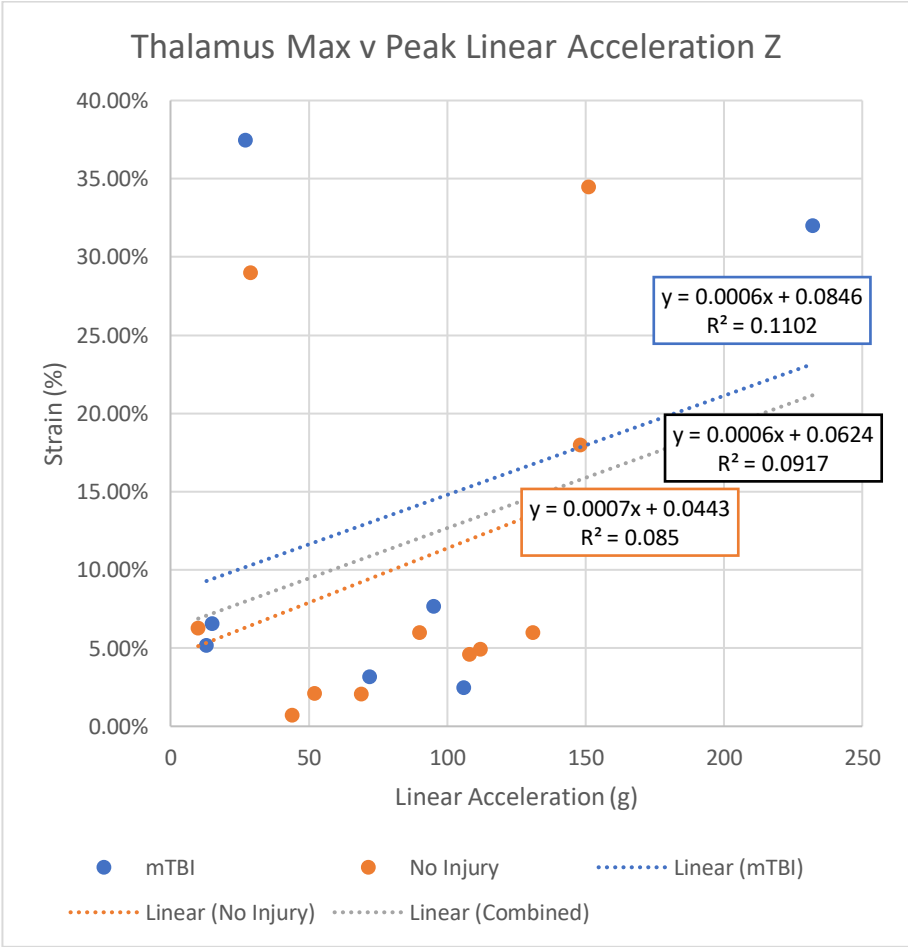
Thalamus Max v Peak Linear Acceleration Z
y = 0.0006x + 0.0846
R² = 0.1102
y = 0.0006x + 0.0624
R² = 0.0917
y = 0.0007x + 0.0443
R² = 0.085
Strain (%)
Linear Acceleration (g)
mTBI
No Injury
Linear (mTBI)
Linear (No Injury)
Linear (Combined)

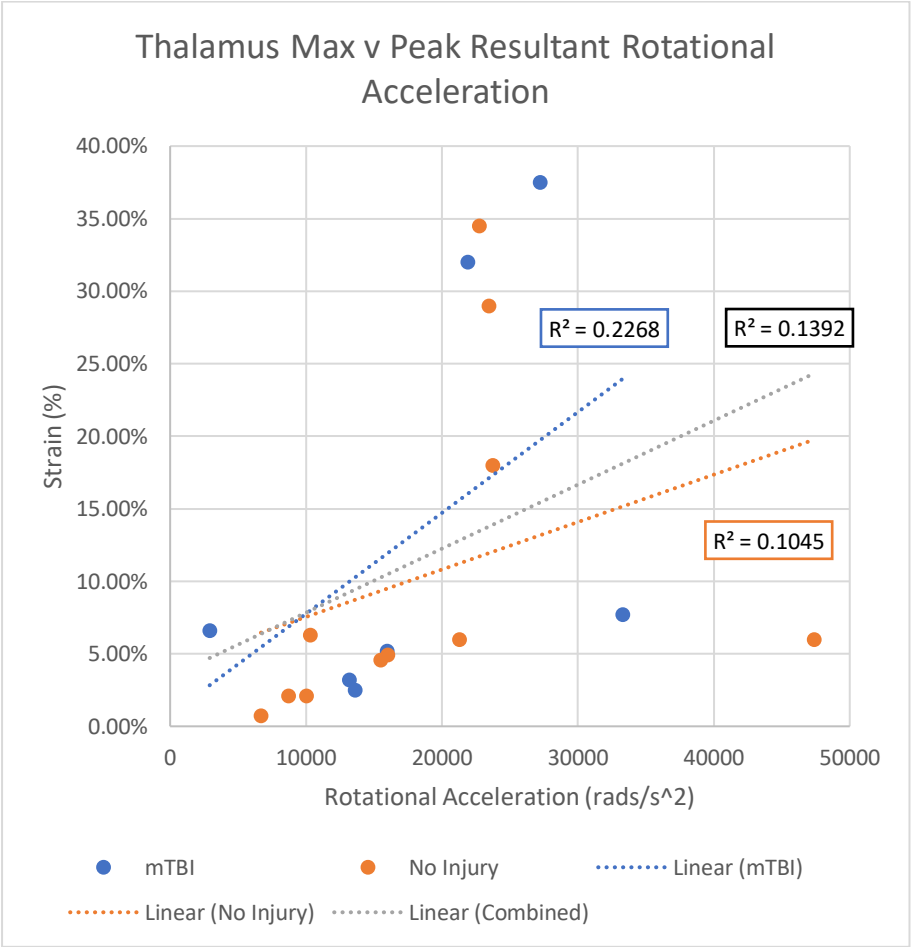
Thalamus Max v Peak Resultant Rotational Acceleration
40.00%
35.00%
30.00%
25.00%
20.00%
15.00%
10.00%
5.00%
0.00%
Strain (%)
0
10000
20000
30000
40000
50000
Rotational Acceleration (rads/s^2)
R² = 0.2268
R² = 0.1392
R² = 0.1045
mTBI
No Injury
Linear (mTBI)
Linear (No Injury)
Linear (Combined)

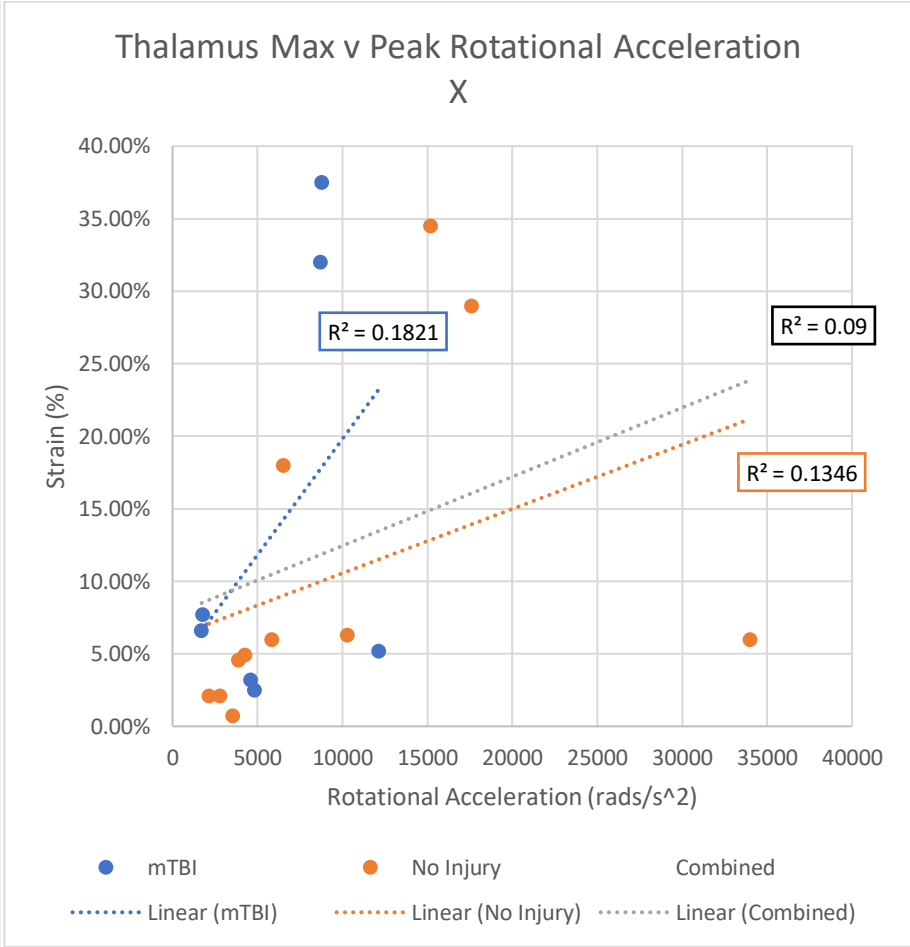
Thalamus Max v Peak Rotational Acceleration X
40.00%
35.00%
30.00%
25.00%
20.00%
15.00%
10.00%
5.00%
0.00%
Strain (%)
0
5000
10000
15000
20000
25000
30000
35000
40000
Rotational Acceleration (rads/s^2)
R² = 0.1821
R² = 0.09
R² = 0.1346
mTBI
No Injury
Combined
Linear (mTBI)
Linear (No Injury)
Linear (Combined)

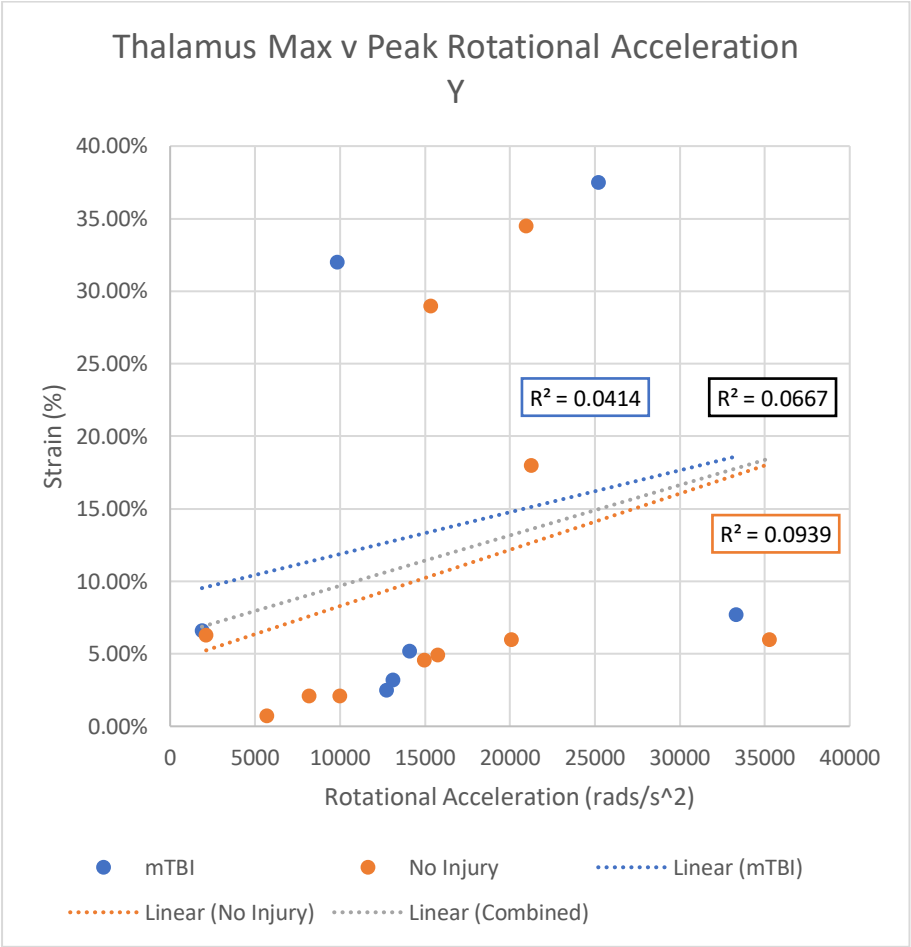
Thalamus Max v Peak Rotational Acceleration
Y
40.00%
35.00%
30.00%
25.00%
20.00%
15.00%
10.00%
5.00%
0.00%
Strain (%)
0
5000
10000
15000
20000
25000
30000
35000
40000
Rotational Acceleration (rads/s^2)
R² = 0.0414
R² = 0.0667
R² = 0.0939
mTBI
No Injury
Linear (mTBI)
Linear (No Injury)
Linear (Combined)

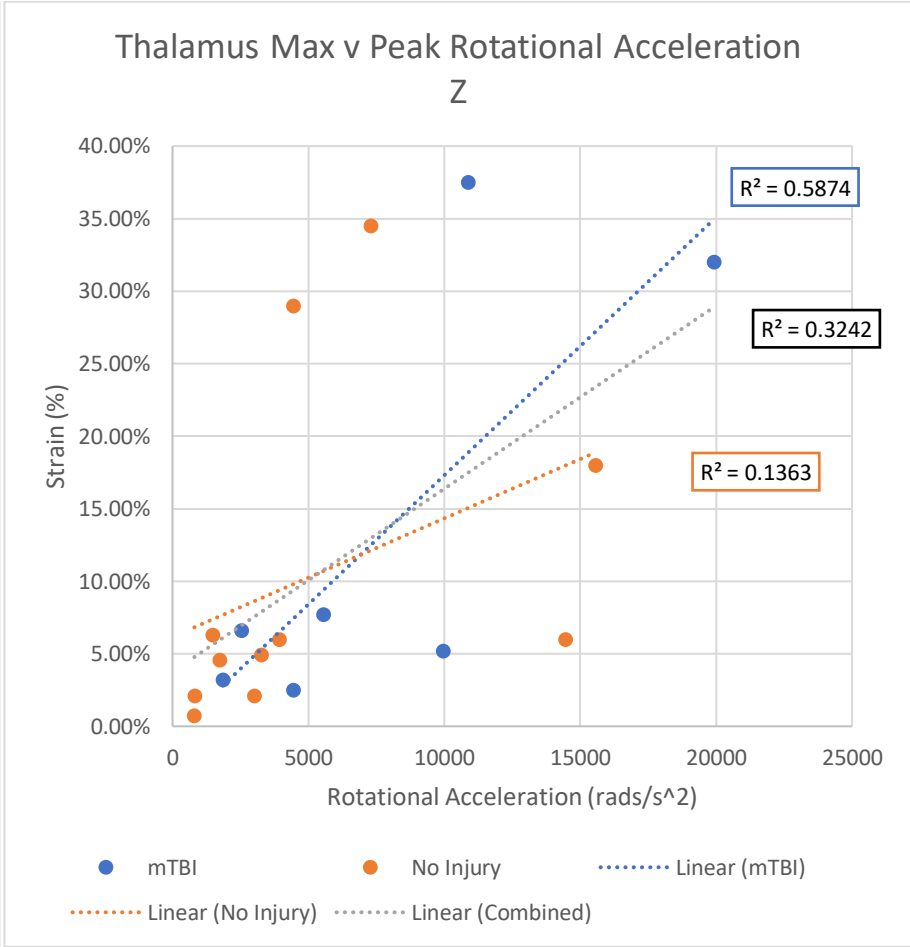
Thalamus Max v Peak Rotational Acceleration
Z
40.00%
35.00%
30.00%
25.00%
20.00%
15.00%
10.00%
5.00%
0.00%
Strain (%)
0
5000
10000
15000
20000
25000
Rotational Acceleration (rads/s^2)
R² = 0.5874
R² = 0.3242
R² = 0.1363
mTBI
No Injury
Linear (mTBI)
Linear (No Injury)
Linear (Combined)

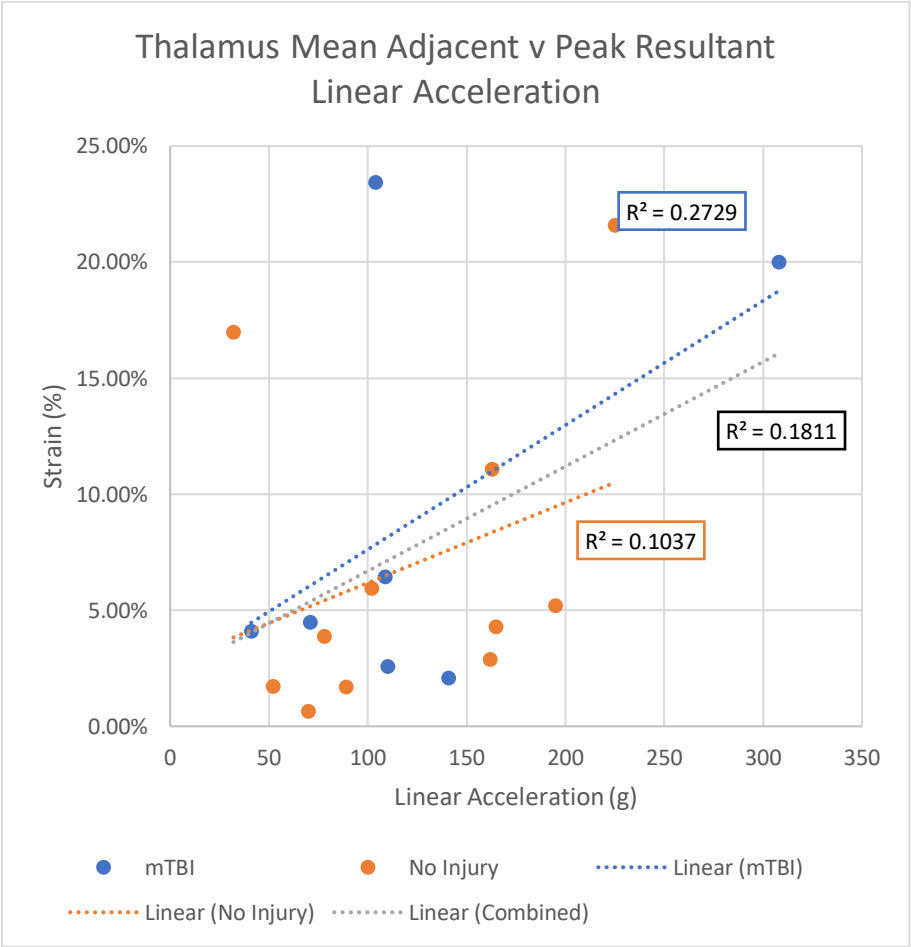
Thalamus Mean Adjacent v Peak Resultant Linear Acceleration
25.00%
20.00%
15.00%
10.00%
5.00%
0.00%
Strain (%)
0
50
100
150
200
250
300
350
Linear Acceleration (g)
R² = 0.2729
R² = 0.1811
R² = 0.1037
mTBI
No Injury
Linear (mTBI)
Linear (No Injury)
Linear (Combined)

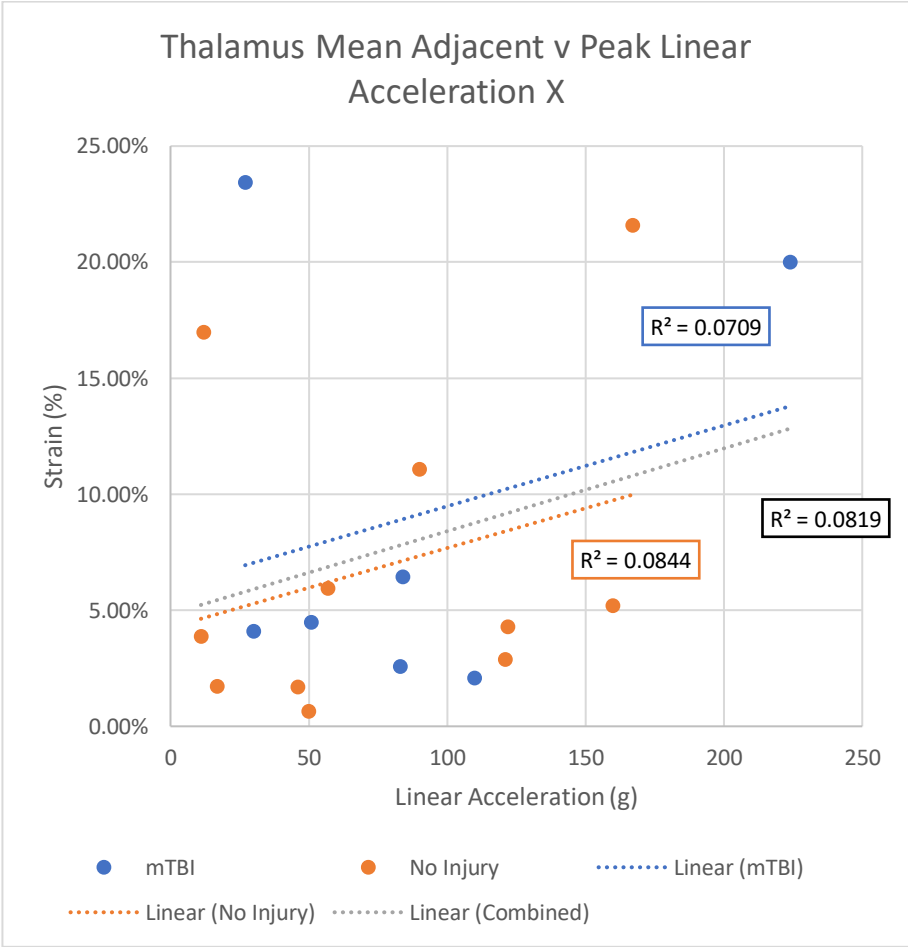
Thalamus Mean Adjacent v Peak Linear Acceleration X
25.00%
20.00%
15.00%
10.00%
5.00%
0.00%
Strain (%)
0
50
100
150
200
250
Linear Acceleration (g)
R² = 0.0709
R² = 0.0819
R² = 0.0844
mTBI
No Injury
Linear (mTBI)
Linear (No Injury)
Linear (Combined)

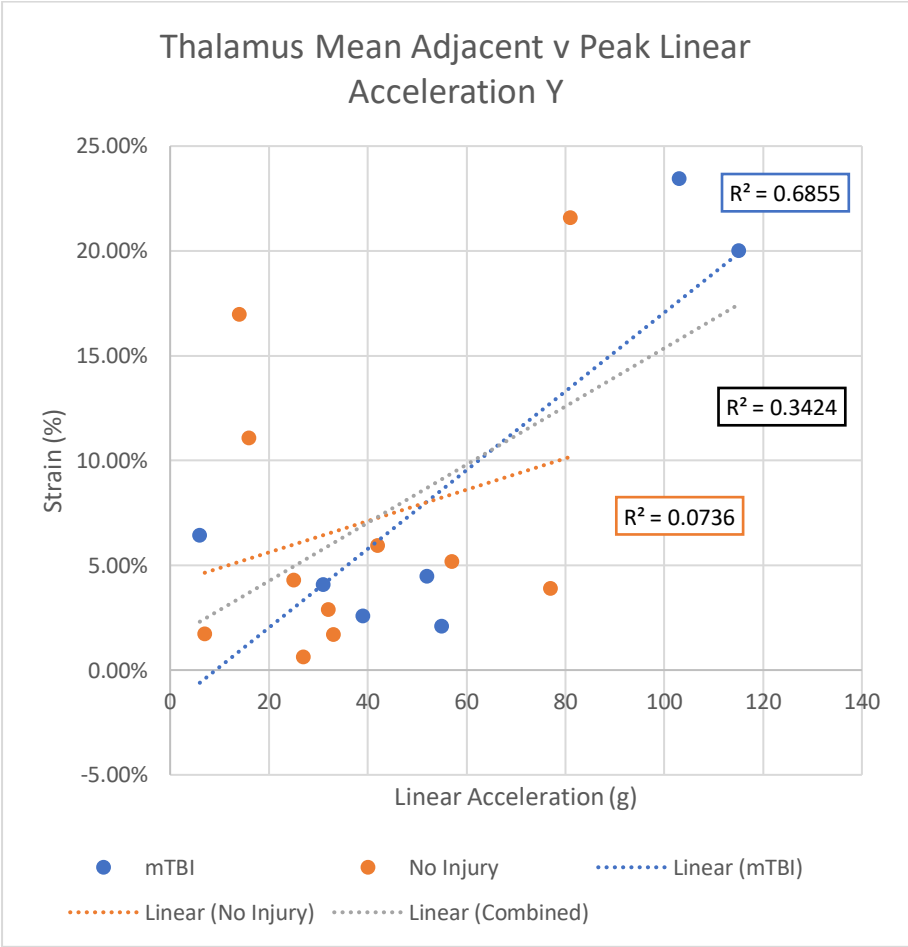
Thalamus Mean Adjacent v Peak Linear Acceleration Y
25.00%
20.00%
15.00%
10.00%
5.00%
0.00%
-5.00%
Strain (%)
0
20
40
60
80
100
120
140
Linear Acceleration (g)
R² = 0.6855
R² = 0.3424
R² = 0.0736
mTBI
No Injury
Linear (mTBI)
Linear (No Injury)
Linear (Combined)

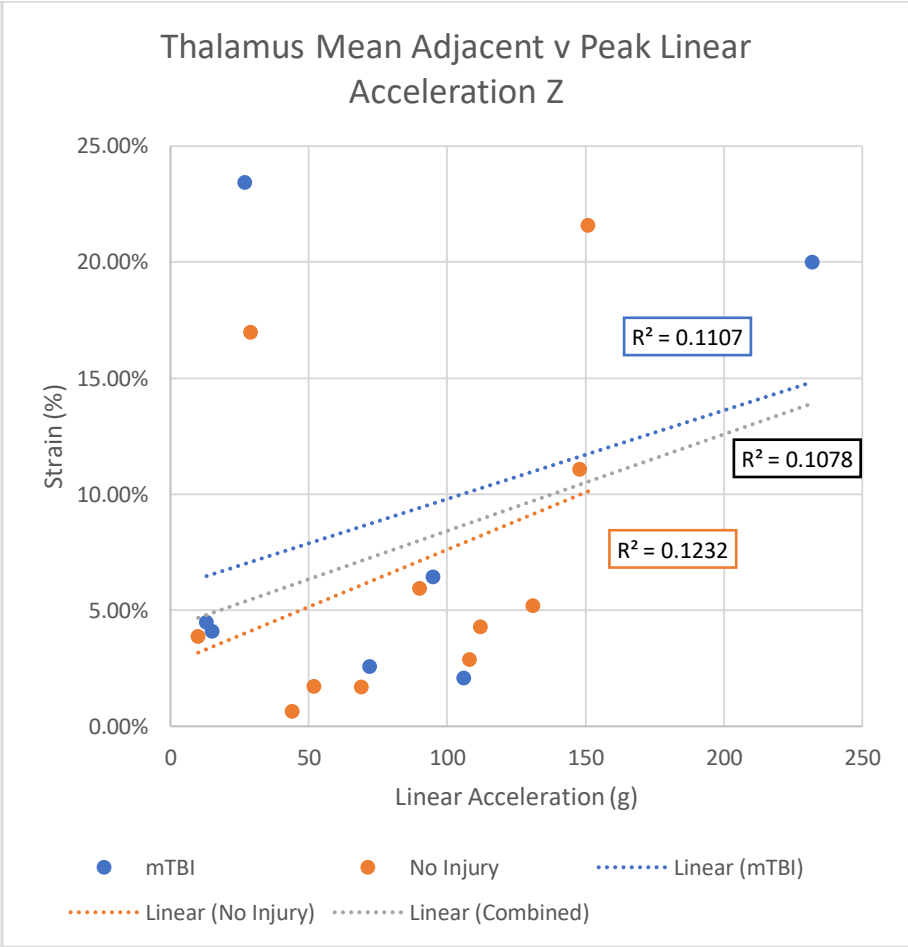
Thalamus Mean Adjacent v Peak Linear Acceleration Z
25.00%
20.00%
15.00%
10.00%
5.00%
0.00%
Strain (%)
0
50
100
150
200
250
Linear Acceleration (g)
R² = 0.1107
R² = 0.1078
R² = 0.1232
mTBI
No Injury
Linear (mTBI)
Linear (No Injury)
Linear (Combined)

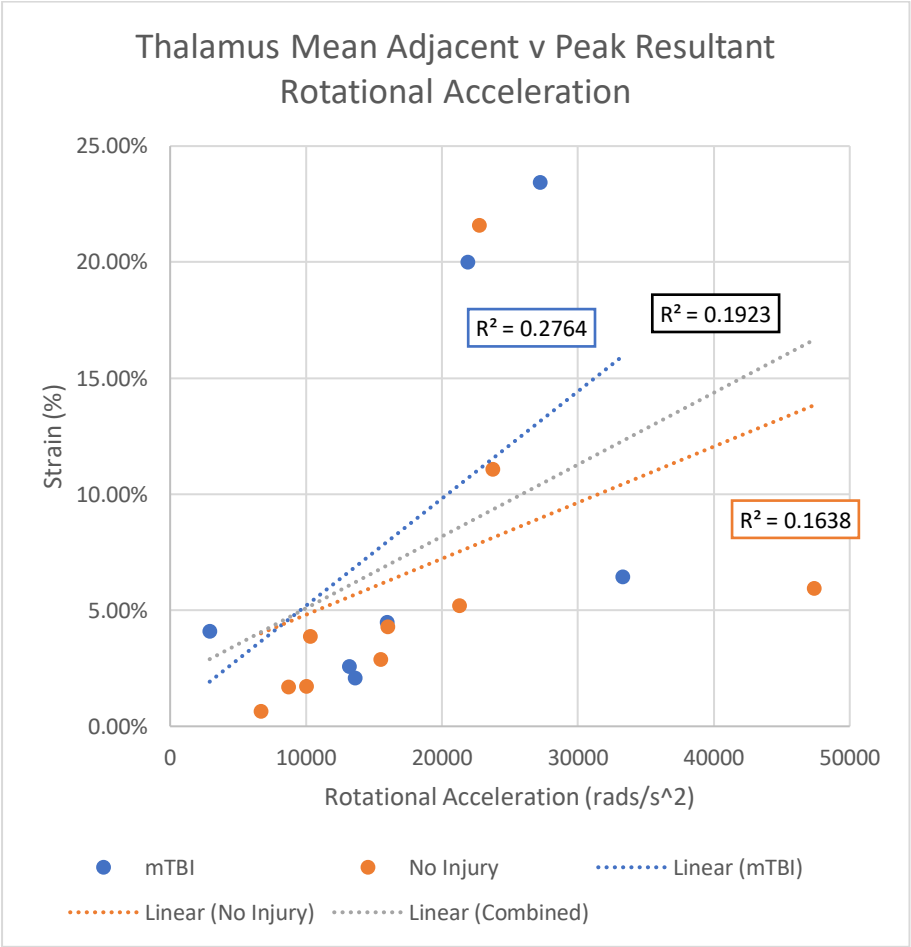
Thalamus Mean Adjacent v Peak Resultant Rotational Acceleration
25.00%
20.00%
15.00%
10.00%
5.00%
0.00%
Strain (%)
0
10000
20000
30000
40000
50000
Rotational Acceleration (rads/s^2)
R² = 0.2764
R² = 0.1923
R² = 0.1638
mTBI
No Injury
Linear (mTBI)
Linear (No Injury)
Linear (Combined)

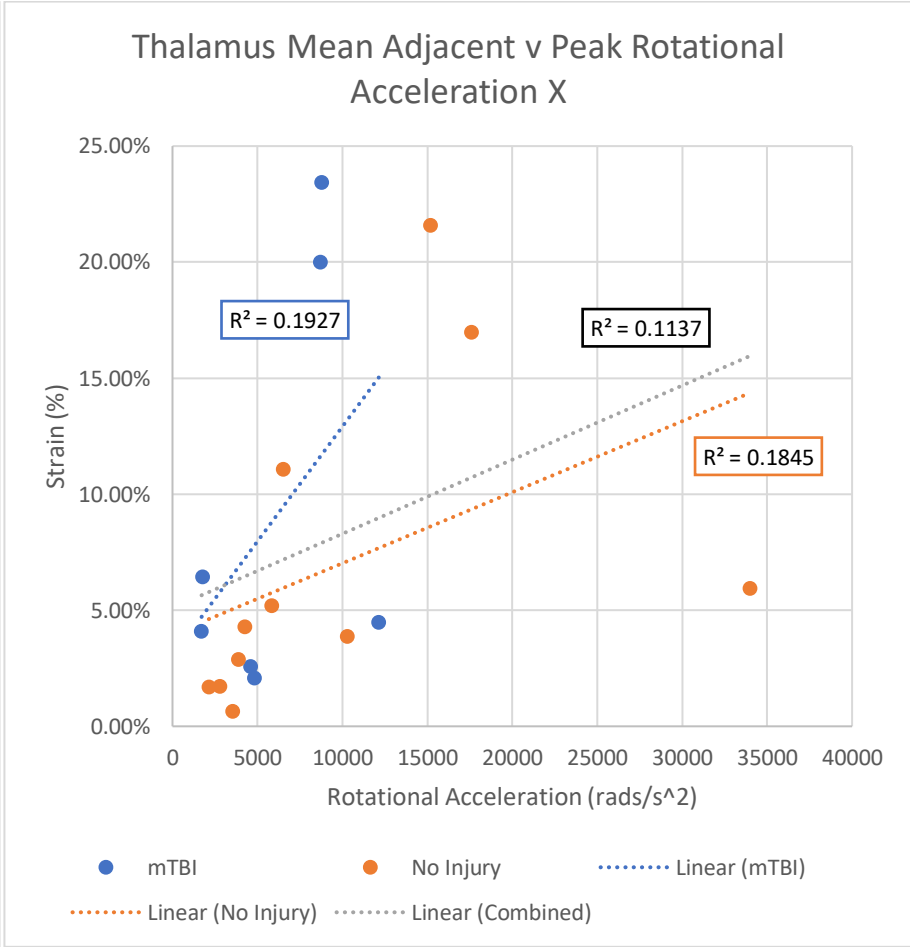
Thalamus Mean Adjacent v Peak Rotational Acceleration X
25.00%
20.00%
15.00%
10.00%
5.00%
0.00%
Strain (%)
0
5000
10000
15000
20000
25000
30000
35000
40000
Rotational Acceleration (rads/s^2)
R² = 0.1927
R² = 0.1137
R² = 0.1845
mTBI
No Injury
Linear (mTBI)
Linear (No Injury)
Linear (Combined)

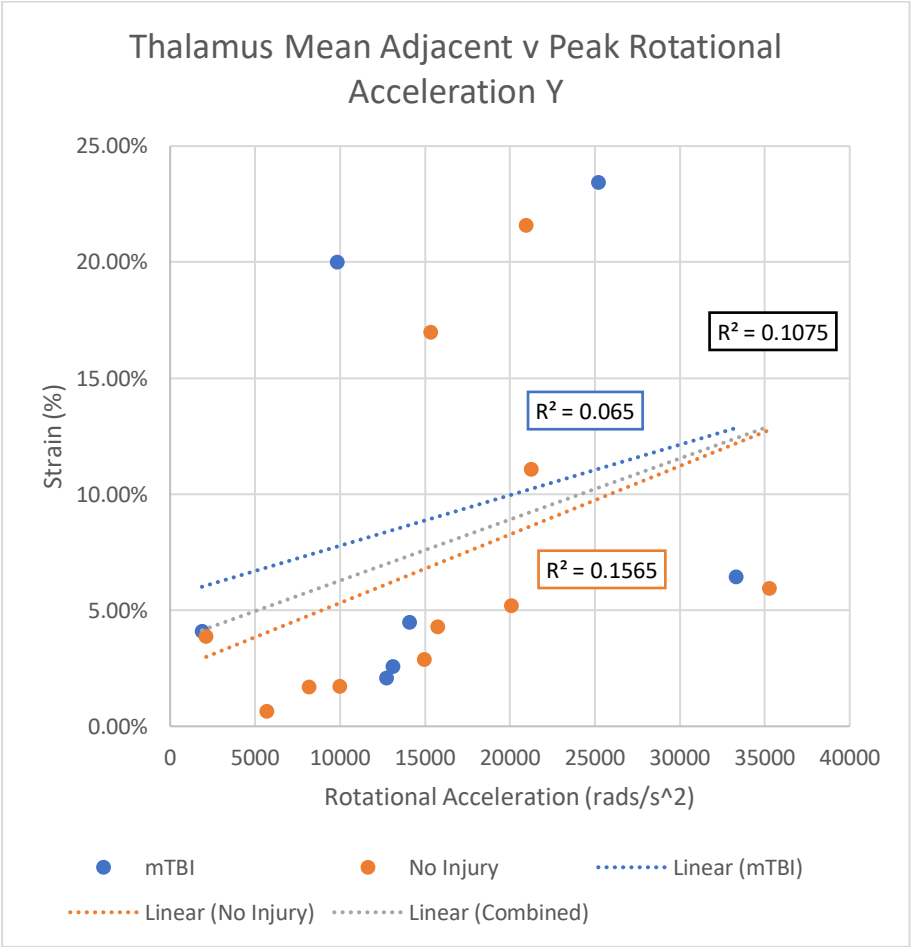
Thalamus Mean Adjacent v Peak Rotational Acceleration Y
25.00%
20.00%
15.00%
10.00%
5.00%
0.00%
Strain (%)
0
5000
10000
15000
20000
25000
30000
35000
40000
Rotational Acceleration (rads/s^2)
R² = 0.1075
R² = 0.065
R² = 0.1565
mTBI
No Injury
Linear (mTBI)
Linear (No Injury)
Linear (Combined)

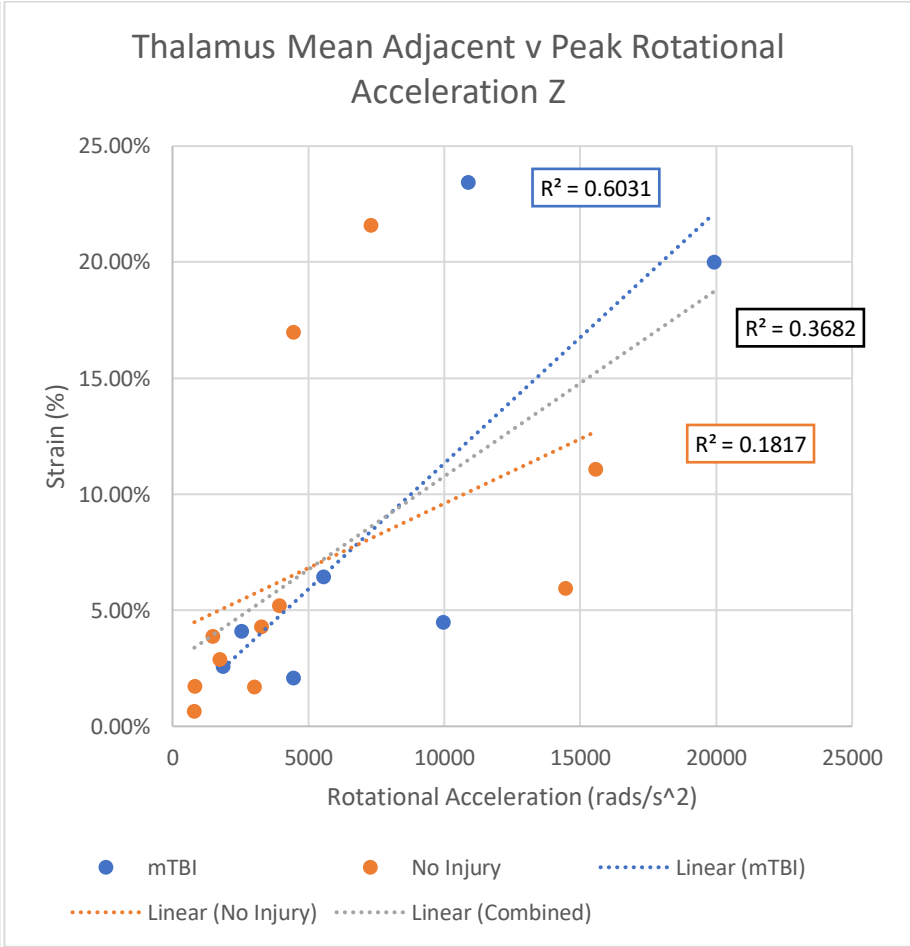
Thalamus Mean Adjacent v Peak Rotational Acceleration Z
25.00%
20.00%
15.00%
10.00%
5.00%
0.00%
Strain (%)
0
5000
10000
15000
20000
25000
Rotational Acceleration (rads/s^2)
R² = 0.6031
R² = 0.3682
R² = 0.1817
mTBI
No Injury
Linear (mTBI)
Linear (No Injury)
Linear (Combined)

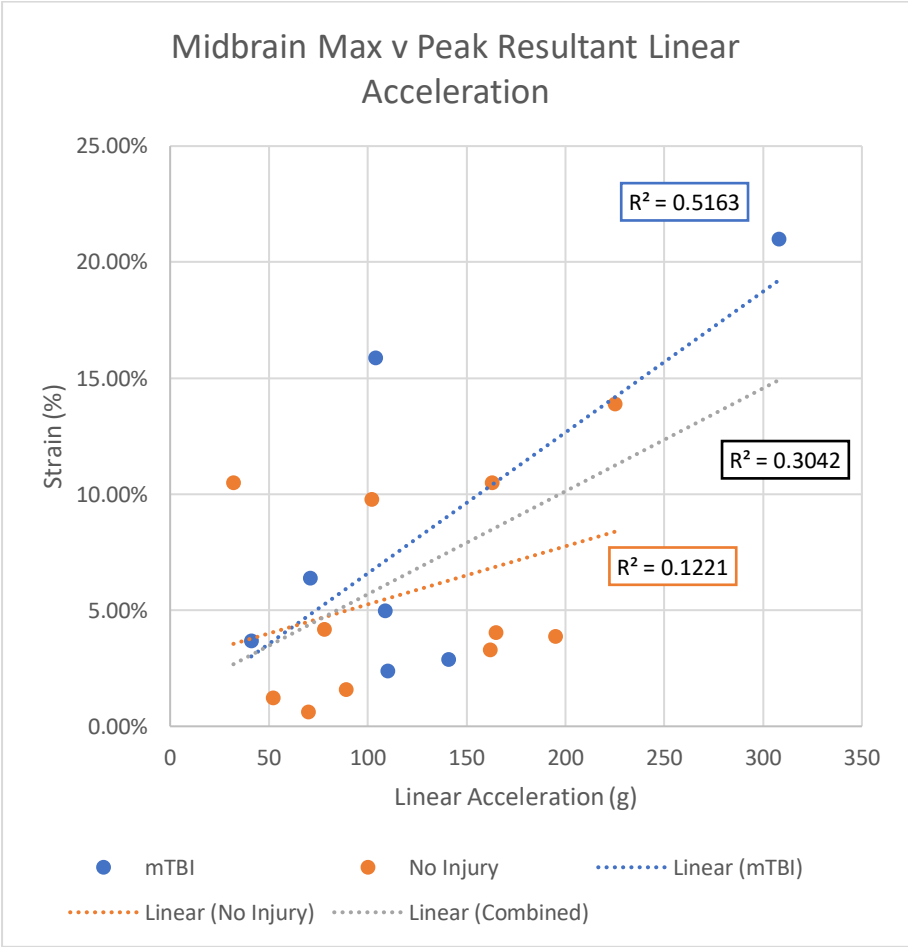
Midbrain Max v Peak Resultant Linear Acceleration
25.00%
20.00%
15.00%
10.00%
5.00%
0.00%
Strain (%)
0
50
100
150
200
250
300
350
Linear Acceleration (g)
R² = 0.5163
R² = 0.3042
R² = 0.1221
mTBI
No Injury
Linear (mTBI)
Linear (No Injury)
Linear (Combined)

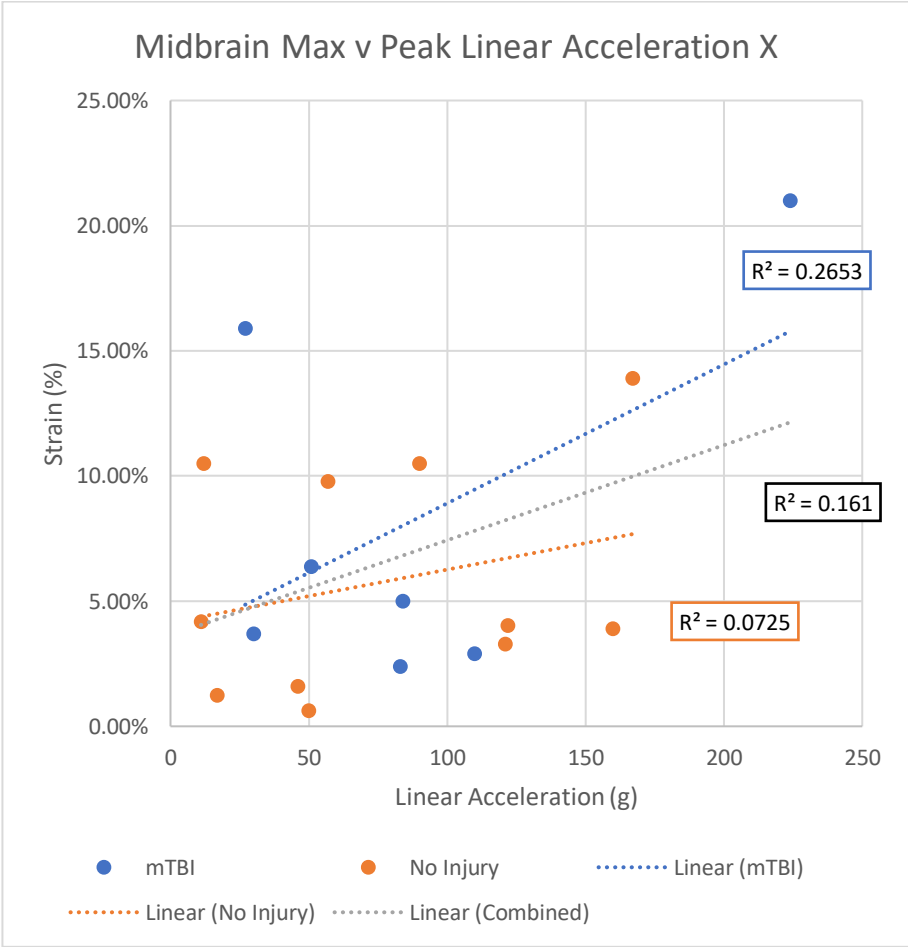
Midbrain Max v Peak Linear Acceleration X
25.00%
20.00%
15.00%
10.00%
5.00%
0.00%
Strain (%)
0
50
100
150
200
250
Linear Acceleration (g)
R² = 0.2653
R² = 0.161
R² = 0.0725
mTBI
No Injury
Linear (mTBI)
Linear (No Injury)
Linear (Combined)

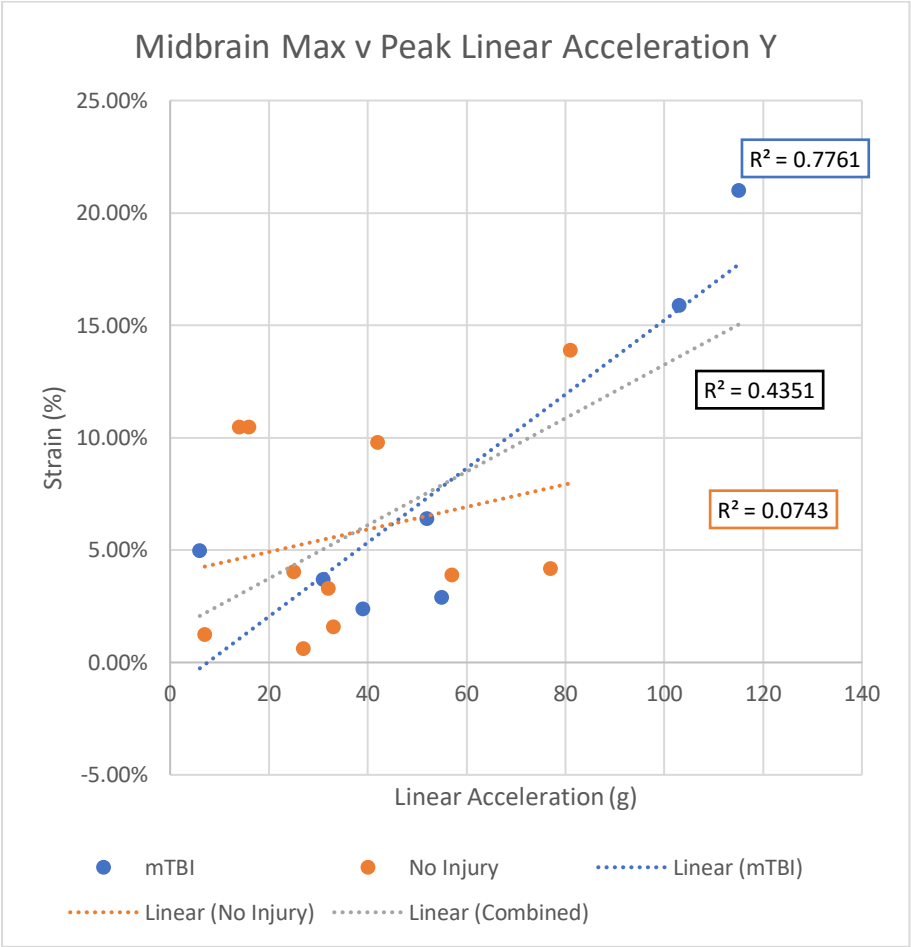
Midbrain Max v Peak Linear Acceleration Y
25.00%
20.00%
15.00%
10.00%
5.00%
0.00%
-5.00%
Strain (%)
0
20
40
60
80
100
120
140
Linear Acceleration (g)
R² = 0.7761
R² = 0.4351
R² = 0.0743
mTBI
No Injury
Linear (mTBI)
Linear (No Injury)
Linear (Combined)

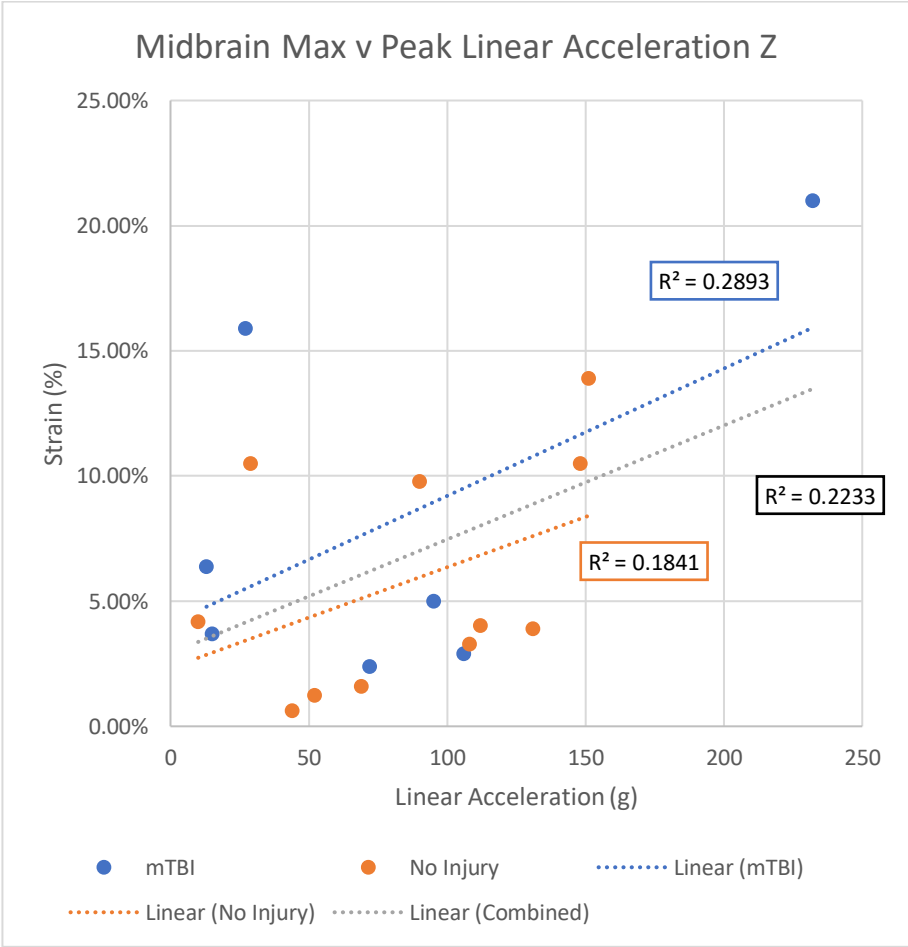
Midbrain Max v Peak Linear Acceleration Z
25.00%
20.00%
15.00%
10.00%
5.00%
0.00%
Strain (%)
0
50
100
150
200
250
Linear Acceleration (g)
R² = 0.2893
R² = 0.2233
R² = 0.1841
mTBI
No Injury
Linear (mTBI)
Linear (No Injury)
Linear (Combined)

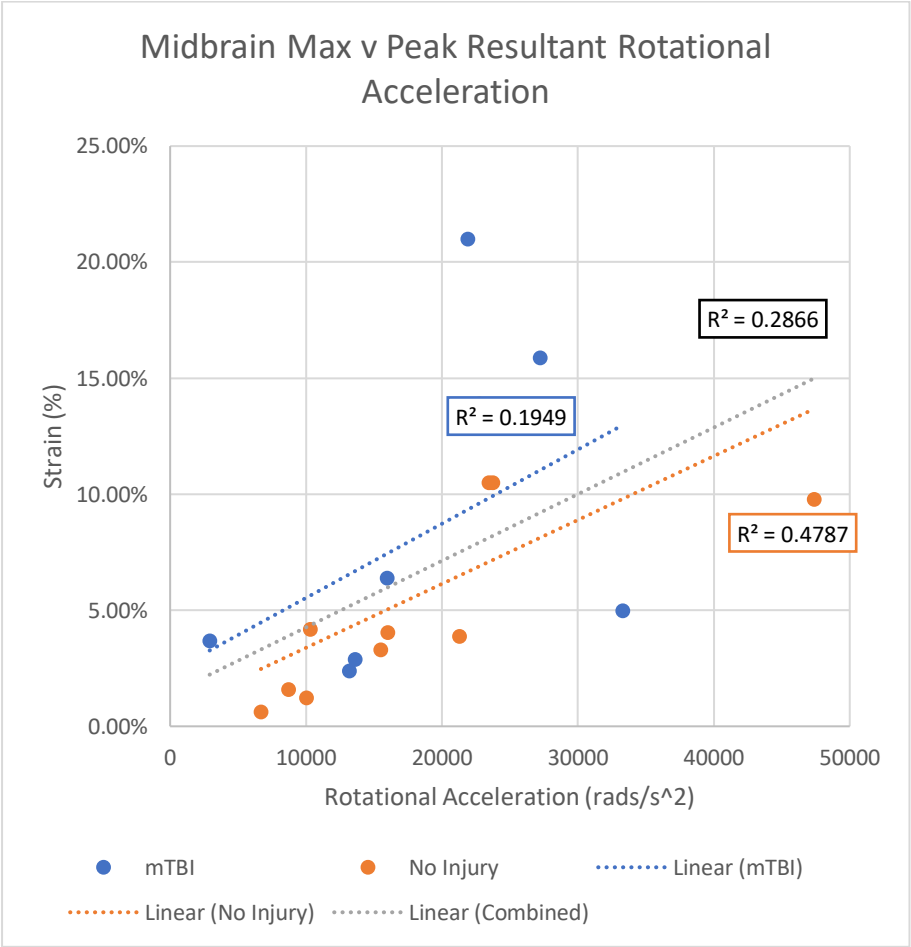
Midbrain Max v Peak Resultant Rotational Acceleration
25.00%
20.00%
15.00%
10.00%
5.00%
0.00%
Strain (%)
0
10000
20000
30000
40000
50000
Rotational Acceleration (rads/s^2)
R² = 0.2866
R² = 0.1949
R² = 0.4787
mTBI
No Injury
Linear (mTBI)
Linear (No Injury)
Linear (Combined)

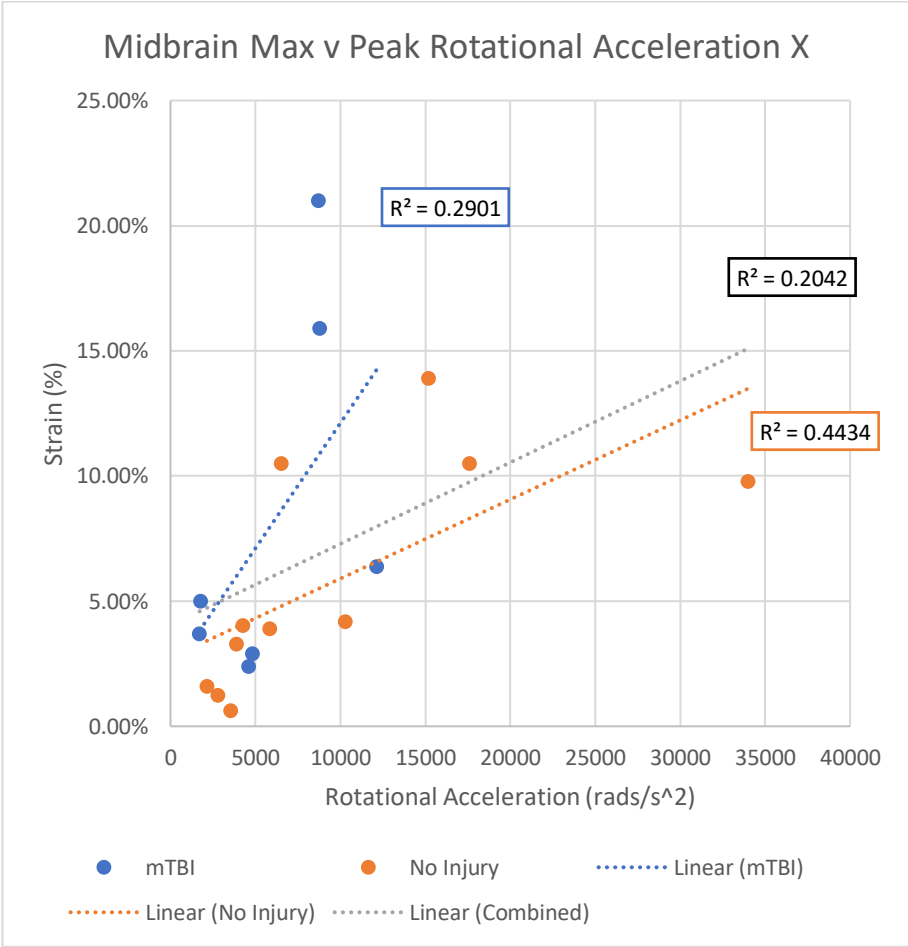
Midbrain Max v Peak Rotational Acceleration X
25.00%
20.00%
15.00%
10.00%
5.00%
0.00%
Strain (%)
0
5000
10000
15000
20000
25000
30000
35000
40000
Rotational Acceleration (rads/s^2)
R² = 0.2901
R² = 0.2042
R² = 0.4434
mTBI
No Injury
Linear (mTBI)
Linear (No Injury)
Linear (Combined)

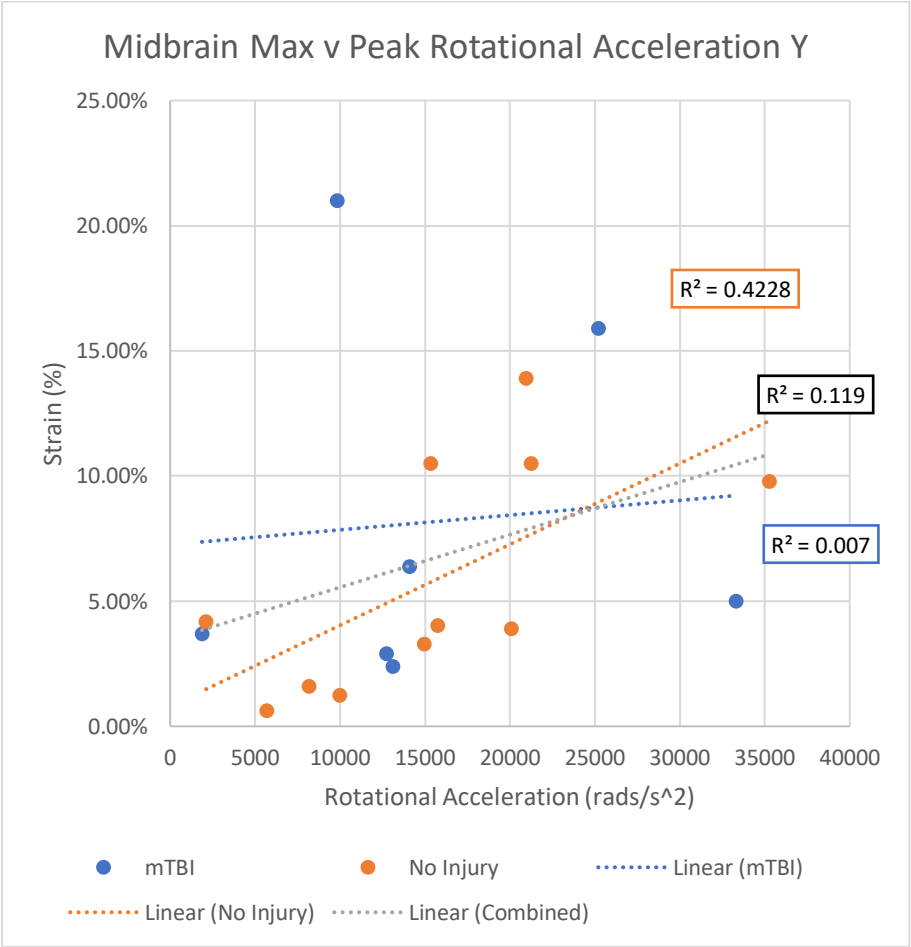
Midbrain Max v Peak Rotational Acceleration Y
25.00%
20.00%
15.00%
10.00%
5.00%
0.00%
Strain (%)
0
5000
10000
15000
20000
25000
30000
35000
40000
Rotational Acceleration (rads/s^2)
R² = 0.4228
R² = 0.119
R² = 0.007
mTBI
No Injury
Linear (mTBI)
Linear (No Injury)
Linear (Combined)

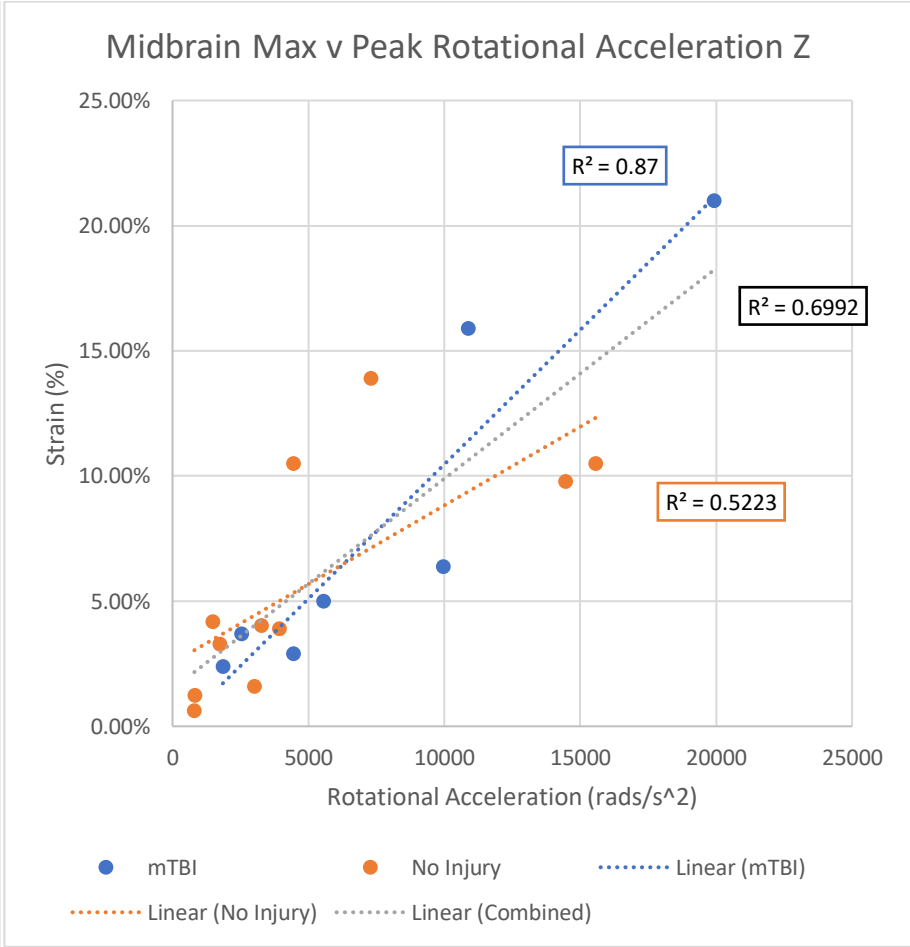
Midbrain Max v Peak Rotational Acceleration Z
25.00%
20.00%
15.00%
10.00%
5.00%
0.00%
Strain (%)
0
5000
10000
15000
20000
25000
Rotational Acceleration (rads/s^2)
R² = 0.87
R² = 0.6992
R² = 0.5223
mTBI
No Injury
Linear (mTBI)
Linear (No Injury)
Linear (Combined)

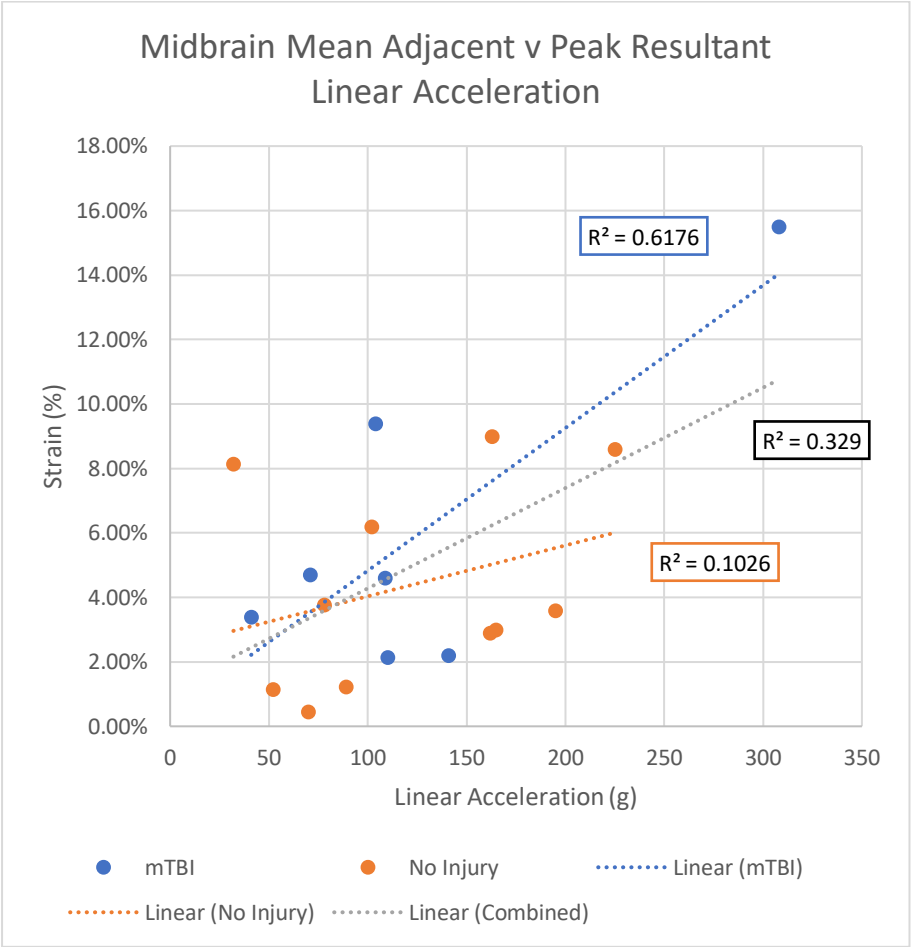
Midbrain Mean Adjacent v Peak Resultant Linear Acceleration
Strain (%)
18.00%
16.00%
14.00%
12.00%
10.00%
8.00%
6.00%
4.00%
2.00%
0.00%
0
50
100
150
200
250
300
350
Linear Acceleration (g)
R² = 0.6176
R² = 0.329
R² = 0.1026
mTBI
No Injury
Linear (mTBI)
Linear (No Injury)
Linear (Combined)

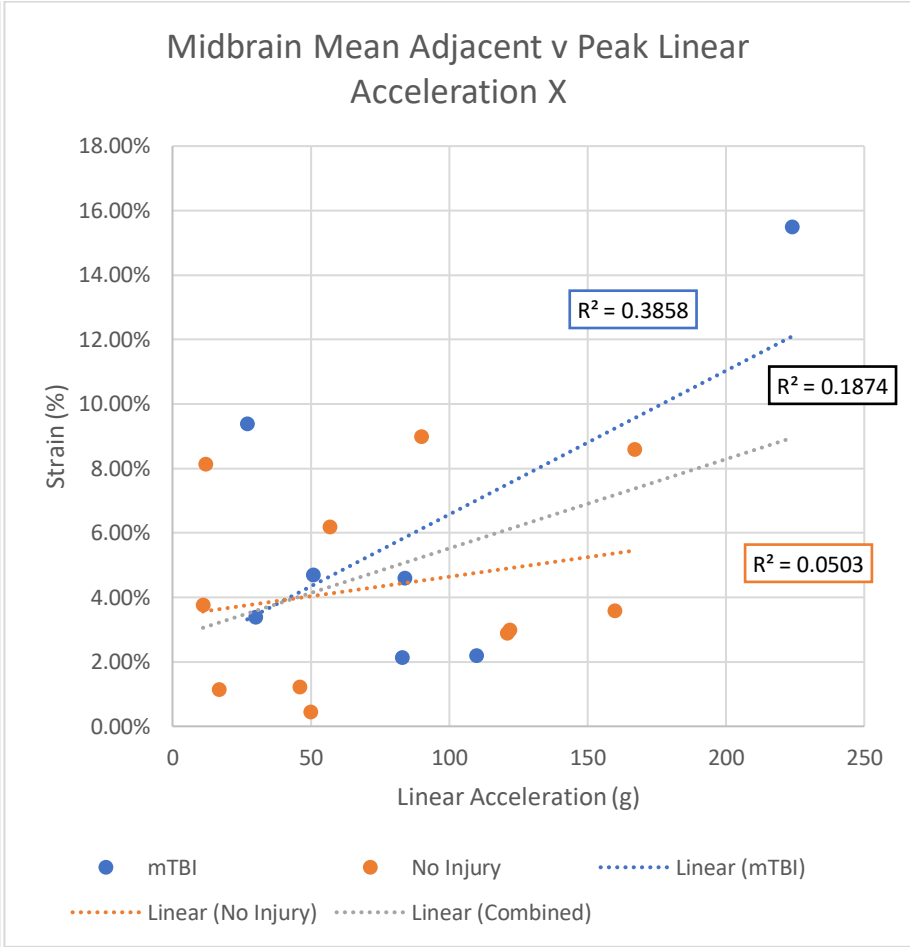
Midbrain Mean Adjacent v Peak Linear Acceleration X
Strain (%)
18.00%
16.00%
14.00%
12.00%
10.00%
8.00%
6.00%
4.00%
2.00%
0.00%
0
50
100
150
200
250
Linear Acceleration (g)
R² = 0.3858
R² = 0.1874
R² = 0.0503
mTBI
No Injury
Linear (mTBI)
Linear (No Injury)
Linear (Combined)

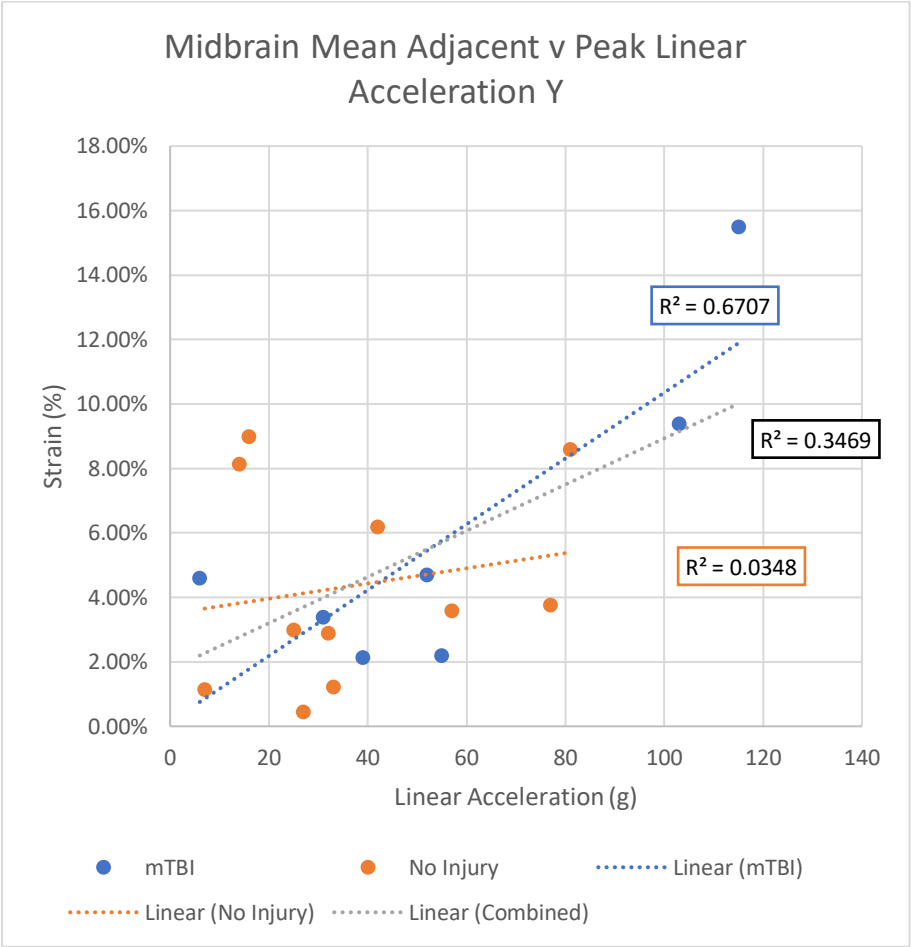
Midbrain Mean Adjacent v Peak Linear Acceleration Y
18.00%
16.00%
14.00%
12.00%
10.00%
8.00%
6.00%
4.00%
2.00%
0.00%
Strain (%)
0
20
40
60
80
100
120
140
Linear Acceleration (g)
R² = 0.6707
R² = 0.3469
R² = 0.0348
mTBI
No Injury
Linear (mTBI)
Linear (No Injury)
Linear (Combined)

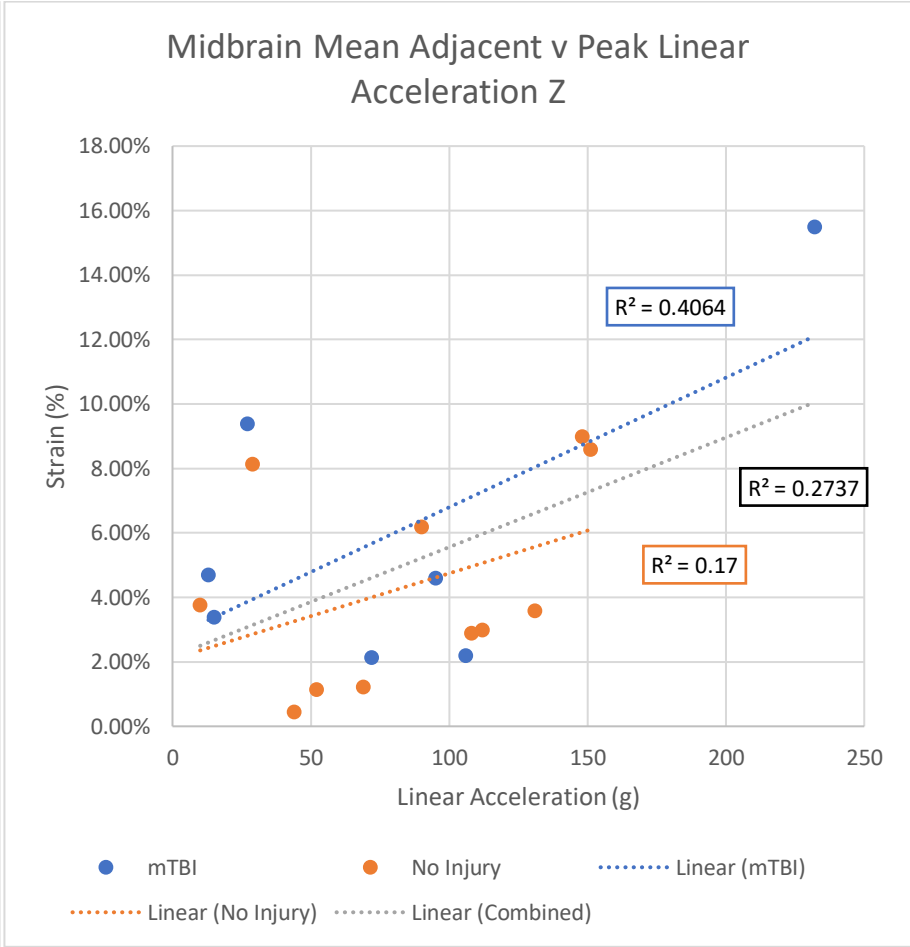
Midbrain Mean Adjacent v Peak Linear Acceleration Z
18.00%
16.00%
14.00%
12.00%
10.00%
8.00%
6.00%
4.00%
2.00%
0.00%
Strain (%)
0
50
100
150
200
250
Linear Acceleration (g)
R² = 0.4064
R² = 0.2737
R² = 0.17
mTBI
No Injury
Linear (mTBI)
Linear (No Injury)
Linear (Combined)

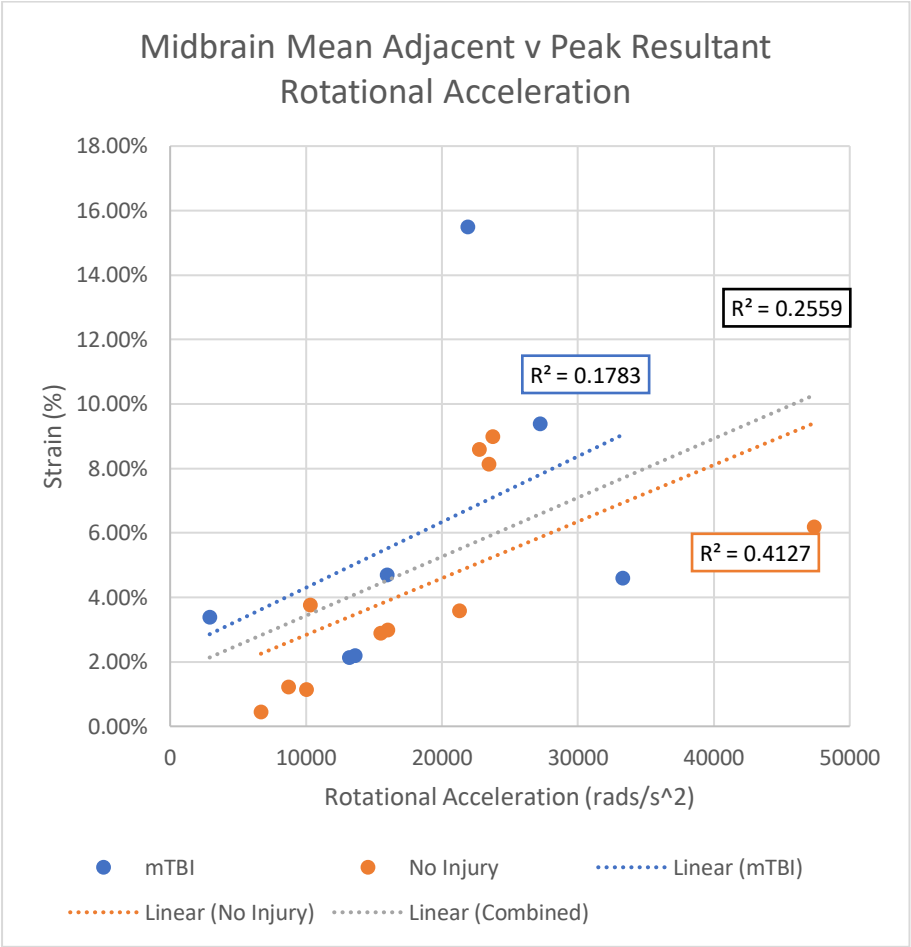
Midbrain Mean Adjacent v Peak Resultant Rotational Acceleration
18.00%
16.00%
14.00%
12.00%
10.00%
8.00%
6.00%
4.00%
2.00%
0.00%
Strain (%)
0
10000
20000
30000
40000
50000
Rotational Acceleration (rads/s^2)
R² = 0.2559
R² = 0.1783
R² = 0.4127
mTBI
No Injury
Linear (mTBI)
Linear (No Injury)
Linear (Combined)

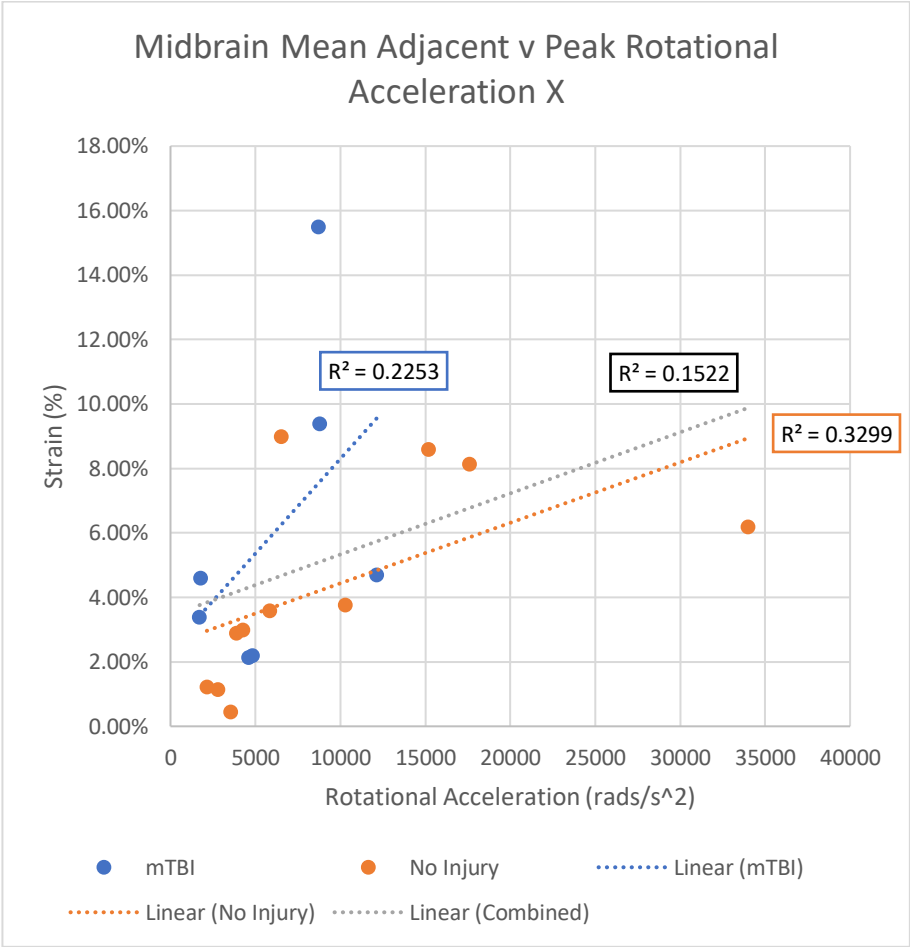
Midbrain Mean Adjacent v Peak Rotational Acceleration X
18.00%
16.00%
14.00%
12.00%
10.00%
8.00%
6.00%
4.00%
2.00%
0.00%
Strain (%)
0
5000
10000
15000
20000
25000
30000
35000
40000
Rotational Acceleration (rads/s^2)
R² = 0.2253
R² = 0.1522
R² = 0.3299
mTBI
No Injury
Linear (mTBI)
Linear (No Injury)
Linear (Combined)

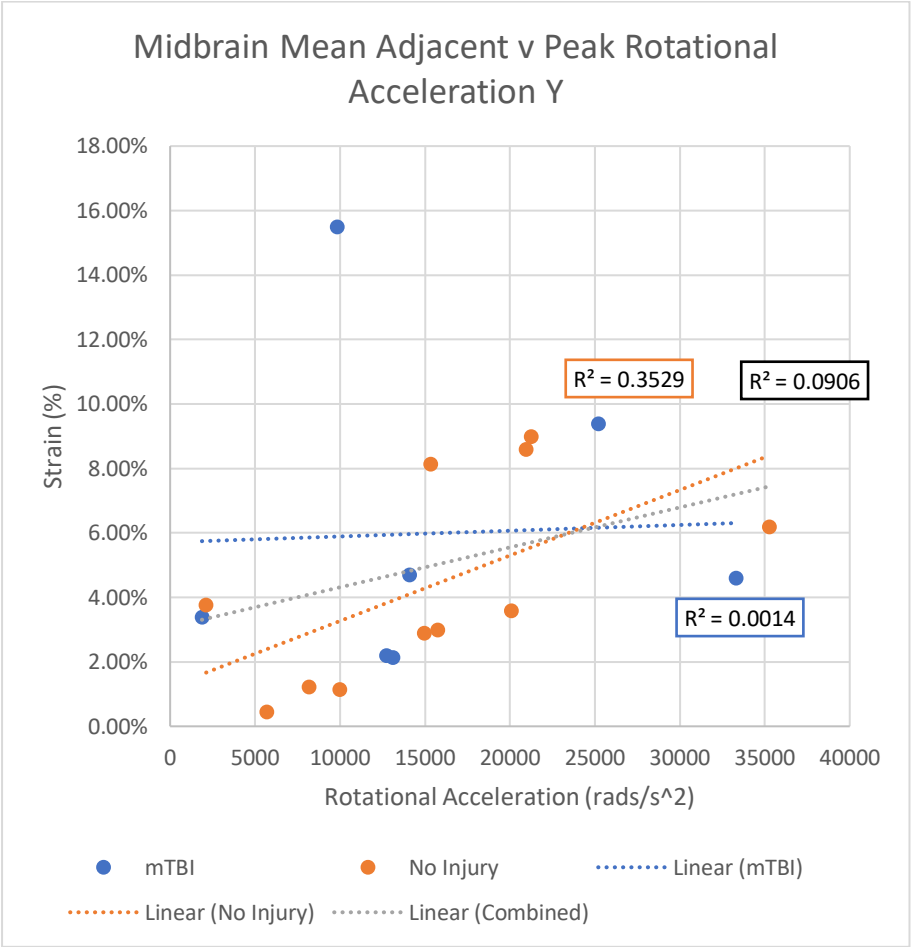
Midbrain Mean Adjacent v Peak Rotational Acceleration Y
18.00%
16.00%
14.00%
12.00%
10.00%
8.00%
6.00%
4.00%
2.00%
0.00%
Strain (%)
0
5000
10000
15000
20000
25000
30000
35000
40000
Rotational Acceleration (rads/s^2)
R² = 0.3529
R² = 0.0906
R² = 0.0014
mTBI
No Injury
Linear (mTBI)
Linear (No Injury)
Linear (Combined)

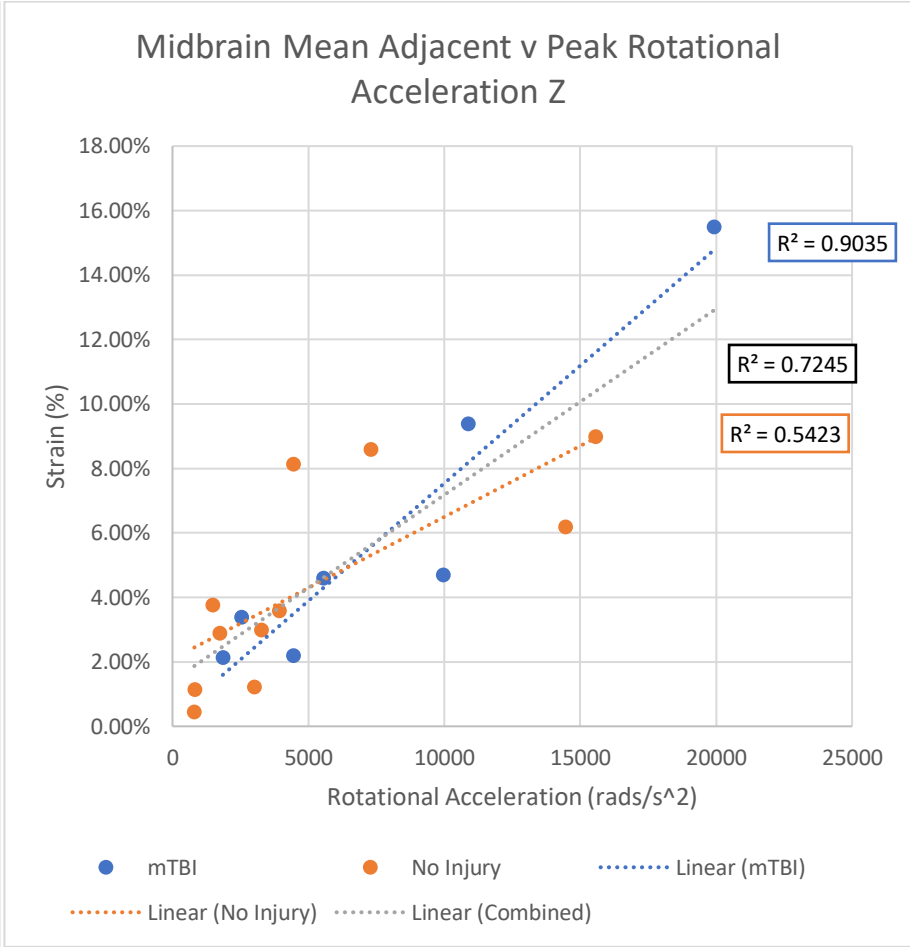
Midbrain Mean Adjacent v Peak Rotational Acceleration Z
18.00%
16.00%
14.00%
12.00%
10.00%
8.00%
6.00%
4.00%
2.00%
0.00%
Strain (%)
0
5000
10000
15000
20000
25000
Rotational Acceleration (rads/s^2)
R² = 0.9035
R² = 0.7245
R² = 0.5423
mTBI
No Injury
Linear (mTBI)
Linear (No Injury)
Linear (Combined)

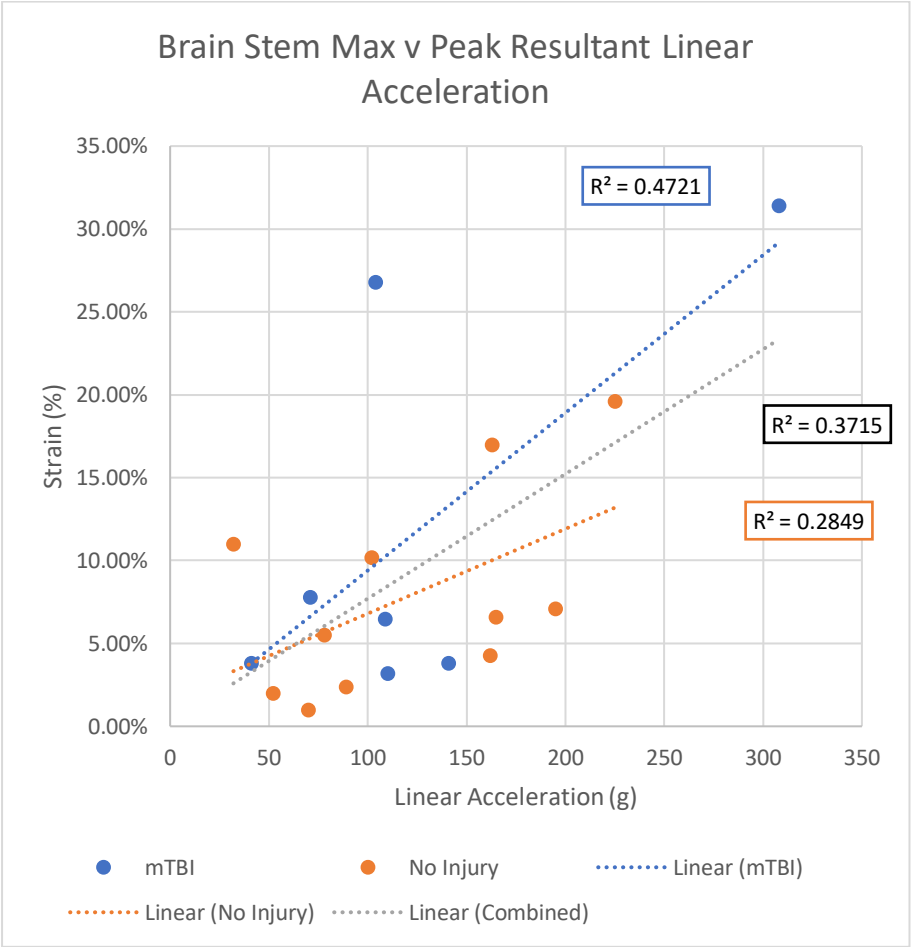
Brain Stem Max v Peak Resultant Linear Acceleration
35.00%
30.00%
25.00%
20.00%
15.00%
10.00%
5.00%
0.00%
Strain (%)
0
50
100
150
200
250
300
350
Linear Acceleration (g)
R² = 0.4721
R² = 0.3715
R² = 0.2849
mTBI
No Injury
Linear (mTBI)
Linear (No Injury)
Linear (Combined)

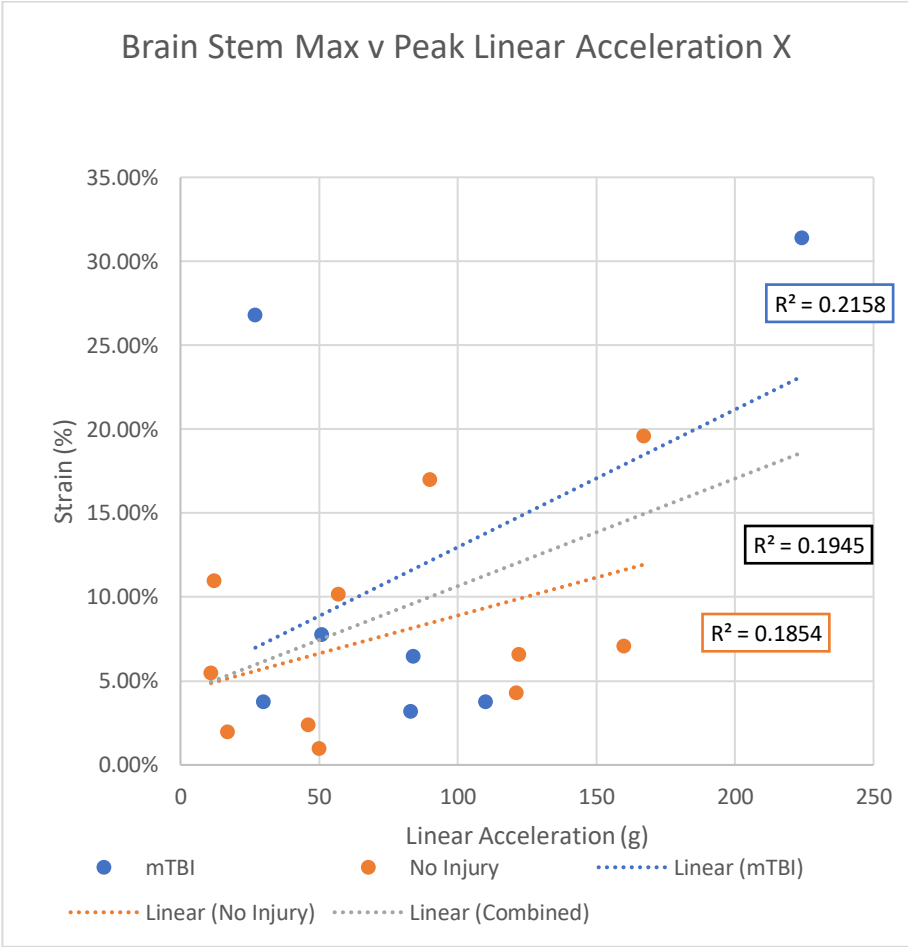
Brain Stem Max v Peak Linear Acceleration X
35.00%
30.00%
25.00%
20.00%
15.00%
10.00%
5.00%
0.00%
Strain (%)
0
50
100
150
200
250
Linear Acceleration (g)
R² = 0.2158
R² = 0.1945
R² = 0.1854
mTBI
No Injury
Linear (mTBI)
Linear (No Injury)
Linear (Combined)

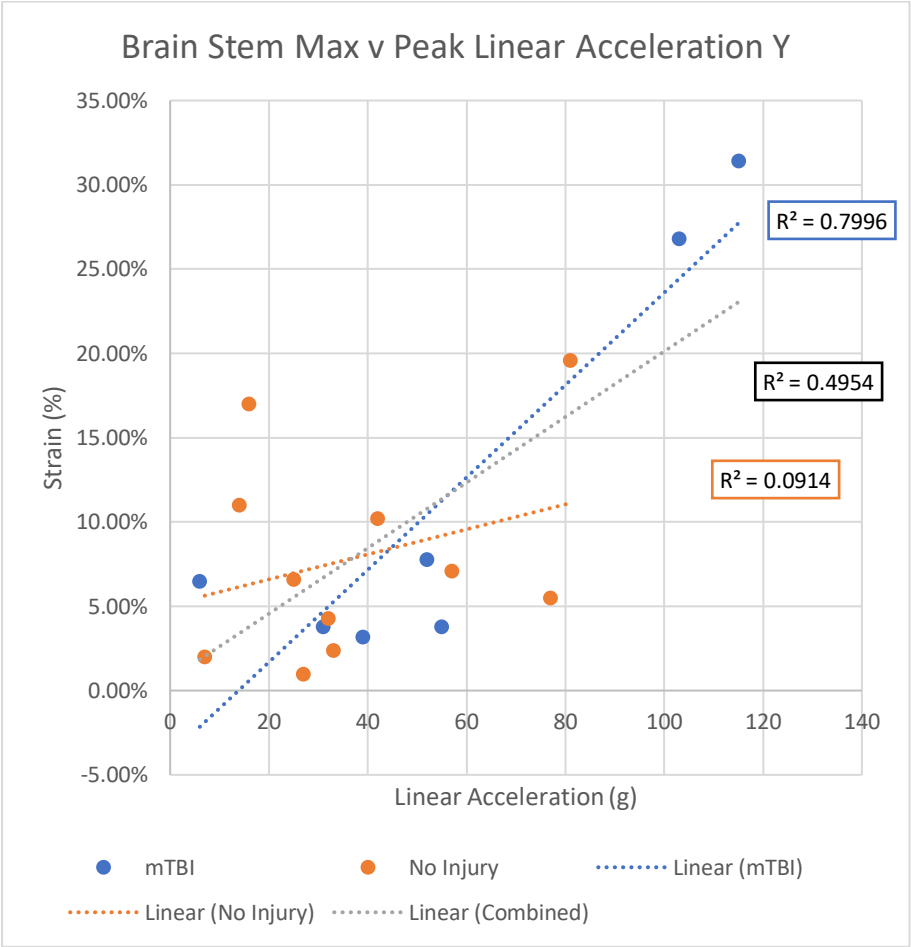
Brain Stem Max v Peak Linear Acceleration Y
35.00%
30.00%
25.00%
20.00%
15.00%
10.00%
5.00%
0.00%
-5.00%
Strain (%)
0
20
40
60
80
100
120
140
Linear Acceleration (g)
R² = 0.7996
R² = 0.4954
R² = 0.0914
mTBI
No Injury
Linear (mTBI)
Linear (No Injury)
Linear (Combined)

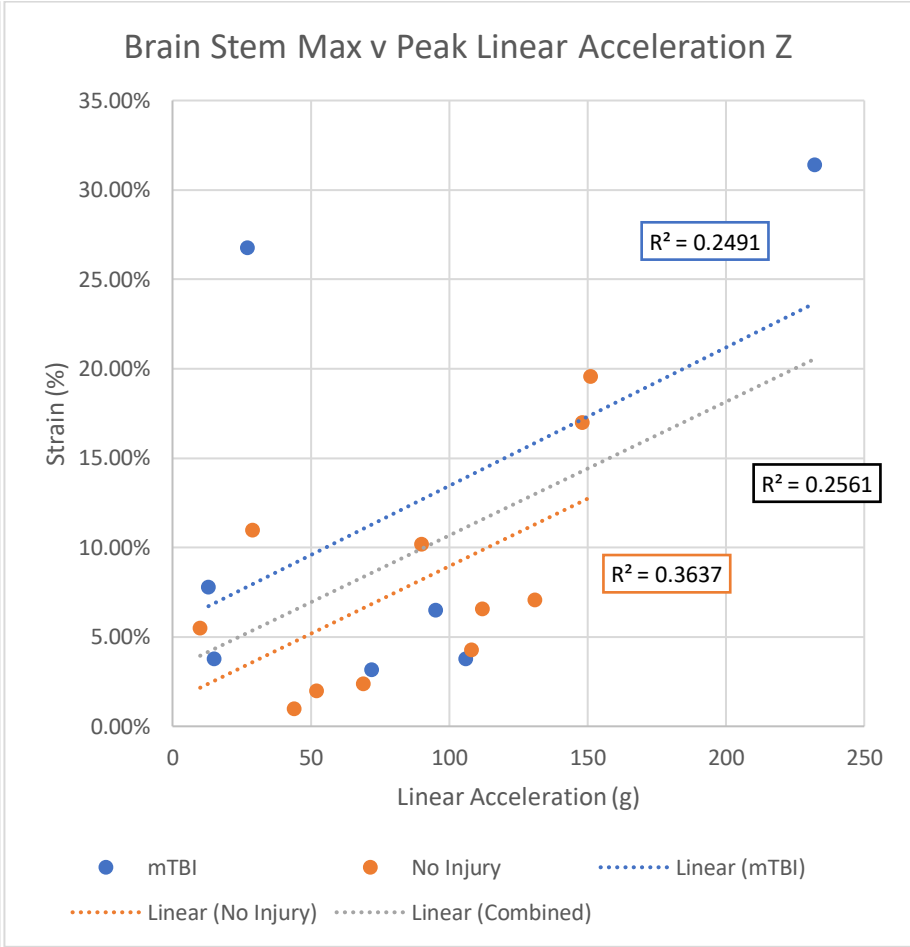
Brain Stem Max v Peak Linear Acceleration Z
35.00%
30.00%
25.00%
20.00%
15.00%
10.00%
5.00%
0.00%
Strain (%)
0
50
100
150
200
250
Linear Acceleration (g)
R² = 0.2491
R² = 0.2561
R² = 0.3637
mTBI
No Injury
Linear (mTBI)
Linear (No Injury)
Linear (Combined)

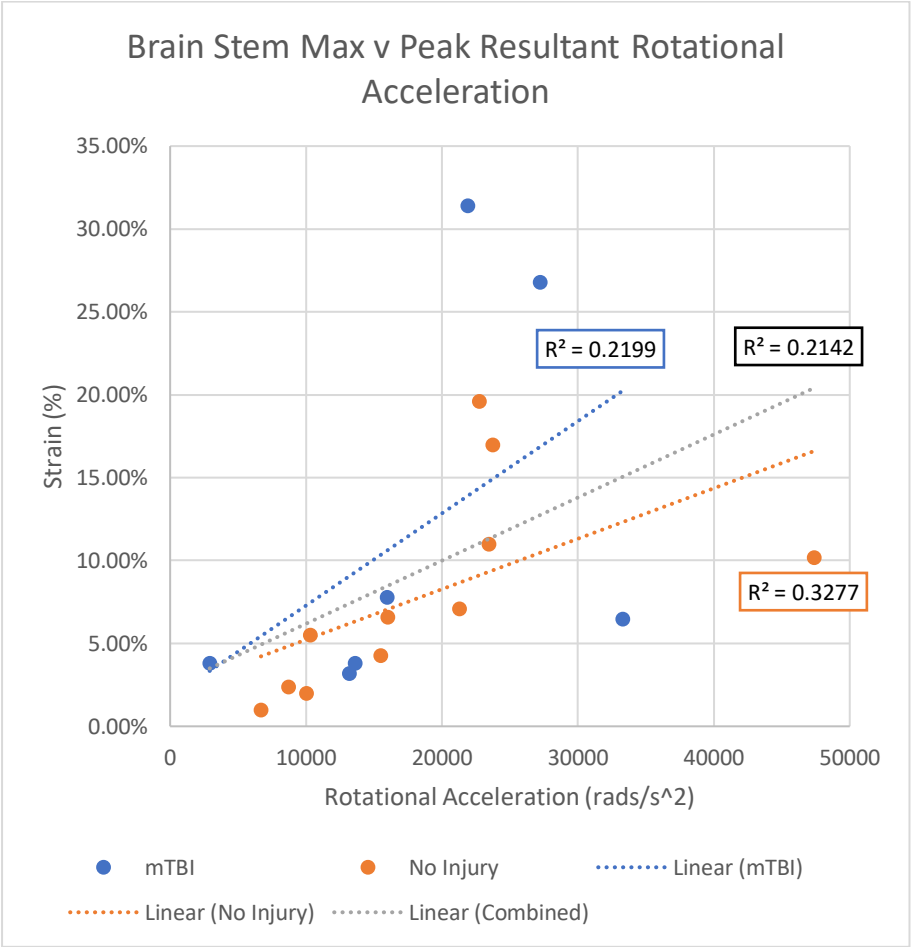
Brain Stem Max v Peak Resultant Rotational Acceleration
35.00%
30.00%
25.00%
20.00%
15.00%
10.00%
5.00%
0.00%
Strain (%)
0
10000
20000
30000
40000
50000
Rotational Acceleration (rads/s^2)
R² = 0.2199
R² = 0.2142
R² = 0.3277
mTBI
No Injury
Linear (mTBI)
Linear (No Injury)
Linear (Combined)

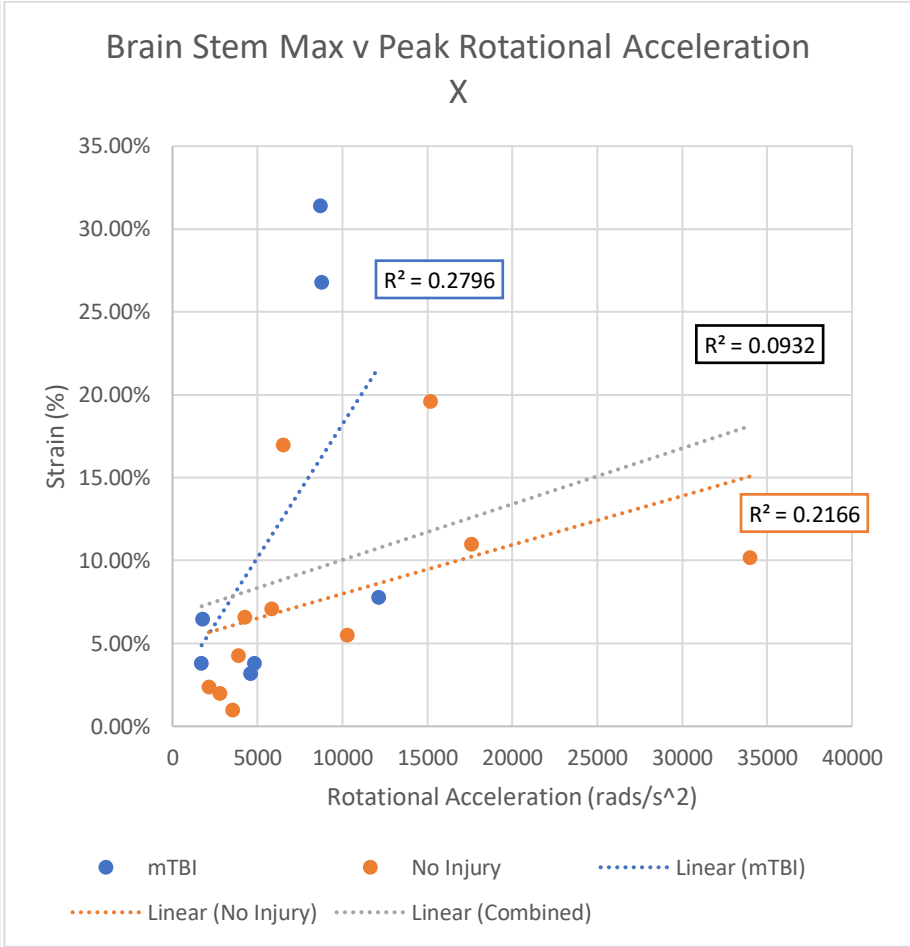
Brain Stem Max v Peak Rotational Acceleration X
35.00%
30.00%
25.00%
20.00%
15.00%
10.00%
5.00%
0.00%
Strain (%)
0
5000
10000
15000
20000
25000
30000
35000
40000
Rotational Acceleration (rads/s^2)
R² = 0.2796
R² = 0.0932
R² = 0.2166
mTBI
No Injury
Linear (mTBI)
Linear (No Injury)
Linear (Combined)

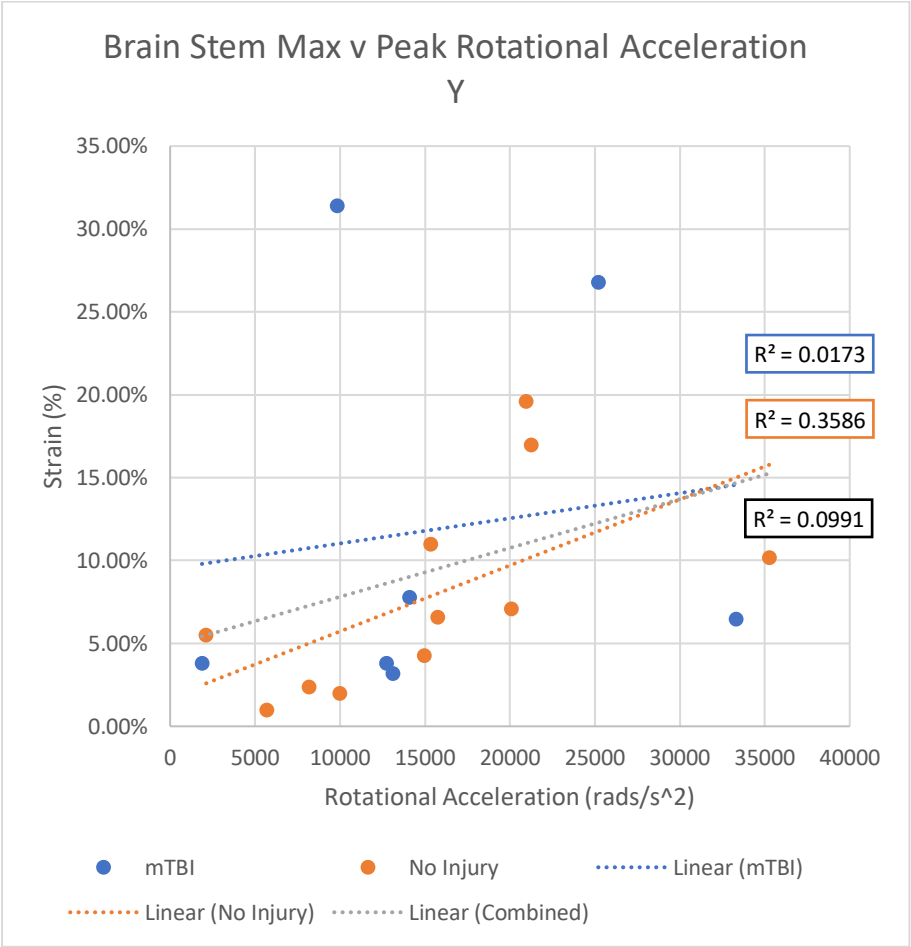
Brain Stem Max v Peak Rotational Acceleration
Y
35.00%
30.00%
25.00%
20.00%
15.00%
10.00%
5.00%
0.00%
Strain (%)
0
5000
10000
15000
20000
25000
30000
35000
40000
Rotational Acceleration (rads/s^2)
R² = 0.0173
R² = 0.3586
R² = 0.0991
mTBI
No Injury
Linear (mTBI)
Linear (No Injury)
Linear (Combined)

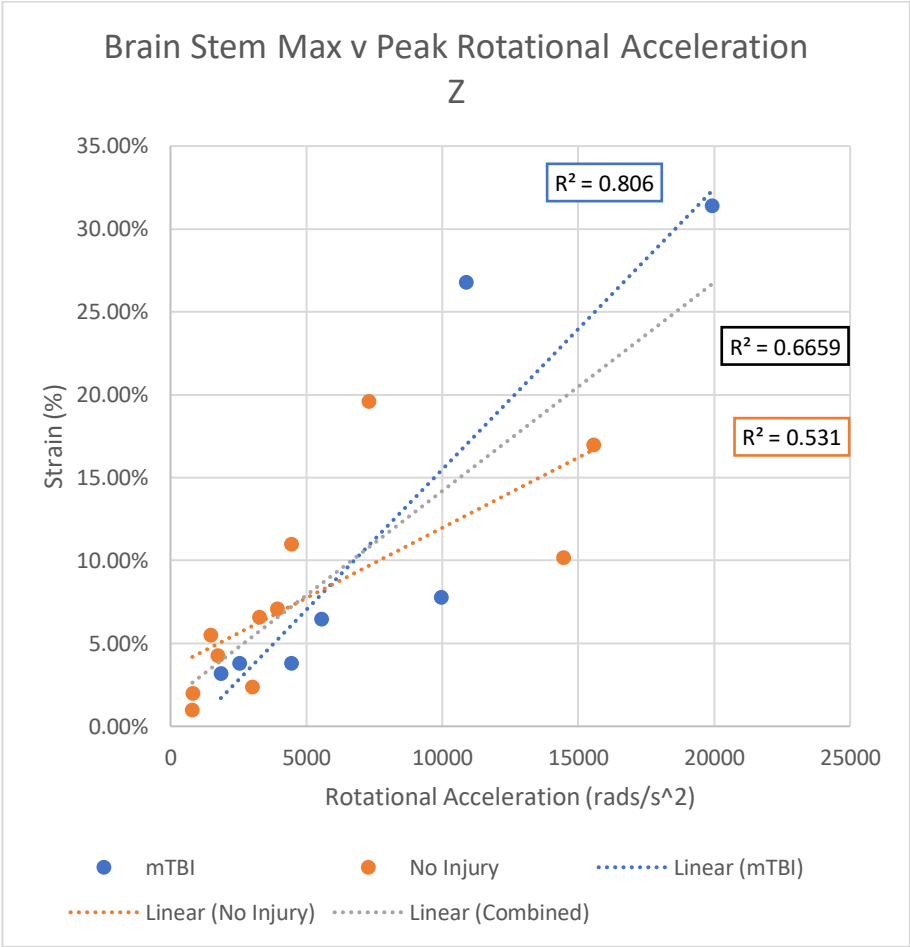
Brain Stem Max v Peak Rotational Acceleration
Z
35.00%
30.00%
25.00%
20.00%
15.00%
10.00%
5.00%
0.00%
Strain (%)
0
5000
10000
15000
20000
25000
Rotational Acceleration (rads/s^2)
R² = 0.806
R² = 0.6659
R² = 0.531
mTBI
No Injury
Linear (mTBI)
Linear (No Injury)
Linear (Combined)

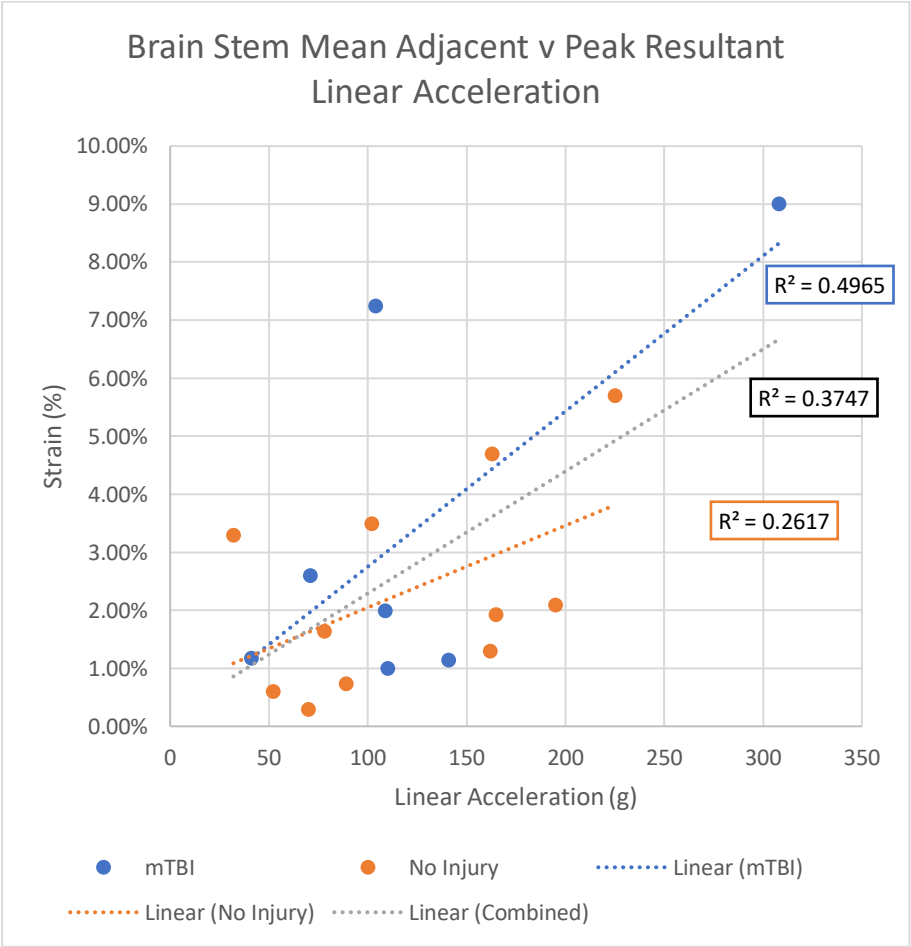
Brain Stem Mean Adjacent v Peak Resultant Linear Acceleration
10.00%
9.00%
8.00%
7.00%
6.00%
5.00%
4.00%
3.00%
2.00%
1.00%
0.00%
Strain (%)
0
50
100
150
200
250
300
350
Linear Acceleration (g)
R² = 0.4965
R² = 0.3747
R² = 0.2617
mTBI
No Injury
Linear (mTBI)
Linear (No Injury)
Linear (Combined)

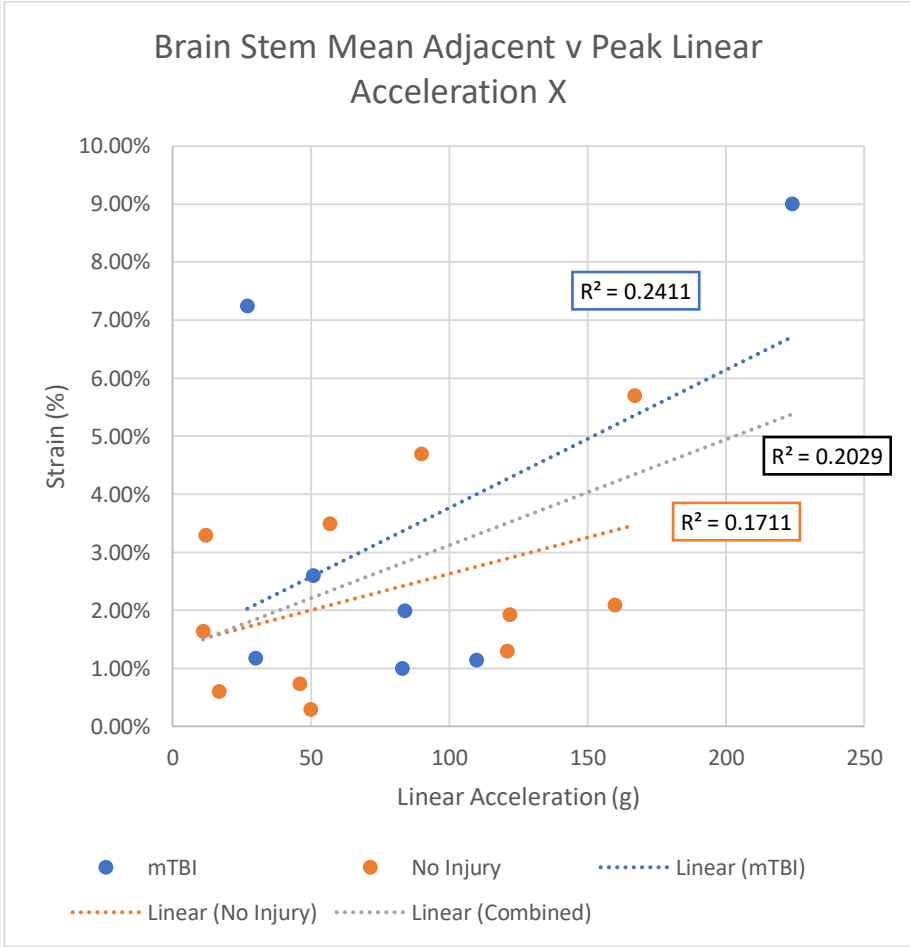
Brain Stem Mean Adjacent v Peak Linear Acceleration X
10.00%
9.00%
8.00%
7.00%
6.00%
5.00%
4.00%
3.00%
2.00%
1.00%
0.00%
Strain (%)
0
50
100
150
200
250
Linear Acceleration (g)
R² = 0.2411
R² = 0.2029
R² = 0.1711
mTBI
No Injury
Linear (mTBI)
Linear (No Injury)
Linear (Combined)

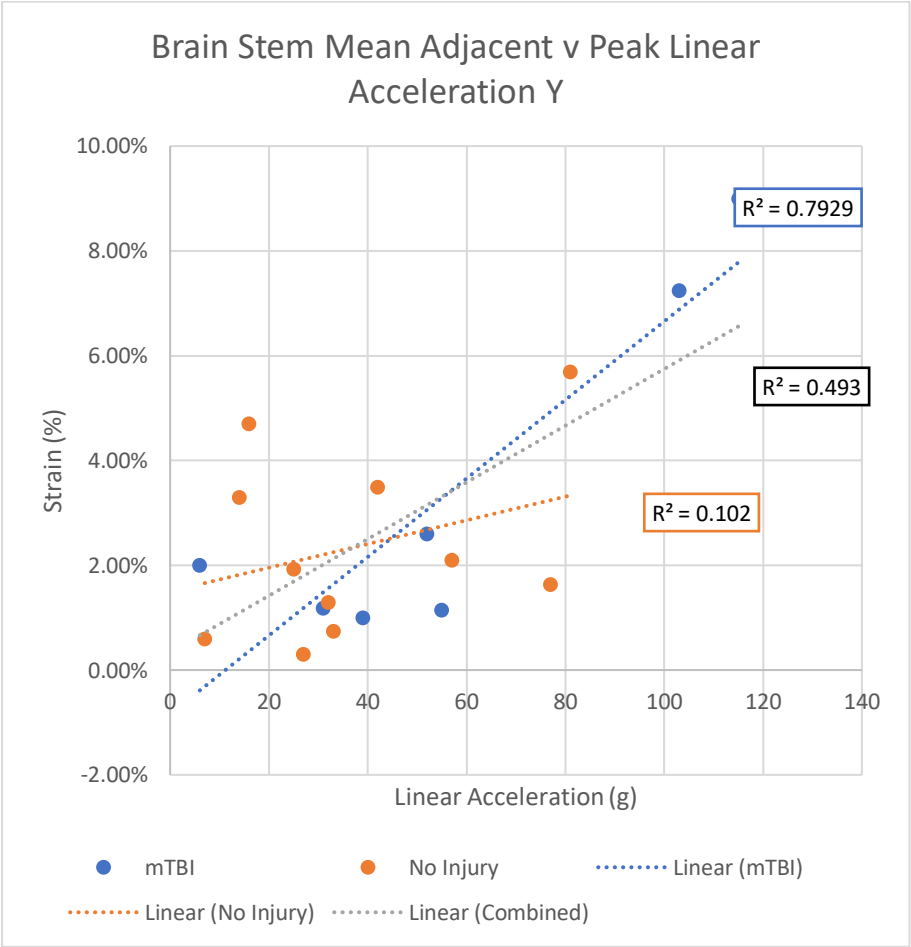
Brain Stem Mean Adjacent v Peak Linear Acceleration Y
10.00%
8.00%
6.00%
4.00%
2.00%
0.00%
-2.00%
Strain (%)
0
20
40
60
80
100
120
140
Linear Acceleration (g)
R² = 0.7929
R² = 0.493
R² = 0.102
mTBI
No Injury
Linear (mTBI)
Linear (No Injury)
Linear (Combined)

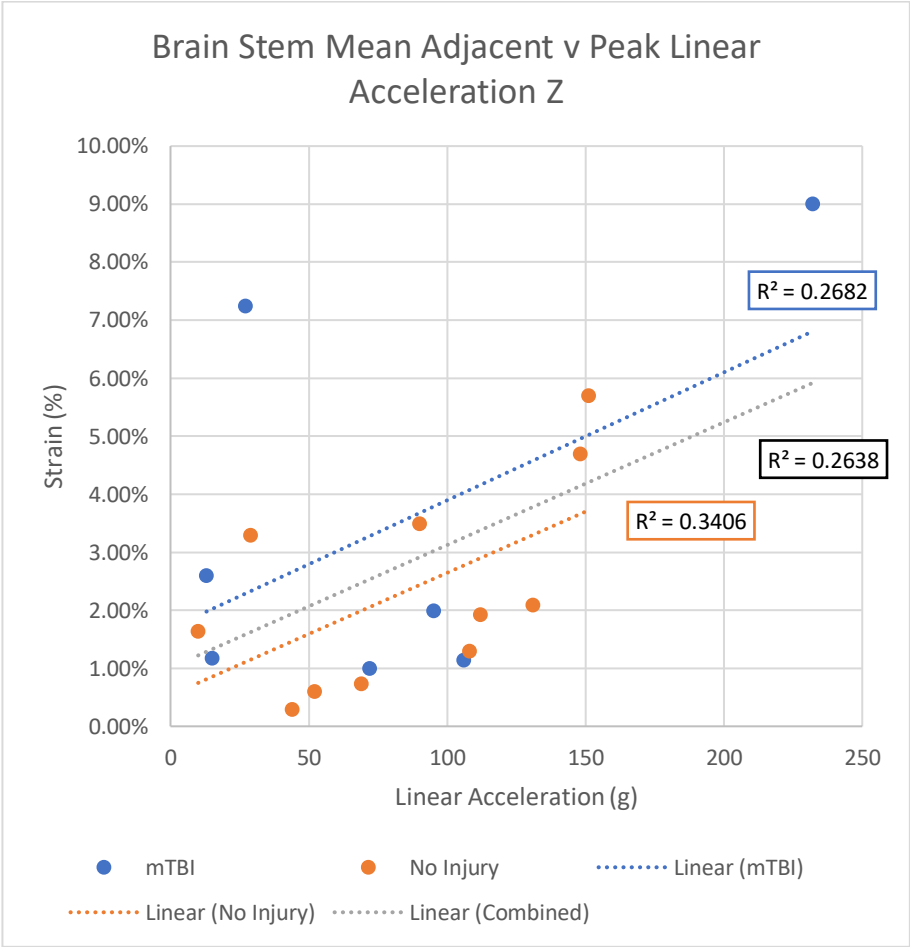
Brain Stem Mean Adjacent v Peak Linear Acceleration Z
10.00%
9.00%
8.00%
7.00%
6.00%
5.00%
4.00%
3.00%
2.00%
1.00%
0.00%
Strain (%)
0
50
100
150
200
250
Linear Acceleration (g)
R² = 0.2682
R² = 0.2638
R² = 0.3406
mTBI
No Injury
Linear (mTBI)
Linear (No Injury)
Linear (Combined)

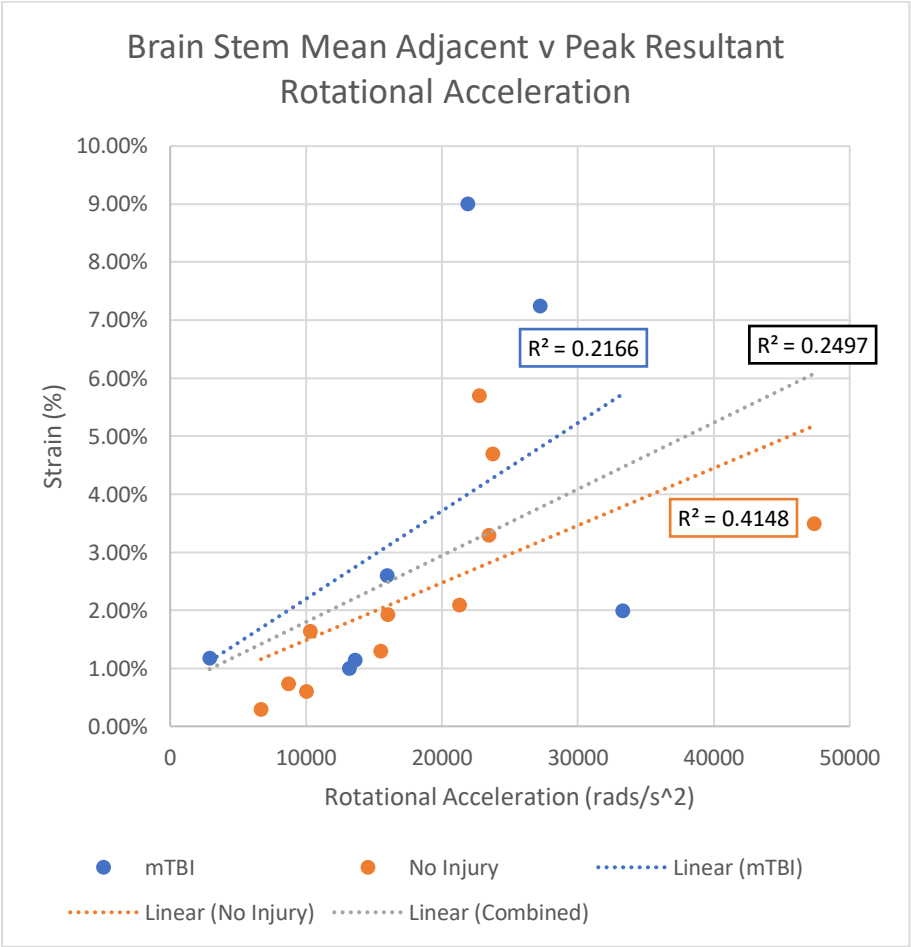
Brain Stem Mean Adjacent v Peak Resultant Rotational Acceleration
10.00%
9.00%
8.00%
7.00%
6.00%
5.00%
4.00%
3.00%
2.00%
1.00%
0.00%
Strain (%)
0
10000
20000
30000
40000
50000
Rotational Acceleration (rads/s^2)
R² = 0.2166
R² = 0.2497
R² = 0.4148
mTBI
No Injury
Linear (mTBI)
Linear (No Injury)
Linear (Combined)

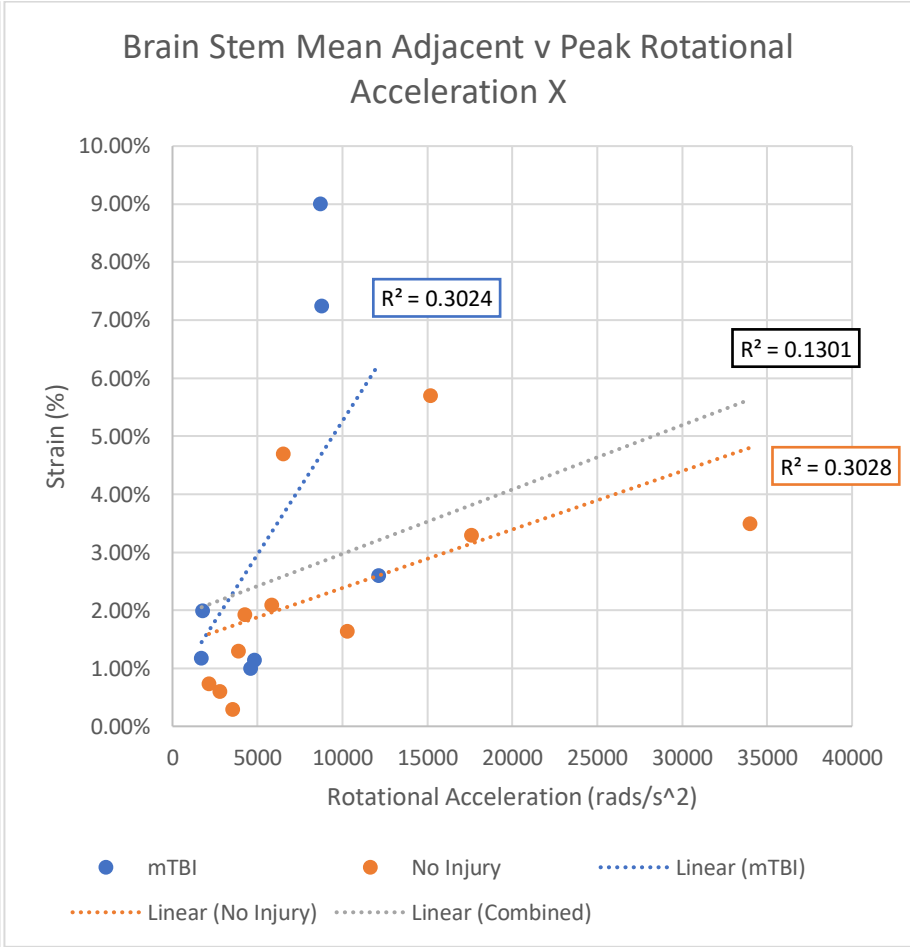
Brain Stem Mean Adjacent v Peak Rotational Acceleration X
10.00%
9.00%
8.00%
7.00%
6.00%
5.00%
4.00%
3.00%
2.00%
1.00%
0.00%
Strain (%)
0
5000
10000
15000
20000
25000
30000
35000
40000
Rotational Acceleration (rads/s^2)
R² = 0.3024
R² = 0.1301
R² = 0.3028
mTBI
No Injury
Linear (mTBI)
Linear (No Injury)
Linear (Combined)

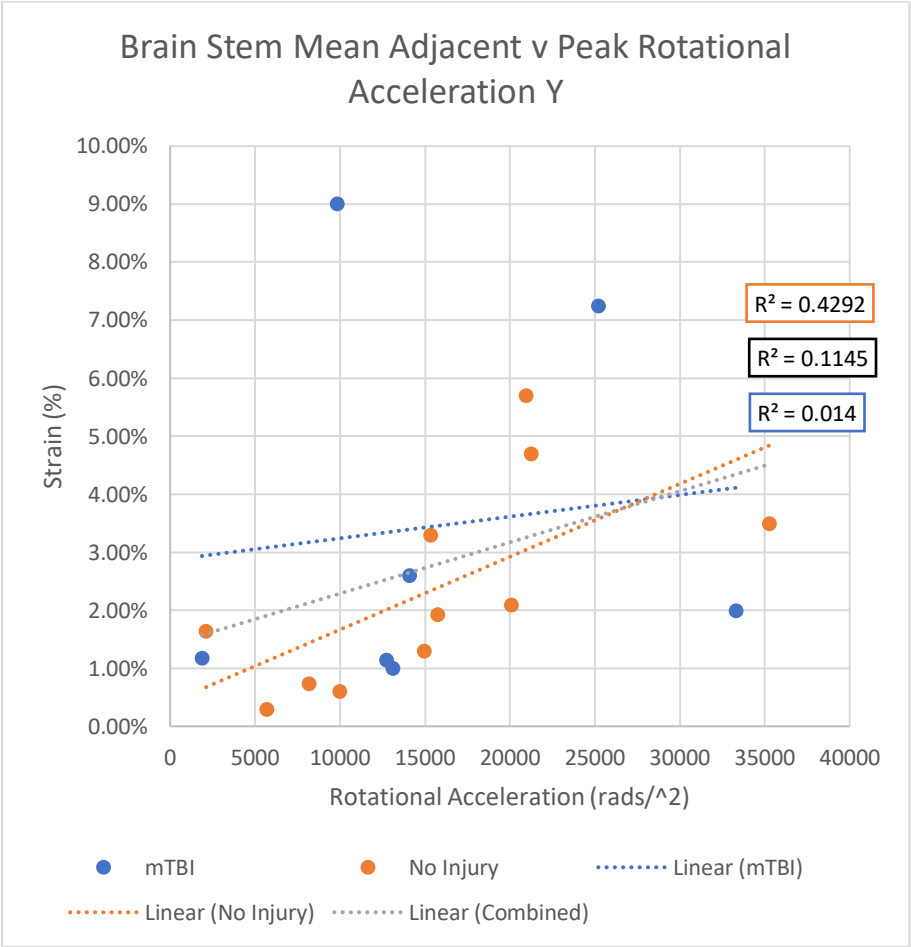
Brain Stem Mean Adjacent v Peak Rotational Acceleration Y
Strain (%)
10.00%
9.00%
8.00%
7.00%
6.00%
5.00%
4.00%
3.00%
2.00%
1.00%
0.00%
0
5000
10000
15000
20000
25000
30000
35000
40000
Rotational Acceleration (rads/^2)
R² = 0.4292
R² = 0.1145
R² = 0.014
mTBI
No Injury
Linear (mTBI)
Linear (No Injury)
Linear (Combined)

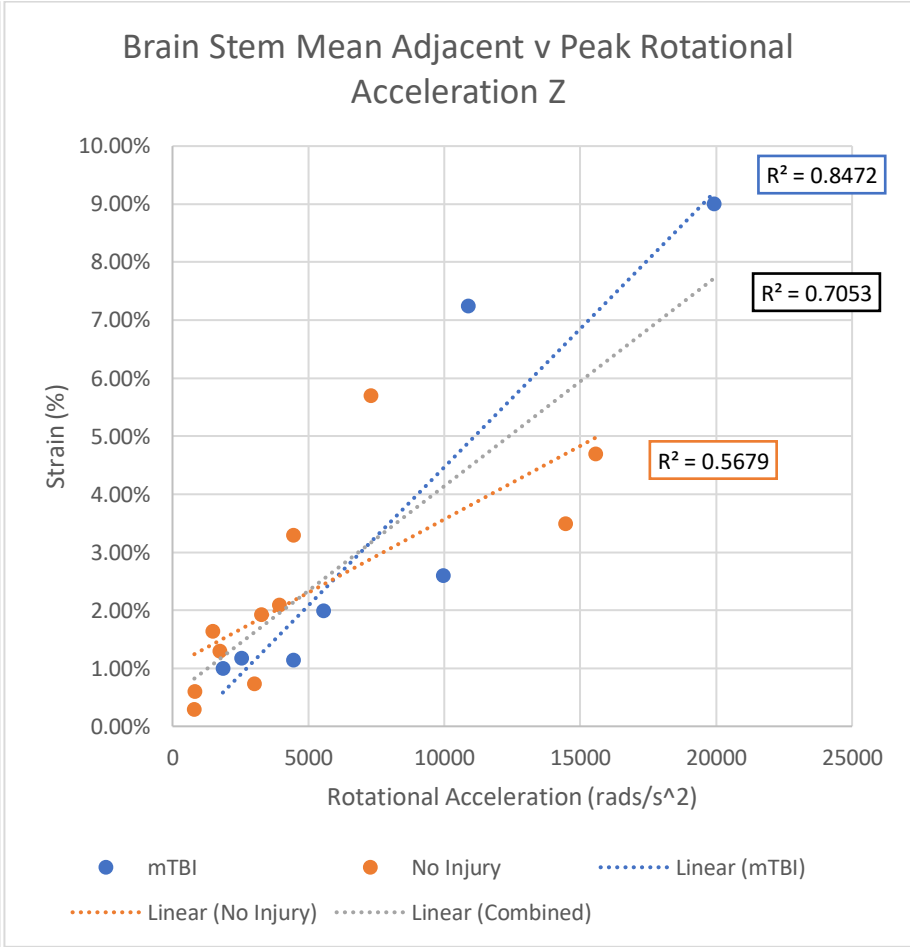
Brain Stem Mean Adjacent v Peak Rotational Acceleration Z
Strain (%)
10.00%
9.00%
8.00%
7.00%
6.00%
5.00%
4.00%
3.00%
2.00%
1.00%
0.00%
0
5000
10000
15000
20000
25000
Rotational Acceleration (rads/s^2)
R² = 0.8472
R² = 0.7053
R² = 0.5679
mTBI
No Injury
Linear (mTBI)
Linear (No Injury)
Linear (Combined)

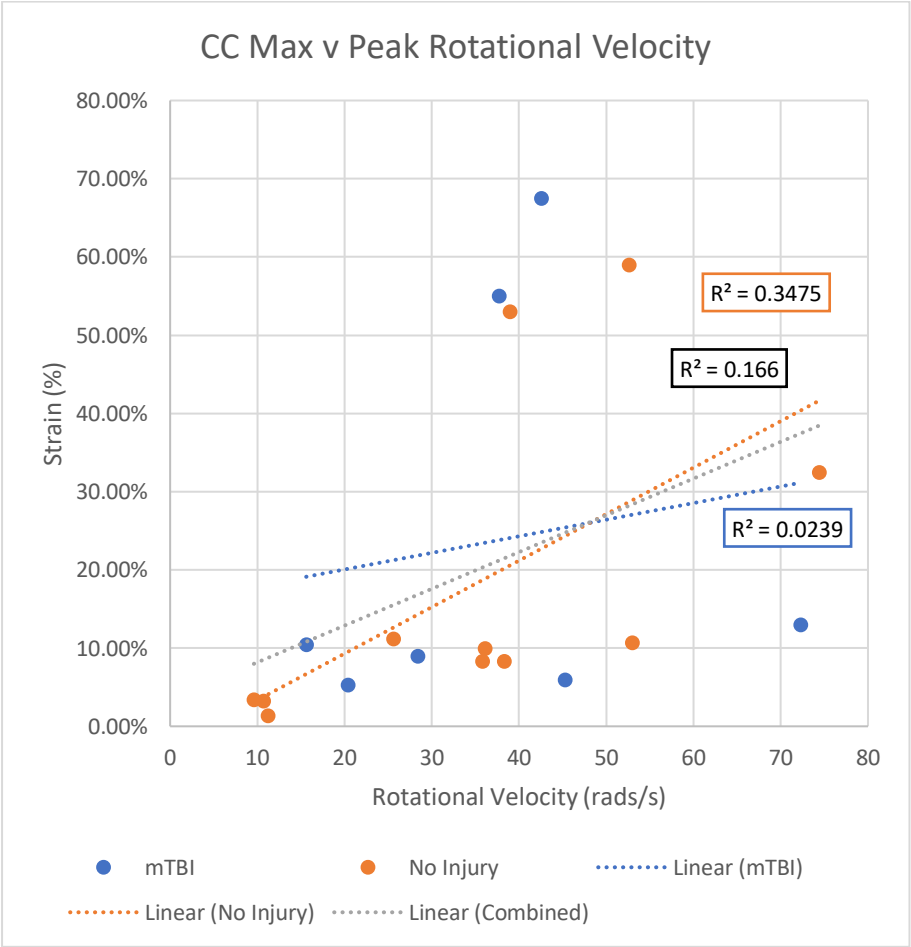
CC Max v Peak Rotational Velocity
80.00%
70.00%
60.00%
50.00%
40.00%
30.00%
20.00%
10.00%
0.00%
Strain (%)
0
10
20
30
40
50
60
70
80
Rotational Velocity (rads/s)
R² = 0.3475
R² = 0.166
R² = 0.0239
mTBI
No Injury
Linear (mTBI)
Linear (No Injury)
Linear (Combined)

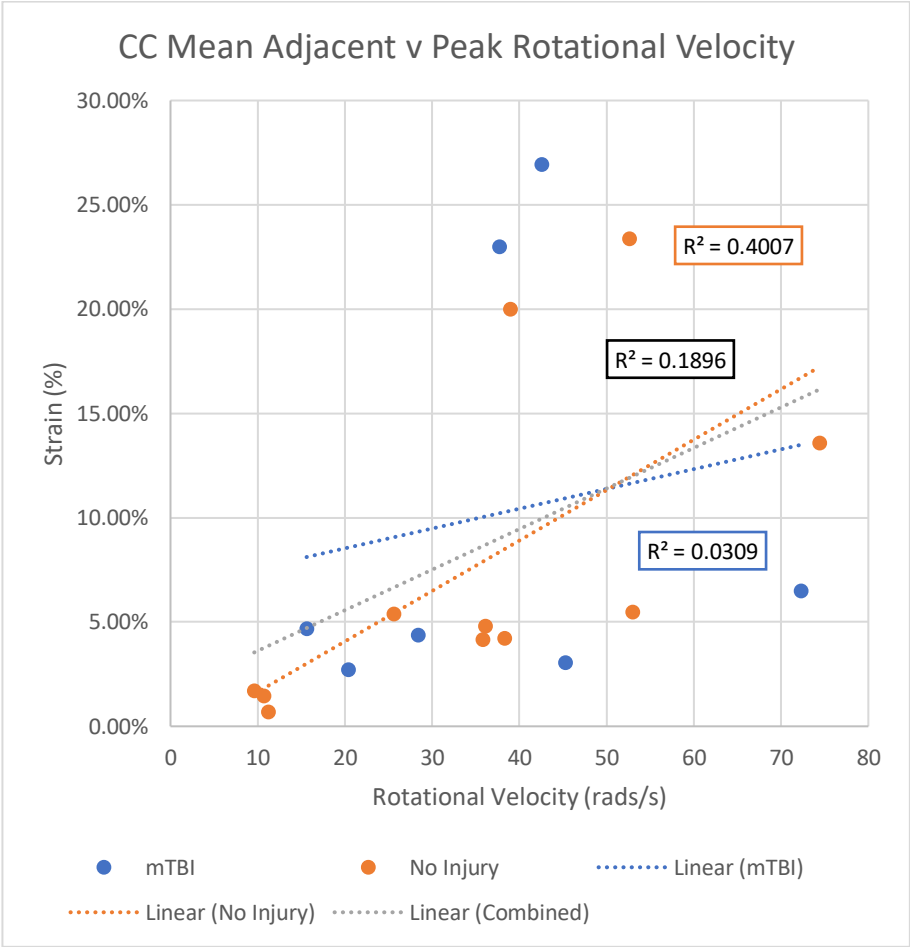
CC Mean Adjacent v Peak Rotational Velocity
30.00%
25.00%
20.00%
15.00%
10.00%
5.00%
0.00%
Strain (%)
0
10
20
30
40
50
60
70
80
Rotational Velocity (rads/s)
R² = 0.4007
R² = 0.1896
R² = 0.0309
mTBI
No Injury
Linear (mTBI)
Linear (No Injury)
Linear (Combined)

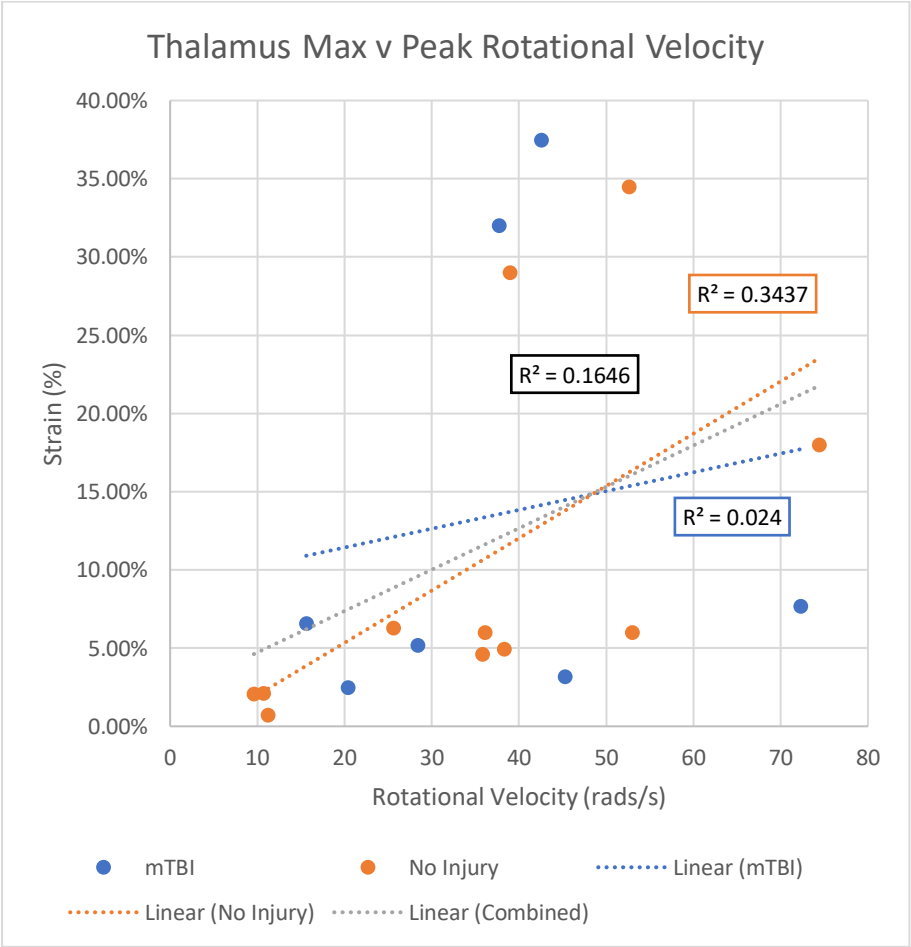
Thalamus Max v Peak Rotational Velocity
Strain (%)
40.00%
35.00%
30.00%
25.00%
20.00%
15.00%
10.00%
5.00%
0.00%
0
10
20
30
40
50
60
70
80
Rotational Velocity (rads/s)
R² = 0.3437
R² = 0.1646
R² = 0.024
mTBI
No Injury
Linear (mTBI)
Linear (No Injury)
Linear (Combined)

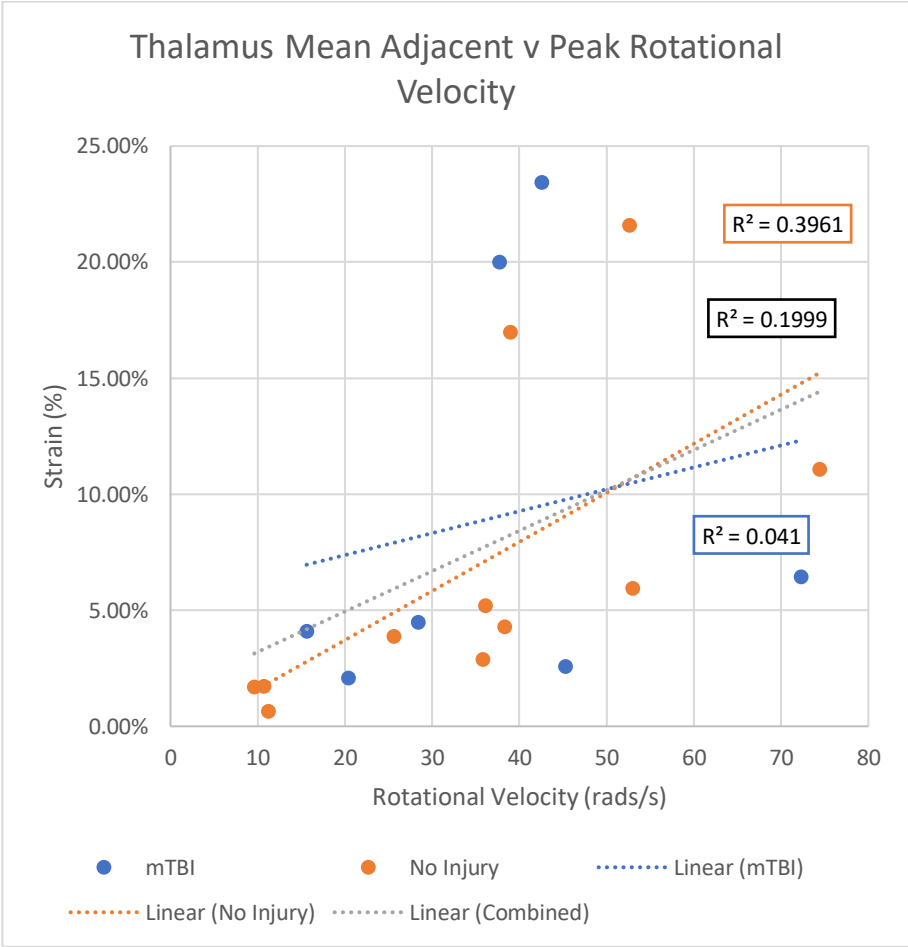
Thalamus Mean Adjacent v Peak Rotational Velocity
Strain (%)
25.00%
20.00%
15.00%
10.00%
5.00%
0.00%
0
10
20
30
40
50
60
70
80
Rotational Velocity (rads/s)
R² = 0.3961
R² = 0.1999
R² = 0.041
mTBI
No Injury
Linear (mTBI)
Linear (No Injury)
Linear (Combined)

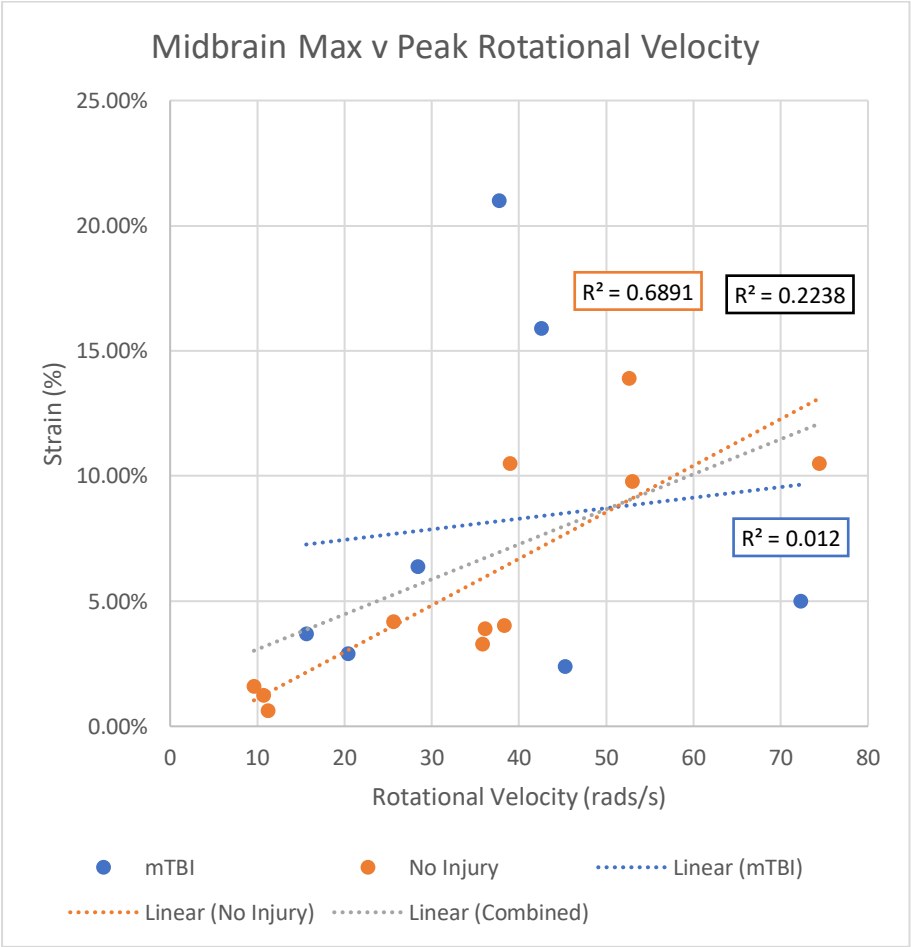
Midbrain Max v Peak Rotational Velocity
Strain (%)
25.00%
20.00%
15.00%
10.00%
5.00%
0.00%
0
10
20
30
40
50
60
70
80
Rotational Velocity (rads/s)
R² = 0.6891
R² = 0.2238
R² = 0.012
mTBI
No Injury
Linear (mTBI)
Linear (No Injury)
Linear (Combined)

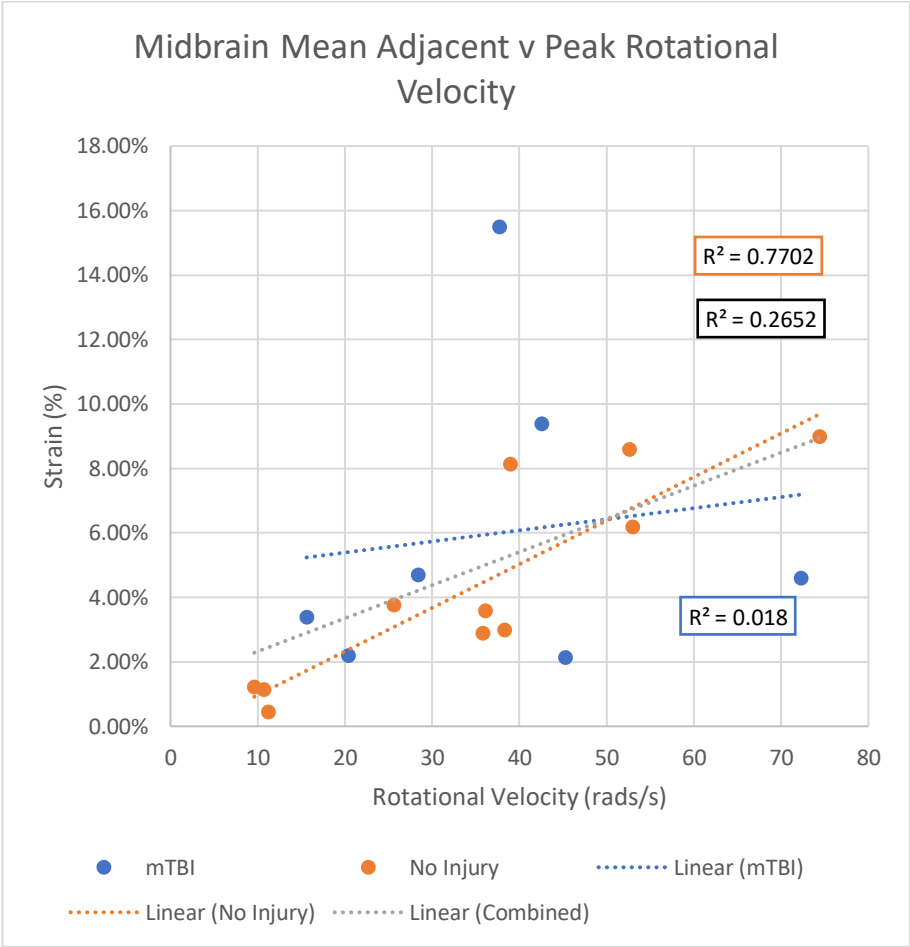
Midbrain Mean Adjacent v Peak Rotational Velocity
Strain (%)
18.00%
16.00%
14.00%
12.00%
10.00%
8.00%
6.00%
4.00%
2.00%
0.00%
0
10
20
30
40
50
60
70
80
Rotational Velocity (rads/s)
R² = 0.7702
R² = 0.2652
R² = 0.018
mTBI
No Injury
Linear (mTBI)
Linear (No Injury)
Linear (Combined)

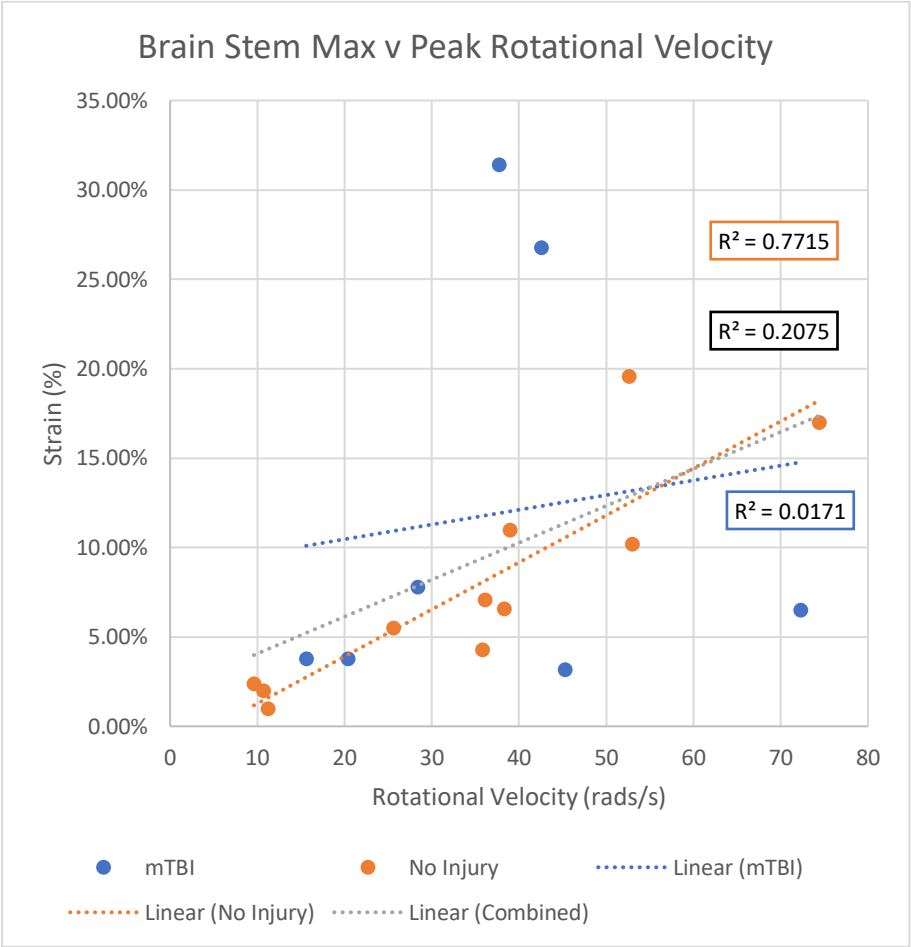
Brain Stem Max v Peak Rotational Velocity
35.00%
30.00%
25.00%
20.00%
15.00%
10.00%
5.00%
0.00%
Strain (%)
0
10
20
30
40
50
60
70
80
Rotational Velocity (rads/s)
R² = 0.7715
R² = 0.2075
R² = 0.0171
mTBI
No Injury
Linear (mTBI)
Linear (No Injury)
Linear (Combined)

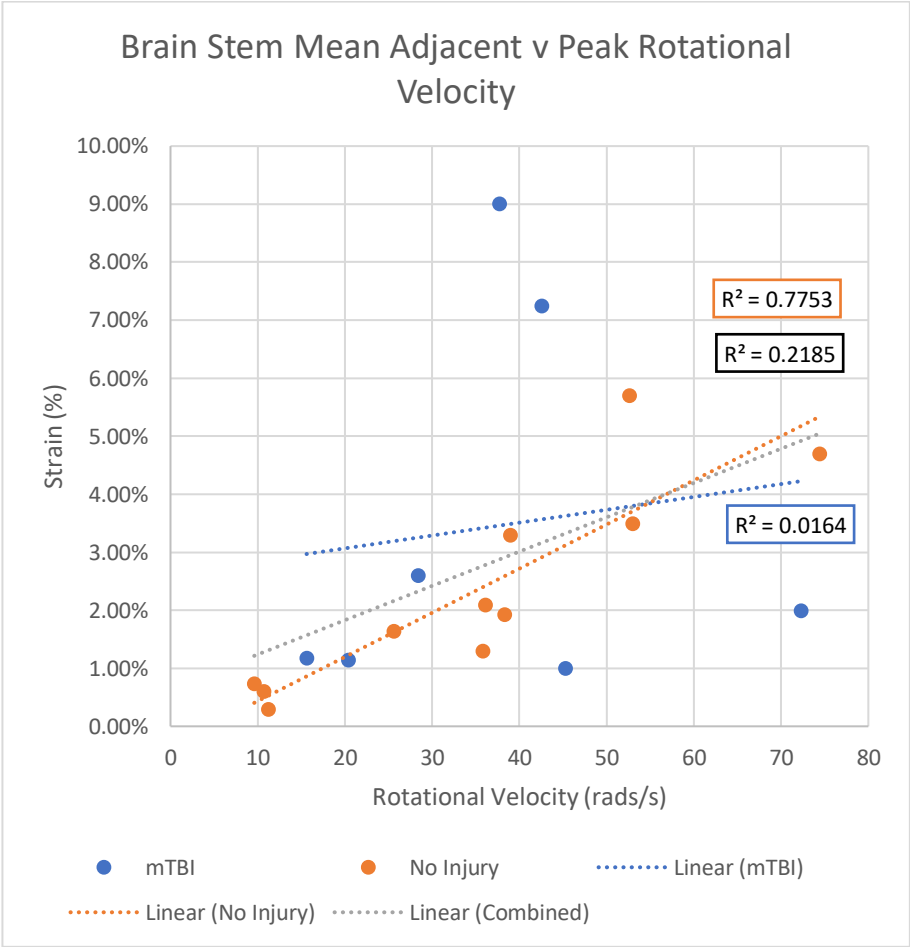
Brain Stem Mean Adjacent v Peak Rotational Velocity
10.00%
9.00%
8.00%
7.00%
6.00%
5.00%
4.00%
3.00%
2.00%
1.00%
0.00%
Strain (%)
0
10
20
30
40
50
60
70
80
Rotational Velocity (rads/s)
R² = 0.7753
R² = 0.2185
R² = 0.0164
mTBI
No Injury
Linear (mTBI)
Linear (No Injury)
Linear (Combined)

Appendix 9

Graphs of HIP against Strain

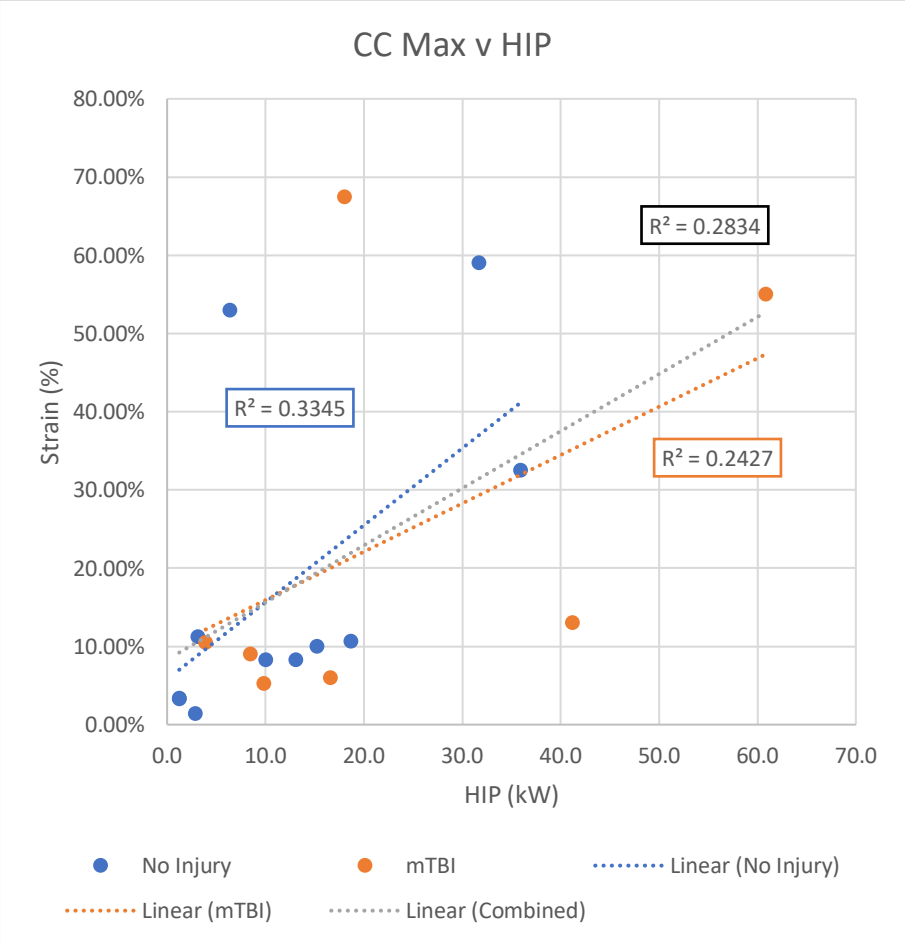

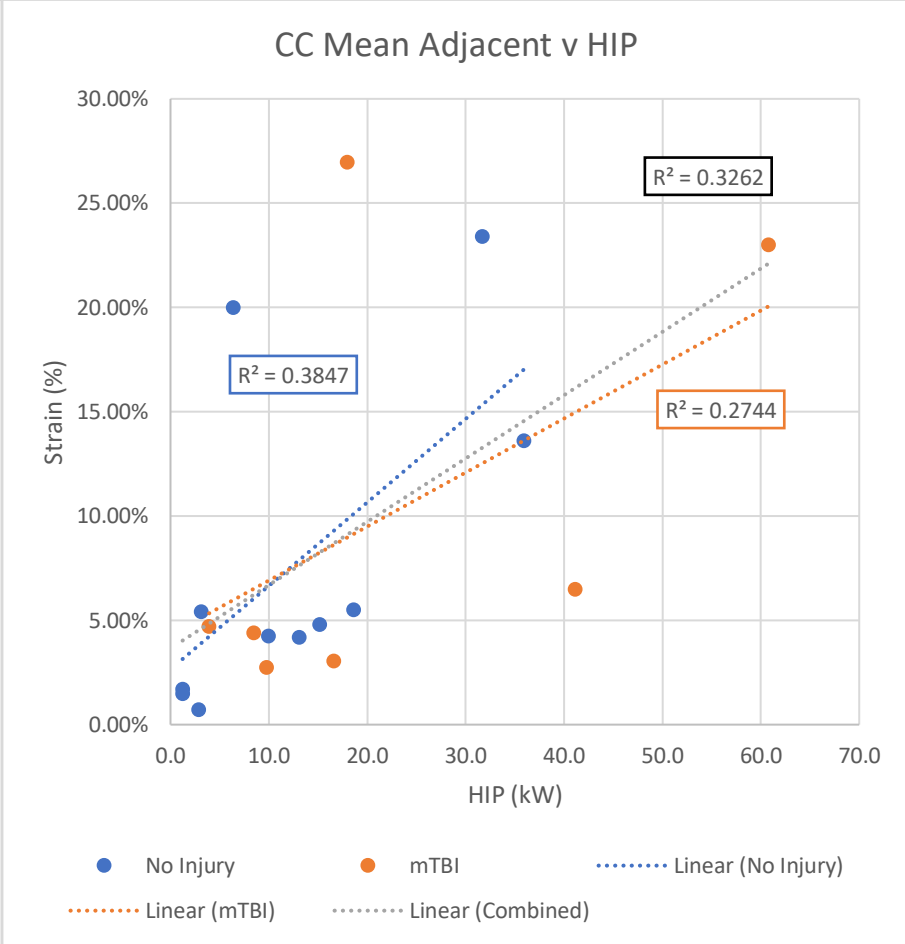

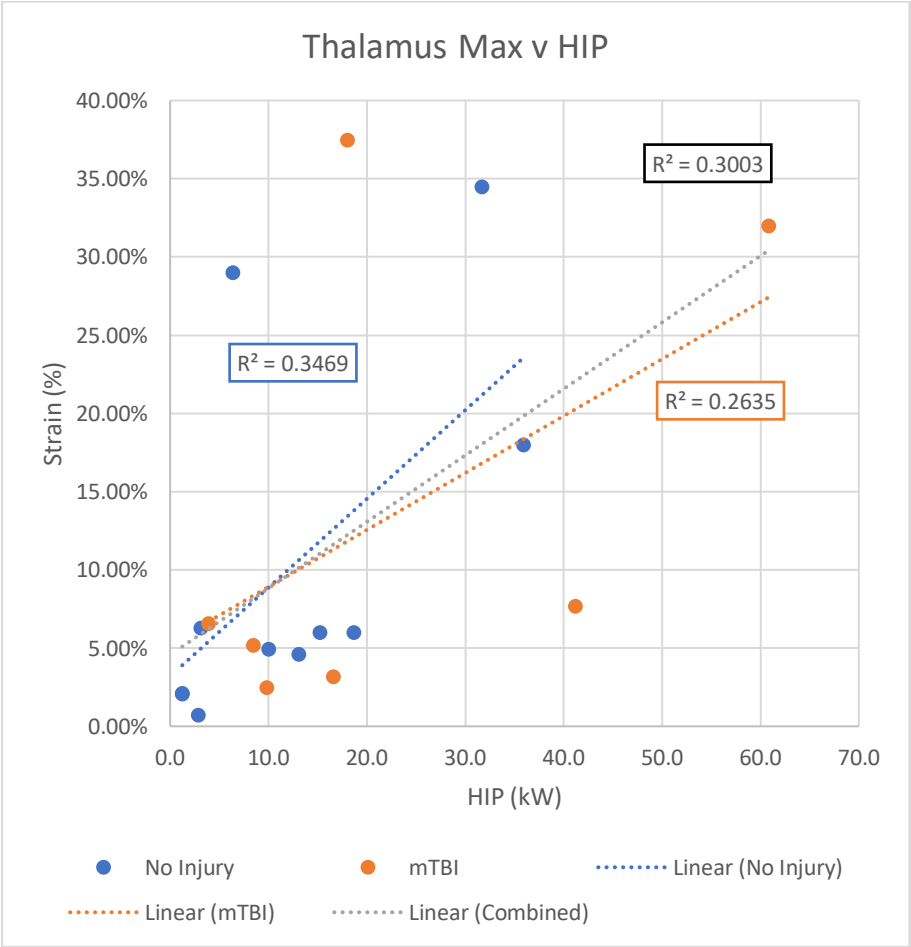
Thalamus Max v HIP
Strain (%)
HIP (kW)
R² = 0.3003
R² = 0.3469
R² = 0.2635
No Injury
mTBI
Linear (No Injury)
Linear (mTBI)
Linear (Combined)

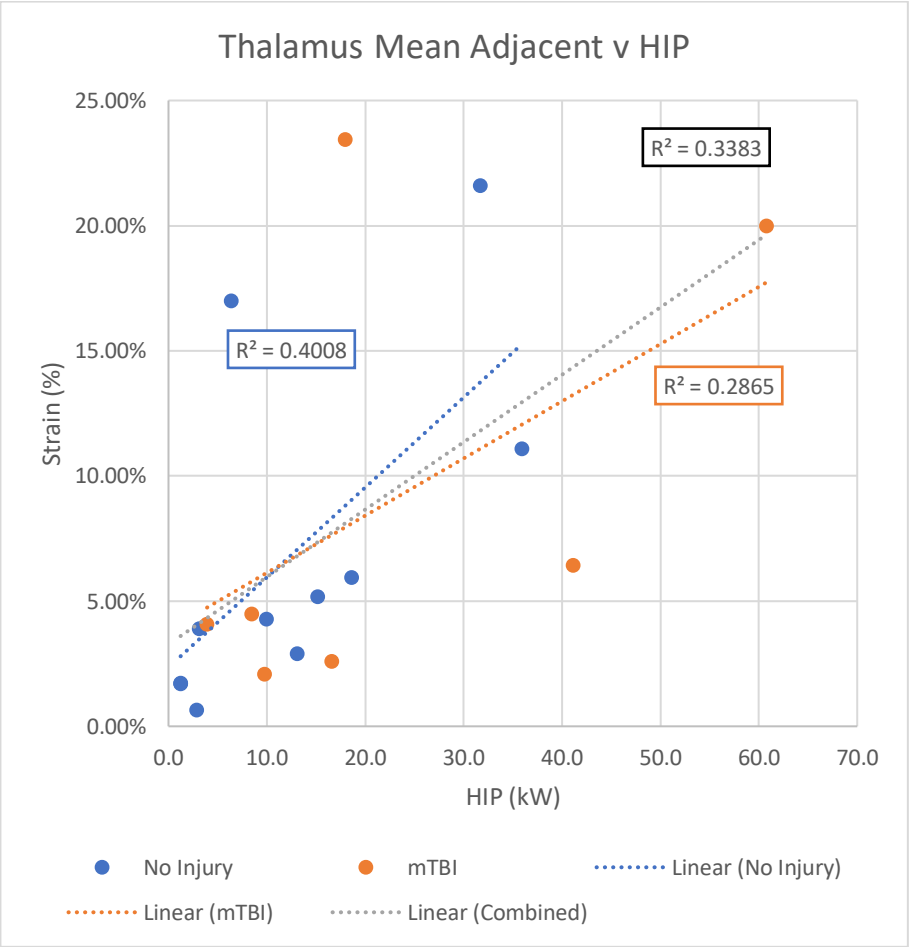
Thalamus Mean Adjacent v HIP
Strain (%)
HIP (kW)
R² = 0.3383
R² = 0.4008
R² = 0.2865
No Injury
mTBI
Linear (No Injury)
Linear (mTBI)
Linear (Combined)

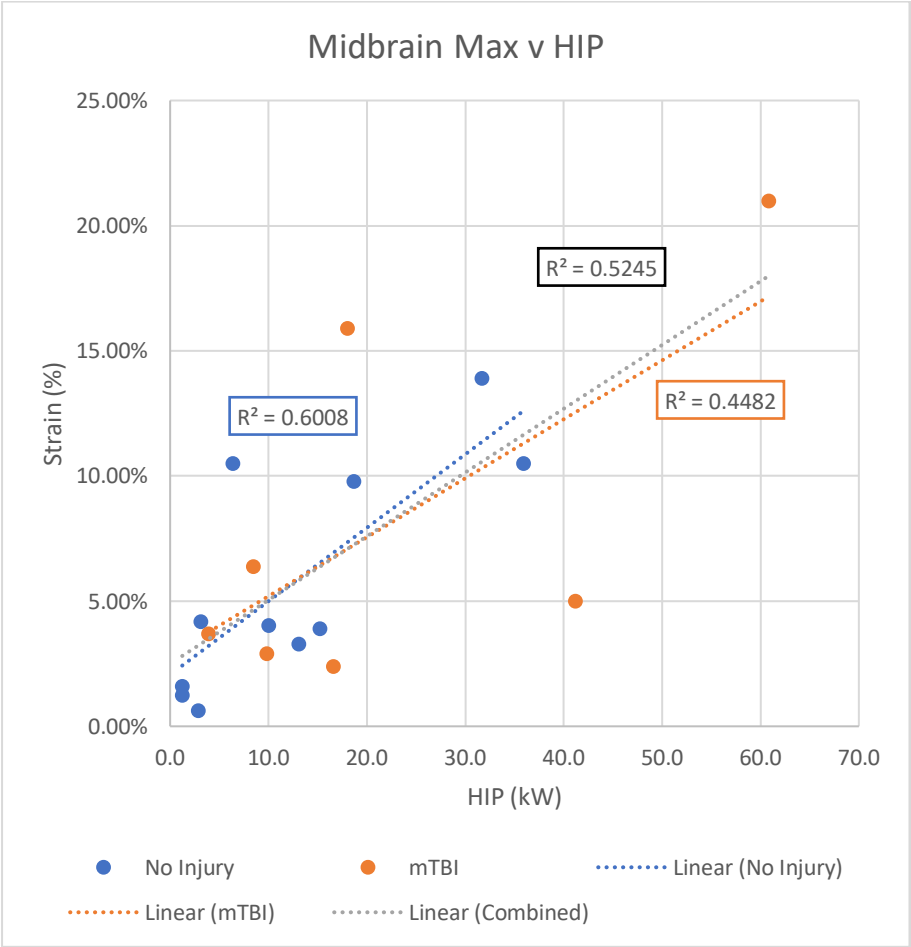
Midbrain Max v HIP
25.00%
20.00%
15.00%
10.00%
5.00%
0.00%
Strain (%)
0.0
10.0
20.0
30.0
40.0
50.0
60.0
70.0
HIP (kW)
R² = 0.5245
R² = 0.6008
R² = 0.4482
No Injury
mTBI
Linear (No Injury)
Linear (mTBI)
Linear (Combined)

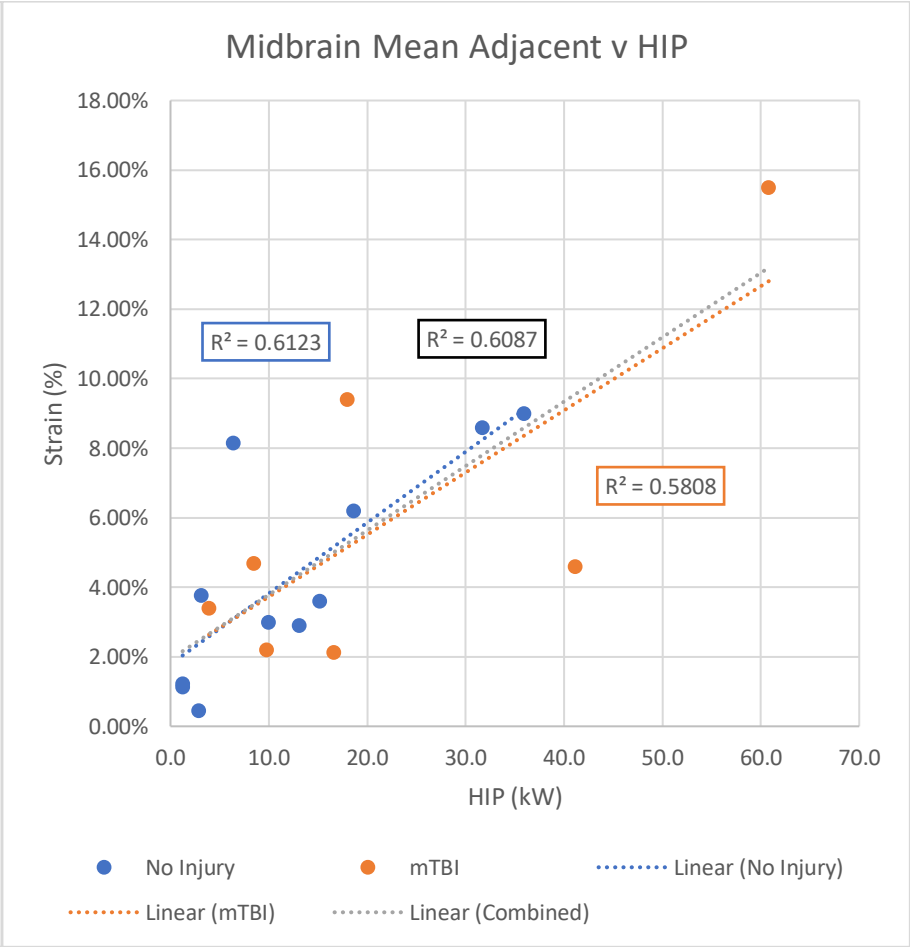
Midbrain Mean Adjacent v HIP
18.00%
16.00%
14.00%
12.00%
10.00%
8.00%
6.00%
4.00%
2.00%
0.00%
Strain (%)
0.0
10.0
20.0
30.0
40.0
50.0
60.0
70.0
HIP (kW)
R² = 0.6123
R² = 0.6087
R² = 0.5808
No Injury
mTBI
Linear (No Injury)
Linear (mTBI)
Linear (Combined)

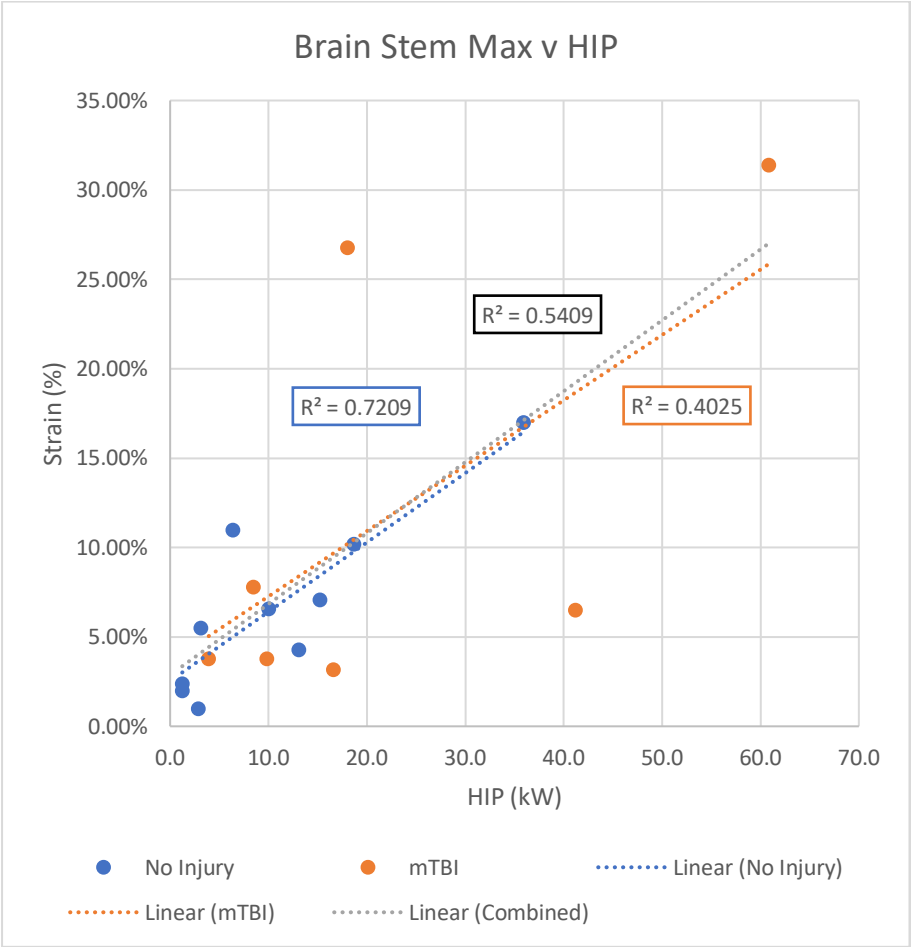
Brain Stem Max v HIP
35.00%
30.00%
25.00%
20.00%
15.00%
10.00%
5.00%
0.00%
Strain (%)
0.0
10.0
20.0
30.0
40.0
50.0
60.0
70.0
HIP (kW)
R² = 0.5409
R² = 0.7209
R² = 0.4025
No Injury
mTBI
Linear (No Injury)
Linear (mTBI)
Linear (Combined)

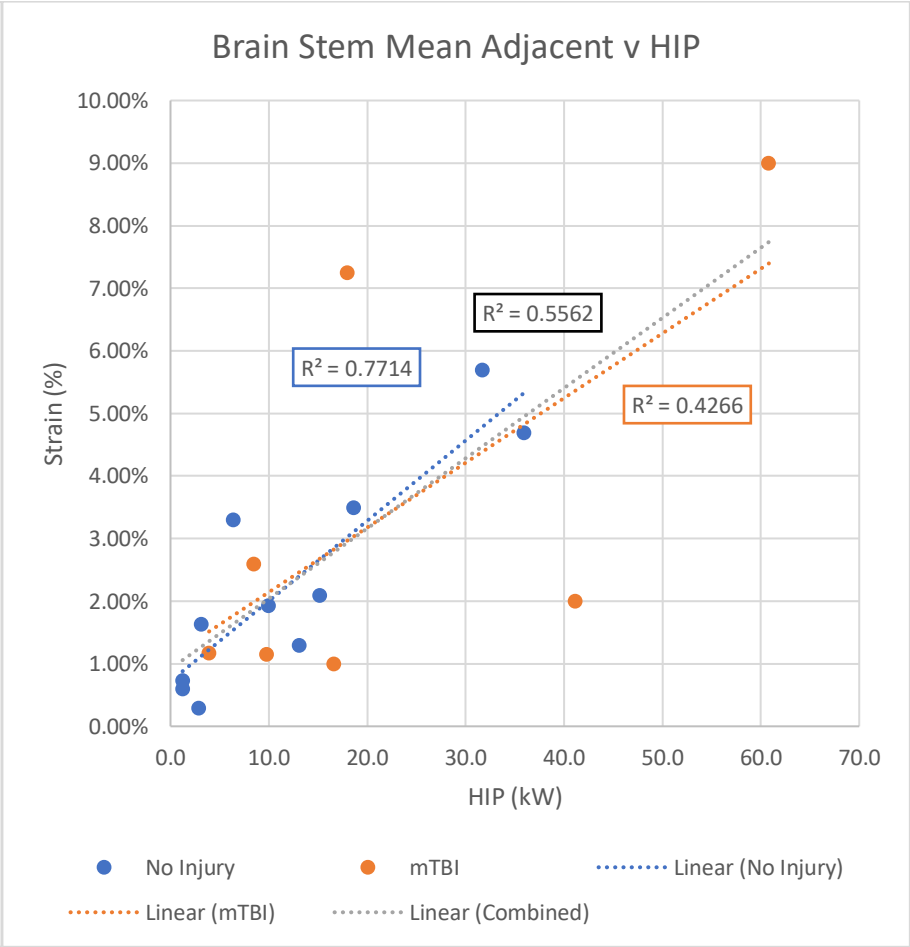
Brain Stem Mean Adjacent v HIP
10.00%
9.00%
8.00%
7.00%
6.00%
5.00%
4.00%
3.00%
2.00%
1.00%
0.00%
Strain (%)
0.0
10.0
20.0
30.0
40.0
50.0
60.0
70.0
HIP (kW)
R² = 0.5562
R² = 0.7714
R² = 0.4266
No Injury
mTBI
Linear (No Injury)
Linear (mTBI)
Linear (Combined)

Publications/Conference Proceedings

Publications

Dynamic blood brain barrier regulation in mild head trauma

Journal of Neurotrauma

Published: 5th September 2019

DOI: https://doi.org/10.1089/neu.2019.6483

Mr. Eoin O'Keeffe, Dr. Eoin Kelly, Dr. Yuzhe Liu, Dr. Chiara Giordano, Dr. Eugene Wallace, Mr. Mark Hynes, Mr. Stephen Tiernan, Mr. Aidan Meagher, Dr. Chris Greene, Ms. Stephanie Hughes, Dr. Tom Burke, Dr. John Kealy, Dr. Niamh Doyle, Dr. Alison Hay, Prof. Michael Farrell, Prof. Gerald Grant, Prof. Alon Friedman, Dr. Ronel Veksler, Prof. Michael Molloy, Prof. James Meaney, Prof. Niall Pender, Dr. David Benjamin Camarillo, Dr. Colin Doherty, and Dr. Matthew Campbell

Conference Proceedings

BINI 2018 – Presentation

Head Impacts: the Effect of Head Size

CADFEM Ansys User Conference 2018 – Presentation

The Measurement and Simulation of Head Impacts

BINI 2019 – Presentation

The Measurement and Simulation of Head Impacts in Mixed Martial Arts

TUD INSPIRE 2019 – Presentation

The Measurement and Simulation of Head Impacts in Mixed Martial Arts

IRCOBI 2019 – Presentation

Measurement and Simulation of Head Impacts in Sport